Development of nanostructured metal based electrocatalyst for electrochemical reduction of carbon dioxide to alcohols

Thesis

Submitted in partial fulfillment for the award of degree

of

Doctor of Philosophy

by

SAUDAGAR BALASAHEB DONGARE

(Registration No.: 901801001)

Under the guidance of

Prof. Haripada Bhunia
Professor
Department of Chemical Engineering,
Thapar Institute of Engineering & Technology
(Deemed to be University), Patiala

Dr. Neetu Singh
Associate Professor
Department of Chemical Engineering,
Thapar Institute of Engineering & Technology
(Deemed to be University), Patiala

Department of Chemical Engineering
Thapar Institute of Engineering & Technology (Deemed to be University)
Patiala – 147004, Punjab (India)
www.thapar.edu

October 2021

Dedicated

to

My Parents

Shr. Balasaheb Dongare & Smt. Jayabai Dongare

My Brothers, Sisters, Friends

and

All My Respected Teachers

CERTIFICATE

This is to certify that the thesis entitled **"Development of nanostructured metal based electrocatalyst for electrochemical reduction of carbon dioxide to alcohols"** being submitted by Mr. Saudagar Balasaheb Dongare to Department of Chemical Engineering, Thapar Institute of Engineering & Technology (Deemed to be University), Patiala for the award of degree of **Doctor of Philosophy**, is a record of bonafide research work carried out by him under our guidance and supervision and has fulfilled the requirements for the submission of this thesis, which to our knowledge has reached the requisite standard.

The results embodied in the thesis have not been submitted in part or full to any other University or Institute for the award of any degree or diploma.

(Haripada Bhunia)
Professor
Department of Chemical Engineering,
Thapar Institute of Engineering & Technology
(Deemed to be University), Patiala

(Neetu Singh)
Associate Professor
Department of Chemical Engineering,
Thapar Institute of Engineering & Technology
(Deemed to be University), Patiala

ACKNOWLEDGEMENTS

The Thapar community has been an inspiring and enriching place to pursue doctoral research and without the many people and programs that are present here, the results presented in this thesis would not have been possible.

First and foremost, I would like to take this opportunity to say thanks to **Dr. P. K. Bajpai** (Ex-Distinguished Professor), Department of Chemical Engineering, Thapar Institute of Engineering and Technology, Patiala for providing scientific advice and technical knowledge through many insightful discussions from very first day of the project. His valuable comments, critical reviews, and suggestions helped me to complete this research work.

I was the first to work on the electrochemical CO_2 reduction project under the guidance of **Prof. H. Bhunia** and **Dr. Neetu Singh** in Chemical Engineering Lab of Thapar Institute of Engineering & Technology, Patiala, India. Progress was slow at first; it took nearly one and half years to develop the facilities required for electrochemical CO_2 reduction, which was frustrating from the perspective of outcomes. However, through the entire time, both my advisors managed to stay upbeat and excited. I never felt limited by experimental cost or conventional wisdom. Their openness to trying new ideas and taking scientific risks was paramount to my own development as an independent researcher and the success of this project. I learnt a lot from them over the course of this Ph.D. work. Their goal oriented style of work, passion towards research, and work ethics have been very inspiring for me. Their daily practice of following up on recent scientific literature is something that I also tried to adopt and greatly benefitted. I really appreciate their unconditional support and encouragement towards doing high-calibre research. It's been a great honour to work under their guidance.

Before joining the Thapar Institute, I have worked with **Prof. Vasant P. Jawanjal** of Department of Petrochemical Engineering, and **Prof. Yogesh S. Mahajan** of Chemical Engineering at Dr. Babasaheb Ambedkar Technological University, Lonere, India. Both of them are extremely dedicated academicians and researchers who demonstrated a level of scientific thoroughness that inspired me to join the Ph.D. program.

I am extremely thankful to **Prof. Prakash Gopalan**, Director, Thapar Institute of Engineering & Technology, **Prof. Rafat Siddique**, Dean of Research & Sponsored Projects, Thapar Institute of Engineering & Technology, and **Prof. Rajeev Mehta**, Head, Chemical Engineering Department for extending the opportunity to undertake this doctoral research.

I would like to profoundly thank to my doctoral committee members **Dr. R. K. Gupta** and **Dr. J. P. Khushwaha** of Chemical Engineering and **Prof. Bonamali Pal**, School of Chemistry & Biochemistry, Thapar Institute of Engineering & Technology for their immense help and guiding me towards the right direction. My heartful thanks to the staff members of Department of Chemical Engineering, Thapar Institute of Engineering & Technology for their valuable contributions, spiritual and moral support.

I would like to thank my Ph.D. course work teachers **Prof. Kulvir Singh**, School of Physics & Materials Science and **Dr. Sumit Chandok**, School of Mathematics for their guidance and motivation in my early stage of Ph.D. I would also like to thank **Dr. Asit Kumar Das**, Head, Refinery R&D and Process Development, Reliance Industries Limited, Jamnagar, Gujarat, India for his help and motivation.

My endless thanks goes to **Mr. Raman Singh Thakur, Mr. Ashutosh Darekar, Dr. Nagendra Singh, Dr. Vinit Kumar, Dr. Anurag Verma, Dr. Manjeet Singh, Dr. Sunil Sable, Dr. Mohit Dhiman, Mr. Ajay Chalotra, Miss. Manju Rawat, Miss. Sanchita, Mr. Daksh Shelly,** and **Mr. Ravi Teja** for their valuable contributions, spiritual and moral support at various stages of my work. I would like to express my myriads of inexpressible thanks and immense gratefulness to my friends and well-wishers who always supported me and made me cheerful in the moments of despair and disappointments.

My deepest gratitude goes to my beloved parents, **Mr. Balasaheb Dongare** and **Mrs. Jayabai Dongare**, my grandmother, **Mrs. Mainabai Dongare**, my sisters and my brothers who have always supported me through highs and lows of life. They have touched my life in many ways. My last word is reserved for **Miss. Vaishali Waghmare** for her support (mental, motivational, and financial) and her true companionship without which I may never have completed this thesis.

I would like to gratefully acknowledge the financial support from **Science and Engineering Research Board, Department of Science & Technology (DST)**, Government of India *(Grant No. EMR/2016/007437, dated March 13, 2018)* throughout the course of this work.

Finally, I wish to thank the "**ALMIGHTY**" God for his sufficiency.

Saudagar Balasaheb Dongare

ABSTRACT

Carbon dioxide (CO_2) is a most common greenhouse gas in our planet. Unfortunately, with the intensified industrial activities by mankind and global consumption of fossil fuels (~ 81.5% of global energy resources) more CO_2 is released to the environment, causing earth–carbon imbalance, leading to possible global warming and climate change issue. In addition, increasing the CO_2 concentration in the atmosphere is resulting in ocean acidification and influencing the growth of many aquatic species present in the ocean. Therefore, the reduction of the CO_2 emissions and the conversion of CO_2 into useful products seem to be important, indeed essential, for the conservation of the environment. Among several existing methods available for CO_2 utilization, electrochemical CO_2 reduction (ECO_2R) has attracted increasing interest in recent years, because it is easily controlled by electrode potential and operated at ambient conditions. Also, electrical energy required to drive ECO_2R can be generated from renewable sources (like geothermal power, wind, tidal, and solar) which help to achieve net-zero carbon footprints. However, CO_2 is a very stable molecule and huge negative potentials are required for triggering ECO_2R reaction. Many useful products like acids, ethers, and alcohols can be derived from ECO_2R but in this work, high energy density products such as alcohols have been targeted due to its application in gasoline blends for fuel. Efficient electro-catalyst is needed which can control the multi-electron and multi-proton transfer pathways for ECO_2R at low over-potential and can also provide high selectivity for alcohols. Therefore, the overall objective of the current Ph.D. work is to develop metal based electro-catalyst for reduction of carbon dioxide to alcohols. To achieve this objective, series of Cu based electro-catalysts were prepared by different techniques. The ECO_2R performance was tested in H-type electrochemical cell in aqueous 0.1 M $KHCO_3$ electrolyte after being characterized through in-situ and ex-situ characterization methods. The in-situ methods involved characterization using cyclic voltammetry (CV), linear sweep voltammetry (LSV), etc. and the ex-situ characterizations included transmission electron microscopy (TEM), scanning electron microscopy (SEM), X-ray diffraction (XRD), X-ray photo-electron spectroscopy (XPS), and Brunauer-Emmett-Teller (BET) method, etc. The liquid products generated after ECO_2R were quantified using high performance liquid chromatography (HPLC), and proton nuclear magnetic resonance (^1H NMR) and the performances were measured in terms of selectivity (Faradaic efficiency), activity (current density), long term stability, etc.

In the first study, highly stable metallic copper nanoparticles (Cu NPs) have been synthesized by wet chemical reduction method. The prepared Cu NPs exhibit porous morphology in pure metallic state with high surface area of 630 m^2 g^{-1}. The total Faradaic efficiency (FE) for the liquid products reached to ~58 % at -0.8 V (vs. RHE) using prepared Cu NPs as an electro-catalyst. In addition, FE for formic acid remained constant around ~40% at −0.8 V (vs. RHE) when reusing the same electrode number of times. The good performance of Cu NPs might be due to the presence of lots of micropores on the surface, which increases CO_2 adsorption for its conversion to chemicals.

In the second study, the nanostructured electro-catalyst consisting of N-doped graphene (NGN) supported Cu nanoparticles (Cu NPs) were prepared and tested for ECO_2R. The electro-catalyst was optimized for loading of Cu NPs on NGN. Results show that the Cu_{20}/NGN (20 wt. % Cu loading on NGN) catalyst showed the highest activity for ECO_2R in the entire potential range studied. It gives a total 54 % FE at -1.0 V (*vs.* RHE) for the liquid products. The study also demonstrated that the electronic and structural properties of the electrode were improved by the addition of Cu NPs on NGN surface, which in turn enhanced the performance of the catalyst as confirmed by potential-controlled electro-catalysis.

Further, oxide derived bimetallic $CuZn_x$ electro-catalysts have been suggested as alternatives for achieving high selectivity for different valuable products. Therefore, in the third study, co-precipitation approach was used to prepare CuO with various quantities of ZnO dopants (x = 5, 10, 15 and 20 wt.%). Amongst studied electro-catalysts, the highest FE of 22.27 % was obtained using CuO-ZnO_{10} at -0.80 V (vs. RHE) with the production rate of about 121 μmol h^{-1} L^{-1}. The optimized electrode (CuO-ZnO_{10}) showed long term stability for at least 12 h. Post characterization of the catalyst was also conducted to obtain an insight into the active sites, which indicated that CO_2 reduction took place on reduced oxide sites (i.e. metallic sites) rather than on metal oxides.

In the fourth study, the oxide-derived Cu and Zn nanoparticles supported on N-doped graphene ($CuZn_x$/NGN) were prepared and ZnO loading was optimized for efficient ECO_2R to multi-carbon products. Results suggest that the FE for multi-carbon products could be tuned by varying the loading of Zn in the $CuZn_x$/NGN. The catalyst with 20 wt.% ZnO loading ($CuZn_{20}$/NGN) gave the highest FE of 34.25 % for ethanol production and 12.38 % for N-propanol at -0.8 V (*vs.* RHE) with the total CD of 3.95 mA cm^{-2}. The $CuZn_{20}$/NGN electrode showed long term stability of at least 24 hours at optimized conditions. It is suggested that CO generated at the reduced ZnO nanoparticles increases the local surface coverage of *CO on the

reduced CuO, which improves the C-C coupling rate, facilitating the multi-carbon production (i.e. ethanol).

Fig. 1 shows the overall thesis outline.

Overall, these studies demonstrate that the activity and selectivity of CO_2 reduction electro-catalysts can be tuned by modifying the elemental composition of the electro-catalyst.

THESIS OUTLINE

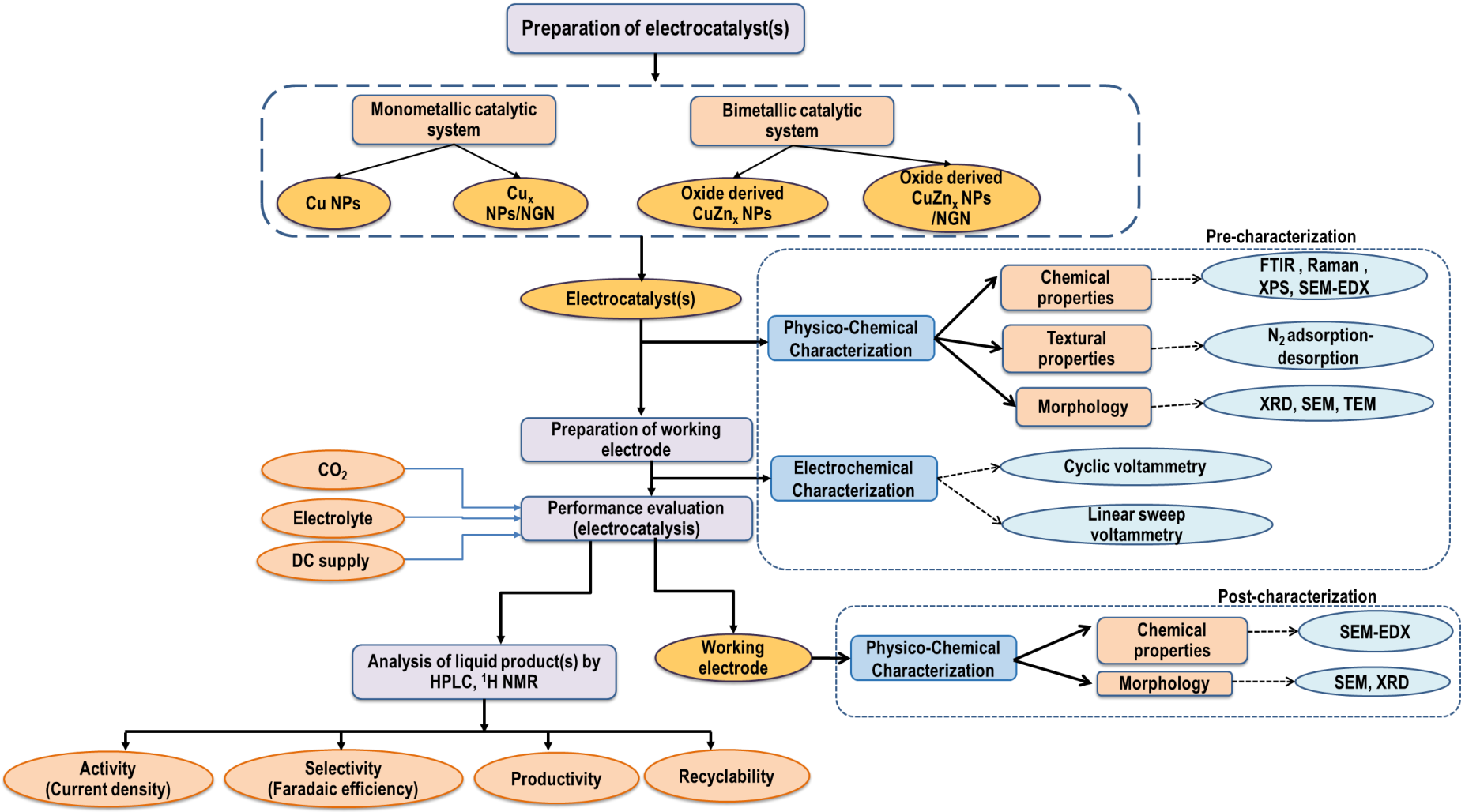

Fig. 1 *Schematic of overall thesis work*

TABLE OF CONTENTS

LIST OF FIGURES

LIST OF TABLES

LIST OF SYMBOLS

C_{dl}	Double-layer capacitance
F	Faraday's constant, F=96485 C.mol^{-1}
h	Hour(s)
I	Current obtained during electrolysis
j	Current density, mA cm^{-2}
$j_{formate}$	Formate partial CD
$j_{ethanol}$	Ethanol partial CD
N	Total number of moles, M
P_{CO_2}	CO_2 partial pressure
Q	Total charge passed across the electrode
R^2	Regression coefficient
S_{BET}	BET surface area, m^2 g^{-1}
t	Time, min
V	Volt, V
V_b	Scan rate, mV sec^{-1}
V_{meso}	Mesopore volume, cm^3 g^{-1}
V_{micro}	Micropore volume, cm^3 g^{-1}
Z	Number of electrons required to produce one molecule of product from CO_2

Greek Letters

θ	Bragg's angle
µm	Micrometer
λ	X-ray wavelength (0.154 nm)
β	Line broadening at half the maximum intensity (FWHM)

LIST OF ABBREVIATIONS

Ag/AgCl	Silver- silver chloride electrode (reference electrode)
B. E.	Binding energy
BET	Brunauer–Emmett–Teller
BJH	Barrett–Joyner–Halenda
CD	Current density
CE	Counter electrode
Cu NPs	Cu nanoparticles
CuO-ZnO_x	Cu-Zn bimetallic oxides where x is weight percentage of ZnO
Cu_x/NGN	N-doped graphene supported Cu NPs where x is weight percentage of Cu
$CuZn_x$/NGN	N-doped graphene supported Cu-Zn NPs where x is weight percentage of Zn
ECASA	Electrochemical active surface area
ECO_2R	Electrochemical CO_2 reduction
EDX	Energy dispersive X-ray spectroscopy
FE	Faradaic efficiency
FESEM	Field emission scanning electron microscopy
FTIR	Fourier-transform infrared spectroscopy
FWHM	Full width at half maximum
HER	Hydrogen evolution reaction
HR-TEM	High resonance-transmission electron microscopy
ILs	Ionic liquids
IPA	Iso-propyl alcohol
JCPDS	Joint committee on powder diffraction standards
MOFs	Metal-organic frameworks
ND	Not detected
NGN	N-doped graphene
OER	Oxygen evolution reaction
ppm	Parts per million
PSD	Pore size distribution

RE	Reference electrode
RHE	Reverse hydrogen electrode (reference electrode)
SCE	Saturated calomel electrode
SHE	Standard hydrogen electrode (reference electrode)
TGA	Thermo-gravimetric analysis
WE	Working electrode
wt.%	weight%
XPS	X-ray photoelectron spectroscopy
XRD	X-ray diffraction

Chapter 1 – Introduction

1.1. Introduction

From last few decades, fossil fuels and coal are used as the world's leading energy sources to meet the growing energy demand. Therefore, atmospheric CO_2 concentrations have increased from 331 to 415 parts per million (ppm) during the period of 1970-2021 [1]. By the end of the 21st century, it is expected to reach 1060 ppm if global energy demand continues to rise which is mostly met with burning of fossil fuels [2]. As a consequence, the average global temperatures will rise by 5 °C [3]. Therefore, many international organizations are working on developing the strategies to reduce atmospheric greenhouse gas concentrations [4]. Among different gas emissions, the CO_2 is the highest emitted greenhouse gas and has a highest impact on greenhouse gas effect. Therefore, reducing this CO_2 emission from the atmosphere is highly desired [5, 6]. There are many approaches for reducing CO_2 emission [7, 8]. Converting waste CO_2 gas into useful goods is a more worthwhile solution than geological CO_2 sequestration due to its high-efficiency use and processing of carbon sources. So far, different methods have been adopted for converting CO_2 into useful chemicals [9], including: (1) thermal; (2) electrochemical; (3) photochemical; (4) biochemical; (5) chemo-enzymatic; and (6) other approaches such as esterification, methanation, hydrogenation, dry reforming, etc. Due to chemical inertness and high stability of CO_2 [10, 11], the traditional CO_2 absorption, activation, and conversion catalytic processes have some drawbacks [9, 12], such as high energy requirement for conversion, slow conversion rate to produce different chemicals, catalyst deactivation, etc. The conversion of CO_2 by electrochemical reduction technique has attracted great attention.

1.2. CO_2 utilization by electrochemical CO_2 reduction

Electrochemical CO_2 reduction (ECO_2R) can produce a variety of products depending on the electro-catalyst material, type of electrolyte, and operating conditions, which allow for reduction routes of two (2), four (4), six (6), eight (8), twelve (12), or eighteen (18) electrons transfer. The half-cell reactions for different valuable products are shown in **Table 1.1** and are categorized as intermediate products, alcohols, hydrocarbons, and acids. The standard reduction potentials ($E°_{redox}$) measured with reference to standard hydrogen electrode (SHE) are also shows in **Table 1.1**.

Table 1.1 *Selected standard potentials (V vs. SHE) of CO_2 to different valuable products in aqueous solutions (at pH=7, 25 °C, 1 atm) [13-18]*

Group	Half reactions	E^o_{redox} (V vs. SHE)
Alcohols	$CO_{2(g)} + 6H^+ + 6e^- \rightarrow CH_3OH_{(l)} + H_2O_{(l)}$	-0.380
	$2CO_{2(g)} + 12H^+ + 12e^- \rightarrow C_2H_5OH_{(l)} + 3H_2O_{(l)}$	-0.329
	$3CO_{2(g)} + 18H^+ + 18e^- \rightarrow CH_3CH_2CH_2OH_{(l)} + 5H_2O$	-0.310
	$3CO_{2(g)} + 18H^+ + 18e^- \rightarrow CH_3CH(OH)CH_{3(l)} + 5H_2O_{(l)}$	-0.30
Hydrocarbons, CO, H_2	$CO_{2(g)} + 2H^+ + 2e^- \rightarrow CO_{(g)} + H_2O_{(l)}$	-0.530
	$CO_{2(g)} + 8H^+ + 8e^- \rightarrow CH_{4(g)} + 2H_2O_{(l)}$	-0.240
	$2CO_{2(g)} + 14H^+ + 14e^- \rightarrow C_2H_{6(g)} + 4H_2O_{(l)}$	-0.270
	$2CO_{2(g)} + 12H^+ + 12e^- \rightarrow CH_2CH_{2(g)} + 4H_2O_{(l)(l)}$	-0.349
Acids, Aldehydes	$CO_{2(g)} + 2H^+ + 2e^- \rightarrow HCOOH_{(l)}$	-0.610
	$2CO_{2(g)} + 8H^+ + 8e^- \rightarrow CH_3COOH_{(l)} + 2H_2O_{(l)}$	-0.31
	$2CO_{2(g)} + 2H^+ + 2e^- \rightarrow H_2C_2O_{4(aq.)} + 2H_2O_{(l)}$	-0.913
	$CO_{2(g)} + 4H^+ + 4e^- \rightarrow HCHO_{(l)} + 2H_2O_{(l)}$	-0.480
H_2 generation	$2H^+ + 2e^- \rightarrow H_{2(g)}$	-0.42

1.3. Prospects and challenges of ECO_2R

Lately the research has shown that by reducing carbon dioxide electrochemically can produce various organic compounds like formic acid, methane, carbon monoxide, hydrogen and others with high current efficiency. Electrochemical reduction of carbon dioxide in recent years have won over other technologies due to unique advantages [19-22], as given in **Table 1.2**.

Table 1.2 *Advantages of electrochemical CO_2 reduction process*

Criteria	Advantages
Valuable products	Different alcohols, hydrocarbons, and other valuable products can be obtained.
Environmental aspect	The net chemical consumption is just water and waste CO_2 since the electrolyte can be entirely recycled.
Clean energy	The electricity used to drive this process can be produced using renewable resources such as hydro, solar, and geothermal energy, resulting in no additional CO_2 emissions.
Temperature/pressure	The electrochemical CO_2 reduction takes place at room temperature and pressure. No high energy requirement.
Selectivity control	The product selectivity and reaction rates can be controlled by changing the applied potentials and temperature.
Ease of operation	The process can be scaled up easily due to its ease of operation and compact cell designs.

The challenges that we face while reducing CO_2 are:

i. Transportation of CO_2 to the reaction system.
ii. Minimizing the catalyst from corroding and poisoning.
iii. Increasing the current densities to achieve high efficiencies.
iv. Collection of the products effectively from the outlet without any wastages.
v. It is important to find new reaction paths and catalysts to produce new products.
vi. Analysis and separation of the products obtained.
vii. Increasing the FE to increase the energy efficiency and reducing the over-potential of the reactions taking place.
viii. Collecting the products from catalyst layer without blocking the catalyst active site.

1.4. Why ECO_2R to alcohols?

As the depletion of crude oil in the reservoirs and increasing global warming issues become more severe, the need for a viable, clean, and renewable liquid fuel as an alternative to replace existing transportation fuels is becoming increasingly important [23, 24]. Therefore, ethanol has become a hot topic in the political, environmental, economic, and scientific areas due to its comparable heating value (1366.8 kJ mol^{-1}), ease of storage and transport than that of gas products. Also, ethanol is used as octane booster (or oxygenate) in the gasoline [25]. India is dependent on crude oil imports for 80% of its requirement and is the third largest importer of energy in the world behind the United States (USA) and China [23]. India has set a goal of 20% blending of ethanol with gasoline to achieve an ambitious target of reducing 50 % crude oil imports by 2030 [23].

Presently, ethanol is majorly produced by the catalytic hydration of ethylene [26] and fermentation of biomass at large scale which is green plant material usually from soybeans, sugarcane, or corn [27, 28]. However, it seems that nature will be unable to supply both food and electricity at a time to worlds rising population and its increasing energy demand. As a result, CO_2 conversion to ethanol powered by renewable energy is a viable option (**Fig. 1.1**) [19].

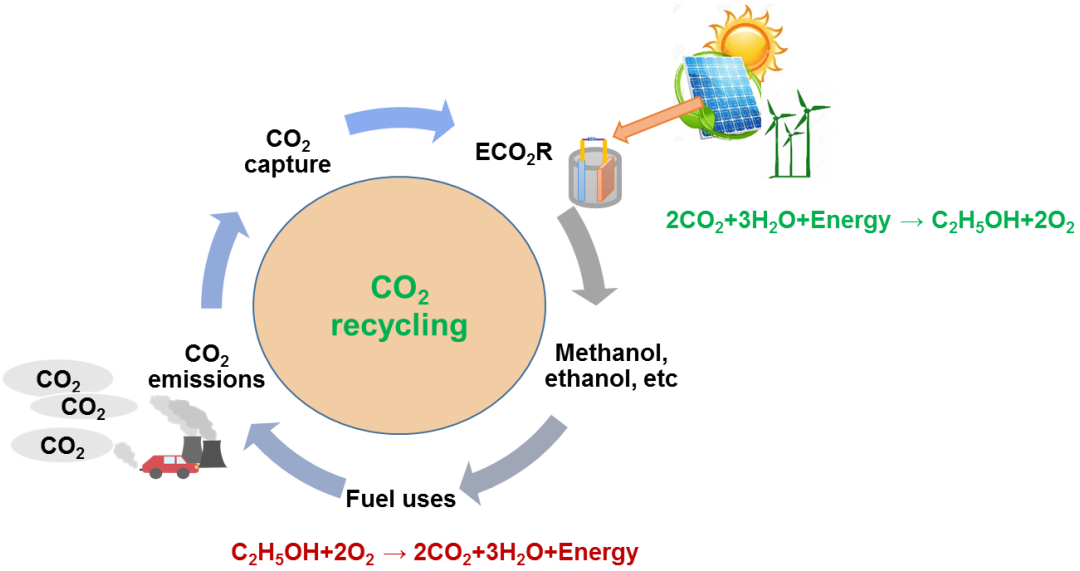

Fig. 1.1 *Schematic illustration of closed loop CO_2 recycling based on ECO_2R*

In the year 1985, Hori et al. [29] first reported a groundbreaking work on electrochemical CO_2 reduction to useful chemicals. Since then, the first direct ECO_2R to C_2H_5OH was reported by same group in 1993 [30]. Later large number of publications [31-35] are available in the literature, especially from last one decade. These efforts have been also summarized in a number of review papers on CO_2 electrochemical reduction [36-38], in which the current state of the art is discussed.

1.5. Motivation and objectives

1.5.1. Motivation

One of the greatest technical challenges in the process of CO_2 conversion is the reduction of CO_2 resulting in a selective product with high efficiencies [13]. To overcome the problem, noble or expensive material as electro-catalyst is used. This research proposal envisages the development of a metal-based nanostructured catalyst by chemical reduction of metal salts on different carbon supports. The product selectivity in ECO_2R will be strongly affected by the operating conditions, such as the catalysts and/or electrodes, electrode potential, electrolyte solution, pH, catalyst loading, CO_2 concentration, and pressure, as well as temperature [39]. The role of carbon supports and composite electro-catalysts need to be studied for better understanding of ECO_2R to alcohols. The role of different heteroatom species in the modified carbon support also remains to be studied. The reusability of optimized electro-catalyst needs to be addressed.

1.5.2. Objectives

The overall objective of the research is to develop metal based electrocatalyst supported on carbon for reduction of carbon dioxide to alcohols.

The specific objectives are:

- To prepare and characterize suitable carbon support for the electrocatalyst
- To prepare and characterize nanostructured metal/metal oxide electrocatalyst (Cu or Cu_2O) on carbon supports and coating of electrocatalyst on electrode
- To evaluate performance of electro-catalysts in terms of activity i.e. CD (current/catalyst area vs. applied potential), selectivity (FE) from the analysis of products for electrochemical reduction of carbon dioxide by changing the different operating parameters (electrolytes, electrolyte concentration, electrocatalyst loading, voltage)
- To study the reusability of optimized electrocatalyst at optimized conditions

1.6. Outline of the thesis

The total thesis has been divided into eight chapters.

Chapter 1 is the general introduction. The background of the global CO_2 emissions, utilization methods, and transportation were first presented. It also points out the various challenges and trends towards CO_2 reduction. Finally, the motivation and objectives of this research are given, which includ investigating ECO_2R performance for production of alcohols using different metal/metal oxide based electro-catalysts.

Chapter 2 provides a literature review of past studies on electrochemical reduction of carbon dioxide to alcohols. A brief study on electro-catalyst composition, its morphology, electrolyte ions and pH, applied potential and the configuration of electrochemical reactor is given. Furthermore, the present status, existing challenges and future prospects are described for future design and planning of high-performance ethanol catalysts.

Chapter 3 lists all experimental methods, tools and equipment employed for the experimental work in this thesis for catalyst preparation, its characterization, fabrication of the electrodes, and conduction of the bulk electrolysis measurements, along with the qualitative and quantitative product analysis.

Chapter 4 *Electrochemical CO_2 reduction on metallic Cu nanoparticles (Cu NPs):* This chapter describes preparation of citrate stabilized metallic Cu nanoparticles (Cu NPs), to be used for ECO_2R in CO_2 saturated aqueous 0.1 M $KHCO_3$ solution. The effect of key governing

parameters like electrolysis potential was explored to obtain the optimal electrolysis condition. Effects of potential on the final product concentration, production rates, and FE (selectivity) were studied. Kinetics is studied by Tafel analysis and dependence of CO_2 partial pressure on product generation is also explored. Moreover, reusability of the electrode at optimized conditions is also discussed. The performance of the Cu NPs is compared with that of commercial Cu foil.

Chapter 5 *Electrochemical CO_2 reduction on nitrogen-doped graphene supported copper nanoparticles (Cu_x/NGN):* This chapter describes preparation of Cu_x/NGN (with different weight percentages of Cu) to be used as electro-catalyst in the electrochemical CO_2 reduction to useful liquid products in aqueous media. The physico-chemical properties of the electro-catalyst were studied using different characterization methods. The effect of catalyst support and composition on different CO_2 reduction products as a function of applied potentials is reported.

Chapter 6 *Electrochemical reduction of CO_2 using oxide based Cu and Zn bimetallic catalyst:* This chapter describes, synthesis of oxide derived Cu-Zn bimetallic oxides (CuO-ZnO_x) using a simple co-precipitation method followed by calcination in air atmosphere, using cupric nitrate and zinc nitrate as Cu and Zn precursor, respectively. The loading percentage of Cu to Zn in the electro-catalysts can be easily adjusted by changing the precursor concentrations. The activity and selectivity of synthesized CuO-ZnO_x were studied by various electrochemical characterization methods.

Chapter 7 *Oxide-derived Cu-Zn nanoparticles supported on N-doped graphene for electrochemical reduction of CO_2 to ethanol:* In this chapter, the oxide-derived Cu-Zn nanoparticles supported on N-doped graphene were prepared by co-precipitation method. The physico-chemical and electrochemical properties of these catalysts were studied by different characterization techniques. The selectivity of CO_2 reduction to ethanol can be regulated by changing the loading of Zn in the oxide derived $CuZn_x$/NGN catalysts. The control experiments were also performed using different ZnO loadings (10 to 40 wt.%) in $CuZn_x$/NGN and CuO/NGN.

Chapter 8 deals with the important conclusions drawn from all the research work of the thesis using different catalyst materials

Chapter 2 – Literature review

2.1. Electro catalysts for reduction of carbon dioxide to ethanol

Although ECO_2R has many advantages as listed earlier, but there are some challenges also which inhibit the CO_2 electro-reduction performance, such as high over-potential (high energy consumption), poor product selectivity, low energy efficiency, and slow kinetics of CO_2 electrochemical reduction reaction, etc. [18]. Therefore, there is a need to develop an electro-catalyst which is highly selective, stable, cheap, and able to produce different chemicals at low over-potential with higher rates without the formation of undesirable byproducts [21, 40, 41]. Numerous strategies have been developed to synthesize alcohol selective electro-catalysts e.g. electrochemical deposition [42-44], hydrothermal synthesis [45], thermal annealing [46, 47], chemical reduction of different metal salts [48-50], soft templating method [51, 52]. Most of these methods undergo oxidation step followed by an in-situ reduction to metallic state during ECO_2R. In this section, the preparation of high performing electro-catalysts for alcohol production and the influence of different synthetic strategies on catalyst composition, morphology on ECO_2R performance have been discussed. In general, there are two types of electro-catalysts that can be used in ECO_2R process:

- Homogeneous electro-catalysts
- Heterogeneous electro-catalysts

2.1.1. Homogeneous electro-catalysts

In homogeneous catalysis, both substrate and catalyst are dissolved in the electrolyte solution and the chemical reactions take place at catalyst surface. Homogeneous electro-catalysts (organics or metal–organic molecules added in electrolyte solutions) show excellent selectivity against CO_2 reduction due to their unique coordinative structures and active centers that can closely interact with dissolved CO_2, gaining significant interest and being extensively investigated since the 1970s [53, 54].

Although homogeneous catalysts have some advantages, they also have some disadvantages. They have high costs, high toxicity, and complex post-separation procedures, which make them unsuitable for large-scale production [54, 55]. Therefore, heterogeneous catalysts have sparked a lot of research interest in recent years due to their high performance, ease of synthesis, environmental friendliness, and its industrial applicability [56-58].

2.1.2. Heterogeneous electro-catalysts

Significant efforts were made to advance the design of heterogeneous electro-catalysts for ECO_2R. A wide range of materials have been examined and evaluated. The materials can be divided into various categories, such as mono-metals [35, 42, 59-61], bimetals/metal alloys [32, 44, 49] , heteroatom doped metals [62, 63], organometallic complexes [58, 64-66], metal organic frameworks [67, 68], supported metals [52, 69, 70] and metal free electro-catalysts [51, 71, 72]. Many researchers have conducted experimental and computational studies in order to enhance the mechanistic understanding of the reaction and the effect of the substance, and it has been reported that the binding energy between different reaction intermediates and the electro-catalyst is a crucial factor regulating the final product distribution [40, 73]. Initially ECO_2R catalysts were pure-metal foils that were directly used as electrodes. However, since the advancement of nanotechnology, other configurations have been employed as catalysts for the ECO_2R with significantly enhanced efficiency. Since nanostructured catalysts have larger surface areas and higher fractions of low-coordination sites, they are frequently studied in last few years, and it has been revealed that nanostructuring improved catalytic efficiency in many cases [34, 74]. Another interesting way is to use composite cathodes for CO_2 reduction for alcohol production with high rates [75]. It has been shown that mixing two or more separate materials into a composite (such as metal-carbon [69, 75], metal-metal oxide [33, 76], etc.) will result in cooperative and synergistic effects, as well as accelerated kinetics, improved selectivity, and enhanced catalyst stability compared to using the individual components.

2.1.2.1. Metal-based electrodes / catalysts

2.1.2.1.1. Monometallic catalysts

Cu and Cu-based materials exhibit notable catalytic properties for the conversion of CO_2 into alcohols and hydrocarbons [31, 46, 77], such as methanol (CH_3OH), ethanol (C_2H_5OH), n-propanol (n- C_3H_7OH), methane (CH_4), ethane (C_2H_6) and ethylene (C_2H_4). During the past few decades, monometallic Cu based electrodes have been widely studied by many researchers for the electrochemical reduction of CO_2 [30, 31, 34, 35, 40, 42, 43, 46, 48, 57, 59, 60, 78-105]. Also, few non Cu-based electrodes are reported for ethanol production like In_2O_3 [106] and Ag [107]. In ECO_2R, the formation of the CO_2^* intermediate has been considered as a rate-determining step [18]. As a result, one of the primary functions of these electro-catalysts is to stabilize this CO_2^* intermediate in order to achieve high energy efficiency during ECO_2R. As compared to untreated metallic Cu [98], the oxide-derived Cu catalysts [35, 46, 59] display

better catalytic efficiency. For example, metallic Cu showing a FE of 9.7% for ethanol at -1.05 V vs. RHE [40] in comparison to several studies on oxide-derived Cu catalyst indicate an improved catalytic activity (FE of 35 % for C_2H_5OH) with a CD of 11.8 mA cm^{-2} at -1.0 V (vs. RHE) [35]. Although, under ECO_2R conditions, the oxide derived copper catalysts (CuO and Cu_2O) are typically rapidly converted to metallic Cu due to application of reduction potentials [108, 109], the other parameters like morphology, local pH changes, defect creation, etc. can affect the activity, selectivity and stability of oxide-derived electro-catalysts. Moreover, the presence of Cu^+ or Cu^{2+} play an important role during ECO_2R [110]. Here, the focus is on some recent progress in the preparation of monometallic electro-catalysts and its catalytic activity towards alcohol formation during ECO_2R.

Recently, Yang et al. [46] proposed a strategy to create grain boundaries (GBs) and micro-strains inside CuO for ECO_2R electro-catalysts. For this, they annealed Cu powder at 500 ^oC for 2 h in a porcelain boat. After annealing, the porcelain boat was immediately dipped into liquid nitrogen for 5 min. It was labeled as CuO-FC. The CuO-FC showed abundant high-density GBs and micron-strains inside CuO electro-catalysts. The CuO-FC electro-catalyst produced ethanol with a 35.7% of FE at a high current density of 127 mA cm^{-2}. The enhanced selectivity of C2 product is ascribed to the higher adsorption capability of *CO intermediates during the electrochemical CO_2 reduction process.

Nanostructured self-supporting Cu electrodes with different morphologies were reported by Wang et al. [80]. In the preparation, the treated Cu substrate is simply dipped into the oxidizing solution at ambient conditions. This oxidation process was controlled for 20, 120 and 720 min to produce Cu nanowires, Cu nanosheets, and Cu nanoflowers, respectively.

The effect of processing conditions on the morphology is summarized in **Table 2.1** and list of monometal/monometal oxide electro-catalysts for ECO_2R to ethanol production with other important parameters are given in **Table 2.2**.

Table 2.1 *Effect of processing on morphology of Cu catalyst*

Sr. No.	Starting material	Processing conditions	Morphology	Ref.
1.	Commercial copper powder	Annealing at 500 ^{0}C for 2 h and cooling at different rates i. Slow cooling (CuO-MC) ii. Fast cooling: by directly dip into water for 20 min (CuO-MC) iii. Fast cooling: Directly dip into liquid nitrogen for 5 min (CuO-FC)	All samples composed of interconnected irregularly nano-crystalline particles, ~50 nm average size but different densities of grain boundaries	[46]
2.	Treated Cu foam	Dipping into oxidizing solution at ambient condition for i. 20 min ii. 120 min iii. 720 min	Cu nanowire Cu nanosheet Cu nano flowers	[80]
3.	Different precursors	Hydrothermal method i. 0.25 M copper acetate and urea aqueous solution ii. 0.025 M copper acetate and urea aqueous solution iii. 1 M cupric nitrate and sodium carbonate aqueous solution	3D spherical 4 µm 3D spherical non-uniform ~ 2 µm 2D structure 200 nm nanosheet of 1 µm	[35]
4.	Copper (I) bromide, olelyamine, and different stabilizers	Standard reflux reaction method i. Trioctylphosphine oxide (2 mmol) ii. Trioctylphosphine (0.8 mmol) iii. Trioctylphosphine (1 mmol)	Cube-like Cu nano single-crystal Hexarhombic dodecahedron-like Cu nano single-crystal Octahedron-like Cu nano single-crystal	[82]
5.	$CuSO_4.5H_2O$ and 3,5-diamino-1,2,4-triazole (DAT) additive at different pH	Electrodeposition; different pH of electrolyte i. pH = 2.5 ii. pH = 1.5 iii. pH = 1.0	Ill-defined shape Wire like shape, 50-70 nm diameter Dot shape/ mixture of wire & dot	[42]

Table 2.2 *Summary of the ECO_2R to ethanol on monometal/monometal oxide electro-catalysts in aqueous electrolyte solutions*

Sr. No.	Catalyst	Preparation techniques	Morphology	Active site	Type of cell	Electrolyte (CO_2 saturated)	Potential, V (vs. RHE)	$j^{\#}$ ($mA \cdot cm^{-2}$)	$FE_{ethanol}$ (%)	Stability (h)	Other C_{2+} products	Ref.
1	Cu NS	Oxidation at room temperature for 120 sec	Nanosheet	Cu^0 species	H-type cell	1 M $KHCO_3$	-0.4	10	35.70	NA	CH_3COOH, C_2H_4,C_2H_6	[80]
2	CuDAT-wire	Electro-deposition	Wire	Nanosize CuDAT particles	Flow cell	1 M $KHCO_3$	-0.85		27.00	8	C_2H_4	[42]
3	H-Cu	NA	Hexarhombic dodecahedron	NA	H-type	0.1 M $KHCO_3$	-1.2	14	25.00	NA	C_2H_4,	[82]
4	Plasma-activated Cu nanocube	Electrochemically anodizing followed by plasma pretreatments in a plasma etcher	Cubic nanostructures	Defects and subsurface oxygen species in Cu^+	H-cell	0.1 M $KHCO_3$	-1.05	50	22.50	NA	C_2H_4	[59]
5	a-Cu	Chemical reduction of $CuCl_2$ by tannic acid	Amorphous	Amorphizing of the materials	Two compartment cell	0.1 M $KHCO_3$	−1.4 (vs. Ag/AgCl)	12.5	22.00	12	NA	[48]
6	Cu_2O TF	DC magnetron sputter deposition	Thin film (100 nm in thickness)	NA	Parallel plate cell	0.05 M Cs_2CO_3	– 1.0	NA	20.00	NA	C_2H_4,	[83]
7	Cu (100)	Sputtering	NA	NA	H-cell	0.1 M $KHCO_3$	-0.95	-5.68	18.00	NA	C_2H_4, C_3H_7OH	[84]

8	Ag-GDEs Cu-GDEs	Supplied by Sigma Aldrich	Spherical nanoparticles	CO is produced in a first step and reduced to multi-carbon products in a second step	Two-step flow cell	1 M $KHCO_3$,	-0.83	300	18.00	14	C_2H_4, C_3H_7OH, CH_3COOH	[85]
9	Cu_2O derived copper	Electro-deposition	Polyhedron	500 nm-sized crystalline Cu0 particles	Two compartment cell	0.1 M $KHCO_3$	−1.0	NA	16.40	NA	C_2H_4, CH_3COOH, C_3H_7OH	[86]
10	Oxide derived Cu catalysts	Electro-deposition and thermal annealing	Nano-dendritic	NA	H-type	0.5 M $KHCO_3$	-1.0	NA	13.00	NA	H_2, CO, CH_4, C_2H_4	[89]
11	Mixture of Cu_2O, CuO and Cu	NA	NA	High concentration of OH at catalyst interface	Flow cell	2.0 M KOH	−0.77	130	9.00	NA	NA	[91]
12	$Cu_{50}/PTFE_{15}$ /Sust	Copper(II)acetate was thermally reduced in a tubular furnace under H_2 atmosphere	NA	NA	Flow cell	0.5 M $KHCO_3$	−1.4	300	9.00	2	C_2H_4	[92]

NA- data not available, $j^{\#}$ - total current density at applied potential mentioned in column 8

2.1.2.1.2. Bimetallic/alloy electro-catalysts

During past few years, the binary mixture/alloys have gained considerable attention in improving alcohol selectivity in the ECO_2R. The electronic structures could be facilely adjusted by changing the bimetallic composition, size, and ordering degree to improve their selectivity and activity by improving the binding energy of the key intermediates. Lee et al. [111] developed Ag-incorporated cuprous oxide (Ag-Cu_2O) for electrochemical reduction of CO_2 to ethanol. For this, electrochemical co-deposition was carried out in either NH_3 or KCN solutions containing Cu and Ag precursors. The characterization results show that the atoms of Ag and Cu are more homogeneously dispersed on Ag-Cu_2O_{PB} (prepared in KCN) surface than on Ag-Cu_2O_{PS} (prepared in NH_3) surface. All the electrode samples had a high atomic Cu content (~66%). Ag-Cu_2O_{PB} displayed selective ethanol formation during ECO_2R.

Recently, Dutta et al. [47] introduced bimetallic AgCu metal foams ($Ag_{15}Cu_{85}$). It was synthesized by additive-assisted electro-deposition method using the dynamic H_2 bubble template approach. Authors reported that Cu and Ag are completely phase separated in the bimetallic foam, with a high degree of dispersion of pure nm-sized Ag domains contained in the Cu matrix. The developed oxide-derived (OD) bimetallic $Ag_{15}Cu_{85}$ foam catalyst selectively produced ethanol with higher FE.

Hoang et al. [112] prepared high surface area and homogeneously mixed CuAg alloy electro-catalyst via electro-deposition in baths containing inhibitor 3,5-diamino-1,2,4-triazole (DAT) with different quantities of Ag dopant. The CuAg alloy film with 6% Ag exhibits the best ECO_2R performance for multi-carbon productions i. e. ethylene and ethanol. Zhu et al. [44] carried out potentiostatic pulse-electro-deposition using the anodic aluminum oxide (AAO) membrane as the template for the preparation of Cu_xAu_y nanowire arrays (NWAs). By regulating the electro-deposition potential, the surface electronic configuration referred to the Cu:Au ratio in the Cu_xAu_y nanowire arrays could be easily controlled, and the as-fabricated Cu_xAu_y NWAs could be directly used as the electro-catalyst for the ECO_2R. The optimized Cu_xAu_y NWAs have a high ethanol selectivity with FEs of 45 to 48 % at -0.5 to -0.7 V (vs. RHE) with a 1.0 mA cm^{-2} specific CD of ethanol formation. Good selectivity was obtained due to the synergistic effect of electronic structure and morphology.

Many other interesting studies are available using CuZn bimetallic electro-catalyst for ethanol production [113-116]. For example, Ren et al. [113] prepared oxide-derived Cu-based catalysts

with different quantities of Zn dopants (Cu_2Zn, Cu_4Zn, and $Cu_{10}Zn$) and used as electro-catalysts in aqueous 0.1 M $KHCO_3$ electrolyte under ambient conditions. Andrews et al. [116] reported vacuum deposition method. All these catalysts showed improved performance of multi-carbon production than Cu alone. This is due to the addition of co-catalyst which improves the binding strength of key intermediate (*CO) for ethanol or other multi-carbon products. The effect of processing conditions on the morphology of bimetallic catalyst is summarized in **Table 2.3** and summary of the ECO_2R to ethanol on bimetal/bimetal oxide electro-catalysts in aqueous electrolyte solutions is shown in **Table 2.4**.

Table 2.3 *Effect of processing on morphology of bimetallic catalysts*

Sr. No.	Starting material	Processing conditions	Morphology	Ref.
1.	$CuSO_4 \cdot 5H_2O$ and $AgNO_3$	Electrochemical co-deposition in different solvents i. NH_3 solutions ii. KCN solutions	Phase-separated Ag/Cu_2O structure Phase-blended Ag/Cu_2O structure	[111]
2.	$CuSO_4$, Ag_2SO_4, $Na_3C_6H_5O_7.2H_2O$	i. Electroplating ii. Electroplating followed by thermal annealing at 200° C for 12 h	Amorphous and crystalline dendrite structures	[47]
3.	$CuSO_4 \cdot 5H_2O$, 3,5-diamino-1,2,4-triazole (DAT), and Ag_2SO_4	Electrodeposition at pH= 1.5	Wire-like morphology	[112]
4.	$CuSO_4$, glycine, $HAuCl_4$, and ethylenediamine	Electrodeposition at different potentials and constant pH= 7.3 i. −0.45 V (CuAu NWAs) ii. −0.5 (Cu_3Au NWAs) iii. −0.4 V ($CuAu_3$ NWAs)	Nanowire arrays Atomic ratio of Cu:Ag 1:1 3:1 1:3	[44]
5.	Cu film	Electrochemical anodization, annealing and immersing Cu_2O in aqueous $HAuCl_4$ solutions with different concentrations of 0.2 mM and 10 mM	Nanowire	[117]

Table 2.4 *Summary of the ECO_2R to ethanol on bimetal/bimetal oxide electro-catalysts in aqueous electrolyte solutions*

Sr. No.	Catalyst	Preparation techniques	Morphology	Active site	Type of cell	Electrolyte (CO_2 saturated)	Potential V (vs. RHE)	$j^{\#}$ ($mA \cdot cm^{-2}$)	$FE_{ethanol}$ (%)	Stability (h)	Other C_{2+} products	Ref.
1	Cu_3Au	Electro-deposition	Nanowire arrays	NA	H-cell	0.1 M $KHCO_3$	-0.7	1	48.00	NA	NA	[44]
2	CuO/TiO_2 (40 wt. % CuO)	Mild hydrothermal synthesis	Nano-floc	TiO_2	H-cell	0.5 M $KHCO_3$	-0.85	NA	37.00	NA	$(CH_3)_2CO$, C_3H_7OH	[32]
3	$Ag\text{-}Cu_2O_{PB}$	Electrochemical co-deposition	Phase-blended	Ag-Cu biphasic boundaries	H-cell	0.2 M KCl	-1.2	3	34.15	3	C_2H_4, C_2H_6	[111]
4	OD-$Ag_{15}Cu_{85}$ foam	Electro-deposition and mild thermal annealing	Dendrites	Metallic Ag and Cu	H-cell	0.5 M $KHCO_3$	-1.0	8.67	33.70	100	C_2H_6, C_2H_4, C_3H_7OH	[47]
5	Cu_4Zn	Galvanostatic deposition on Cu disks	NA	NA	Two compartment	0.1 M $KHCO_3$	−1.05	8.2	29.10	5	C_2H_4	[113]
6	40 wt. % Cu/TiO_2	Citrate-protecting method	Three-dimensioned (3D) irregular nanoblock structure	Cu NPs stabilized by TiO_2	Two compartment cell	0.2 M KI	-1.45	8.66	27.40	25	C_3H_7OH	[33]
7	Nanoporous copper−silver alloys	Additive-controlled electrode position	Wire	CuAg wire	Flow cell	1 M KOH	−0.7	300	25.00	NA	C_2H_4	[112]

8	Au-nanoparticles-covered Cu_2O	Electrochemical anodization, annealing, and immersion In aqueous $HAuCl_4$	Intertwined nanowires	Presence of Au enhanced *CO-coverage on Cu	H-cell	0.1 M $KHCO_3$	-1.05	42	23.00	NA	C_2H_4, CH_3COOH, CH_3CHO, C_3H_7OH	[117]
9	CuO/ZnO (3:7)	NA	NA	NA	H-cell	0.1 M KH_2PO_4	-1.32 (vs. Ag/AgCl)	0.5	17.30	NA	C_2H_4, C_3H_8	[114]
10	Cu/ZnO(1010)	Vacuum deposition	NA	Cu-Zn interfaces	2-compartment (fritted) glass cell	0.1 M $KHCO_3$	−1.4 (vs. Ag/AgCl)	12	10.20	NA	C_2H_4	[116]
11	Oxidized Cu-Ni intermetallic alloys	Reduction of copper (ii) acetylacetonate and Ni(II) chloride	NPs	Mixture of Cu (Cu^0) and Cu-O (Cu^+) species	Single compartment	0.05 M $KHCO_3$	-1.2	3	9.00	5	C_2H_4	[49]
12	Cu_2O:Al-140	Solvothermal	NA	Stabilizing effect of Al on Cu^+ species	NA	0.1 M $KHCO_3$	−0.8	NA	2.00	12	C_2H_4	[45]

NA- data not available, $\mathbf{j}^{\#}$ - total current density at applied-potential mentioned in column 8

2.1.2.1.3. Organometallic complex

Organometallic complexes are one of the most popular classes of materials in the field of electrochemical CO_2 reduction. These metal complexes stabilize radical intermediates thus providing an effective pathway to facilitate C–C coupling. There are many reported examples having varied molecular structures and ligands extensively used by many scientists in this field [58, 64, 65, 118, 119]. For example, cobalt(III) triphenylphosphine corrole (Co-corrole) complex was demonstrated by Gonglach et al. [58]. This Co-corrole complex contains three polyethylene glycol residues attached at the meso-phenyl groups. In the synthesis of Co-corrole, cobalt(II)acetate tetra hydrate was used as Co-precursor and was mixed with H_3TpFPC(-S-PEG(7)-OMe)$_3$ and triphenylphosphine. This reaction mixture further heated to reflux for 1 h. During ECO_2R, the cobalt(III) converted to cobalt(I) by removal of the axial ligand, thus resulting in a square-planar cobalt(I) complex. Corrole modified carbon paper electrode showed a FE of 48 % towards ethanol production in moderately acidic aqueous medium (pH = 6.0). Li et al. [120] reported a strategy for functionalizing the copper surface with a family of porphyrin-based metallic complexes that catalyze CO_2 to CO. The high concentration of local CO concentration creates CO-rich environment at the molecule–metal interface increasing the coverage of *CO on Cu surface, which further enhances carbon–carbon coupling and steers the reaction pathway towards ethanol. Authors reported a CO_2-to-ethanol FE of 41% and 124 mA cm^{-2} partial current density at −0.82 V (vs. RHE). The Summary of the ECO_2R to ethanol on organometallic complex electro-catalysts in aqueous electrolyte solutions is given in **Table 2.5**.

Table 2.5 *Summary of the ECO_2R to ethanol on organometallic complex electro-catalysts in aqueous electrolyte solutions*

Sr. No.	Catalyst	Preparation techniques	Complex structure/ morphology	Active site	Type of cell	Electrolyte (CO_2 saturated)	Potential, V (vs. RHE)	j# ($mA \cdot cm^{-2}$)	$FE_{ethanol}$ (%)	Stability (h)	Other C_{2+} products	Ref.
1	$Ni^{II}L^{NH2}$	Reaction	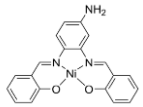	$–NH_2$ group	H-cell	0.5 M $KHCO_3$	-1.60 (vs. Ag/AgCl)	6	52.50	NA	NA	[64]
2	Co-corrole catalyst.	Chemical reaction	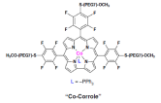	Co(III) site	H-cell	0.1M $NaClO_4$	-0.8	2.5	48.00	65	CH_3COOH, $(CHO)_2$	[58]
3	Cu-Cu_2O-1,3,5-H_3BTC/Cu	Electro-deposition	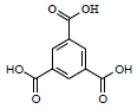 Dendritic 3D structure	Cu^I/Cu^0	H-cell	0.1 M KCl	-0.4	11.5	39.2	5	CH_3COOH	[121]
4	[PYD]@Cu-Pd	Reduction of $PdCl_2$ and $CuCl_2$ mixture by zinc powder in a PYD aqueous solution.	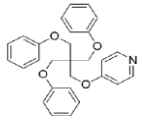 Metallic nanocrystallites, macroporous solid	PYD and Cu	Two compartment cell	0.5 M KCl	-0.64	5	12.00	14	NA	[119]

5	Polymer/ metal complex-immobilized Pt mesh	NA	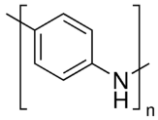	NA	NA	0.5 M KCl	0.8 (vs. Ag/AgCl)	NA	11.10	3	CH_3COOH	[122]
6	Cu-C_3N_4	Mixing $CuCl_2$ aqueous solutions with dicyandiamide (DCDA) in room temperature.	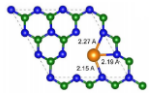	NA	H-cell	0.1 M $KHCO_3$	-1.6 (vs. Ag/AgCl)	8	5.00	NA	C_2H_4, C_2H_6	[123]

NA- data not available, $\mathbf{j}^{\#}$ - total current density at applied potential mentioned in column 8

2.1.2.1.4. Heteroatom-doped transition metals

During CO_2 electro-reduction, the oxidation state of Cu electrodes has been shown to have a major impact on product selectivity. It has been shown that the interface between Cu^+ species and their neighboring metallic Cu sites are beneficial for C-C coupling, allowing ethanol formation more easily [63]. However, due to the decomposition of CuO/Cu_2O to metallic Cu during CO_2 reduction, the catalytic activity of CuO/Cu_2O for ethanol formation rapidly decreases [35]. Introducing modifier elements has been proposed as a viable method for increasing Cu^+ stability in a long-term manner. During ECO_2R, this would help in better understanding of CO_2 reduction to C_2 as well as its realistic application. Therefore, Cu electro-catalysts have been prepared with other dopants than oxygen in recent research, such as boron [62], chloride [110], fluorine [63] etc. as summarized in **Table 2.6**.

Recently, Cu-CuI composite catalyst has been reported by Li et al. [124] which has abundant Cu/Cu^+ interfaces. This Cu-CuI composite was prepared by mixing CuI powders and Cu NPs. When compared with CuI or Cu alone, the composite catalyst exhibited greater overall CD and high ethanol selectivity. Many other researchers reported boron doped Cu for ethanol production [50, 62, 125, 126]. For example, Zhou et al. [62] reported boron to adjust the $Cu^{\delta+}$ to Cu^0 active sites ratio in ECO_2R for improving the stability and C2-product selectivity. Authors reported one-step process of chemical reduction of copper(II) chloride ($CuCl_2$) using sodium borohydride ($NaBH_4$) for the synthesis of boron-doped copper (B-Cu). In the year 2019, another interesting study on chloride (Cl)-induced bi-phasic cuprous oxide (Cu_2O_{Cl}) and metallic copper (Cu) electrode was published by Lee et al. [110]. The bi-phasic cuprous oxide (Cu_2O_{Cl}) was prepared by electro-deposition method and in-situ formed Cl-induced bi-phasic Cu_2O–Cu (Cu_2O_{Cl}) by applying cathodic potential in the Cl-containing CO_2 electrolytic system. Ma et al. [63] also reported fluorine-modified copper catalyst for the ECO_2R to ethanol and ethylene in a flow cell reactor configuration using a gas diffusion electrode. It was reported that the fluorine-modified copper catalyst is highly selective for C_{2+} product generation as shown in **Table 2.7**.

Table 2.6 *Synthesis strategy of different heteroatom doped transition metals*

Sr. No.	Catalyst	Materials		Processing conditions	Morphology	Ref.
		Metallic precursor	**Dopant source**			
1.	Cu-CuI	Commercial Cu NPs	Commercial CuI powders	Physical mixing at molar ratio =1 followed by electrochemical pretreatment in 1 M KOH electrolyte	Cubic morphology	[124]
2.	B-doped Cu	Copper(II) chloride	Sodium borohydride	Chemical reduction of copper(II) chloride in frozen water (~0 °C) at different copper(II) chloride amounts i.e. i. 400 mg (Cu(B)-1) ii. 300 mg (Cu(B)-2) iii. 200 mg (Cu(B)-3) iv. 100 mg (Cu(B)-4) v. 25 mg (Cu(B)-5)	Porous dendritic morphology **B/Cu (%)** 1.3 1.7 1.9 2.0 2.2	[62]
3.	B-Cu-Zn	Copper(II) chloride, Zinc sulphate	Sodium borohydride	Physical mixing of B-Cu nanoparticles and Zn nanosheets on a carbon paper with different Zn loading i. 0.01 mg cm^{-2} ii. 0.025 mg cm^{-2} iii. 0.05 mg cm^{-2} iv. 0.075 mg cm^{-2}	B-Cu nanoparticle sizes in the 23~31 nm range. The as-synthesized Zn sample exhibits nanosheet morphology.	[50]
4.	Cu_2O_{Cl}	$CuSO_4$	KCl	Electrodeposition for Cu_2O preparation followed by in situ preparation of Cu_2O_{Cl}.	Crystallographic cuboctahedral shape	[110]
5.	MT-Cu	Commercial Cu film	Dimethyl disulfide	Direct casting of dimethyl disulfide solution on pretreated Cu film	Roughened surface on Cu	[118]
6.	F-Cu	$Cu(NO_3)_2 \cdot 3H_2O$	Ammonium halides (NH_4HF_2, NH_4Cl, NH_4Br or NH_4I)	Solvothermal synthesis at 160 °C for 4 h	Copper particles with 102–136 nm size	[63]
7.	Cu	$CuSO_4.5H_2O$	$NaH_2PO_2.H_2O$	Electrodeposition at -1.1 V (vs. Ag/AgCl) for 20 min at 70℃ and pH=8	Nanoflakes	[125]

Table 2.7 *Summary of the ECO_2R to ethanol on heteroatom doped metallic electro-catalysts in aqueous electrolyte solutions*

Sr. No.	Catalyst	Preparation techniques	Morphology	Active site	Type of cell	Electrolyte (CO_2 saturated)	Potential, V (vs. RHE)	$j^{\#}$ ($mA \cdot cm^{-2}$)	$FE_{ethanol}$ (%)	Stability (h)	Other C_{2+} products	Ref.
1.	Cu-CuI composite	Physically mixing Cu nanoparticles and CuI powders	Cubic	Presence of residual Cu^+ and adsorbed iodine species	Flow cell	1 M KOH	-0.87	700	28.00	85	C_3H_7OH, C_2H_4, CH_3COOH	[124]
2.	Boron-doped copper (Cu(B))	One-step process using $CuCl_2$ and $NaBH_4$	Porous dendritic	Boron stabilizes the oxidation state of copper	H-cell	0.1 M KCl	− 1.1	70	27.00	40	C_2H_4, C_3H_7OH	[62]
3.	Cu electrode modified with methanethiol monolayers	Direct casting	NA	Combination of Cu^+ on the Cu surface	NA	0.1 M $NaHCO_3$	-1.8 (vs. Ag/AgCl)	2	14.00	1	C_2H_4	[118]
4.	B-doped Cu-Zn (B-Cu-Zn)	Physical mixing of B-Cu nanoparticles and Zn nanosheets	Nanoparticle morphology with agglomeration	Presence of Cu^+ species under ECO_2R	H-cell	1 M KOH	−0.54	200	24.00	4	C_2H_4, C_2H_6, CH_3COOH, C_3H_7OH	[50]

5.	Chloride-induced bi-phasic Cu_2O-Cu	Electro-deposition method	Irregular shape	Synergistic effect between the Cu_2O structure and Cl adsorption	H-cell	0.1 M K_2CO_3	-1.6	-7	24.00	7	C_2H_4, C_2H_6	[110]
6.	Chlorine-modified copper	Electro reduction of a Cu(OH)Cl precursor, synthesized by a solvothermal method	Cubic	Chlorine enhances CO adsorption by increasing surface $Cu^{\delta+}$ sites.	Flow cell	1 M KOH	-0.8	800	21.00	NA	C_2H_4	[63]
7.	Fluorine-modified copper	Electro-reduction of a Cu(OH)F precursor, synthesized by a solvothermal method	Cubic	Fluorine enhances CO adsorption by increasing surface Cuδ+ sites.	Flow cell	2.5 M KOH	-0.54	800	16.00	40	C_2H_4	[63]
8.	Chemically plated boron-doped Cu	Chemically deposition	Densely packed nanoparticles	B- doped Cu (111)	H-cell	0.1 M $KHCO_3$	-1.08	NA	16.30	NA	C_2H_4, C_3H_7OH	[125]

NA- data not available, $j^{\#}$ - total current density at applied potential mentioned in column 8

2.1.2.1.5. Metal-organic framework electro-catalyst

Metal-organic frameworks (MOFs) are a type of ordered crystalline coordination polymers that are gaining popularity in electro-catalyst design. This is due to its unusual combination of heterogeneous and homogeneous properties such as addition of well-defined and highly active sites into stable framework guarantee enhanced catalytic performance; the superior mass transfer due to highly porous metrics, and the catalytic reaction can be tuned by molecularly defined catalytic environment around the active site. In this section, the MOF-based electro-catalyst design and ECO_2R performance are discussed.

In 2016, Albo et al. [68] reported variety of Cu-based MOFs and mesoporous metal-organic aerogel (MOA) namely HKUST-1, CuDTA, CuAdeAce, and CuZnDTA. All these materials were synthesized by solvent free synthesis method. For example, the preparation of HKUST-1T MOF, homogeneous mixture of copper(II) acetate monohydrate and benzene-1,3,5-tricarboxylic acid was heated to 120 ^oC at 2 $^oC\ h^{-1}$ heating rate for 50 h. Preparation techniques for other MOFs and MOAs have also been mentioned. The electrodes have large surface area and greater availability of the Cu catalytic sites, as well as favorable ECO_2R performance. The HKUST-1 and CuZnDTA show a FE of 10.3 %, and 6.5 %, respectively for ethanol formation at -0.9 V and -1.25 V (vs. RHE) respectively. The ethanol selectivity on HKUST-1 and CuZnDTA is higher than that on other two CuAdeAce MOFs and CuDTA MOA. The lower ethanol FE on CuAdeAce MOFs and CuDTA MOA may be due to steric hindrance from the surrounding ligands, which affects the availability of the pentacoordinate Cu(II) sites for C-C coupling. Besides, HKUST-1 and CuZnDTA- electro-catalysts exhibited significantly stable ECO_2R for 17 and 12 h, respectively at optimum conditions.

Karapinar et al. [127] introduced a simple pyrolytic route to prepare Cu-N-doped carbon (CuN-C) consisting of single Cu atoms with a CuN_4 coordination environment, atomically dispersed in a N-doped conductive carbon matrix. The catalyst was prepared in two steps. First dry-phase mixing of ZIF-8, a Zn based zeolitic imidazolate framework, phenanthroline ligand (N-source), and Cu(II) chloride by low-energy ball milling is done. This mixture was pyrolyzed at 1050 °C under Ar flow resulting in $Cu_{0.5}NC$ electro-catalyst powder, comprising 1.4 wt.% Cu with Cu^+ and Cu^{2+} ions and pyrrolic, porphyrin, pyridinic, and graphitic-like N atoms in carbon. This material reduced CO_2

selectively into ethanol with FE of 55% and CD of 16.2 mA cm^{-2} under optimized conditions (potential: -1.2 V vs. RHE, electrolyte: 0.1 M $CsHCO_3$, and gas-phase recycling set up). During electrolysis, the Cu^{+} and Cu^{2+} sites converted into metallic copper nanoparticles, which are likely to be the catalytically active species.

Sakamotu et al. [67] reported self-assembled cuprous coordination polymer nanoparticle (Cu-SCP) for ECO_2R to ethanol. Cu-SCPs can be synthesized with different types of ligands with different numbers of phenyl groups. The $[Cu_2(\mu\text{-}Br)_2(PPh_3)_2(\mu\text{-}DPB)]n$ (represented by DPB-SCP) shows highest selectivity for ethanol with FE of 35 % at -1.34 V (vs. RHE) with overall CD of -32 mA cm^{-2} in CO_2 saturated 0.5 M $KHCO_3$. DPB ligand with Cu atoms inhibits conversion of Cu(I) oxidation state into Cu metal particles.

The N-doped carbons decorated with Cu nanoparticles (Cu-NC) for ECO_2R was studied by Cheng et al. [128]. The Cu-NC was synthesized using carbonization of a benzimidazole modified MOF at different temperatures ranging from 200-800 ^{o}C. It was reported that electro-catalyst produced at 400 °C (Cu-NC400) exhibited maximum amount of pyrrolic-N and Cu(I)-N active sites which are considered as excellent CO_2 adsorption sites and enhance the C-C coupling reaction rate for higher ethanol and ethylene selectivities. The Cu-NC400 electro-catalyst produces ethanol with FE of 18.4 % and ethylene with FE of 11.2 % at -1.01 V (vs. RHE) along with other C1 products like CO and formate.

The summary of the ECO_2R to ethanol on metal organic framework electro-catalysts in aqueous electrolyte solutions is given in **Table 2.8**.

Table 2.8 *Summary of the ECO_2R to ethanol on metal organic framework electro-catalysts in aqueous electrolyte solutions*

Sr. No.	Catalyst	Preparation techniques	Morphology	Active site	Type of cell	Electrolyte (CO_2 saturated)	Potential, V (vs. RHE)	$j^{\#}$ ($mA \cdot cm^{-2}$)	$FE_{ethanol}$ (%)	Stability (h)	Other C_{2+} products	Ref.
1	CuNC	Carbonization of a ZIF-8/Cu^{2+} mixture	Amorphus	Cu clusters in matrix	H-cell	0.1 M $CsHCO_3$	−1.2	16.2	43	60	-	[127]
2	Cu-SCP	Cu-SCPs with [Cu2(μ-Br)2(PPh3)2(μ-DPB)]n ligands	Nanorods	Presence of Cu(I) and suitable ligands surrounding the Cu atoms	Flow cell	0.5 M $KHCO_3$	-1.34	32	35.00	10	C_2H_4, C_3H_7OH	[67]
3	MOFs-derived copper@nitrogen-doped carbon (Cu-NC)	Calcination of N-containing benzimidazole modified Cu-BTC	Cuboctahedral profiles with diameters of 400-600 nm.	pyrrolic-N and Cu-N species	H-cell	0.1 M $KHCO_3$	-1.01	6.5	18.4	8	C_2H_4	[128]
4	H_Zn8	NA	Heaped sub-micrometric crystals.	NA	Micro flow Cell	0.5 M $KHCO_3$	-1.79 (vs. Ag/AgCl)	NA	12.85	NA	NA	[129]
5	HKUST-1	Solvent free synthesis	Porous	N-donor ligands	Micro flow Cell	0.5m $KHCO_3$	-0.9 (vs. Ag/AgCl)	10	10.30	17	NA	[68]

NA- data not available, $j^{\#}$ - total current density at applied potential mentioned in column 8

Table 2.9 *Summary of the ECO_2R to ethanol on supported electro-catalysts in aqueous electrolyte solutions*

Sr. No.	**Catalyst**	**Preparation techniques**	**Morphology**	**Active site**	**Type of cell**	**Electrolyte (CO_2 saturated)**	**Potential, V (vs. RHE)**	**$j^{\#}$ ($mA \cdot cm^{-2}$)**	**$FE_{ethanol}$ (%)**	**Stability (h)**	**Other C_{2+} products**	**Ref.**
1	Carbon-supported copper (Cu)	Amalgamated Cu–Li method	Atomically dispersed copper	A transformation from atomically dispersed $Cu^{+}2$ to metallic Cu3 or Cu4 under a reducing potential	Single compartment	0.1 M $KHCO_3$	−0.7	1	91.00	16	NA	[69]
2	Ag-G-NCF	Direct carbonization of melamine foam loaded with graphene oxide and silver salt	3D interconnected network macroporous structure	Pyridinic N species and Ag	Double electrolytic cell	0.1 m $KHCO_3$	-0.6	NA	85.20	10	CH_3COOH,	[130]
3	Cu/NPC-800	Pyrolysis or organic salt and Cu deposition	Hierarchical porous structure with different open pores in multidirectional channels	Pyridinic N and Cu sites	H-cell	0.2 M $KHCO_3$	-1.05	12.5	64.60	10	C_2H_4, C_3H_7OH	[77]

4	GO-VB_6-Cu	Chemical reduction of $Cu(NO_3)_2$ by $N_2H_4•H_2O$	Transparent paper-like structure	Pyridinic N and metallic Cu	H-cell	0.1M $KHCO_3$	−0.250	4.7	56.30	24	NA	[70]
5	OD Cu/C-1000	Carbonization of Cu-based MOF (HKUST-1).	Octahedral with a uniform size of ∼10 μm	Highly dispersed copper and the matrix of porous carbon	Two-bath cell	0.1 M $KHCO_3$	-0.5	0.75	34.80	15	NA	[131]
6	Pt/NCNFs/Cu-foil	Carbonization	Three-dimensional nanofiber web	NA	Divided glass cell	0.1 M $KHCO_3$	-1.0	NA	31.00	50	NA	[132]
7	Graphene (GN)/Cu_2O	Modified Hummers methods	Cubic	NA	Two compartment	0.5 M $NaHCO_3$	−0.9 (vs. Ag/AgCl)	0.5257	9.93	0.333	NA	[133]
8	1-CuCNT-ImR	Conventional impregnation route	Nanowire	NA	Compact cell, (Plexiglas)	NA	NA	NA	10.40	4	NA	[134]

NA- data not available, $j^{\#}$ - total current density at applied potential mentioned in column 8

2.1.2.1.6. Supported catalyst

The "support" material suitable for ECO_2R must be conductive enough to keep the flow of electrons from anode to cathode without Ohmic losses. The incorporation of metals on the carbon supports not only decreases the quantity of metal content, but it also helps stabilize NPs against uncontrolled NP aggregation during the reaction process and provides more active sites. Moreover, dopants in carbon supports (like pyridinic N) provides a CO-producing site and copper may assist in C–C coupling between *C1 or *C2 intermediates and *CO. Thus, pyridinic N contents facilitated CO_2 adsorption and produced CO which transferred to adjacent Cu active sites [77]. Also, appropriate size of Cu NPs with an improved electronic structure, which helps in the generation of *C1 or *C2 intermediates, further reacted with CO. Graphitic carbon, Vulcan carbon, carbon nanotubes and the graphene sheets are few examples which can be used for better charge transfer. However, the reactivity and product selectivity can be controlled by the morphology, structure, pore size and BET surface area of the carbon material used.

Han et al. [77] demonstrated Cu NPs supported on N-doped porous carbon (Cu/NPC) for ECO_2R. The N-doped porous carbons were synthesized using direct carbonization of sodium citrate followed by heat treatment of in-situ polymerized pyrrole and the Cu/NPC were synthesized by reduction of $Cu(NO_3)_2.xH_2O$ in NPS suspended solution. Different pyridinic N contents were obtained at different temperature. The pyridinic N content in the N-doped porous carbon materials had a substantial impact on the selective formation of multi-carbon alcohols on Cu/NPC hybrid catalysts.

Another study on CoO-anchored N-doped carbon catalyst (MC-CNT/Co) was reported by Du et al. [52]. The MC-CNT/Co was prepared using silica template method which consisted of mesoporous carbon, carbon nanotube, and oxide derived cobalt. The excellent selectivity for ethanol was obtained with 60.1% FE and current density reached to 5.1 mA cm^{-2} at −0.32 V (vs. RHE). Xu and researchers [69] studied the effect of atomically dispersed Cu on carbon support. Authors reported amalgamated Cu–Li method for the synthesis of carbon-supported copper materials. During the synthesis, the bulk Cu was first added in molten lithium until complete dissolution under sonication. Later Li is converted to LiOH under humidified air for the formation of Cu–LiOH mixture. Cu–LiOH mixture is mixed with a carbon support (XC-

72), and lastly, LiOH is removed by leaching with water. Formed Cu-C electro-catalyst showed excellent performance in ECO_2R.

Yuan et al. [75] prepared Cu/TiO_2 NPs modified N-doped graphene ($Cu/TiO_2/NG$) catalyst for converting CO_2 into different alcohols by ECO_2R. The $Cu/TiO_2/NG$ nanocomposite was prepared by reduction of $Cu(NO_3)_2{\cdot}3H_2O$ salt with hydrazine hydrate. During the synthesis, they used sodium citrate to stabilize Cu^{2+}. The characterization results showed the metallic state of Cu and higher pyridinic N content in $Cu/TiO_2/NG$. When used in ECO_2R, it shows outstanding selectivity to produce ethanol with FE up to 43.6% at −0.75 V (vs. RHE). The summary of the ECO_2R to ethanol on supported electro-catalysts in aqueous electrolyte solutions is given in **Table 2.9**.

2.1.2.1.7. Non-copper metallic electro-catalysts

Cu-based electro-catalysts are currently the most promising materials for ECO_2R to ethanol production. However, they face significant obstacles in terms of long term stability, selectivity, high over-potentials, and reusability. Therefore, some non-Cu based electro-catalysts have been recently introduced to have good multi-carbon product selectivity at low over-potentials. This opens up a new direction to study novel non-Cu electro-catalysts. In this section, the non-Cu electrodes for ECO_2R to ethanol formation in aqueous electrolytes are discussed with a particular focus on synthesis strategy and the C–C bond forming mechanisms. **Table 2.10** shows the summary of the ECO_2R to ethanol on non-copper electro-catalysts in aqueous electrolyte solutions.

Recently, Sun and group [135] reported excellent copper free electro-catalyst for efficient ECO_2R to various chemicals and fuels. Authors prepared FeP nanoarray on titanium mesh (FeP NA/TM) by reduction of Fe salt ($FeCl_3.6H_2O$) by Na_2SO_4 in autoclave followed by mild heat treatment with NaH_2PO_2 environment. In their another work [136], the $Fe_2P_2S_6$ nanosheets were prepared by heating the mixture of elements (Fe, P and S with 99.99% purity) in the required stoichiometric ratio in evacuated (~ 10^{-4} Pa) quartz tube at 700 °C. Both the electro-catalysts are capable of achieving ethanol selectivity as discussed in section 3.1.

2.1.2.2. Non-metallic electro-catalysts

Carbon-based metal-free electro-catalysts consist of B and N co-doped nanodiamond [71], Nitrogen-doped mesoporous carbon [51], pyridoxine functionalized graphene oxide (GO-VB6-4) [137], N-doped graphene quantum dots (NGQDs) [72] and boron-doped diamond (BDD)

[138], are reported for ECO_2R to ethanol. In the year 2017, Liu et al. [71] worked on B and N codoped nanodiamond (BND) for selective ethanol formation in ECO_2R. The authors used hot filament chemical vapor deposition method for the preparation of BND electrodes using Si substrate under flowing $CH_4/B_2H_6/N_2/H_2$ gas mixture. Song et al. [51] reported soft-template method via the self-assembly of resol (the carbon precursor), dicyandiamide, and F127 (the soft template) to synthesize N-doped ordered cylindrical mesoporous carbon (c-NC) for CO_2 electro-reduction. Yuan et al. [137] explored N-doped graphene oxide (GO) catalysts with different N-precursors like 4-aminopyridine, 8-hydroxyquionline, pyridoxine, 5-amino-1,10-phenanthroline, and 4-hydroxypyridine for ECO_2R to ethanol. Among the different N-sources, the pyridoxine modified on GO sheets shows the maximum catalytic performance for ECO_2R. Pyridoxine modified on GO sheets exhibited 2.32% pyridinic N content of (GO-VB6). The summary of the ECO_2R to ethanol on non-metallic electro-catalysts in aqueous electrolyte solutions is given in **Table 2.11**.

Table 2.10 *Summary of the ECO_2R to ethanol on non-copper electro-catalysts in aqueous electrolyte solutions*

Sr. No.	**Catalyst**	**Preparation techniques**	**Morphology**	**Active site**	**Type of cell**	**Electrolyte (CO_2 saturated)**	**Potential, V (vs. RHE)**	**$j^{\#}$ ($mA \cdot cm^{-2}$)**	**$FE_{ethanol}$ (%)**	**Stability (h)**	**Other C_{2+} products**	**Ref.**
1.	FeP nanoarray on Ti mesh	FeP NA/TM was derived from Fe_2O_3 NA/TM via well-established topotactic conversion process	Nanoarray	Fe atoms	H-cell	0.5 M $KHCO_3$	−0.20	1.5	14.10	39	NA	[135]
2.	$Fe_2P_2S_6$	Annealing and liquid exfoliation	Nanosheet	Fe atom	H-cell	0.5 M $KHCO_3$	−0.20	0.1	23.10	30	NA	[136]

NA- data not available, $j^{\#}$ - total current density at applied potential mentioned in column 8

Table 2.11 *Summary of the ECO_2R to ethanol on non-metallic electro-catalyst in aqueous electrolyte solutions*

Sr. No.	Catalyst	Preparation techniques	Morphology	Active site	Type of cell	Electrolyte (CO_2 saturated)	Potential, V (vs. RHE)	$j^{\#}$ ($mA \cdot cm^{-2}$)	$FE_{ethanol}$ (%)	Stability (h)	Other C_{2+} products	Ref.
1	B and N codoped nanodiamond	Hot filament chemical vapor deposition method	Pyramidal nanoparticles	B and N codoping	H-cell	0.1 M $NaHCO_3$	-1.0	1	93.20	48	NA	[71]
2	N-doped mesoporous carbon	Soft-template method via the self-assembly of resol	Ordered cylindrical mesoporous carbon	The nitrogen heteroatoms and the cylindrical channel configurations	Two-compartment electrolysis cell	0.1 M $KHCO_3$	-0.56	0.20	77.00	24	NA	[51]
3	Pyridoxine functionalized graphene oxide (GO-VB_6-4)	Graphting of pyridine derivatives on GO sheets	Sheets like and transparent	Pyridinic N	Two compartment cell	0.1 M $KHCO_3$	-0.40	0.8	36.40	NA	$(CH_3)_2CO$	[137]
4	N-doped graphene quantum dots (NGQDs)	Autoclave at 200 C for 10 h	Hexagonal	Pyridinic N	NA	1 M KOH	-0.78	24	16.00	NA	NA	[72]

NA- data not available, $j^{\#}$ - total current density at applied potential mentioned in column 8

2.2. Factors influencing the ECO_2R performance

The product selectivity in ECO_2R can be decided by a number of variables, including composition of electro-catalyst, electrode potential, type of electrolyte, its pH, reactant concentration, and reactor configuration. If all other operating conditions are same, the composition of electro-catalyst, structure, and morphology control the product selectivity in ECO_2R. As a result, many researchers reported variety of electrode materials for ECO_2R that are sufficiently active to transform CO_2 to ethanol at high production rates. Moreover, the pH of the electrolyte solution is also important parameter to consider during ECO_2R, especially when reducing CO_2 in an aqueous medium, since pH affects CO_2 solubility and HER. In this section, some key parameters are highlighted that affect ECO_2R performance for selective production of ethanol.

2.2.1. Composition of catalyst

Many studies have shown that *CO is a key intermediate in ethanol production by ECO_2R. The sufficient binding strength between *CO and electrode surface and/or availability of high concentration of CO near electrode surface is required for initial coupling of vicinal *CO intermediates. Therefore, binding strength and surface coverage of *CO intermediates on Cu-based catalysts can be improved by introducing cocatalyst (such as, Zn, Au, or Ag). In such Cu bimetallic systems, the CO is generated on Zn, Au, or Ag and transported to neighboring Cu active sites on the surface that are active for the *CO dimerization. The short diffusion path is required from Ag, Zn, or Au to Cu in the catalytic systems for this 'CO spillover' effect. In **Table 2.4**, different bimetallic electro-catalytic systems are reported in terms of the active sites and ECO_2R performance.

Few reports are available on Ag-Cu bimetallic catalysts for selective ethanol formation from ECO_2R [47, 111, 112]. The phase-separated Ag-Cu_2O electro-catalyst produces ethanol with a 34% FE at −1.2 V (vs. RHE) in KCl electrolyte [111]. However, using Cu_2O-Cu as electro-catalyst (without the Ag) shows higher selectivity for H_2 with FE of 48.5 % and the main C2 product was observed to be ethylene along with ethanol (9.7% FE). No clear reason for the obtained selectivity was given. The oxide derived bimetallic Ag-Cu metal foams (OD-$Ag_{15}Cu_{85}$) produce ethanol with 33.7% FE at -1.0 V (vs. RHE) [47]. It shows long term stability of 100 h with stable CD response of 26 mA cm^{-2}. Higher stability and selectivity for ethanol production on OD-$Ag_{15}Cu_{85}$ is attributed to the high dispersion of nanosized metallic Ag

(responsible for selective CO production) and Cu (responsible for C-C coupling) in the bimetallic catalyst. In an another report, the CuAg alloy with 6% Ag exhibited 25% C_2H_5OH selectivity at −0.7 V (vs. RHE) with total CD of 300 mA cm^{-2} [112]. Such high activity and selectivity is due to higher local CO intermediate availability on CuAg surface.

Ethanol was produced with 15 % FE using Cu_2O derived Cu and 22 % FE using Cu_2O derived CuAu electro-catalysts at -1.05 V (vs. RHE) along with other C_{2+} products ethylene, and n-propanol [117]. Also, the suppression of hydrogen evolution at lower over-potential from -0.60 V to -0.80 V (vs. RHE) indicate that the presence of Au in bimetallic CuAu helps in reducing the relative *H-coverage in this potential range, which further indicates that higher active sites are available for *CO coupling for ethanol formation.

Many interesting studies are available on CuZn bimetallic electro-catalyst for ethanol production [113-116]. For example, oxide-derived Cu_4Zn catalysts reported by Ren et al. [113] shows maximum 29.1% FE for ethanol at -1.05 V (vs. RHE) with CD of 8.2 mA cm^{-2}. It was suggested that the CO produced by the Zn active sites could have reacted with the Cu surface to produce ethanol.

Other than Cu based electro-catalysts, few non-Cu metallic electro-catalysts like FeP nanoarray on titanium mesh [135], $Fe_2P_2S_6$ nanosh [136], etc. are also reported for ethanol production by CO_2 electrochemical reduction in 0.5 M $KHCO_3$ solution. $Fe_2P_2S_6$ nanosheets produced ethanol with 23 % FE and FeP nanoarray produced ethanol with 14 % FE at applied potential of −0.20 V (vs. RHE). Fe atoms on the $Fe_2P_2S_6$ surface are active for alcohol production. DFT calculations suggest that the dimerization of two *CO species are responsible for the C–C coupling in $Fe_2P_2S_6$ [136] and FeP(211) [135] catalysts. However, the potential-determining step for $Fe_2P_2S_6$ and FeP(211) are *CO/ 2(*CO) (ΔG=0.35 eV) and *CO to *CO–*COH (ΔG=1.33 eV), respectively. This reveals that ethanol formation on FeP is more difficult than on $Fe_2P_2S_6$.

Reports are also available on doping different heteroatoms in Cu for efficient ECO_2R to ethanol production. As previously stated, the oxidation state of Cu catalyst plays significant role in multi-carbon product selectivity during ECO_2R. At low over-potentials, metallic Cu produces CO and HCOOH as the major products, and CH_4 or C_2H_4 at higher over-potentials [139]. However, CuO and Cu_2O are commonly reported to produce ethanol with high efficiency [50, 62, 110, 124]. The reports also reveal that the interface between oxide Cu species and adjacent

metallic Cu sites is responsible for higher production of C_{2+} products by improved C-C coupling [63]. $Cu^{\delta+}$ sites in copper electro-catalysts have been considered as active sites for ethanol production via ECO_2R; indeed, incorporating $Cu^{\delta+}$ into copper catalysts has resulted in producing ethanol with higher selectivity. $Cu^{\delta+}$ has been introduced in copper based catalysts using oxygen-containing species. However, during ECO_2R, high applied reducing potentials needed to generate C_2 products, the resulting $Cu^{\delta+}$ species initially present on surface of catalyst are subject to being reduced to Cu^0 within the first few hours of the reaction [35]. This has made investigating the function of $Cu^{\delta+}$ difficult, and it is likely that it undergoes phase change during ECO_2R. Introducing modifier elements has been proposed as a viable method for increasing $Cu^{\delta+}$ stability for longer duration. This would lead to increased ethanol selectivity. Many researchers reported Cu materials with other dopants such as boron [62], chloride [110], fluorine [63] etc. as summarized in **Table 2.7**.

B-doped CuO catalyst showed 27 % FE for ethanol, higher than that of boron free CuO (7 %) at -0.45 V (vs. RHE) [50]. Further, the catalyst with a composition of 0.5B-Cu:0.025Zn exhibited increased FE for ethanol (31%) and n-propanol (3%) at −0.45 V (vs. RHE) with total CD of −200 mA cm^{-2}. Further, the FE of C_2H_5OH was decreased at higher Zn loading due to the competing HER and excess CO production by Zn. In-situ Raman measurements showed that the addition of boron and Zn maintains stability of Cu^+ species during ECO_2R resulting increased ethanol selectively and the long-term stability on B-Cu-Zn.

2.2.2. Morphology of catalyst

Morphology of electro-catalyst is also important factor while designing the electrode materials. Till date, many researchers studied effect of different morphologies on ethanol production during ECO_2R. For example, Wang et al. [80] reported highest 35.7% FE at -0.4 V (vs. RHE) in 1 M $KHCO_3$ on nanostructured Cu nanosheets (CuNS) compared to other Cu morphologies like nanowires ($FE_{ethanol}$= 0 %) and nanoflowers ($FE_{ethanol}$= 15 %) under same studied conditions. The superior performance of nanosheet morphology attributed to better stabilization of the intermediate state products than that of other two morphologies.

Three-dimensional spherical structure (~4 µm size) was reported for highest selectivity of ethanol with 36.1% FE at -1.7 V (vs. SCE) [35]. Better performance of 3-dimensional spherical structure (~4 µm size) is attributed to its highest specific surface area of 45.4 m^2 g^{-1}. At the same experimental conditions, the 3 dimensional spherical structure ~2 µm non-uniform size,

2 dimensional structure 200 nm size, nanosheet of 1 μm size and uniform nanorod structure of 150 nm size electro-catalysts produced ethanol with 17.5%, 15 %, 12.5%, and 9.5% FE respectively. All samples showed long term stability of 5 h without appreciable change in CD response under optimized conditions. The nano-porous copper films and the CuDAT-wire shape were reported by Hoang et al. [42]. The CuDAT-wire shape catalyst showed the best CO_2 reduction performance with 20% FE for ethanol at -0.5 V (vs. RHE).

2.2.3. Surface ligands

Functionalizing metal based electro-catalysts with different surface ligands is an effective way to enhance ECO_2R performance. Iijima et al. [118] reported Cu electrode modified with methanethiol monolayers (MT−Cu) for ECO_2R. The roughened surface and the Cu^+ moiety, generated due to methanethiol during ECO_2R, promote C_2 product formation. Bose et al. [64] reported Ni^{II} complex with free amine functional group $[Ni^{II}L^{NH2}]$ for ECO_2R. The complex produced ethanol with 49% FE at −1.60 V (vs. Ag/AgCl). The authors reported that the electron transfer can be improved by anchoring amine functional group to the metal ion Ni(II). Another interesting study on cobalt(III) triphenylphosphine corrole complex was presented by Gonglach et al. [58]. The Co-corrole– carbon paper electrode showed 48 % FE for methanol and ethanol at −0.8 V (vs. RHE) This Co-corrole– carbon paper electrode also exhibited 140 h of operational stability which is highest reported so far.

[PYD]@Cu–Pt [65] and PYD]@Cu-Pd composite [119] were used for CO_2 reduction in 0.5 M KCl solution. Using [PYD]@Cu–Pt electro-catalyst, the FE of ethanol reached to 27% at -1.2 V (vs. SCE). Moreover, the CD value was maintained at a steady value at around 22 mA cm^{-2} for at least 22 h at -0.6 V (vs. SCE). When using [PYD]@Cu-Pd composite, ethanol with 12% FE was obtained at -0.64 V (vs. RHE).

Although remarkable progress was achieved in last few years in the development of organometallic complexes, there are still several issues related to production rates, reusability of electrodes, and achieving high current densities for industrial deployment of the process, that need to be addressed.

2.2.4. Non-metallic electro-catalysts

As mentioned above, metals, metal oxides, or metal complexes such as Cu (100) [84], copper(I) oxide [34], Cu_4Zn [113], and Cu/TiO_2 [33, 140] have been used as electro-catalysts for

electrochemical reduction of CO_2. However, issues related to higher over-potential for C_2 product generation, high cost, and poor selectivity need to be addressed. Therefore, the study of metal-free carbon based electro-catalysts has opened a new door due to their higher surface area, low cost, and superior electrical conductivity between metal and carbon supported materials. Doping of different heteroatoms like nitrogen and boron to carbon materials may additionally improve its electronic properties [72]. For example, N-doped carbons have higher electrical conductivity than carbons because N is more electronegative than carbon. Also, N-doped carbons show suitable binding strength to active intermediates. In view of the above-mentioned benefits, few review papers are also available on metal-free electro-catalysts for ECO_2R [21, 141-143].

Liu et al. [71] introduced B and N codoped nanodiamond (BND) for selective reduction of CO_2 to ethanol. The electrode with highest N content (BND3 with 4.9 atm% N) gives highest FE of 93.2% at -1.0 V (vs. RHE) for ethanol than that of other electrodes i.e. BND1 (3.1 atm% N), and BND2 (3.6 atm% N). The superior performance of BND is attributed to the high N content, synergistic effect of B and N codoping, and high over-potential for HER. Authors also revealed the possible reaction pathway by DFT study as $CO_2 \rightarrow *COOH \rightarrow *CO \rightarrow *COCO \rightarrow *COCH_2OH \rightarrow *CH_2OCH_2OH \rightarrow C_2H_5OH$. The BND3 electrode showed constant 93.2% FE for ethanol production at -1.0 V (vs. RHE) during 16 sequential ECO_2R study with each run lasting for 3 h.

N-doped graphene quantum dots (NGQDs) exhibited 16% FE for ethanol at -0.78 V (vs. RHE) which is higher than that of GQDs (without N doping) [72]. The Tafel slope of GQDs electrode (371 mV dec^{-1}) has a greater value than that of NGQDs electrode (198mV dec^{-1}), indicating superior kinetics for ECO_2R on NGQDs electrode. Among the most common N configurations like pyrolytic, pyridinic and graphitic N, the pyridinic N is the most active site for CO_2 reduction due to its Lewis basicity in carbon nanostructures [144].

2.2.5. Catalyst support

While designing electro-catalyst for ECO_2R, the metal NPs need to be dispersed uniformly to achieve maximum catalysis. This can be achieved by supporting metal NPs on the carbon supports. Carbon supports prevent the uncontrolled NP aggregation during catalyst synthesis and provide more active sites for ECO_2R. It also reduces the amount of metal content. Different carbon supports like carbon nanotubes [52, 145], N-doped graphene [70, 75], porous carbons [77], etc. have been reported in literature. Twenty wt.% Cu nanoparticles supported on N-doped

porous carbon (Cu/NPC-800) [77] exhibited 64.6% and 8.7% FE for C_2H_5OH and C_3H_7OH respectively at −1.05 V (vs. RHE). Authors also reported that the higher pyridinic N contents are responsible for improved CO_2 adsorption and thus produced CO which transferred to neighboring Cu sites for ethanol formation.

The CoO-anchored N-doped carbon material (MC-CNT/Co) produced ethanol with the FE of 60.1% at −0.32 V (vs. RHE) and CD reached to 5.1 mA cm^{-2} [52]. Xu et al. [69] studied carbon-supported copper (Cu) catalyst. When used in CO_2 reduction, the prepared catalyst was capable of producing ethanol with highest FE of 91% at −0.7 V (vs. RHE) and onset potential as low as −0.4 V (vs. RHE). The catalyst showed long term stability and constant FE for ethanol over 16 h at −0.7 V (vs. RHE).

When using Ag-G-NCF as electro-catalyst for CO_2 reduction, the ethanol was obtained with 82.1 to 85.2% FE at -0.6 to -0.7 V (vs. RHE) [130]. The pyridinic N species exhibited the higher bonding strength toward CO* intermediate, and Ag particles gradually converted CO* to OC-COH intermediate of ethanol production.

2.2.6. Applied potential

The product selectivity is greatly affected by the applied potential in ECO_2R. As reported by Chi et al. [35], the total FE increased from 2 % to 36.1 % with increase in cathode potential from -1.4 V to –1.7 V (vs. SCE) and further increase in potential to -2.0 V (vs. SCE), the FE decreased to 3.8 %. (**Fig. 2.1a**). However, the total CD increased with increasing applied potential, the highest CD for ethanol ($j_{ethanol}$) was observed at -1.7 V (vs. SCE). It is common that, at higher negative potentials, the selectivity for CO_2 reduction products decreases and selectivity for H_2 production increases due to the mass transport limitation of CO_2 to the electrode surface, as CO_2 has a poor solubility in aqueous electrolytes (~34 mM at 25 °C). Similar trend was observed by Lee et al. [111] when using Ag-Cu_2O_{PS} and Ag-Cu_2O_{PB} in 0.2 M KCl electrolyte solution. Furthermore, when the overall current increased with applied over-potential, a buildup of OH^- at the electrode surface occurred, resulting rise in pH near electrode surface (**Fig. 2.1b**). This decreased the local CO_2 concentration at the electrode surface which further decreased the FE of targeted products during ECO_2R in H-type cell configuration. Ren et al. [146] presented theoretical study on local pH values and CO_2 concentrations at the Cu surface (using Cu-10 as the model). The local pH increased from 6.8 to 11.5, whereas the local

CO_2 concentration decreased from 34 mM to 6.5 mM as the simulated current increased to 90 mA cm^{-2} [147].

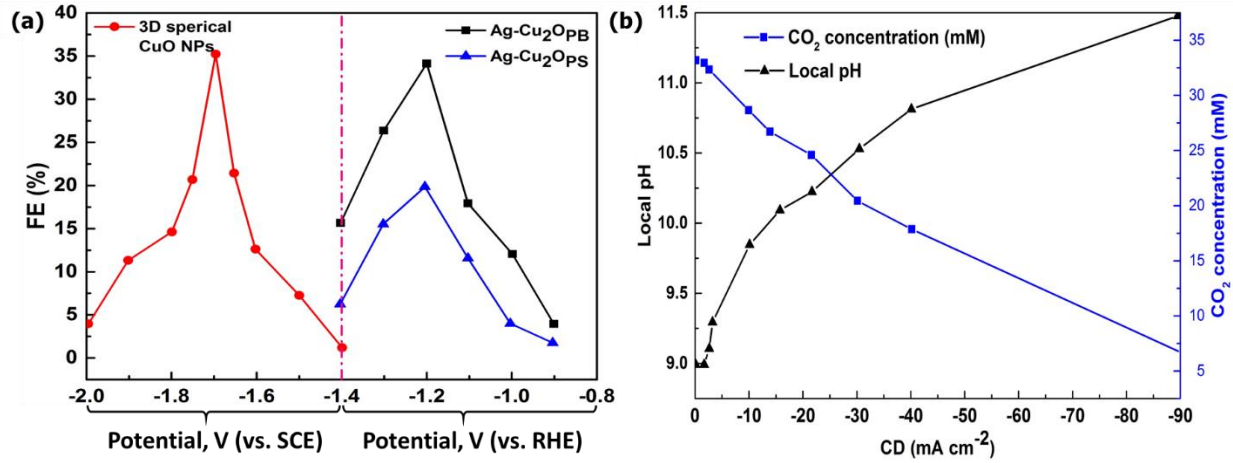

Fig. 2.1 ***(a)*** *The Faradaic efficiency for C_2H_5OH as a function of applied potential using 3 dimensional spherical structure in the ~4 µm size CuO nanoparticles in 0.2 M KI electrolyte solution [35], and using Ag-Cu_2O_{PS}, Ag-Cu_2O_{PB} in 0.2 M KCl electrolyte solution [111];* ***(b)*** *Simulated local pH values and local concentration of CO_2 as a function of CD on Cu-10 catalyst [146]*

2.2.7. Electrolyte

Electrolyte plays a significant role in any electro-catalytic system as it interacts with reactants and intermediate products. As a result, the electrolyte selection has gained lot of attention in ECO_2R. The main purpose of electrolyte is to transmit ionic charge between working and counter electrodes. An electrolyte is made up of three components, i.e. the solvent, an inert electrolyte or salt, and the electroactive species. A good solvent should have a high solubility of CO_2, electrochemically stable, low viscosity, chemically compatible with electro-catalysts and easy to handle, storage, and safe for transportation. Water is the most popular solvent for ECO_2R electrolyte since it has all the above features and can operate as both a proton donor and acceptor, allowing for the formation of a variety of useful products. Different electrolytes, such as aqueous electrolytes, solid oxide electrolytes, organic electrolytes, and ionic liquids have been studied in recent years [22, 148-150]. Although CO_2 solubility in an aqueous medium is low (for example, the concentration of CO_2 in aqueous 0.1 M $KHCO_3$ is 33 mM at 25 °C) [151-153], many scientists prefer to work with aqueous solutions because of their numerous advantages, including cost effectiveness, high ionic conductivity, and environmental friendliness. KOH solutions (> 0.5 M concentration) are commonly used electrolyte in flow cell configurations for excellent activity and selectivity of ECO_2R products. It is attributed to

its stronger electrolyte conductivity, low Ohmic resistance, and low over-potentials for ethanol production [22, 154]. The presence of OH^- ions may reduce the energy barrier for CO dimerization, increasing multi-carbon product compared to H_2 and C_1 products [155]. However, in semi batch reactor configurations, the highly alkaline KOH could not be employed as electrolyte because of chances of bicarbonate formation by reacting CO_2 with KOH solutions [156]. Stationary electrolyte (in H-type cells) increases the local pH near electrode surface reducing ECO_2R performance. In continuous flow cells, the gaseous CO_2 is transferred through the GDE to electro-catalyst and finally to electrolyte, where ECO_2R occurs immediately.

Wang et al. [80] reported the product distribution using different electrolytes and Cu nanosheet electrode. The highest total FE was reported using 1 M $KHCO_3$ solution (86.9%) at −0.4 V (vs. RHE) as compared to other electrolytes such as KH_2PO_4 (1.0%, -0.9 V (vs. RHE)) and KCl (54.7%, -0.5 V (vs. RHE)). Further, effects of electrolyte anions (0.1 M $KClO_4$, KI, KBr and KCl electrolytes) on the ECO_2R to C_{2+} products on Cu single crystal surfaces was studied by Huang et al. [60]. The selectivity of ethanol and ethylene on Cu single crystal surfaces increased as the electrolyte was changed from $ClO_4^- \rightarrow Cl^- \rightarrow Br^- \rightarrow I^-$. For example, on Cu(100) at -1.23 V (vs. RHE), as the electrolyte anion changed from ClO_4^- to I^-, the $FE_{ethanol}$ increased from 7 to 16%. The presence of an electrolyte anion can lead to increased adsorbed *CO intermediate, which facilitates C-C coupling and the generation of multi-carbon products with excellent selectivity. Karapinar et al. [127] studied effect of size of the cation on ECO_2R and reported that the bigger cations act as good buffering agents and thus enhancing local CO_2 concentration. The ECO_2R performance is improved in the order of $Cs^+ > K^+ > Na^+ > Li^+$ with the increasing cation size.

2.2.8. Temperature and pressure

ECO_2R performance greatly affected by temperature and pressure because of CO_2 solubility, conductivity of electrolytes, viscosity, and its effect on mass transfer rates. The stability of electrolyzer components like electrodes, membranes, and the sealing gaskets may also be affected by temperature. Also, increase in pressure can increase the CO_2 concentration in the electrolytic solution but also increases operational complexity and cost of electrolyzer [22], so optimization of the pressure is necessary in designing ECO_2R eletrolyzers. Ahn et al. [151] performed ECO_2R experiments at different temperatures ranging from 2.0 °C to 42.0 °C. While increasing temperature, the dissolved CO_2 concentration in H_2O is decreased (73 mM at 2 °C to 21 mM at 42 °C) and increasing the bulk pH. At lower temperatures, more CO_2 is available

for ECO_2R reaction however at higher temperatures concentration of CO_2 is less, thus HER is more kinetically facile [157], resulting in higher selectivity for H_2. Till now there is no correlation is reported between electrolyzer temperature & pressure and product selectivity of ECO_2R

2.2.9. Membrane

Two types of membranes (anion exchange membrane (AEM) and cation exchange membrane (CEM)) are commonly used in an electrochemical cell. The primary function is to transport the charge between the electrodes and prevent the mixing of ECO_2R products. The effects of using CEM vs. AEM on polarization losses in a 1 M $KHCO_3$ electrolyte were studied by Singh et al. [158] (**Fig. 2.2**). When AEM is used, the polarization loss increases by around 10 mV at 10 mA cm^{-2} compared to when there is no membrane. On the other hand, when CEM is used, the polarization losses increased to infinite with current density. The polarization losses in the presence of a CEM are larger than those in the absence of a membrane or with an AEM. Furthermore, the limiting current density achievable with a CEM is substantially lower than with an AEM. Unfortunately, most of the studies are available using Nafion 117 CEM membrane in both H-type and flow cell electrolyzers.

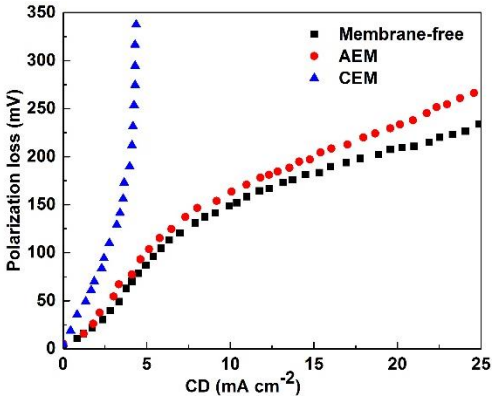

Fig. 2.2 *Comparison of polarization losses in the membrane-free 1 M $KHCO_3$ electrolyte with the electrolyte separated by a cation exchange membrane (CEM) and anion exchange membrane (AEM) [158]*

2.2.10. Metal loading

Electro-catalyst is coated on the GDE as the active component to enhance the production of ethanol and inhibit HER. Despite the fact that the amount of metal utilized is a major factor in the economic consideration, there have only been a few studies reporting impact of metal loading on ECO_2R performance.

In 2017, Yang's group [159] reported ECO_2R performance on different Cu NPs loadings supported on carbon paper. The electrode with the highest loading (x22.5) exhibited the best selectivity towards C_{2+} product. Recently, Xu et al. [69] reported five catalysts with increasing Cu loading (i.e. 0.1, 0.8, 1.6 and 6 wt.%) over carbon support (XC-72). LSV results show that increase of the Cu loading over these catalysts show a rise of ECO_2R current density, since more active metal sites are available for ECO_2R or HER.

In other way, many reports [160-162] are available on optimizing quantity of catalyst material on working electrodes. For this, electrodes containing various quantities of metal ranging from 0 to 10 mg cm^{-2} were prepared and their performance is measured in terms of Faradaic efficiency, specific current density, as well as the long term stability. A rise in electrode activity at increased metal loading was reported due to increased roughness factors at a given over-potential. In addition, as per some reports [160], reduced electrode activity at higher catalyst loading (i.e., beyond 1.5 mg cm^{-2}) is likely due to a particle agglomeration, which includes poor accessibility of the active sites for the reactants.

2.3. Electrochemical cells

Apart from electro-catalysts and electrolytes, designing suitable electrochemical reactor is an successful way to improve ECO_2R efficiency, especially in terms of production rate [163]. Significant development has been made in the design and fabrication of novel electrochemical reactors for ethanol production. A ECO_2R process involves several key steps in any electrolyzer system, such as (1) mass transfer of gas phase CO_2 to the bulk electrolyte, (2) transport of dissolved CO_2 and chemical absorption on the cathode surface, (3) proton migration and/or electron transfer to break C–O bonds and formation of *CO, *COH, *CHO, and *COOH intermediates at the cathode catalyst, (4) rearrangement of these intermediates to form desired product, (5) desorption of product from electrode and transfer into bulk electrolyte. The electrochemical reactors are broadly divided into two types based on their method of operation.

- Batch/semibatch reactors
- Continuous reactors

Batch and semi-batch electrochemical reactors like the H-type cell (**Fig. 2.3a**) are often used in ECO_2R studies. H-type cell consists of a cathode (i.e. working electrode where CO_2 conversion takes place) kept in cathodic compartment; an anode (i.e. counter electrode where water splitting reaction takes place ($2\ H_2O(l) \rightarrow O_2(g) + 4\ H^+(aq) + 4e^-$)) placed in anodic

compartment; an electrolyte for the transfer of dissolved CO_2 to cathode surface for conversion and to transport of ions between anode and cathode compartments; an ion-exchange membrane to separate the anode and cathode compartments; and lastly, an external voltage source to transfer electrons from anode to cathode [60, 158]. Due to its simple construction and low cost, it allows for rapid testing of new electrolytes and electro-catalysts. Treatment of large volumes of CO_2 gases are not possible due to the low CO_2 solubility (0.034 M) in aqueous electrolyte under ambient conditions [152] and slow CO_2 mass transfer rates to the cathode surface (even with the vigorous stirring of catholyte), resulting in low measured current densities up to few mA cm^{-2}. Furthermore, cations (e.g. Na^+, K^+) that move through the membrane accumulate in the cathode compartment, and this accumulation will further decreases the CO_2 solubility and ECO_2R selectivity during longer duration.

To solve these issues, the ECO_2R was performed in continuous flow reactor assembly by many groups [63, 67, 124, 129, 164] for its industrial applications. As shown in **Fig. 2.3b**, continuous flow reactor includes current collectors for both electrodes, chambers for electrolytes, membrane, and GDEs. For the working electrode, a GDE is commonly used, while the counter electrode can be either a catalyst supported on a hydrophilic substrate or GDE. The catholyte and anolyte chambers are separated by an ion-exchange membrane to prevent the mixing of CO_2 reduction products in anolyte. The catalyst side of GDE is facing to the membrane and other side is pressed against the current collector. To reduce the Ohmic drop on the anode side, the working electrode is placed very close to the membrane. During operation, gaseous CO_2 diffuses through the carbon substrate and microporous layer to the coated catalyst, where it comes in contact with the catalyst and liquid electrolyte solution, allowing the ECO_2R reaction to occur. Many flow cell studies are available in the literature on different electrodes such as micro-strain-rich CuO [46], nanosize In_2O_3 [106], grain-boundary-rich metallic copper [31], CuDAT-wire [42], Cu [43, 88, 91], nanoporous copper−silver alloys [112], phase-separated CuPd [165], Cu-CuI composite [124], chlorine-modified copper [63], fluorine-modified copper [63], HKUST-1 [68], N-doped carbon supported Cu [164].

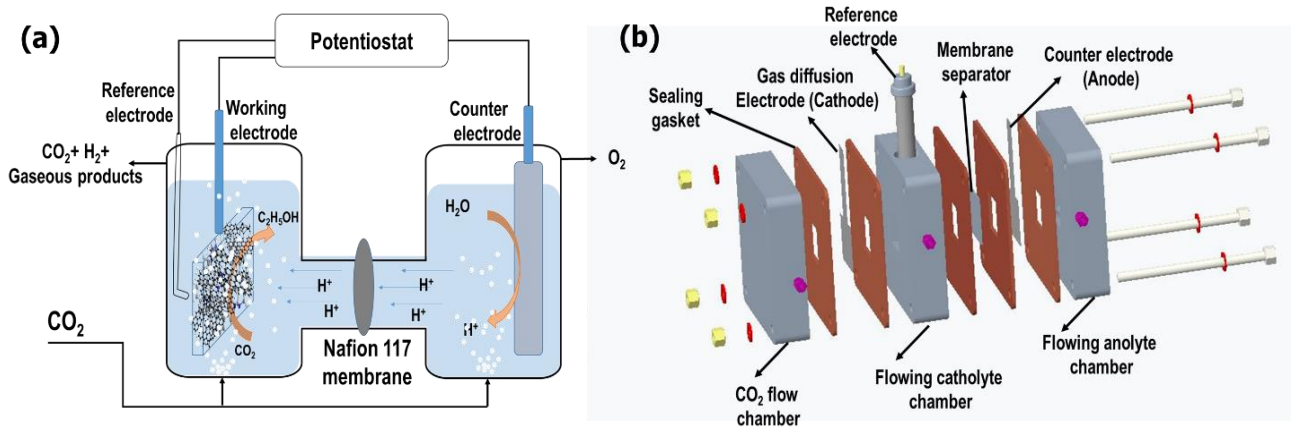

Fig. 2.3 (a) *Schematic illustration of H-type cell;* ***(b)*** *A figure showing the structure and components of flow cell*

2.4. Electrochemical reactions and mechanisms

As discussed in introduction section, the ECO_2R is multi-electron and -proton transfer process and involves different reaction intermediates. As a result, more than 16 different gaseous and liquid products are formed in aqueous solutions [40]. Many researchers reported that the C2 species are generated by reacting two *CO intermediates adsorbed on the catalyst surface. With this approach, the possible reaction pathway for ethanol and ethylene formation is shown in **Fig. 2.4.** The coupling of two *CO intermediates into 2*CO is considered as a rate determining step.

Initially, CO_2 is adsorbed on the surface of electro-catalyst and forms adsorbed CO_2(ad) species. As CO_2 is a stable molecule, it requires a large negative potential to break down the stable structure to form CO_2(ad) species. A portion of the CO_2(ad) species receives an electron and then transforms into the transition state CO_2(ad), a portion of which then interacts with the surrounding H^+, which is formed from H_2O, and is further converted into reaction intermediates (like *COOH and then to *CO) at the catalyst surface and desorbed. *CO is confirmed to be a common intermediate for the production of different valuable products, especially to produce multi-carbon products [167]. For the multi-carbon production, the catalyst surface requires strong binding ability for the CO intermediate during ECO_2R, therefore generated *CO further undergoes C-C coupling via multiple proton-electron (H^+/e^-) transfer from solution to adsorbed species formed on the surface of catalysts [166]. It has been widely reported that, the nanostructured Cu electrode can stabilize both CO_2(ad) and CO* transition states, allowing for further hydrogenation and isomerization to occur [80]. Sufficient surface coverage of reaction

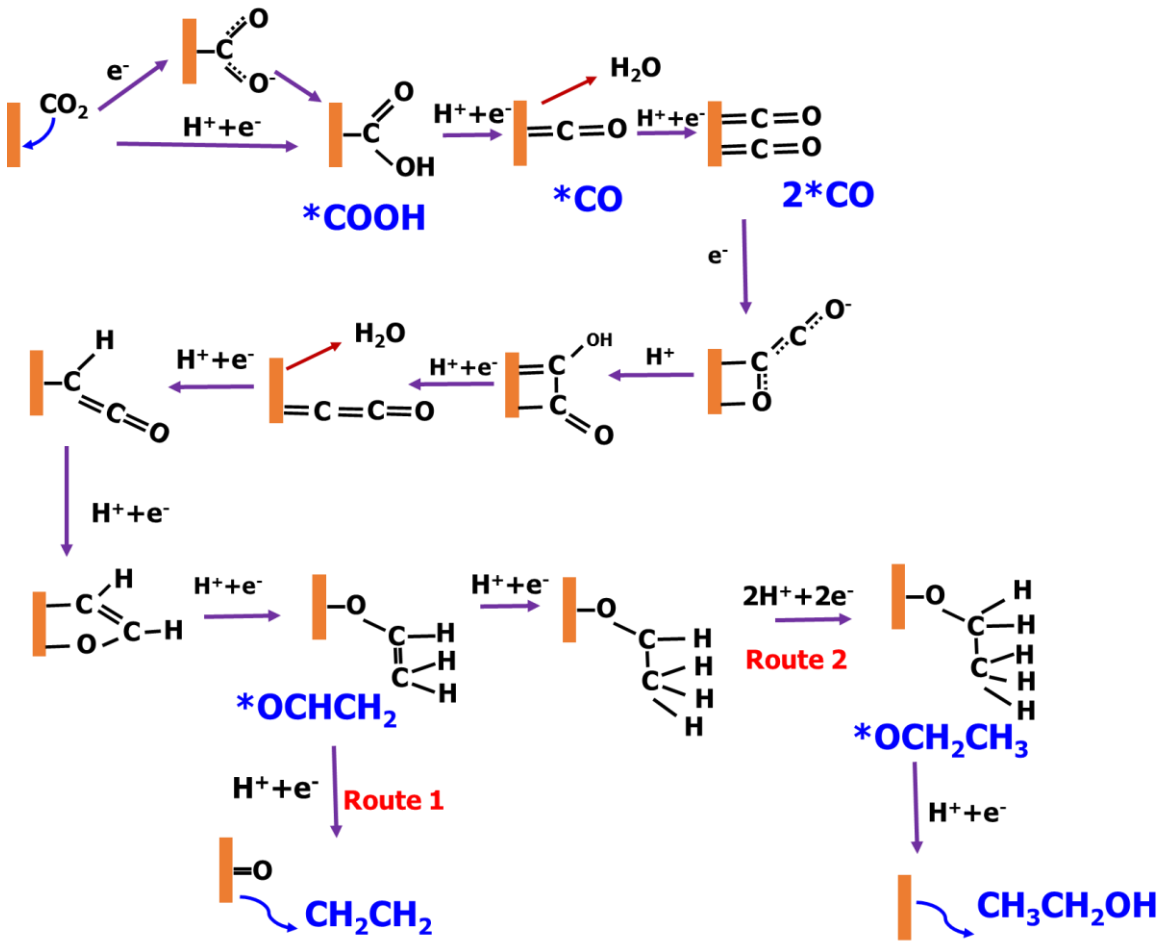

Fig. 2.4 *Possible ECO_2R reaction pathways on Cu metal based on recent work [166]. (Orange bars indicates the catalyst surface and * indicate different adsorptive reaction intermediates)*

intermediates (*CO) and favorable reaction energetics are needed for *CO dimerization to occur. This can only happen if two C-containing adsorbates are close to each other [40]. *CO dimerizes to form $*C_2O_2^-$ (a rate-limiting step), which is then rapidly hydrated to *CO-COH through the Eley-Rideal (ER) mechanism with $H_2O + e^-$ (H_2O_{ad}). The selectivity-determining intermediate i.e. vinyl alcohol ($*CH_2$=CHO) can be generated by further reduction of *CO-COH. The pathway then divided into ethanol-forming and ethylene-forming pathways [98]. The protonation of a carbon in $*CH_2$-CHO produces acetaldehyde, which is then converted to ethanol by an ethoxy ($*CH_3CH_2O$) intermediate [168].

2.5. Present status

Table 2.2 to **Table 2.11** show the brief summary of ECO_2R performance data for alcohol production reported in the literature from 1985 to April 2021. Note that many parameters such as electrode material, supports, cell configuration, electrolyte (composition and pH) and

operating conditions are not consistent but this information is only meant to give a general idea about the developments in ECO_2R. Many electro-catalysts and reactor configurations have been reported revealing a high activity and selectivity, but stability, reproducibility and reusability is a challenge. Presently, most of electro-catalysts are studied in H-type electrochemical reactors exhibiting lower current densities, which limit its use in large scale application. Many research organizations around the world are working on different projects to create a more effective technology and improved manufacturing process for alcohol production using the ECO_2R approach (**Table 2.12**).

For instance, CO_2 electro-reduction to CO with high Faradaic efficiency (FE) and low over-potential has already been demonstrated [165, 169], and a few start-up firms are trying to commercialize this technology [170, 171]. Mantra Energy, Canada, Techwin Co., Ltd. South Korea, Det Norske Veritas, Norway scaled up the electro-catalytic CO_2 reduction process for the production of formate/formic acid and CO. On the other hand, the production of alcohol is still at lab scale due to poor catalyst stability, low selectivity, high over-potential, etc. Therefore, Spurgeon et al. [172] suggested different possible routes for the synthesis of ethanol and other high density liquid fuels through electro-synthesized CO. As shown in the route (i) of **Fig. 2.5a,** the conversion of electro-synthesized syngas mixture (CO and H_2) to liquid fuel i.e. ethanol by Fischer-Tropsch synthesis. The route (ii) suggests direct ECO_2R to ethanol which is more challenging as it involves the adsorption of *CO intermediates to electrode active sites to enable C-C bond formation. Several attempts have been made to design electro-catalysts for direct CO_2 to C_2H_5OH conversion. Marginal Faradaic efficiencies have been achieved at high over-potentials [63, 67, 124, 129, 164]. The route (iii) is also aimed at generating ethanol by ECO_2R, but it employs a two-step cascade system. In the first step, CO_2 is first transformed to CO with high selectivity, and in next step, generated CO is electro-reduced to ethanol with high selectivity at a low over-potential [57]. The two-step ECO_2R to ethanol cascade electrolyzer configuration (CO_2 - CO-C_2H_5OH) divides the complex 12-electron ethanol synthesis into two different reactions where optimum conditions can be used for both individual reactions to increase ethanol selectivity at minimum over-potential. The overall research progress in ECO_2R is shown in **Fig. 2.5b**.

Table 2.12 *List of representative pilot commercial projects on the ECO_2R to useful chemicals*

Project name	Organization	Description	Reference
Opus 12	Opus 12 Inc., Berkeley, California	CO_2 to chemicals	https://www.opus-12.com/
ECO_2RECT	Bayer Technology Services Science	CO_2 to chemicals	http://co2chem.co.uk/carbon-utilisation/ECO_2Rect
PhasKat	Siemens Gas and Power GmbH & Co. KG	CO_2 to chemicals	https://co2-utilization.net/de/projekte/elektro-und-photokatalyse/phaskat/
Carbon2Chem	ThyssenKrupp AG	Converts CO_2 emissions from top gases of the steel production to chemicals	https://www.thyssenkrupp.com/carbon2chem/de/carbon2chem

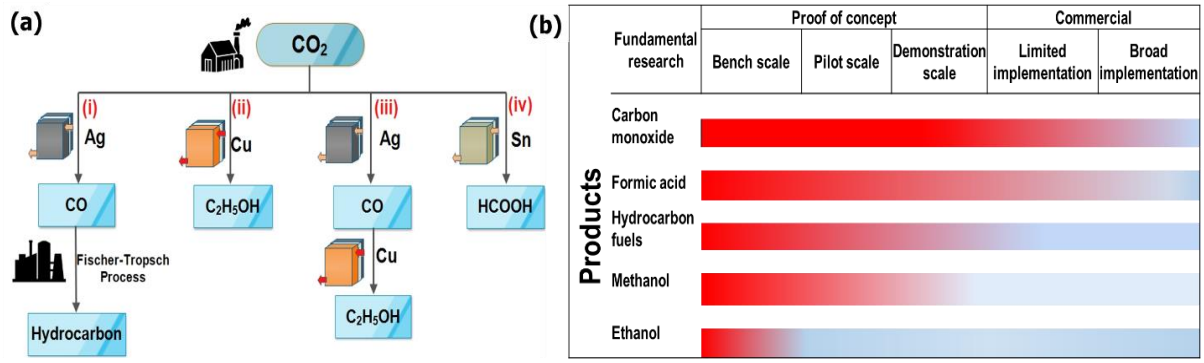

Fig. 2.5 (a) *Schematic of the pathways for ECO_2R to liquid products for technoeconomic analysis [171, 172],* ***(b)*** *Stages of research activity in ECO_2R for target products (The denser red color in the chart indicates sufficient research progress in that stage whereas blue areas correspond to need more progress in that stage, indicating gaps in research activity for different products.) [173]*

2.6. Summary

After surveying the state-of-the-art of electrochemical CO_2 reduction, it is clear that catalyst material and reactor configuration play important role in catalytic systems. Although enormous efforts have been given to develop efficient electro-catalysts to increase the selective production of ethanol at lab scale only, however, the state-of the-art CO_2 reduction catalysts are still not suitable for industrial applications due to issues related to the CO_2 solubility, energy efficiency, complicated reaction kinetics, production rate, and catalytic stability. Another need is to improve the selectivity of the catalysts for such products which can be directly used as fuels (e.g. hydrocarbons and alcohols). In spite of the significant efforts made for enhancing

the Faradaic efficiency, there is scope for further improvement. Further, to overcome the high over-potential issues, designing of new class of electro-catalysts is essential. In this direction, combined effect of two or three metals can be studied, because combination of metals results in some of the unique properties which cannot be obtained with single metals.

Chapter 3 – Experimental: materials, methods, and characterization

3.1. Materials

3.1.1. Chemicals for preparation of electro-catalysts

Cupric chloride dihydrate (99.9%) ($CuCl_2.2H_2O$), Cu foil (99.7%, approx. 0.1 mm thickness), hydrazine hydrate (80%) ($N_2H_4.H_2O$), and trisodium citrate dihydrate (99%) ($C_6H_5Na_3O_7.2H_2O$) were purchased from Loba Chemie Pvt. Ltd, India. Copper(II) nitrate trihydrate ($Cu(NO_3)_2 \cdot 3H_2O$), Zinc nitrate hexahydrate ($Zn(NO_3)_2 \cdot 6H_2O$), and sodium carbonate (Na_2CO_3) were obtained from S. D. Fine Chemicals Ltd. (India). N-doped graphene (purity >99%, thickness 1-5 nm, length 1-5 μm, amine content 10-15 wt.%) was purchased from the Platonic Nanotech Pvt. Ltd., India.

3.1.2. Chemicals for electrochemical CO_2 reduction experiment

Potassium bicarbonate (99.99 %) ($KHCO_3$), Nafion® 117 solution (~5 wt. % in a mixture of water and lower aliphatic alcohols), cation exchange membrane (Nafion-117), sulfuric acid (99.99 %) (H_2SO_4) were procured from Sigma-Aldrich. Porous carbon paper (approx. 0.18 mm thickness and 77 % porosity) was purchased from Ce-Tech Japan. Carbon dioxide (99.999%) and nitrogen (99.999%) were procured from Sigma Gases and Services, India. All reagents were used as received without any further purification. All the aqueous solutions were prepared in double-distilled water.

3.1.3. Chemicals for liquid product analysis

Methanol, n-propanol, iso-propanol, formic acid, ethanol, acetic acid, and sulfuric acid (all HPLC grade, 99.9%) were also obtained from Sigma Aldrich. HPLC grade water (obtained from S. D. Fine Chemicals Ltd) was used to prepare HPLC solvents. Deuterium oxide (99.9 atom % D) and dimethyl sulfoxide (DMSO, 99.7 %) were purchased from Sigma-Aldrich.

3.2. Methods

3.2.1. Preparation of electro-catalysts

Four different types of electro-catalysts were prepared in this work.

i. Metallic Cu nanoparticles (Cu NPs)
ii. Cu supported on N-doped graphene (Cu_x/NGN)
iii. Oxide derived Cu-Zn nanoparticles ($CuZn_x$)

iv. Oxide derived Cu-Zn nanoparticles supported on N-doped graphene ($CuZn_x$/NGN)

The detailed preparation method is given in subsequent chapters.

3.2.2. Preparation of electrolyte solution

For ECO_2R study, aqueous 0.1 M $KHCO_3$ electrolyte was used. Electrolyte solution was prepared by mixing the corresponding amount of high purity $KHCO_3$ (99.99 %) in double distilled water and stirred for complete dissolution. High purity nitrogen gas was sparged in the electrolyte solution for the first 30 min to remove any dissolved oxygen and then CO_2 was passed for another 30 min under stirring.

The value of pH was measured in 0.1 M $KHCO_3$ solution as a function of time during purging of N_2 at a flow rate of 20 mL min^{-1}. The pH value was found to increase from 8.50 to 8.75 (**Table 3.1**) in 100 min. Increasing value of pH with time suggests that CO_2 dissolved in solution is escaping due to continuous N_2 flow as per equation 3.1. As CO_2 level is decreased, more OH^- ions are produced.

$$HCO_3^- \rightleftharpoons CO_2 + OH^- \qquad 3.1$$

Table 3.1 *The pH value of 0.1 M $KHCO_3$ solution on continuous bubbling of high purity N_2 at a flow rate of 20 mL min^{-1}*

Time (min)	0	5	10	15	20	30	40	70	100
pH	8.50	8.54	8.57	8.60	8.61	8.62	8.64	8.70	8.75

The pH values were also measured during CO_2 purging to find out time required to reach CO_2 saturation level in 0.1 M $KHCO_3$. During continuous purging of high purity CO_2 at a flow rate of 20 mL min^{-1}, pH of the solution decreased from initial 8.50 to 6.96 in 30 min. After that, pH value was stable (**Table 3.2**). Stable pH value suggests that the solution might be saturated with CO_2 in 30 min. Knonche et al. [174] suggested possible equation 3.2.

$$CO_2 + H_2O \rightleftharpoons H_2CO_3 \rightleftharpoons HCO_3^- + H^+ \rightleftharpoons CO_3^{2-} + 2H^+ \qquad 3.2$$

Table 3.2 *The pH value of 0.1 M $KHCO_3$ solution on continuous bubbling of high purity CO_2 at a flow rate of 20 mL min^{-1}*

Time (min)	0	5	10	15	20	25	30	50
pH	8.50	8.17	7.93	7.17	7.03	6.99	6.96	6.96

3.3. Physico-chemical characterization methods

3.3.1. Fourier-transform infrared (FTIR) spectroscopy

In FTIR spectroscopy, IR radiation is passed through a sample. Some amount of the infrared radiation is absorbed by the sample while some amount of it is passed through (transmitted). This results in a spectrum, which represents the molecular absorption and transmission by the sample. Each molecular structure produces a unique infrared spectrum.

To get the spectrum, sample is prepared by grinding approximately 1-3 mg of solid sample with approximately 350 mg of infrared-inert matrix material viz. KBr (FTIR grade). Before use, KBr should be dried overnight at 110°C to remove any trace of moisture. Since, there is need of a relative scale for the absorption intensity; a background spectrum must be created with only KBr (without sample) in the beam. This background spectrum is compared with the spectrum obtained with the sample, and thus percent transmittance is produced. The FTIR spectra of electro-catalysts were obtained in a Bruker Vector 27 spectrophotometer to identify the various functional groups present in the sample. The FTIR spectra of the electro-catalysts were collected at a resolution of 4 cm^{-1} in the 400–4000 cm^{-1} region.

3.3.2. X-ray photoelectron spectroscopy (XPS)

X-ray photoelectron spectroscopy (XPS) is a surface analysis technique widely used to determine the elemental composition and oxidation states of elements at the surface of electro-catalysts by excitation of inner orbital and bonding electrons by a focused X-ray beam. It also determines the binding states of the elements. The XPS spectrum is obtained by measuring the kinetic energy and quantity of electrons.

The XPS analysis of electro-catalysts was performed on ESCALB Xi^+ (Thermo Fischer Scientific Inc., USA) system. A monochromatic Al-K_α source operated at anode potential of 15 kV is used on 900 μm size area to record XPS spectra. The survey spectra were recorded with a pass energy of 50 eV while the high resolution spectra with a pass energy of 20 eV operating at an anode potential of 15 kV and emission current of 10 mA. The pressure in the analysis chamber was less than 2×10^{-9} torr. XPSPEAK41 software was used for the data processing and the core level spectra were fitted with mixed Gaussian-Lorentzian convoluted function (80/20) and Shirley function was used for background subtraction.

3.3.3. Raman spectroscopy

Raman spectroscopy is a spectroscopic technique used to detect vibrational, rotational, and other states in a molecular system, capable of probing the chemical composition of materials. Raman spectra were recorded at room temperature using a Confocal LabRam HR800 spectrometer (HORIBA Scientific, India) with 532 nm radiations.

3.3.4. Surface area and pore size distribution

The surface area of the synthesized electro-catalysts was determined using Brunauer-Emmett-Teller (BET) gas adsorption method. This gas adsorption method is based on the physical adsorption of a gas (inert) on the surface of the solid (electro-catalyst). Physical adsorption results from relatively weak vander Waals force which develops due to dipole-dipole interaction between the adsorbate gas molecules and adsorbent surface (test sample). The amount of adsorbate gas corresponding to a monomolecular layer on the surface is calculated to evaluate the surface area of the sample.

The surface area and pore volume of the electro-catalysts were determined by using a N_2 adsorption-desorption isotherms, acquired using a physisorption apparatus (Autosorb iQ Station 1, Quantachrome Instruments, Germany) at -196 °C. Approximately, 0.3 to 0.5 g of powder was placed in a test tube and allowed to degas at 473 K under vacuum for 12 h before any adsorption measurements. This removes contaminants such as water vapor and adsorbed gases from the sample. The sample was then weighed under air-tight conditions; after which it was inserted into the analysis port for further analysis at liquid nitrogen temperature. Multipoint adsorption method was employed to obtain the results of Brunauer–Emmett–Teller (BET) surface area. Total pore volume (VP) of the prepared carbons was assessed from the amount of N_2 adsorbed at a relative pressure of 0.99 and micropore volume was estimated from t-plot method [175]. The mesopore volume and pore size distribution were derived from the adsorption branch of isotherm by using the Barrett–Joyner–Halenda (BJH) model [176].

3.3.5. X-ray diffraction (XRD) analysis

X-ray diffraction is an effective method for determining crystal structure of materials. It is a rapid analytical technique primarily used for phase identification of a crystalline material and can provide information on unit cells. The material to be analyzed is finely ground, homogenized, and average bulk composition is determined. X-ray diffraction results from the constructive interference between X-rays and electrons of the sample material. The X-rays are

produced using a cathode ray tube. These X-rays are filtered to produce monochromatic radiation and collimated to concentrate before directing towards the sample. Constructive interference is produced when the conditions satisfy Bragg's law according to equation 3.3. These diffracted X-rays are then detected, processed and counted. Diffraction peaks are converted to d-spacing, which allows identification of the substance because each substance has a set of unique d-spacings. Usually this is carried out by comparison of d-spacings with standard reference patterns.

$$n\lambda = 2d\sin\theta \qquad 3.3$$

Where λ is the wavelength, d is the spacing between the two crystal planes, and θ is the Bragg angle, which is the angle between incident and reflected beam.

The crystallite size was calculated using Debey-Sherrer equation (3.4).

$$d = 0.9\frac{\lambda}{\beta}\cos\theta \qquad 3.4$$

Where λ is the wavelength (0.154 nm), β is the line broadening at half the maximum intensity (FWHM) and θ is the Bragg angle.

X-ray diffraction (XRD) analysis of the electro-catalysts and electrodes was carried out using an X'Pert³ MRD (Malvern Panalytical Technologies, UK) X-ray diffractometer, with a PIXcel^{3D} detector and Cu Kα source (λ = 0.1543 nm, 40 kV, 30mA). Diffraction patterns were recorded at a scan rate of 6^{o} min^{-1} between $20^{o} \geq 2\theta \geq 80^{o}$.

3.3.6. Scanning electron microscopy (SEM)

Scanning electron microscopy (SEM) is used very effectively for analyzing surface morphology of solid materials. This microscopy uses a focused beam of high energy electrons to generate a variety of signals at the surface of solid samples. The signals produced are derived from the interactions between electrons and sample. The signals generated during analysis produce a three-dimensional image and render information about the external morphology of the sample. In SEM, a beam of highly energetic electrons (primary electrons) is directed towards a sample. These electrons collide with the sample and give rise to secondary electrons, back scattered electrons, as well as X-rays. For imaging samples, secondary electrons and backscattered electrons are commonly used. There is no volume loss in the sample during

analysis, and hence the same material can be used to generate images repeatedly. Hence, SEM is termed as non-destructive analytical technique.

The SEM analysis was performed using scanning electron microscope (make: JEOL JSM-6510 LV) operated at 20 kV which was able to magnify the samples in the wide range of 10X to 20 kX. In order to avoid charging of samples under electron beam, samples were coated with gold film (of 50 μm thickness) in an automatic sputter coater (Polaron) prior to SEM studies.

3.3.7. Transmission electron microscopy (TEM)

Transmission electron microscopy is another technique to analyze the morphological details of a specimen. The basic difference between SEM (or FESEM) and TEM is that SEM is based on scattered electrons while TEM is based on transmitted electrons. In SEM, back scattered electrons, secondary electrons, and characteristic X-rays generated after the collision with the sample, produce 3-dimensional images, while in TEM, the transmitted electrons from the samples are utilized to produce two-dimensional images. As the electrons need to pass through the samples in TEM, the specimen has to be thin enough to transmit electrons (i.e. electronically transparent). TEM provides higher resolution than SEM and is able to analyze the sample at nano level.

The TEM analysis was performed using JEM 2100 transmission electron microscope (TEM) (JEOL Ltd., Japan) operated at 200 kV. The samples for TEM analysis were dispersed ultrasonically in appropriate solvent for 30 min. The homogenously dispersed sample was put over 300 mesh size copper grid using micropipette. The sample kept over the grid was then placed in a Petridish and dried in a vacuum oven to remove the volatile contents. Thereafter, the grid having sample was mounted in the single axis tilt sample holder to insert into TEM column for analysis.

3.3.8. Energy dispersive X-ray (EDX) spectroscopy

Energy dispersive X-ray spectroscopy is a qualitative and quantitative non-destructive X-ray microanalytical technique, which provides information about the chemical composition of the samples having elements with atomic number (z) > 3. In EDX spectroscopy, an electron beam is focused on the sample in either a scanning electron microscope (SEM) or transmission electron microscope (TEM). The electrons from the primary beam penetrate the sample and interact with the atoms of the sample. After interaction, the X-rays are detected by an energy dispersive detector and signal is displayed as spectrum of intensity vs. X-ray energy. The

sample does not require any special preparation for EDX analysis. It is done in the same way as in case of SEM or TEM analysis.

The EDX spectra of the electro-catalysts were obtained using INCA X-act detector (Oxford Instruments, UK) connected to scanning electron microscope (SEM) (make: JSM-6510, model: JEOL Ltd., Japan) and transmission electron microscope (make: JEOL, model: JEM 2100).

3.3.9. Thermogravimetric analysis (TGA)

Thermogravimetric analysis (TGA) measures weight changes in a material as a function of temperature (or time) under a controlled atmosphere. Its principle uses include measurement of a material's thermal stability, filler content in polymers, moisture and solvent content, and the percent composition of components in a compound.

TGA analysis was performed on TGA Q500 (TA instruments, USA). In a typical experiment, about 10 mg of sample was heated from 30 °C to 900 °C at a heating rate of 10 °C min^{-1} under dry nitrogen at a flow rate of 50 cm^3 min^{-1}.

3.3.10. Hydrodynamic size distribution

The hydrodynamic size distribution of Cu nanoparticles was determined on Brookhaven 90 plus particle size analyzer. The measured autocorrelation function is determined on MAS OPTION software by fitting the data in a lognormal particle size distribution function. From the best fit, the hydrodynamic size was determined.

3.4. Electrochemical characterization

The most popular electrochemical characterization methods include cyclic voltammetry, linear sweep voltammetry, rotating disk voltammetry, and electrochemical impedance spectroscopy. Some techniques derived from these methods like electrochemical active surface area (ECASA) are also used for electrode characterization. These methods give the information related to electrode surface, like active surface area and surface activity. A good electrode should have larger surface area and activity to enhance surface reactions. To study the stability of electrode and product distributions at different applied potentials, chronoamperometry is largely used. In current research work, following characterization techniques were used.

3.4.1. Cyclic voltammetry

Cyclic voltammetry is an electrochemical technique widely used for electrode characterization. It consists in sweeping the potential along a triangular wave between two values using a certain

scan rate (dU/dt) while measuring the current response (see **Fig. 3.1**). The outcome current comes as a consequence of all the processes occurring at electrode at a specific potential. A positive current is recorded if the processes at the working electrode assume net shuffling of electrons in direction from the WE to the CE. Similarly, negative currents are measured in a CV if the processes occurring on the WE involve transfer of electrons from its surface. This means that not only processes of oxidation or reduction of the electrode surface are possible to identify, but also all other processes that involve transfer of electrons such as oxidation or reduction of atoms (metals) or molecules (gases or organic impurities), electrolyte adsorption, surface reconstructions, as well as changes in double layer capacitance.

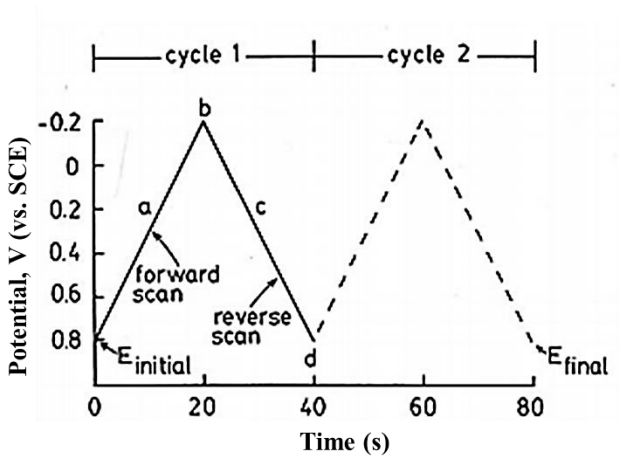

Fig. 3.1 *Typical excitation signal for cyclic voltammetry – a triangular potential waveform with switching potentials at 0.8 V to -0.2 V vs. SCE*

The cyclic voltammetry studies were performed in a high purity N_2 as well as CO_2 saturated 0.1 M $KHCO_3$ electrolyte solution at a scan rate of 10 mV s^{-1} between -0.2 V to -1.8 V (vs. AG/AgCl).

3.4.2. Linear sweep voltammetry (LSV)

The electro-catalytic performance of the different electrodes was studied by recording LSVs in CO_2 and N_2 saturated 0.1 M $KHCO_3$ aqueous solutions. The electrodes were pre-reduced by performing multiple scans at a scan rate of 50 mV s^{-1} before each LSV experiments. In linear sweep voltammetry (LSV), a fixed potential range is employed much like potential step measurements. However, in LSV the voltage is scanned from a lower limit to an upper limit as shown in **Fig. 3.2**. In current work, the LSV was conducted in N_2, or CO_2 saturated environment at a scan rate of 10 mV s^{-1} between −0.2 V and −1.8 V (*vs.* Ag/AgCl).

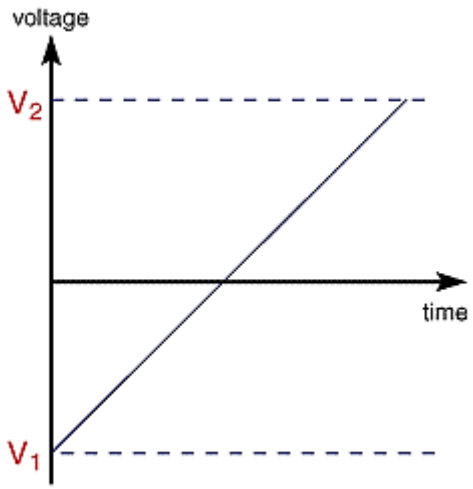

Fig. 3.2 *Typical excitation signal for linear sweep voltammetry*

3.4.3. Electrochemical active surface area (ECASA)

The electrochemical active surface area (ECASA) has an important effect on the electro-catalytic activity. Therefore, the ECASA of the electro-catalysts was evaluated by electrochemical double-layer capacitance (C_{dl}), which was obtained from the CVs taken within non-Faradaic region at different scan rates of 10, 20, 30, 40, 50, 60, 70, 80, 90, and 100 mV s^{-1}. Then the double-layer capacitance (Cdl) was estimated by plotting the current densities obtained at midrange of applied potential range as a function of the scan rate. Further, it can be calculated using the equation 3.5:

$$C_{dl} = \frac{d(\Delta CD)}{2dV_b} \qquad 3.5$$

Where, V_b is the scan rate (mV sec^{-1}).

3.4.4. Chronoamperometry

In this method, a pulse potential is applied to a working electrode and the current passing through the cell is determined versus time [177]. Such experiments receive the name of chronoamperometry (**Fig. 3.3**), and they are mainly used to accumulate products of a reaction at a given potential. CO_2 reduction is typically measured using this method. Operation at a constant potential presents the disadvantage that contaminants may accumulate at the electrode surface.

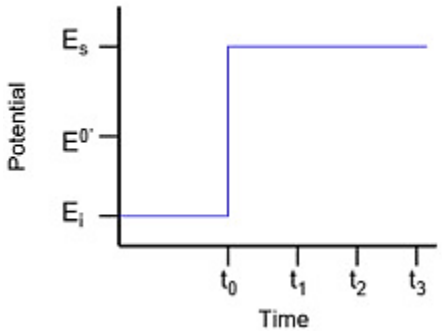

Fig. 3.3 *Typical excitation signal for chronoamperometry*

3.5. Evaluation of electro-catalysts

The ECO_2R experiments were performed using a "Wave Driver 20" Bi-potentiostat (Pine Instruments, USA) with a three-electrode system in customized H-type cell as discussed below.

3.5.1. Experimental set-up

The H-type electrochemical cell was used to evaluate the electrochemical CO_2 reduction performance of the prepared electro-catalysts. **Fig. 3.4** shows the schematic representation of the experimental setup used in the present study. It consisted of gas humidification system, H-type electrochemical cell, liquid product analysis system and data acquisition and data processing system. Gas humidification section consists of mass flow controllers, pre-mixer and non-return valves. Two mass flow controllers (Bronkhorst, Netherlands), each for high purity CO_2 and N_2, were used to regulate flow rates of pure nitrogen and carbon dioxide gases entering the customized humidification chamber. Then the gas is passed through the cathode and anode compartment of H-type electrochemical cell at a flow rate of 10 ml min^{-1}. The H-type electrochemical cell (having 30 mL total volume of each compartment) made up of borosilicate glass and filled with 20 mL electrolyte solution in each compartment where CO_2 is continuously bubbled to maintain the CO_2 saturation level. Here, the electrolyte volume is fixed to a minimum level to generate detectable quantities of CO_2 reduction products. Anode, cathode and reference electrodes are connected to electrochemical workstation "Wave Driver 20" Bi-potentiostat (Pine Instruments, USA) through connecting cable as shown in **Fig. 3.4.** The silver/silver chloride (Ag/AgCl) containing saturated solution and platinum coil was used as a reference electrode (RE) and counter electrode (CE), respectively. The carbon paper coated with electro-catalyst was used as a working electrode (WE). Working electrode and reference electrode were placed in the cathodic compartment, whereas platinum coil was placed in another chamber (anodic compartment). Distance between RE and WE were kept minimum

(0.5 mm) to minimize uncompensated solution resistance [178]. The actual photograph of electrochemical CO_2 reduction set up with high pressure liquid chromatograph is shown in **Fig. 3.5**. The area of counter electrode is much larger than that of the working electrode, which can reduce the polarization of the Pt electrode and prevent the dissolution of Pt electrode. Pretreated Nafion-117 membrane was used to separate the anode and cathode compartments to prevent diffusion of products generated at working electrode [109]. The process for the pretreatment of Nafion membrane is given in section 3.5.3. During ECO_2R experiments, all the potentials measured against an Ag/AgCl reference were converted to the reverse hydrogen electrode (RHE) by using the equation 3.6. All the experiments were carried out at ambient conditions.

$$V_{vs.RHE} = V_{measuredvsAg/AgCl} + 0.197 + 0.059 * pH \qquad 3.6$$

At the end, liquid product is analyzed by HPLC and ^1H NMR as explained in section 3.6. of this chapter.

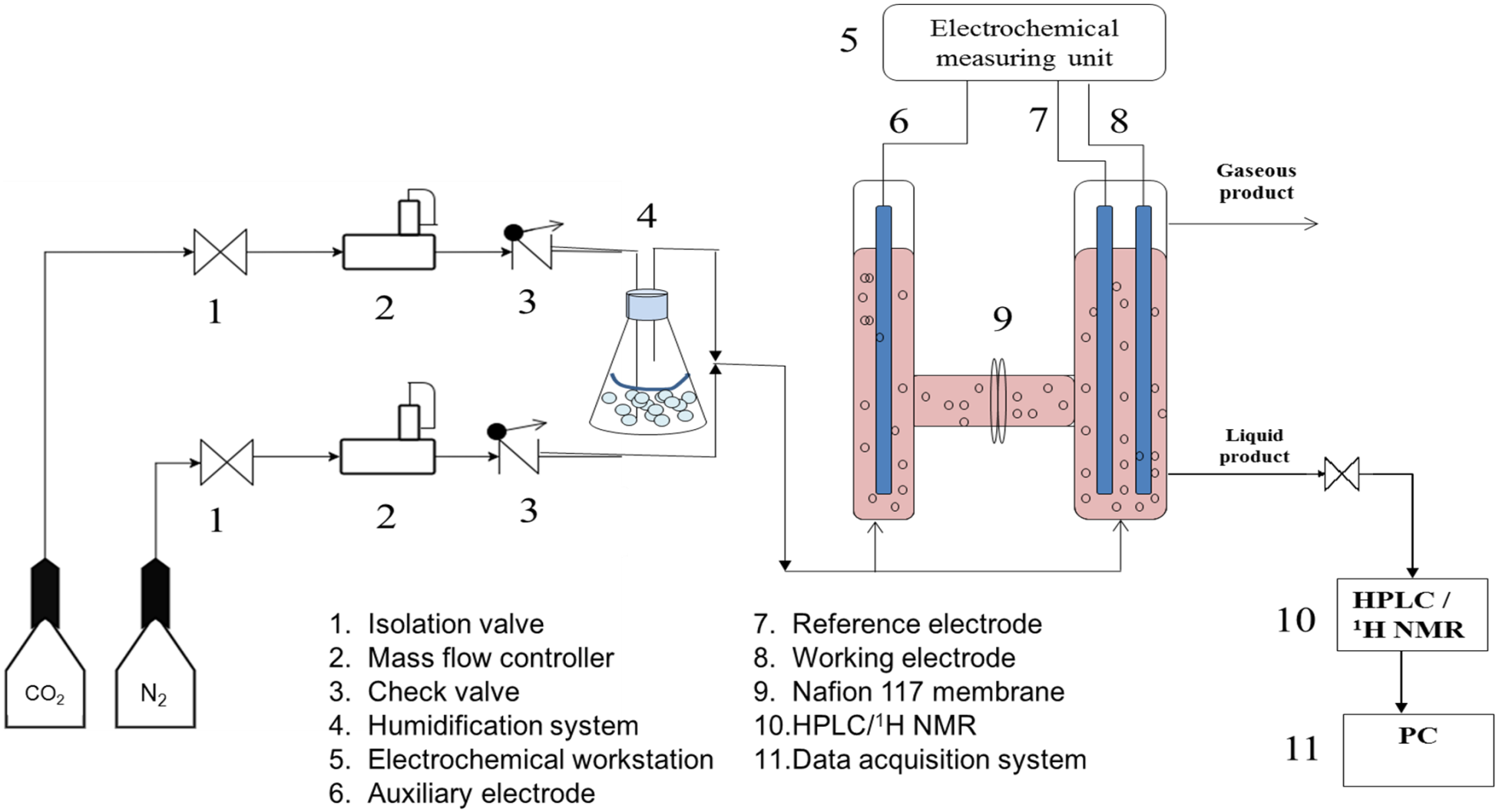

Fig. 3.4 *Schematic diagram of the experimental setup*

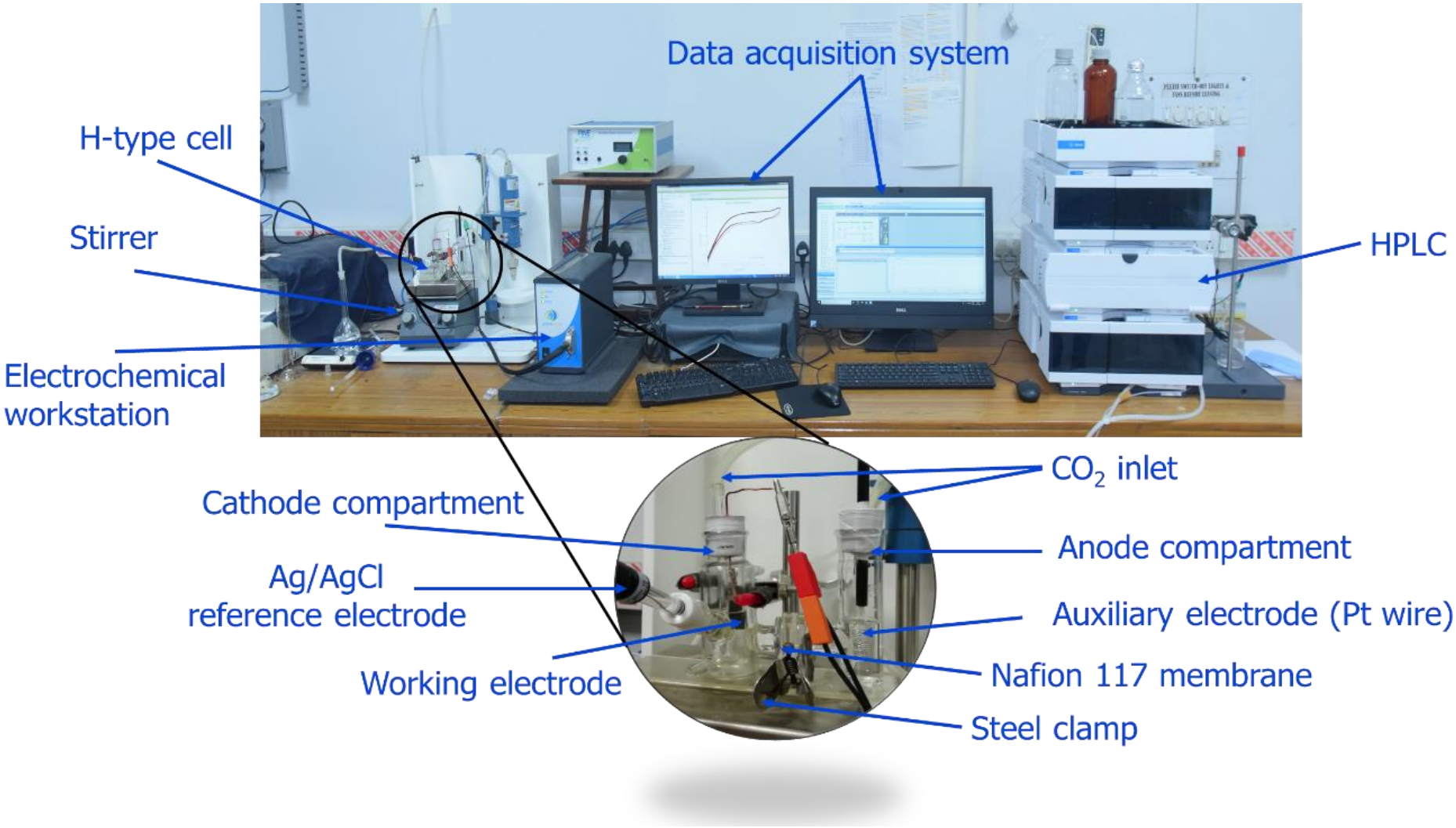

Fig. 3.5 *The actual photograph of electrochemical CO_2 reduction set up with high pressure liquid chromatograph for liquid product analysis*

3.5.2. Preparation of working electrode

Surface preparation of purchased porous carbon paper was carried out to remove dust so that electrochemical activity could truly be attributed to the coated electro-catalysts. For this, the carbon paper was cut into 2 cm x 2 cm or 1 cm x 1 cm dimensions. These pieces were ultrasonically treated in pure acetone for 5 min and then the carbon paper was properly dried. The mixture of catalyst powder, Nafion® 117 solution and isopropanol was sonicated for its uniform distribution. Obtained mixture is also called as catalyst ink. This catalyst ink was then sprayed onto a carbon paper using N_2 carrier gas. The ink coated carbon paper was dried at 60 °C for 2 h to remove the solvents. Dried carbon paper was denoted with corresponding coated electro-catalyst and used as working electrode in further experiments. For example, carbon paper coated with Cu nanoparticles electro-catalyst was denoted as Cu electrode. Approximately 0.5 to 2.0 mg cm^{-2} catalyst loading was achieved on different electrodes.

The detailed preparation method is given in subsequent chapters.

3.5.3. Pretreatment of Nafion membrane

For separating the working and counter electrode compartments, proton conducting membranes were used. The ionic conductivity of Nafion based membranes is high enough to provide a fast transport of H^+ from the CE, where they are produced in Oxygen Evolution Reaction (OER), to the WE compartment where they are consumed in CO_2 reduction reaction. Nafion 117 perflourinated membrane (0.007-inch-thick obtained from Sigma Aldrich) was used. The membrane was carefully cut into pieces of appropriate size. The pieces of membrane were then cleaned in 10% water solution of H_2O_2 by boiling for 1 hour. Afterwards, the Nafion was boiled in 10 % H_2SO_4 for 1 hour, followed by several rinsing with ultrapure water. The membrane pieces as prepared contain an excess of protons. In contact with the working electrolyte, this proton excess could easily shift the pH value of the electrolyte to lower values. To avoid this, the cleaned membrane pieces were sonicated for 1 hour in 0.1 M $KClO_4$ solution to exchange the excess H^+ by K^+. Outline for pretreatment of Nafion membrane is shown in **Fig. 3.6.**

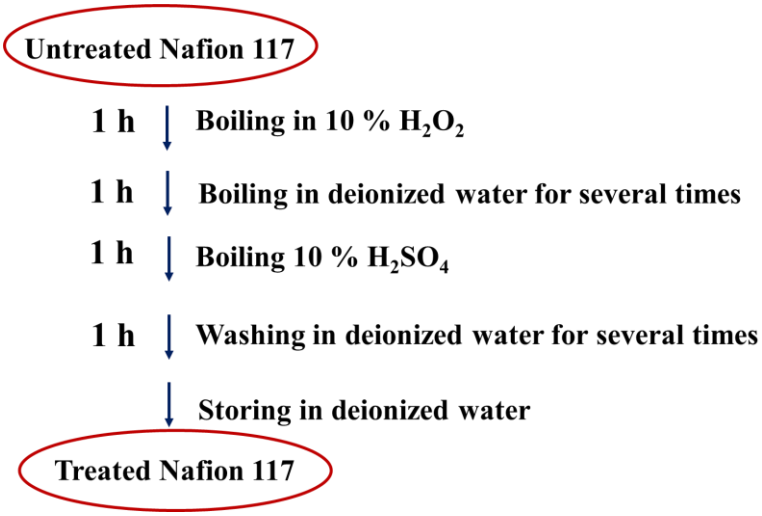

Fig. 3.6 *Step by step procedure for Nafion membrane pretreatment [109]*

3.5.4. Performance evaluation

During CO_2 reduction several reactions run in parallel, including the hydrogen evolution reaction as a competitive reaction (**Table 1.1**). Hence, initially, the approach was focusing on what controls the activity and the selectivity of the catalyst at a set of fixed parameters (i.e. electrolyte 0.1 M $KHCO_3$, 20 mL catholyte volume, 20 mL min^{-1} CO_2 flow rate). The effect of key governing parameters like electrolysis potential was explored to obtain the optimal electrolysis condition. In the case of CO_2 reduction reaction, it is essential to not only measure the total current densities (monitored by the potentiostat), but also to perform both qualitative and quantitative analysis of all the reaction products coming from the entire catalyst surface. For this purpose, bulk CO_2 electrolysis was performed in the H-type electrochemical cell at ambient temperature and pressure. After a given time, the liquid products were collected, for analysis using suitable methods and tools, such as HPLC and ^1H NMR. Experiments were usually run for up to 120 minutes. Furthermore, care was taken to carry out product analysis immediately after the reaction. Otherwise, the products could be lost due to various reasons like loss of volatile products from the liquid phase. Then, effects of potential on the final product concentration, production rates, and FE (i.e. selectivity) were studied for each electrode. Kinetics was studied by Tafel analysis and dependence of CO_2 partial pressure on product generation was also explored. Reusability and long term performance of the optimized electrode was also studied for changes in surface morphology, exposure to impurities and poisoning.

3.6. Analysis of reaction products

The information about the catalyst selectivity, thus on partial activities towards specific compounds in relation to CO_2 reduction, relies on identification, detection and quantification of all reaction products. A valuable indication of the accuracy of product quantification is obtained by the total balance between the integrated charge measured by potentiostat and the charge that would be required for the formation of all the detected products. There are several techniques that can be used for the analysis of CO_2 electro-reduction products in order to access the total charge. In this study, two different techniques were used for the detection of liquid products, high performance liquid chromatography (HPLC) (useful for the quantification of carboxylic acids as well as alcohols) and nuclear magnetic resonance (^{1}H NMR) (useful for all products, especially identification of new products). To access the catalytic activities towards different products, one must produce all products with concentrations higher than the detection limits of the analysis methods. Also, comparing the productivity and Faradaic efficiency equations (equation 3.7 and equation 3.8), one can easily conclude that there are two major parameters influencing the concentration of liquid products in solution: total reaction charge (at constant j dependent on the electrode roughness factor and the reaction time) and the electrolyte volume. The minimum electrolyte volume was fixed for the equipment. Hence, either high surface area of catalyst or longer reaction times may ensure meeting the required concentrations.

3.6.1. High performance liquid chromatography (HPLC)

Liquid chromatography has been employed primarily for detection of carboxylic acids, such as formic acid, acetic acid, and alcohols. The principle of separation of the products in liquid phase depends on the separation column used; in this work it was based on different polarities of the compounds. A small amount of liquid (20 μL) is manually injected through 1 mL sample injection. The needle injects the aliquot to the mobile phase which passes through the column for products separation (follow **Fig. 3.7**). A good separation is achieved by setting the optimal values for temperature of the column, flow rate of the mobile phase, as well as its composition, pH value, etc. Upon leaving the column, the separated compounds should be detected by an appropriate type of detector.

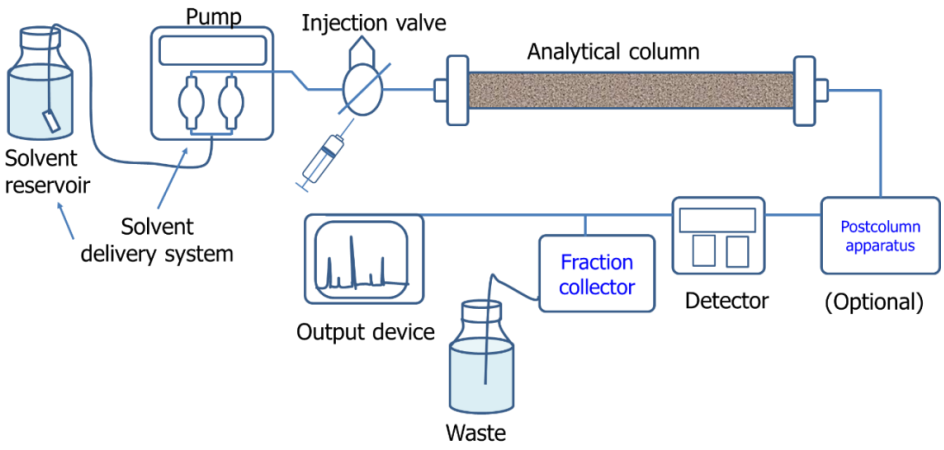

Fig. 3.7 *Flow chart of the HPLC (high performance liquid chromatograph) system. Figure reprinted from [179]*

In this work, refraction index detector (RID) was used to detect the products.

Refraction Index Detector (RID): The differences in refractive index between the mobile phase and the sample allow the detection and quantification by this method. **Fig. 3.8** shows a beam of light passing through a dual compartment flow cell. One of the compartments, filled with pure eluent (mobile phase), is reference cell. Through the other compartment (sample cell) flows both the eluate and the eluent (the mobile phase). A signal is obtained as a difference in refraction indices of the contents of the two cells at different times.

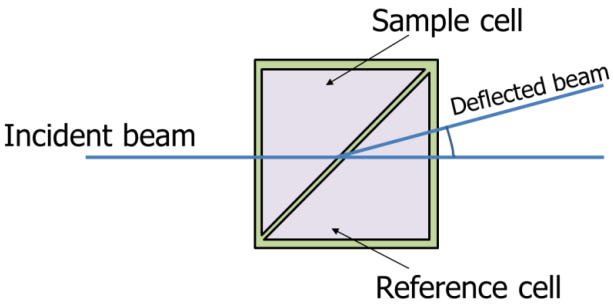

Fig. 3.8 *Principle behind detection in Refractive Index Detector (RID) in HPLC system*

*Equipment details and procedure***:** After every ECO_2R experiment, samples were collected from the reactor and analyzed (without any further treatment) with HPLC (1260 Infinity II series, Agilent Technologies, Germany). Sample vials were placed in a low temperature environment (10 ^oC) before injection and 20 µL of each sample was injected through a 0.22 µm Nylon syringe filter (Raj Analytical Solutions Pvt. Ltd. India). Hi-Plex H column (Agilent Technologies, Part No. PL1170-68730) was used for product separation. The column oven was kept at a constant temperature of 60 ^oC with a flow rate of 0.6 $mL.min^{-1}$ of 1 mM H_2SO_4

prepared in HPLC grade water (S. D. Fine Chem Ltd, India) as eluent. For identifying the product concentration in the sample, the effluent stream exiting the column was passed through a refractive index detector (Agilent Technologies, Part No. G71628). HPLC system was conditioned along with a column for 6 h before analysis. After the analysis, the column was cleaned for 1 h by passing 1mM H_2SO_4.

Calibration of HPLC: The peak area in liquid chromatography is proportional to the compound concentration. The HPLC was calibrated using known concentrations (0.05, 0.1, 0.25, 0.5, 1, 2.5 and 5 mM L^{-1}) of formic acid, acetic acid, methanol, ethanol, and n-propanol prepared in CO_2 saturated 0.1 M $KHCO_3$ solution. The product concentration in the sample was calculated using the calibration curve (**Fig. 3.9**). Accuracy was checked every time with a standard mixture of formic acid, acetic acid, ethanol and n-propanol (0.1, 0.5, 1, and 5 mM, respectively) in CO_2 saturated 0.1 M $KHCO_3$ solution.

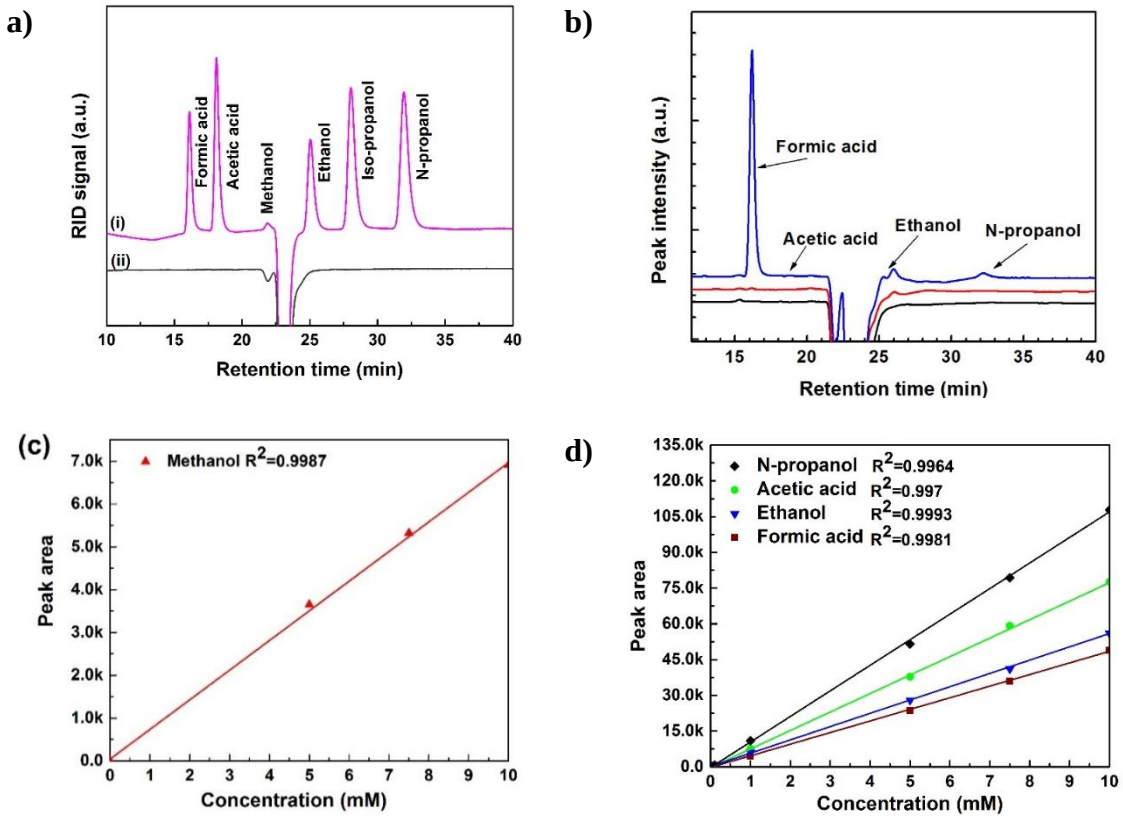

Fig. 3.9 *HPLC chromatograms of* ***a)*** *5 mmol L^{-1} standard mixture (i) and blank 0.1 M KHCO3 electrolyte solution (ii);* ***b)*** *HPLC chromatogram of fresh CO_2 saturated 0.1 M $KHCO_3$ solution taken before electrolysis (black), product collected after 2 h of electrolysis in N_2 (red) and CO_2 saturated (blue) at -0.8 V (vs. RHE) at Cu NPs/carbon paper;* ***c)*** *HPLC calibration curve for methanol; d) HPLC calibration curves for formic acid, acetic acid, ethanol and n-propanol*

3.6.2. Nuclear magnetic resonance (^{1}H NMR) spectroscopy

NMR spectroscopy is a unique technique for identification of the compounds, based on the magnetic properties of a given nuclei. In particular, ^{1}H-NMR, spectroscopy allows the identification of different types of protons on a given sample. Moreover, the signals observed in NMR are proportional to the concentration of each compound, so it facilitates an acceptable quantification of almost all compounds with low detection limits. For this reason, ^{1}H-NMR spectroscopy was employed as means of quantification of the products from CO electro-reduction in alkaline media. This study involved strict considerations of cleanliness, use of internal standards and chemical shift references, sample shipping and preparation, as well as obtaining the calibration curves for some of the most interesting products and detection and quantification on the unknown samples. It turns out that NMR was able to detect traces of organic impurities coming from fingerprints, various types of plastics, gloves, etc. For obtaining clean spectra, all the glassware, weighing cups, plastic pipettes and tubes used for accurate measuring, weighing and storage of standard solutions should be cleaned of organic impurities with piranha solution; plastics by multiple sonication in heated ultrapure water).

The basic NMR spectrometer analyzes using a magnetic field and a special detector to assess the changes. The different components of NMR spectrophotometer are shown in **Fig. 3.10**. The strength of the external magnetic field causes electrically charged nucleus to move from a lower energy level (E1) to a higher energy level (E2) and the difference between E2 and E1 is symbolized as ΔE which is dependent on the power of the magnetic field and size of the nuclear field moment. The electromagnetic radiation rhythm attains the NMR signal with a frequency (v) causing the nuclei to move to a higher energy level (E1/E2). When this electromagnetic radiation is stopped, it causes the nuclei to relax and accomplish thermal equilibrium. This release of energy from the nuclei is recorded in the form of spectra on the computer [180].

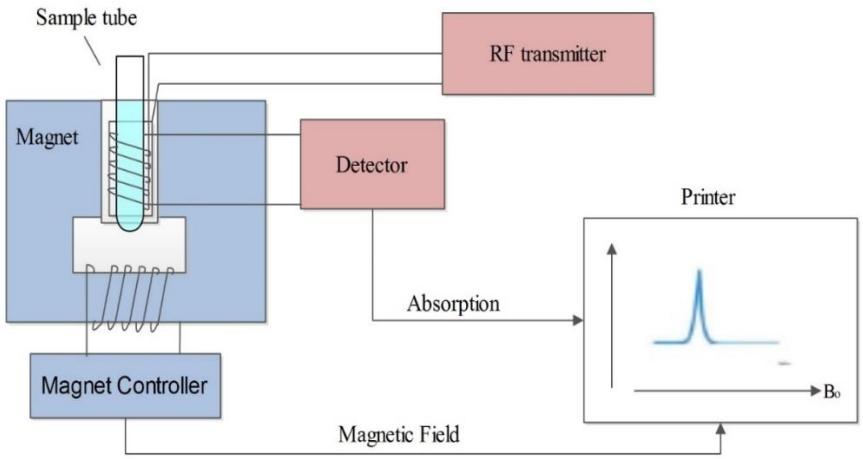

Fig. 3.10 *Schematic presentation of a typical nuclear magnetic resonance spectrometer showing the relationship of various components (magnet, magnetic field, and detector). Figure reprinted from [180]*

Preparation of NMR standards for calibration: The absolute peak area in an the NMR spectrum depends on several factors. That is the reason why the peak areas in NMR must be compared to the peak area of an internal standard of known concentration to find the accurate concentration of a specific product. Apart from use of internal standard, aliquots based on aqueous solutions need to be added deuterized water (D_2O) in order to suppress the wide peak coming from water.

For each measurement, 1 mM DMSO solution was used as internal standard. DMSO stock solution was made by dissolving a corresponding amount of DMSO in 0.1 M $KHCO_3$. All samples have been made up as follows:

All the standards were prepared in the working electrolyte solution (CO_2 saturated 0.1 M $KHCO_3$). An accurately measured amount of high purity compound (liquid) was added in order to make solutions of 5 mM, or in some cases 10 mM (to match the volume of ca. 50-100 µL for pipette's accuracy). These starting solutions were further diluted to obtain 2.5 mM, 1 mM, 0.5 mM, 0.25 mM and 0.1 mM solutions. A mixture of liquid products from ECO_2R (500 µL), D_2O (200 µL), and internal standard (1 mM DMSO) (100 µL) was transferred into a nuclear magnetic resonance (NMR) sample tube in order to collect NMR spectrum and obtain the calibration curves (**Fig. 3.11** and **Fig. 3.12**).

Equipment details and procedure: Spectra were recorded on nuclear magnetic resonance spectroscope (Jeol JNM-ECS 400, 400 MHz). The water peak was suppressed using solvent suppression function. The time of d1 was 5 seconds and the number of scan was 64 in all the NMR measurements. The peaks used for quantification are highlighted with green color in

Table 3.3. The peak area of a given product is normalized to the internal standard and used to determine the concentration of the product. Identical NMR acquisition parameters were used for all measurements. **Fig. 3.11** and **Fig. 3.12** show the sample ^{1}H NMR spectra and calibration curves for formic acid/formate, acetic acid/acetate, methanol, ethanol, and n-propanol. Accuracy of the assay was checked before and after experimental runs, with a standard mixture of formic acid, acetic acid, ethanol and n-propanol (0.1, 0.5, 1, and 5 mM, respectively) in CO_2 saturated 0.1 M $KHCO_3$ solution.

Analysis of unknown sample: Samples with unknown concentrations of compounds were stored for short-term before shipping to the NMR facility, where DMSO was added as internal standard. Shipping was done using thermally insulated packaging containing dry ice to avoid evaporation of the volatile ECO_2R products or their possible degradation at elevated temperatures. After the measurement, the obtained peaks are identified and integrated and their areas expressed relative to the internal standard peaks areas. The calibration curves are then used to determine the unknown concentrations of the compounds detected.

Table 3.3 *^{1}H NMR peaks of the standards (Peaks used for quantification are highlighted.)*

Assignment		**Chemical Shift**	
Probed nucleus	**Product name**	**^{1}H splitting**	**Chemical shift**
HCOO-	Formate	S	8.33
CH_3CH_2OH	Ethanol	Q	3.53
$CH_3CH_2CH_2OH$	N-propanol	T	3.44
CH_3OH	Methanol	S	3.23
DMSO	Internal standard	S	2.60
$CH_3C(=O)O$-	Acetate	S	1.87
$CH_3CH_2CH_2OH$	N-propanol	Sextet	1.42
CH_3CH_2OH	Ethanol	T	1.06
$CH_3CH_2CH_2OH$	N-propanol	T	0.77
S: singlet, T: triplet, Q: quartarate			

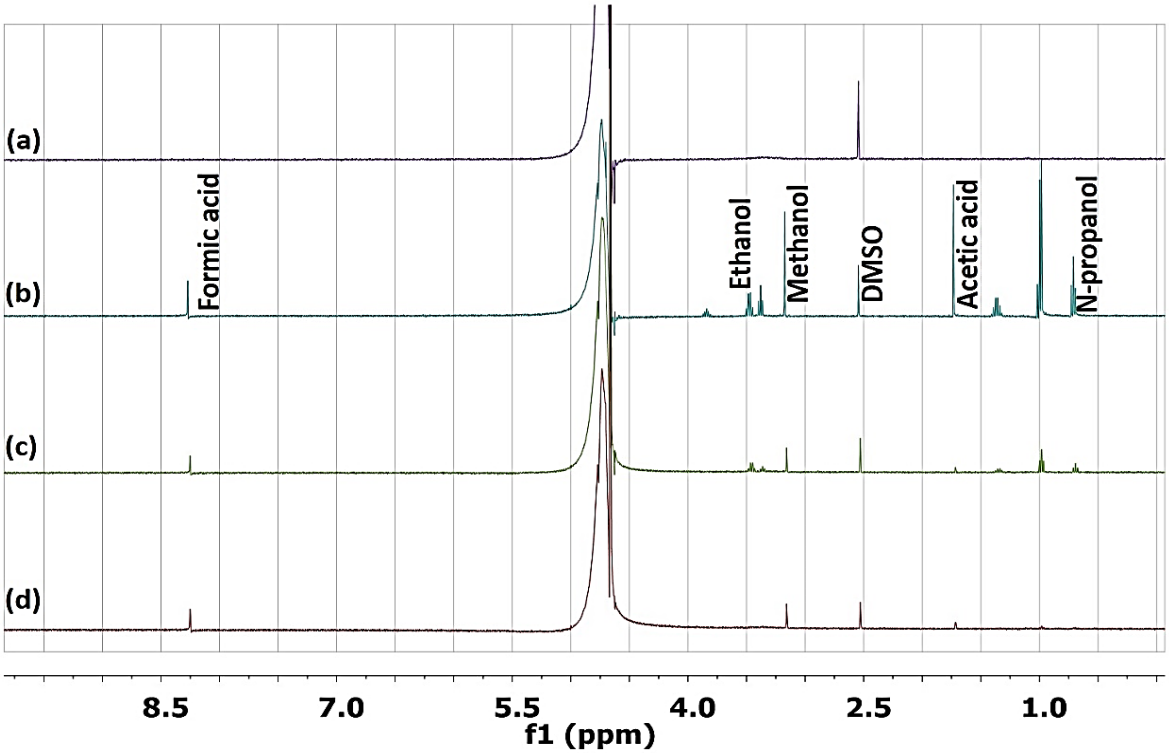

Fig. 3.11 *Representative ^{1}H NMR spectrum of* ***(a)*** *the blank 0.1 M $KHCO_3$ electrolyte,* ***(b)*** *standard mixture of 2.5 mmol L^{-1} each of methanol, ethanol, n-propanol, formic acid, and acetic acid,* ***(c)*** *liquid products after 2 h electrolysis at -0.8 V (vs. RHE) using $CuZn_{20}$/NGN catalyst,* ***(d)*** *liquid product after 2 h electrolysis at -0.8 V (vs. RHE) using CuO/NGN catalyst* (Only the peaks used for quantification are labelled.)

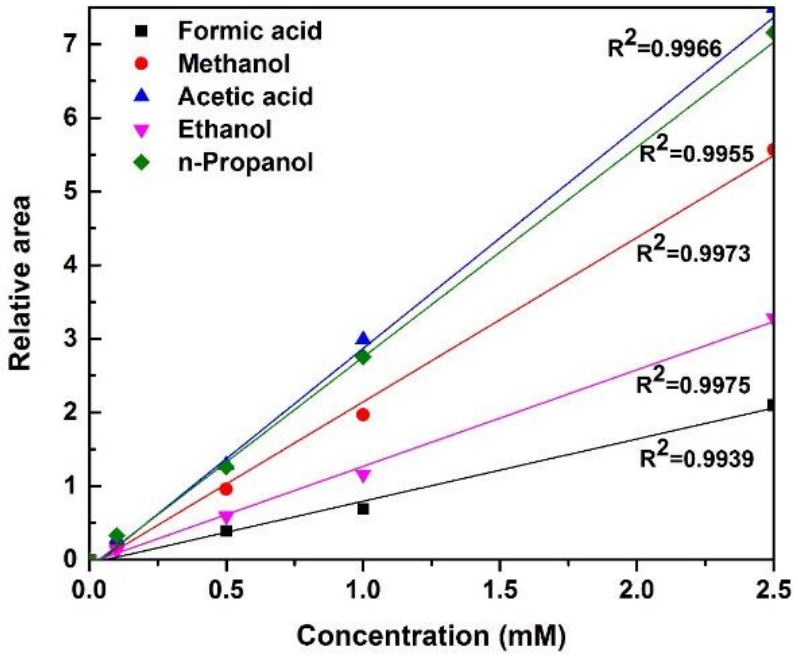

Fig. 3.12 *Calibration of six liquid products from known concentrations of standard solution by ^{1}H NMR* (The relative peak area of products is normalized to the peak area of DMSO.)

3.7. Performance metrics

After ECO_2R reduction experiments and analysis of liquid products, the performance is measured in terms of productivity, selectivity (FE), activity (CD), and stability for longer duration & reuse run test as mentioned below.

3.7.1. Productivity

The production rate (in μmol h^{-1} L^{-1}) of all liquid products were calculated using equation 3.7:

$$\text{Productivity} = \frac{N}{t} \qquad 3.7$$

Where, N is product concentration (μmol L^{-1}) and t is a total electrolysis time (2 h).

3.7.2. Selectivity

As multiple electrochemical reactions are possible on a single catalyst surface, an important parameter in CO_2 reduction is the FE, also known as selectivity. This parameter can be used to describe the percentage of charge consumed to different reaction products. An ideal catalyst would minimize all competing reactions such that only a singular, target product is produced. The FE for any product was calculated by using equation 3.8.

$$FE(\%) = \frac{ZnF}{Q} \times 100 \qquad 3.8$$

Where, Z is number of electrons required to produce one molecule of product from CO_2 (here, Z = 2, 8, 6, 12 and 18 for formic acid, acetic acid, methanol, ethanol and n-propanol respectively); n represents the moles produced; F is Faraday's constant (F=96485 $C.mol^{-1}$); and Q represents the total charge passed across the electrode ($Q = I \times t$ where I represents the current passed during electrolysis and "t" is the electrolysis time.).

3.7.3. Activity

The rate that products are created within electrochemical reactions is most frequently reported as geometric CD, denoted by j. CD is a function of the total applied current divided by the planar area of active catalyst. The total CD measured accounts for all the reaction products formed (HCOOH, CH_3COOH, CH_3OH, CH_3CH_2OH, etc.) and any catalyst surface reductions that may occur. The CD can also be described using the electrochemically active surface area rather than the geometric area to account for the explicit activity of the catalyst.

3.7.4. Long term performance and reusability study

Electrode stability is one of the least studied aspects in literature but one of the most important for industry. As commercial catalysts need to last for thousands of hours to be cost-effective and reliable, the applied voltage, CD and selectivity of the electrolyzer should remain constant during extended and cyclical operation. Unfortunately, high stability is difficult to achieve due to the number of mechanical, chemical and electrochemical failures that can occur. It is common for designed nanostructures to mechanically break-off, catalysts to dissolve and redeposit elsewhere and for impurities in the electrolyte to contaminate the reduction catalyst. Nevertheless, stability is an important design consideration for catalysts which show promise in other performance metrics. Furthermore, the reusability of the working electrodes was also studied. For this, electrodes were easily washed with water and then reused for next reaction run under the same conditions.

In current research work, stability and reuse tests were performed at optimized conditions as described in respective chapters.

3.8. Softwares used

i. OriginPro 2016 64Bit software was used for fitting the experiments data, determination of error, and to draw required 2D and 3D plots.
ii. XPSPEAK41 was used for fitting raw XPS data.
iii. X'Pert HighScore Plus (2.2.0) software was used to process raw XRD data by identifying possible crystal structures.
iv. ImageJ software was used to measure the particle sizes of NPs and to study particles size distribution by SEM and/or HR-TEM images.
v. AfterMath (1.5.9509) to capture data points from electrochemical workstation and process raw data wherever required.
vi. MestReNova (6.0.2-5475) was used to identify ^{1}H NMR data and quantification of different liquid products.

Chapter 4- Electrochemical CO_2 reduction on metallic Cu nanoparticles (Cu NPs)

4.1. Synthesis of Cu nanoparticles

Citrate stabilized metallic copper nanoparticles were synthesized using the method reported by Chatterjee et al. [181]. In brief, 60 mL of double-distilled water was taken in 500 mL of round bottomed flask and 10 g of cupric chloride dihydrate was dissolved in it. The color of the solution changed to royal blue, indicating the formation of hexaaquacopper(II) complex ions. Subsequently, about 10 g of trisodium citrate dihydrate was mixed to the above solution. Then, the temperature of this precursor solution was raised to 60 ^oC. Hydrazine hydrate was heated separately to 60 ^oC, and 20 mL of this was added in the Cu precursor solution (at once) under vigorous stirring. After this, the solution turned to dark brown signifying the reduction of $CuCl_2.2H_2O$ to metallic Cu. Stirring was continued for another 20 min and then the temperature was lowered down to 25 ^oC. Obtained copper solution was kept undisturbed for overnight at room temperature. During this step, suspended Cu NPs slowly settled at the bottom and clear solution was obtained in supernatant. The settled material was thoroughly washed with water and subsequently with ethanol then it was dried in vacuum oven for 15 h at 50 ^oC. Fine powder was obtained by crushing dried nanopowder in a mortar-pestle. Schematic of synthesis of citrate stabilized Cu NPs is given in **Fig. 4.1**.

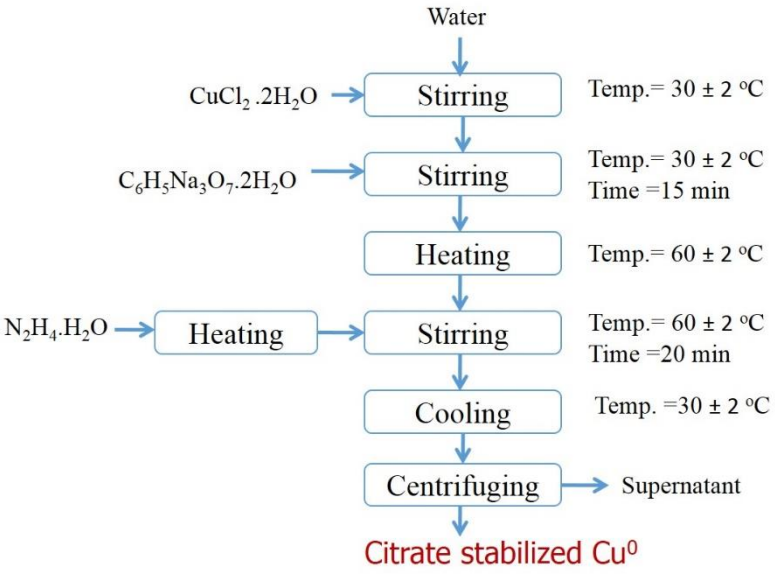

Fig. 4.1 *Schematic of synthesis of citrate stabilized Cu nanoparticle*

4.2. Preparation of working electrodes

Cleaned carbon paper (section 3.5.2. was cut into 2 cm x 2 cm dimensions. These pieces were ultrasonically treated in pure acetone for 5 min. and then the carbon paper was properly dried at 105 ^{o}C for 2 h. The mixture of 8±0.2 mg of the Cu NPs, 1 mL of IPA and 50 μL Nafion® (5 wt. % solution) was sonicated for 30 min in a 2 mL vial to obtain homogeneous catalyst ink. Obtained suspension ink was dropped on to a pretreated carbon paper and dried under the incandescent lamp. This was used as a working electrode (WE) and represented as Cu NPs/carbon paper in further discussion.

4.3. Results and discussion

4.3.1. Physico-chemical characterization

4.3.1.1. X-Ray diffraction

The XRD pattern of citrate stabilized Cu NPs recorded from a powder sample, reflects three diffraction characteristic peaks at 2θ of 43.3^{o}, 50.4^{o}, 74.1^{o} which are assigned to (220), (200), and (111) planes of Cu cubic crystal respectively [JCPDS card no. 01-085-1326] as shown in **Fig. 4.2a**. They also exhibit small peaks at 2θ = 35.75° and 38.9° associated with the presence of CuO phase [JCPDS card no. 01-089-5899].

4.3.1.2. X-ray photoelectron spectroscopy

XPS was used to study the oxidation state of copper. It shows the two strong peaks at 951.4 eV and 931 eV, which correspond to Cu $2p_{1/2}$ and Cu $2p_{3/2}$ core levels respectively, confirming the metallic structure of the Cu nanoparticles [182]. The deconvoluted XPS spectrum is shown in **Fig. 4.2b**. Small satellite peak at 945.5 eV [112] was also observed suggesting that Cu NPs contain some oxide (at least on the surface) in minor proportion. The XRD also indicated the presence of CuO in the sample. It is important to note that because nano-sized Cu can be readily oxidized by O_2, it is possible that the observed CuO phase was formed during sample handling in air following insitu reduction [156].

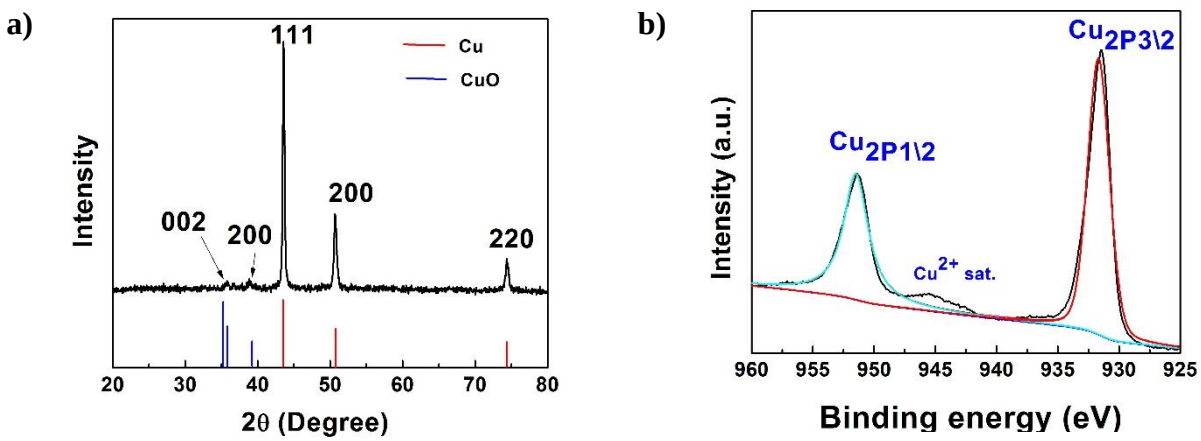

Fig. 4.2 a) *XRD patterns and* ***b)*** *High-resolution XPS spectrum recorded for citrate stabilized Cu NPs*

4.3.1.3. SEM and TEM analysis

Morphology and dispersion of nanoparticles greatly affect the electrode performance and selectivity [109]. **Fig. 4.3*a*** shows HR-TEM image of citrate stabilized Cu NPs together with their selected area electron diffraction patterns (**Fig. 4.3b**). The particles are observed to be nanostructured. The mean diameter of the Cu NPs is 20-30 nm. Large aggregates are observed due to the separation of Cu NPs from solvent. Selected area electron diffraction (SAED) image shows that Cu NPs are highly crystalline in nature with (111), (200) and (220) cubic planes of metallic Cu. EDX analysis shows that all the peaks are related to the chemical composition of nanoparticles and substrate, made of Cu, C, and O as shown in **Fig. 4.3*c*.** The elemental analysis of the sample confirmed the formation of 99 wt. % pure Cu NPs, which is in good accord with the results of XRD and XPS.

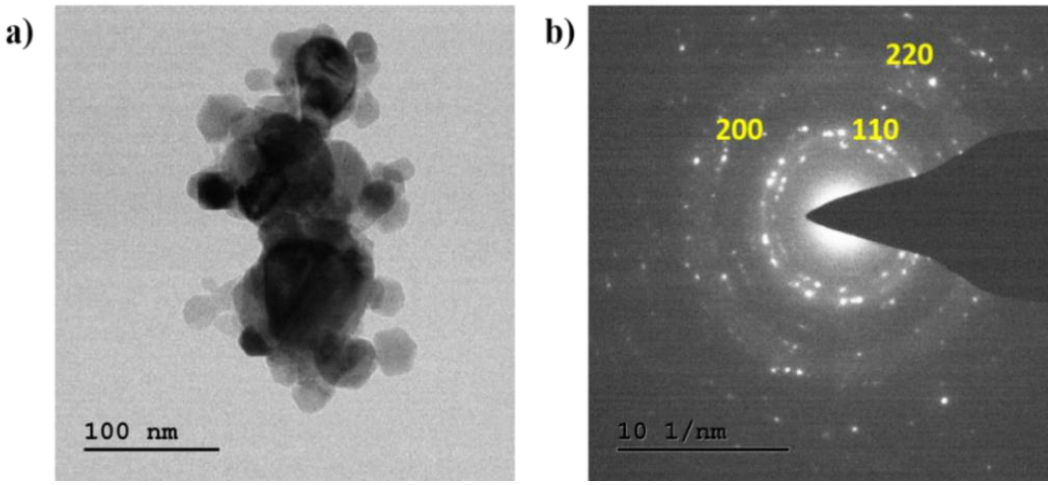

c)

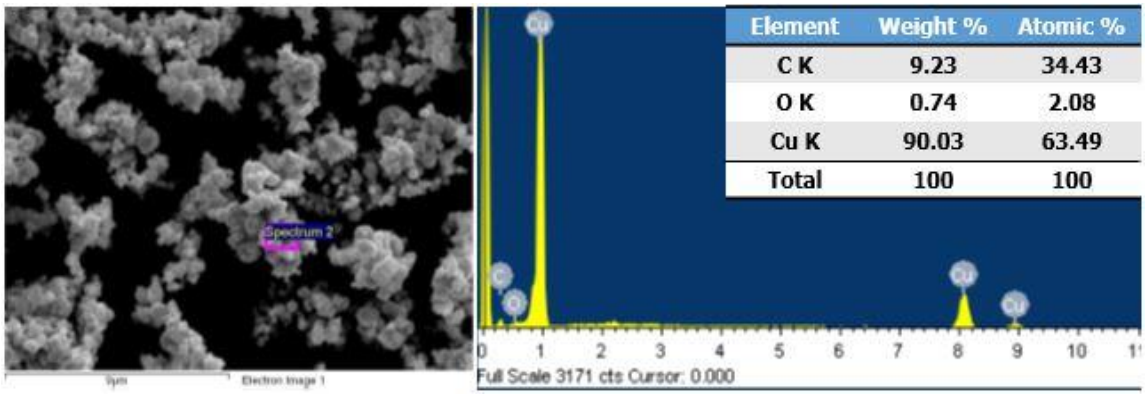

Fig. 4.3 a) *TEM image,* ***b)*** *SAED pattern, and* ***c)*** *SEM-EDX image of citrate stabilized Cu NPs*

4.3.1.4. Hydrodynamic size distribution

The hydrodynamic size distribution histogram of citrate stabilized Cu NPs is shown in **Fig. 4.4.** The mean hydrodynamic size of as synthesized Cu NPs was found to be 130 nm.

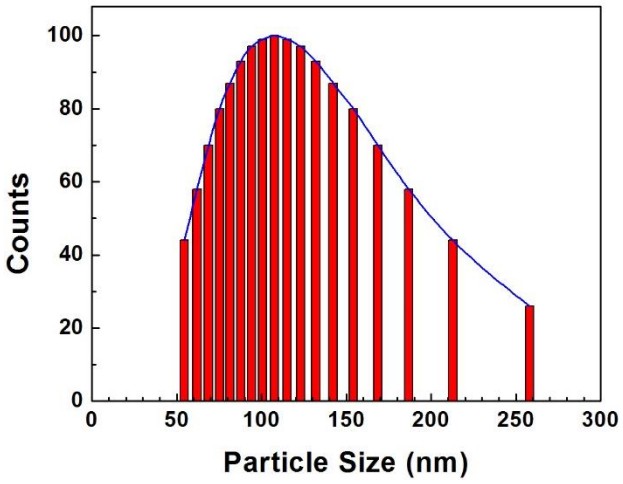

Fig. 4.4 *Hydrodynamic size distribution of citrate stabilized Cu NPs*

4.3.1.5. N_2 adsorption isotherms

Total surface area and pore size were studied by N_2 sorption method. As shown in **Fig. 4.5,** the effective pore diameter for Cu NPs is centered around 3-4 nm with maximum surface area of 630 $m^2.g^{-1}$. The synthesized Cu NPs have lots of micropores and high surface area, which favour the adsorption of CO_2 [183]. Summary of BET result is shown in **Table 4.1**.

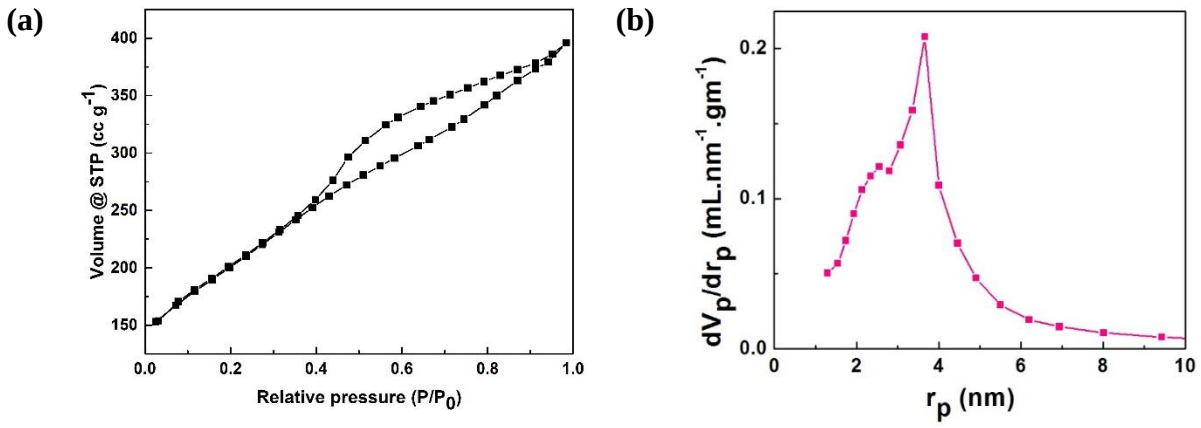

Fig. 4.5 (a) *Nitrogen adsorption/desorption isotherm and (b) pore size distribution by t-plot method of citrate stabilized Cu NPs*

Table 4.1 *Textural properties of Cu NPs (calculated from nitrogen adsorption-desorption)*

Material	Total surface area ($m^2 g^{-1}$)	Micro pore area ($m^2 g^{-1}$)	Total pore volume ($cm^3 g^{-1}$)	Micro pore volume ($cm^3 g^{-1}$)	Mesopore volume ($cm^3 g^{-1}$)
Citrate stabilized Cu NPs	630	115	0.528	0.062	0.466

4.3.1.6. Fourier-transform infrared spectroscopy

FTIR measurements were performed to study the surface modification of Cu NPs by citrate ions. **Fig. 4.6** shows FTIR spectra of (a) citrate stabilized Cu NPs, and (b) pure tri-sodium citrate crystal. In FTIR spectrum of the pure tri-sodium citrate, the bands at 1386 cm^{-1} and 1581 cm^{-1} are attributed to the symmetric and asymmetric stretching of COO− respectively. However, the FTIR spectrum of citrate stabilized Cu NPs shows many small peaks. Smaller bands at about 1386 cm^{-1} and 1561 cm^{-1} pertain to the symmetric and asymmetric stretching of COO− respectively. This low signal/noise ratio is attributed to low amount of citrate ions with respect to the copper [184]. The band at 1270 cm^{-1} and 1269 cm^{-1} corresponds to the –CO stretching in trisodium citrate and citrate stabilized Cu NPs respectively. Bonding of copper with trisodium citrate through –CO functionalities was indicated by decrease in its spectrum intensity of bands at 1270 cm^{-1} and 1269 cm^{-1}. Also, a wide band at 3445 cm^{-1} in pure trisodium citrate and citrate capped Cu NPs attributed to –OH stretching suggesting the capping of citrate ions on Cu surface.

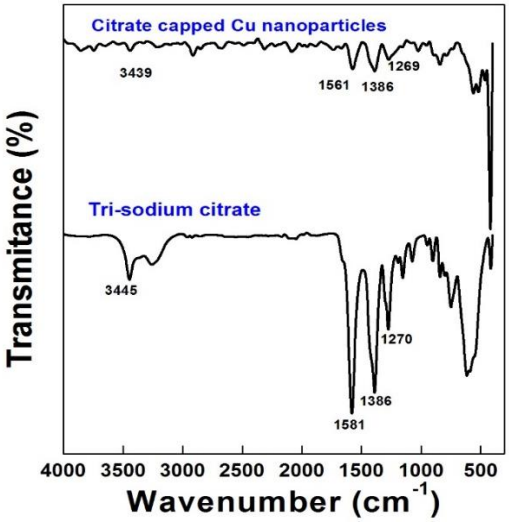

Fig. 4.6 *FTIR spectra of pure tri-sodium citrate and citrate capped Cu NPs*

4.3.2. Electrochemical characterization and performance measurement

4.3.2.1. Cyclic voltammetry (CV) study

Fig. 4.7a shows the cyclic voltammogram of the Cu NPs/carbon paper in N_2 (inert) and CO_2 saturated 0.1 M $KHCO_3$ taken at a scan rate of 10 mV s^{-1} between -0.4 V to -1.2 V (vs. RHE). Appreciable amount of CD response was observed in N_2 (inert) and CO_2 saturated 0.1 M $KHCO_3$ solutions. The CD observed in an inert atmosphere is primarily due to the electro-catalyst reduction and HER [185]. The CD in CO_2 saturated electrolyte solution is observed to be higher as compared to that in N_2 atmosphere. This increase in CD may be due to ECO_2R activity along with electro-catalyst reduction and HER. The saturation concentration of CO_2 in 0.1 M $KHCO_3$ (≈ 35 mM) [13]) leads to a downward shift of the CD curves suggesting the ECO_2R activity along with HER [89].

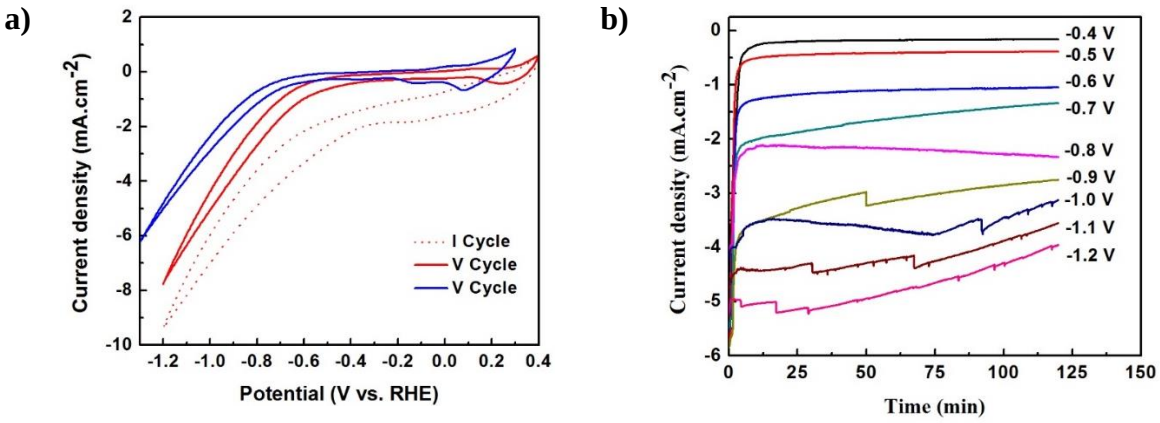

Fig. 4.7 a) *CV curves of Cu NPs/carbon paper in the N_2 (blue) and CO_2 (red) saturated 0.1M $KHCO_3$ electrolyte,* ***b)*** *Controlled-potential electrolysis curves for Cu NPs/carbon paper in 0.1 M $KHCO_3$ with continuous CO_2 bubbling at 20 mL min^{-1}*

4.3.2.2. Electrochemical CO_2 reduction and product distribution

Since CO_2 reduction and water splitting both are occurring at applied potentials during full CV study, it cannot give direct proof for any specific type of reaction occurring on the cathode surface. Therefore, controlled-potential electrolysis (CPE) was studied in a range from - 0.4 to -1.2 V (vs. RHE) for 2 h in CO_2 saturated 0.1 M $KHCO_3$ solution with continuous CO_2 supply to produce the CO_2 reduction products. **Fig. 4.7b** shows the CD normalized by geometric area versus time data for different applied potentials. It can be seen that a rapid decrease in CD from very high to a low value was observed at initial stage and further, it got stabilized. No product was observed (as per HPLC analysis) during this period, which indicates that all of the charge supplied was consumed for the electro-catalytic reduction itself.

At all the studied conditions, a mixture of reduction product with different selectivity was obtained, similar to reported in previous literature [35, 40, 186]. To verify the liquid products derived from dissolved CO_2, the electro-catalytic experiment was performed in N_2 saturated $KHCO_3$ solution (without CO_2 purging) at -0.8 V (vs. RHE). No peaks were observed in HPLC analysis after electrochemical reduction for 2 h, indicating all liquid products were coming from CO_2 rather than from the reduction of functional groups (i.e. HCO_3^-, COO^-, CO) present in stabilizing material of Cu NPs or electrolyte.

4.3.2.3. Electrochemical active surface area (ECASA)

The ECASA of the as-prepared working electrode after reduction was estimated based on the double layer capacitance (C_{dl}). More details on C_{dl} measurements were given in section 3.4.3. The CVs were taken between 0.30 and 0.50 V (vs. RHE) at various scan rates as shown in **Fig. 4.8**. It can be seen that Cu NPs/carbon paper has the C_{dl} of 1.17 mF cm^{-2}, which is much larger than that of bare carbon support (38 µF cm^{-2}), suggesting its largest effective ECASA for reduction of CO_2. Further, to estimate the surface roughness factor, the capacitance value of bare carbon paper support was subtracted from the capacitance value measured for Cu NPs/carbon paper, and divided by 0.036 mF cm^{-2} (reported capacitance value for electropolished copper foil) [159]. High roughness factor of 31.44 indicates that prepared electrode has more active sites for reduction of CO_2.

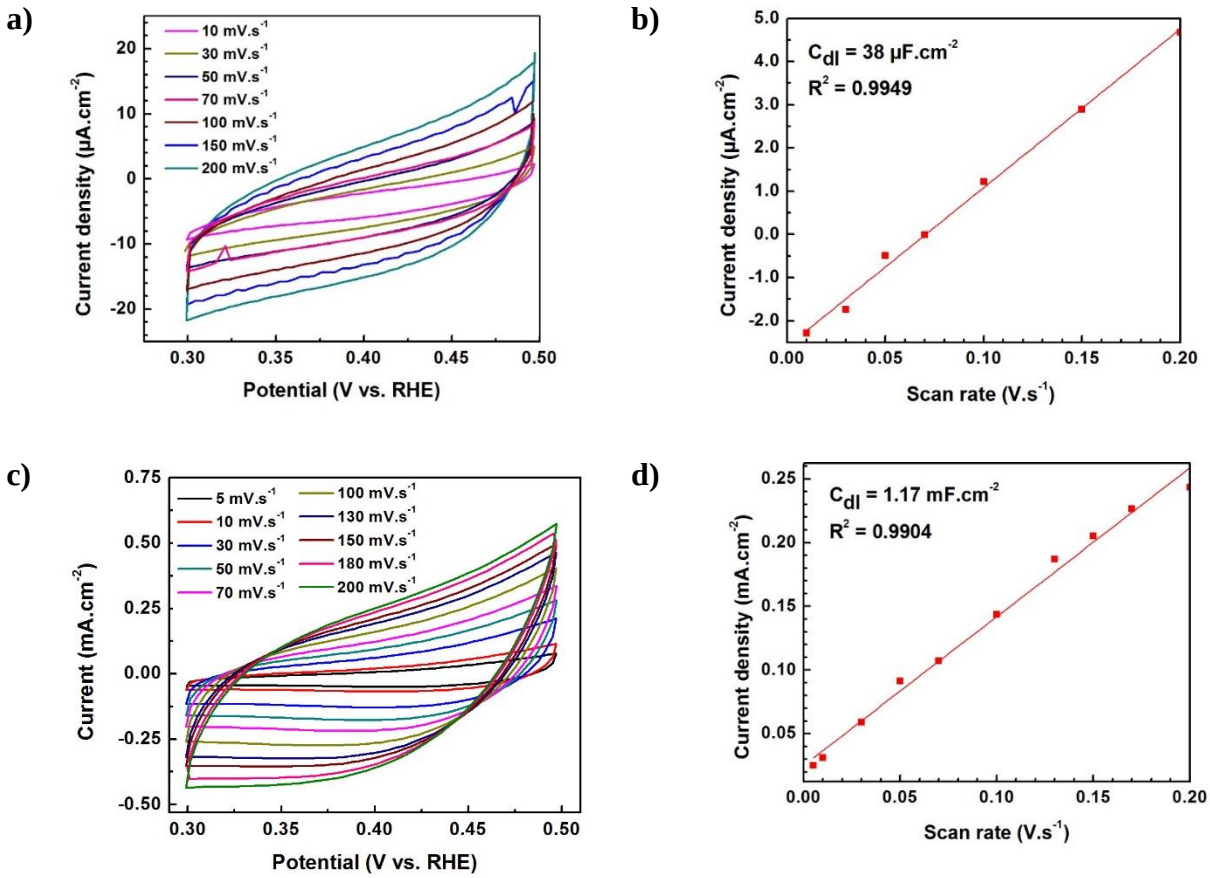

Fig. 4.8 *The cyclic voltammetry (CV) curves vs. RHE at the different scan rates (indicated by different colors) for the calculation of double layer capacitance of* ***a)*** *bare carbon support and* ***c)*** *catalyst coated electrode, The linear fitting of non-faradic current of various CV curves vs. different scan rates of* ***b)*** *bare carbon support and* ***d)*** *catalyst coated electrode*

4.3.3. Products vs. potential

Fig. 4.9 displays the concentrations of products, obtained after 2 h of reaction time at different electrode potentials, which are divided into two groups viz., major and minor products. Formic acid was identified as the major reaction product. At lowest applied potential (-0.4 V vs. RHE), the formic acid/fomate concentration was about 58 µM. It was increasing with increasing applied potential up to -0.9 V (vs. RHE) where a maximum formic acid concentration of 2.91 mM was observed and it decreased to 1.10 mM with further increase in applied potential to -1.2 V (vs. RHE). Similar trend was observed for other minor products. The minimum concentration of ethanol, n-propanol and acetic acid was detected at -0.8, -0.7 and -0.6 V (vs. RHE), respectively. The final concentration of all these products increased with an increase in applied potential from -0.6 to -1.0 V (vs. RHE), and a further increase in applied potential, resulted in decreased concentration. This may be due to the limited availability of CO_2 in CO_2 saturated aqueous 0.1 M $KHCO_3$ and the formation of gaseous products at such a high negative

potential greatly restricts the formation of more complex multi-carbon liquid products in higher concentrations.

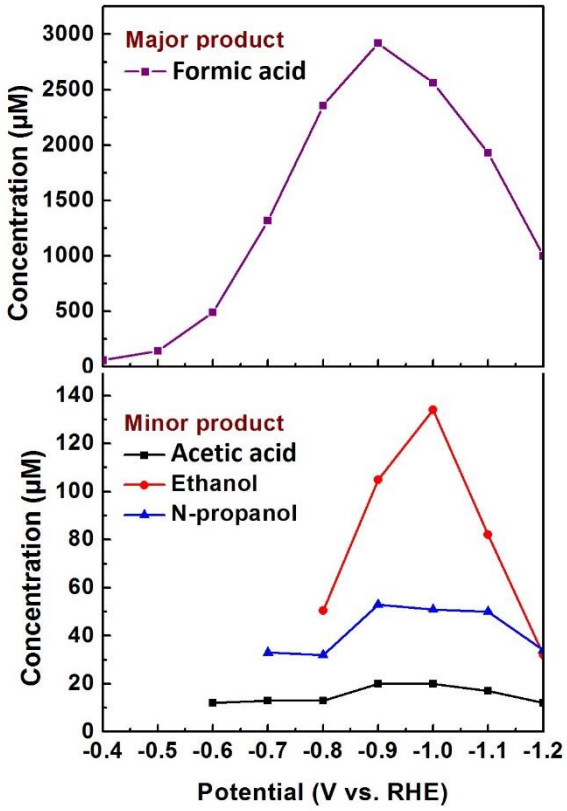

Fig. 4.9 *Concentration of liquid products produced after ECO_2R at different controlled potentials*

As shown in **Fig. 4.10**, formic acid formation rates at Cu NPs/carbon paper electrode are quite high ranging from 29 to 1460 μmol L^{-1} h^{-1} as compared to other products. Acetic acid yield ranged from 6 to 10 μmol L^{-1} h^{-1}, ethanol yield ranged from 16 to 67 μmol L^{-1} h^{-1} and n-propanol yields from 16 to 26 μmol L^{-1} h^{-1}. No acetic acid, ethanol, and N-propanol was not detected between -0.4 to -0.5 V (vs. RHE), -0.4 to -0.7 V (vs. RHE), and -0.4 to -0.6 V (vs. RHE) respectively. Formation rates of products typically increased with potential from –0.4 V (vs. RHE) and reached a maximum near - 0.9 V (vs. RHE), then decreased significantly at potentials more cathodic than - 0.9 V (vs. RHE) along with enhanced gas *bubble formation* at electrode surface probably due to hydrogen evolution or gaseous product generation.

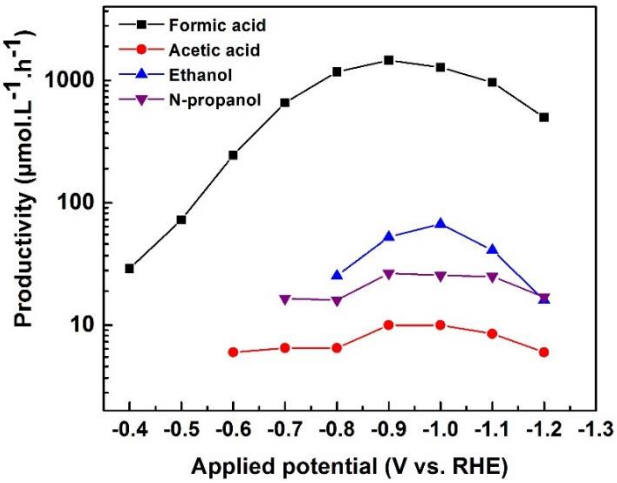

Fig. 4.10 *Productivity of liquid products at difference applied potentials*

Though from a practical point of view, final product concentration and production rate hold great relevance but the FE calculations are of critical importance for studying the product selectivity. **Fig. 4.11** shows the FE of liquid products as a function of applied potential. The maximum formic acid/formate concentration was obtained at -0.9 V (vs. RHE), but the FE was low ($FE_{(formate)}$= 25 %), which indicates that at this potential, the maximum charge was utilized in the formation of other product(s). Highest FE for formate/formic acid was 45.4 % at -0.8 V (vs. RHE). At lowest applied potential (i.e. -0.4 V), $FE_{(formate)}$ was 13.4 %. This is increased with applied potential up to -0.8 V (vs. RHE) and on further increase in potential the $FE_{(formate)}$ decreased. This can be explained by considering the mass transport of the reactants to the electrode surface. With an increase in current densities, significant reduction of the CO_2 concentration at the electrode surface takes place due to higher rate of CO_2 consumption and stronger HER. Due to the higher concentration in the bulk and higher diffusion coefficient, these protons become the dominant substrate. The maximum of 1.70 % FE for acetic acid was found at -0.6 V (vs. RHE) with a high and stable average CD of -1.3 $mA.cm^{-2}$. Similarly, maximum $FE_{(ethanol)}$ and $FE_{(n\text{-}propanol)}$ was around at -1.0 and -0.7 V (vs. RHE) with CD of -3.5 and -1.8 $mA.cm^{-2}$ respectively. Further, only formate was observed in liquid product using flat metallic copper foil at all applied potentials (**Fig. 4.12**), which is consistent with a previously reported ECO_2R of Cu polycrystalline foil [40, 187, 188]. Therefore, it is concluded that the porous structure of Cu NPs with more active surface area could facilitate adsorption and desorption of CO_2 and promote the accessibility of active sites, which are beneficial to the ECO_2R process. This hypothesis is supported by the fact that the porous Cu NPs prepared in this work was more effective than the non-porous metallic Cu foil reported by Yang et al. [189]

and Sen et al. [190]. The FE values obtained in this work are compared with other published reports in **Table 4.2**. Cu NPs used in this work represent one of the most effective electro-catalysts that can reduce CO_2 to liquid products. Moreover, the total FE for all liquid products are less than 60 % at –1.2 V (vs. RHE), Therefore, remaining charge (i.e. 40 %) may have been utilized in generating H_2, CO, etc.

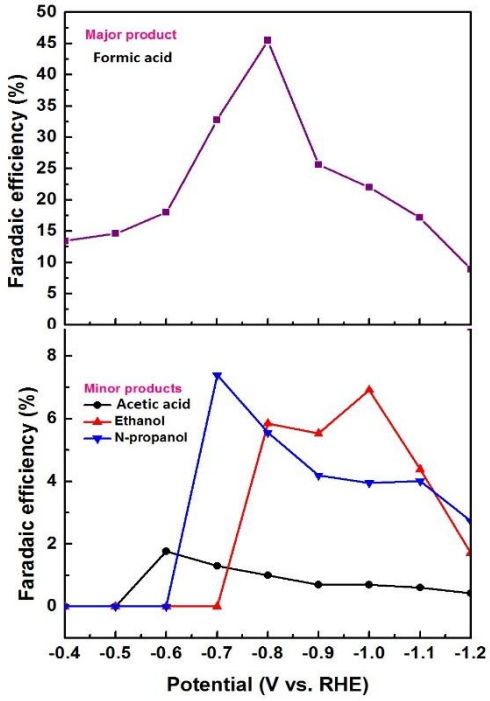

Fig. 4.11 *FE for product formation at different applied potentials*

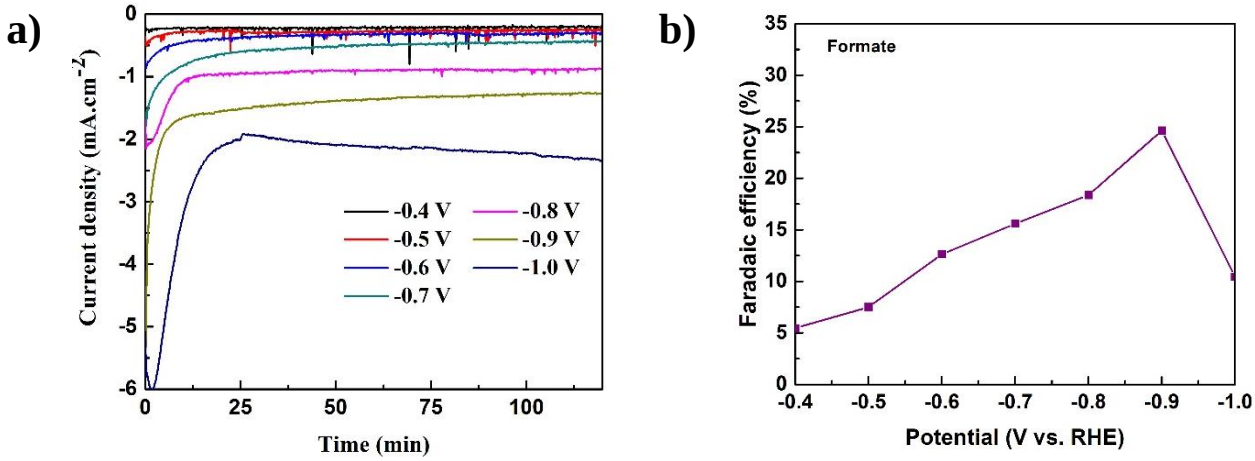

Fig. 4.12 a) *Controlled-potential electrolysis curves for flat Cu foil in 0.1 M $KHCO_3$ with continuous CO_2 bubbling at 20 mL.min^{-1},* ***b)*** *FE for product formation at different applied potentials*

Table 4.2 *Comparison of liquid products' FE obtained in this work with literature reported values*

Sr. No.	Electrode	Applied potential (V *vs.* RHE)	Electrolyte	FE (%)					Reference
				Methanol	Formic acid	Ethanol	Acetic acid	N-propanol	
1	Copper nanocrystals	-1.1	0.1 M $KHCO_3$	1	20	5	1.1	1	[191]
2	Cu_2O-derived Cu electrode	-1.0	0.1 M $KHCO_3$	NR	10	8.7	NR	NR	[34]
3	Cu foil	-1.15	0.1 M $KHCO_3$	1	5	9.8	0.3	3	[40]
4	Cu_2O derived Cu films	-0.98	0.1 M $KHCO_3$	NR	6	7.1	NR	5	[192]
5	Cu NPs/Cu disc	-0.95	0.1 M $KHCO_3$	ND	4.54	12.8	0.4	6.65	[193]
6	Cu NPs/carbon paper	-0.86	0.1 M $KHCO_3$	2	NR	16.6	0.6	12	[159]
7	Polycrystalline Cu	-1.41	0.1 M $KHCO_3$	NR	9.7	6.9	NR	3.0	[194]
8	Electrodeposited Cu_2O	−1.1	0.1 M $KHCO_3$	NR	22	NR	NR	NR	[195]
9	Electrodeposited Cu_2O	−1.22	0.1 M $KHCO_3$	NR	8	NR	NR	NR	[196]
10	Cu mesocrystals	−0.99	0.1 M $KHCO_3$	NR	4.3	NR	NR	NR	[197]
11	Cu NPs/carbon paper	-0.8	0.1 M $KHCO_3$	NR	45.4	5.84	1.00	5.55	**Present work**

**NR- Not reported*

4.3.4. Reaction kinetics/Tafel plot

The mechanistic insight on a Cu NPs and flat Cu foil was studied by Tafel analysis using partial CD of formate in 0.1 M $KHCO_3$ solution. Tafel slope of Cu NPs and flat Cu foil was found to be 154 mV dec^{-1} and 206 mV dec^{-1} respectively (**Fig. 4.13**). Decrease in the Tafel slope of Cu NPs compared to flat Cu foil further demonstrates the inherently improved efficiency of Cu NPs [188]. It is also observed that, at higher over-potentials, Tafel slope has increased indicating the effect of another rate-limiting step. In this case, the other consideration is most likely mass transport problems concerning the diffusion of products and reactants from / in the nanopores [198]. More experiments were conducted to provide further insight into the mechanism for reducing CO_2 on Cu NPs. The dependence of CO_2 reduction activity on CO_2 partial pressure was investigated from 0.1 to 1 atm, which shows an approximate first-order dependence on the concentration of CO_2 in the electrolyte (**Fig. 4.14**).

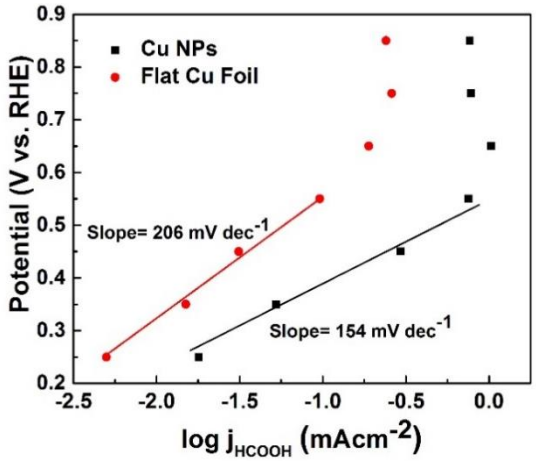

Fig. 4.13 *Tafel analysis on electrochemical CO_2 reduction on Cu NPs*

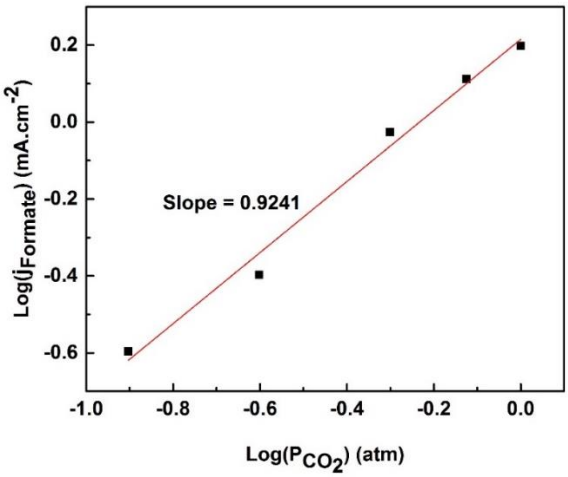

Fig. 4.14 *Formate partial CD ($j_{Formate}$) of Cu NPs vs. CO_2 partial pressure (P_{CO_2}) at constant potential of -0.8 V (vs. RHE)*

At lowest onset potential, only formate was observed which required two electrons. However, at higher over-potentials, more reduced products were observed. This suggests that, formate is generated with lowest kinetic barrier. Further, generation of C2-C3 products have higher kinetic barriers [40], and are generated at higher over-potential. As stated earlier, similar trend was observed for C2 and C3 product generation. For multi-carbon products, sufficient surface coverage and favorable reaction energies are required [199]. C-C coupling rate was initially increased with increasing over-potential and decreased with further increase in over-potential. This can be due to the mass transport problems as explained in previous paragraph. There are many possible explanations on reaction mechanism of different products. Based on some reports, *CO intermediates are more strongly bound on the Cu surface and converted into alcohols or hydrocarbons by *CO dimerization [194, 200]. It is also assumed that *CO dimerization is the key step in the selective reduction of *CO intermediates to $*C_2O_2$ or formyl species (*CHO) to produce alcohols on copper electrodes [167]. The different reaction pathways of Cu-based electro-catalysts and their corresponding main products (including CO, CH_4, C_2H_4, alcohols, etc.) are illustrated in **Fig. 4.15**. Here, * denotes a catalytic active site.

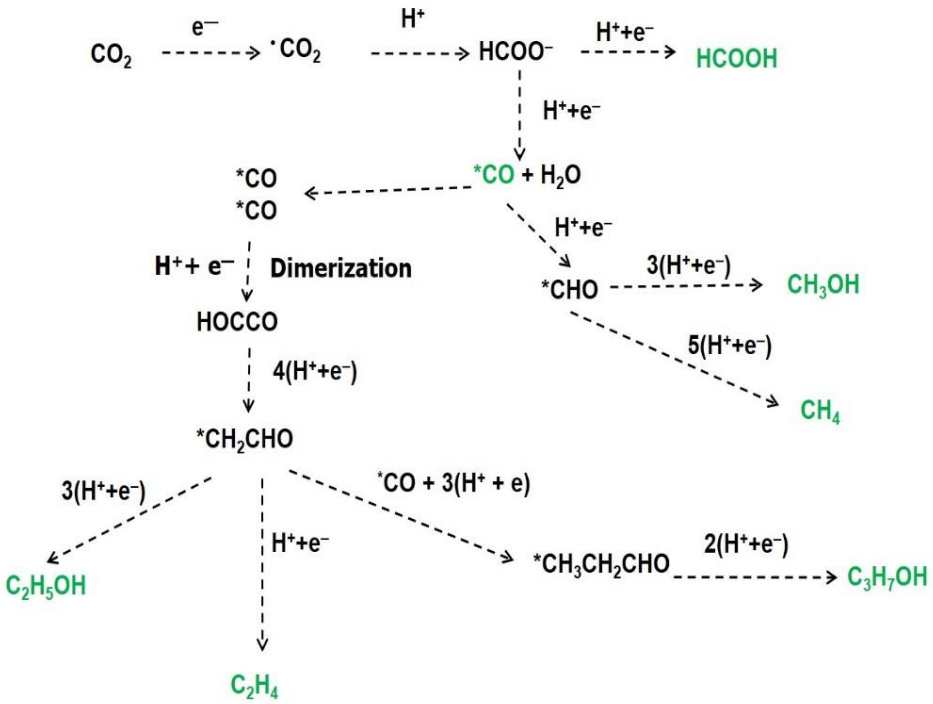

Fig. 4.15 *Possible reaction pathways for the electro catalytic reduction of CO_2 to products on Cu electrode (* in above equations denote a catalytic active site.)*

4.3.5. Long term performance and reusability study

The reusability of the working electrode after electrolysis was also studied. It is worth noting that the electrode after use could be easily washed with water and then reused for next reaction run under the same conditions. The FE of formate/formic acid could be maintained around 40±5 % for at least ten runs of repeated electrolysis at − 0.8 V (vs. RHE) as presented in **Fig. 4.16*a***, but the total FE of acetic acid, ethanol, and n-propanol reduced from 23% to about 5 %. The electro-catalytic activity of copper for C2 products decreased significantly with the deposition of poisoning species (i.e. graphitic carbon) on the electrode surface as reported by Bard et al. [201] and other investigators [167, 202]. Also, metallic impurities from electrolyte solution can be adsorbed on catalyst surface due to a higher rate of OH− production (or H+ consumption) and K+ transfer into the catholyte at higher current densities. This is supported by appearance of K signal in EDX analysis after 20 h of ECO_2R (**Fig. 4.18**). Hydrogen evolution continued at this very negative potential on the poisoned surface, but CO_2 reduction to products, which requires active Cu surface, decreased. Long term performance of Cu NPs was also tested at constant cathode potential of −0.8 V (vs. RHE) for 20 h. The CD was kept a steady value at around 2.5 mA cm^{-2} throughout the duration of the test (in **Fig. 4.16b**). A slight disturbance in CD was observed due to minor fluctuations in CO_2 flow rate.

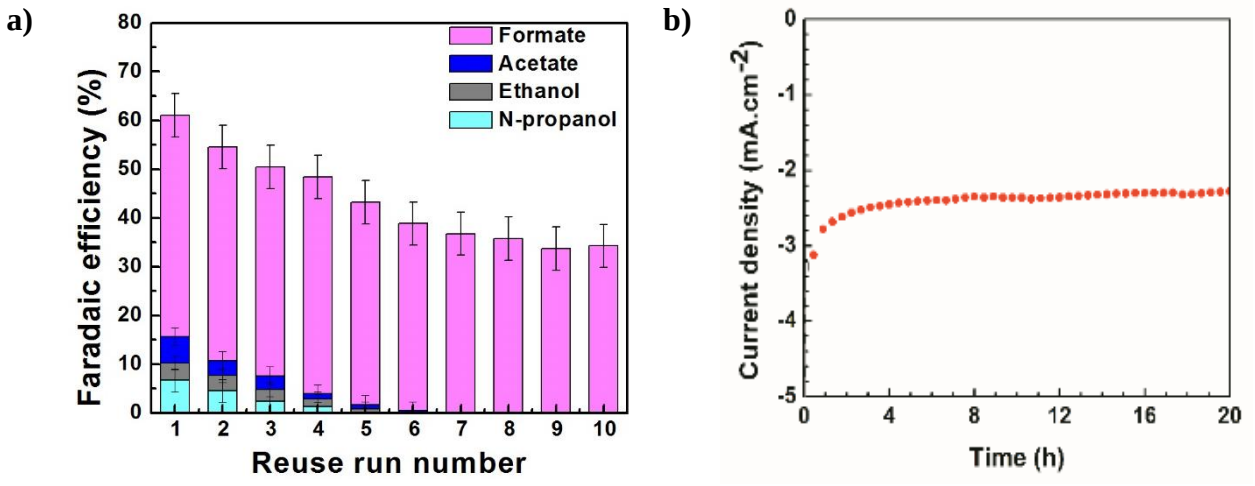

Fig. 4.16 a) *FE of products during reuse test performance and* ***b)*** *Long-time test performed at -0.8 V (vs. RHE) cathode potential using Cu NPs/carbon paper as working electrode*

4.3.6. Post characterization

To further study the morphology and phase of electro-catalyst after the CO_2 electro-reduction reaction for 20 h, post characterizations like SEM and XRD have been carried out, and the corresponding results are shown in **Fig. 4.17** and **Fig. 4.18**. Before ECO_2R, the characteristic XRD peaks at 2θ of 43.3º, 50.4 º, 74.1º are assigned to (220), (200), and (111) planes of Cu cubic crystal respectively [JCPDS card no. 01-085-1326]. Two small peaks at 35.7 º and 38.4 º are assigned to oxidized CuO and Cu_2O species, respectively, indicating that the minor amount of Cu^+ and Cu^{2+} phase is also present in Cu NPs. After the ECO_2R, the initial small peaks at 35.7 º and 38.4 º of Cu^{2+} and Cu^+ species disappeared due to the electrochemical reduction. The metallic Cu remained in cubic crystal shape after long term performance for 20 h ECO_2R, indicating the relative stability of the as-made Cu NPs. Furthermore, no apparent changes were observed in morphology (**Fig. 4.18**), implying the good stability of the Cu NPs.

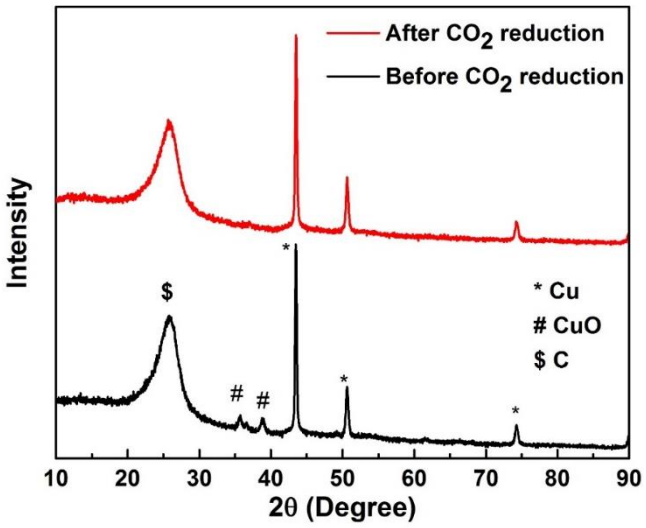

Fig. 4.17 (a) *XRD patterns of Cu NPs/CP before and after electro-catalytic test*

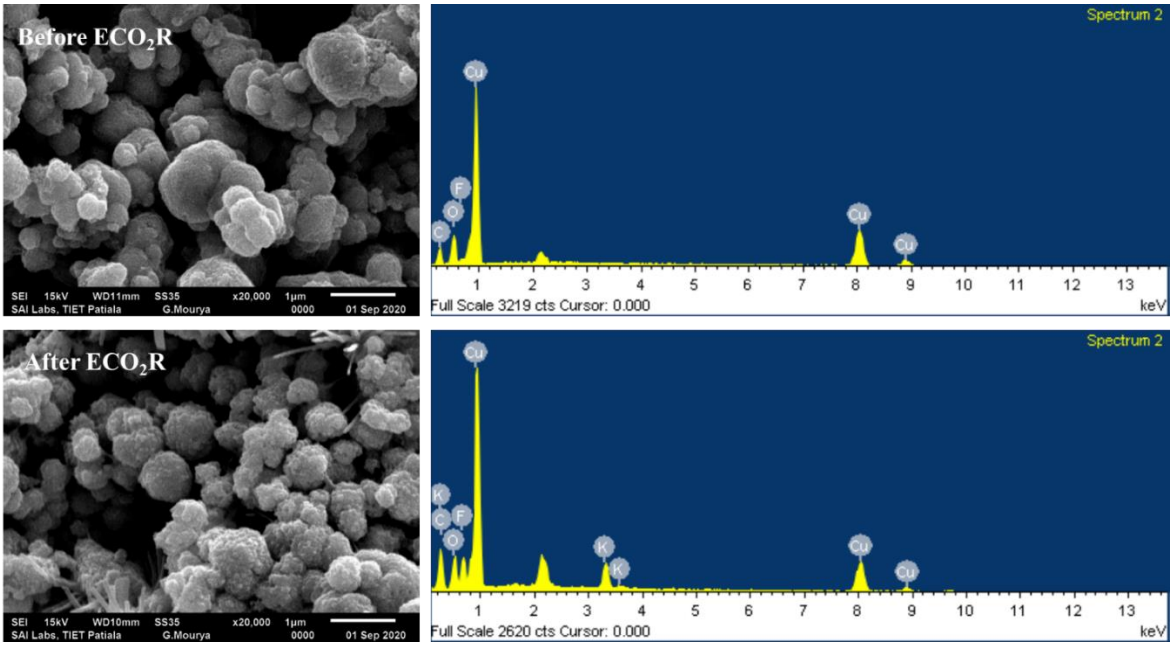

Fig. 4.18 *SEM image and corresponding EDX analysis of Cu NPs/CP before and after ECO_2R, In EDX spectra, C signals arise from carbon paper, stabilizing agent and Nafion, O and F elements are attributed to Nafion*

4.4. Conclusions

Copper nanoparticles having a high surface area (630 $m^2\ g^{-1}$) and total pore volume of 0.528 $cm^3.g^{-1}$ with micropore volume of 0.062 $cm^3.g^{-1}$ have been synthesized and found to be in pure metallic state. The electro-catalytic properties of the nanoparticles towards CO_2 reduction to chemicals in aqueous electrolyte have been studied. The synthesized nanoparticles show electro-catalytic reduction activity towards formate/formic acid, acetate, ethanol and n-propanol formation after coating on the carbon paper. In 2 h ECO_2R, total ~58% FE is observed for the liquid products. The favorable electrode potential is fund to be 0.8 V (vs. RHE) and at this potential, the concentration of formic acid/formate, acetic acid, ethanol and n-propanol are about 2.35, 0.013, 0.050 and 0.032 mM respectively. It is believed that nanoporous Cu NPs have great potential in developing efficient and green routes for ECO_2R to produce useful chemicals and fuels.

(This work has been published in Applied Surface Science, 537 (2021) 148020. DOI: https://doi.org/10.1016/j.apsusc.2020.148020 (IF = 6.707))

Chapter 5- Electrochemical CO_2 reduction on metallic Cu_x/NGN

5.1. Synthesis of Cu_x/NGN

In the first step, the mixture of 200 mg NGN and 200 mL deionized water was sonicated for 30 min to obtain a uniform dispersion. Then, under continuous stirring, the desired amounts of copper(II) chloride salt and tri-sodium citrate were added. The homogeneous suspension of the NGN consisting of Cu ions and citrate ions was heated to 60 ^oC in a water bath. The desired amount of preheated (60 ^oC) hydrazine hydrate was then added gradually and stirred for another 30 min to reduce copper(II) chloride salt and allow Cu nanocrystal growth on the surface of NGN. Later, the temperature of suspension was lowered to room temperature and dispersed Cu_x/NGN (here, x represents wt.% of copper on NGN) was separated by centrifugation. The supernatant was discarded and the sediment consisting Cu_x/NGN was washed by ultrapure water and ethanol for several times. Finally obtained catalyst was then dried overnight at 80 ^oC. The amounts of the precursors and reagents used for preparation of all the electro-catalysts are listed in **Table 5.1**. The block diagram for the synthesis of Cu_x/NGN is shown in **Fig. 5.1**.

Table 5.1 *Amounts of ingredients used in the preparation of Cu_x/NGN catalysts*

Sr. No.	Sample	NGN (mg)	$CuCl_2.2H_2O$ (mg)	Water (mL)	$N_2H_4.H_2O$ (mL)	$Na_3C_6H_5O_7 \cdot 2H_2O$[#] (gm)	Expected mass content of Cu (wt.%)
1	NGN	200	0.00	200	5	2	0
2	Cu_{10}/NGN	200	59.60	200	5	2	10
3	Cu_{20}/NGN	200	133.66	200	5	2	20
4	Cu_{30}/NGN	200	230.09	200	5	2	30

[#] The amount of $Na_3C_6H_5O_7 \cdot 2H_2O$ is adequate for complexing Cu^{2+}

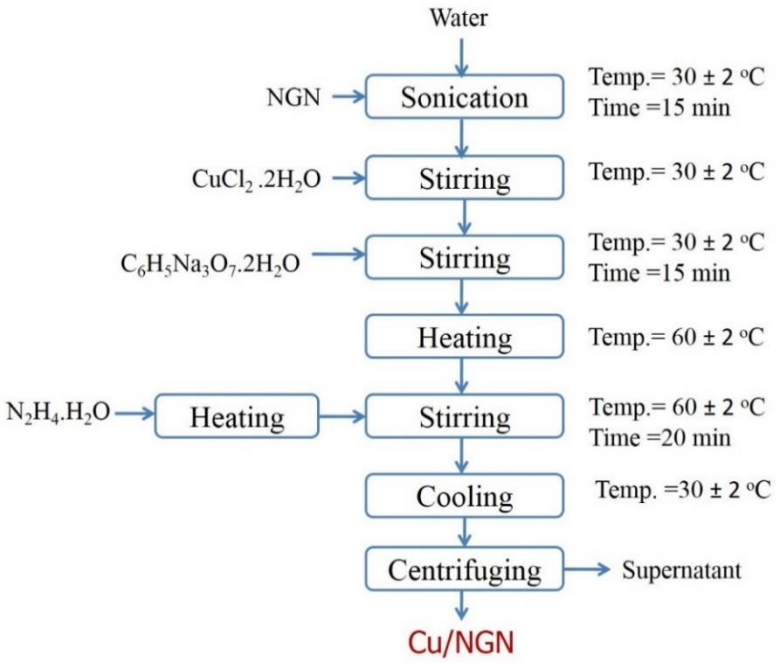

Fig. 5.1 *Block diagram for the preparation of Cu_x/NGN*

5.2. Preparation of working electrodes

The working electrode was prepared using following procedure. The mixture of electro-catalyst powder (4 mg), iso-propanol (1 mL), and Nafion solution (30 µL) was sonicated for 30 min to obtain homogeneous catalyst ink. One part of obtained ink (250 µL) was coated on the pretreated carbon paper (refer section 3.5.2. to get 1 mg cm^{-2} catalyst loading. Further, coated carbon paper was dried overnight in an oven at 80 °C to obtain a final working electrode.

5.3. Results and discussion

5.3.1. Physico-chemical characterization

5.3.1.1. X-Ray diffraction (XRD)

The crystal structures of the Cu_x/NGN were studied by XRD analysis. **Fig. 5.2** shows the XRD patterns of the four electro-catalysts of different Cu loadings. The peak at 2θ = 26.18° shows the diffractions of the (002) planes of crystalline structure of NGN (JCPDS# 03-065-6212). For all the Cu_x/NGN catalysts, other than the characteristic NGN peak, diffraction peaks of cubic metallic Cu phases of (111), (200), and (220) at 2θ = 43.38°, 50.30°, and 74.01° respectively, were identified (JCPDS number 01-085-1326). This indicates that Cu NPs were successfully deposited on the surface of NGN. Interestingly, stronger peak intensities were observed for higher Cu loading than the lower Cu loading on NGN. This reveals that the

formation of larger size Cu NPs due to agglomeration at higher loadings resulted in stronger XRD pattern. Also, the intensity of diffraction peak of C for NGN is decreasing with an increase in Cu loading due to the relatively higher peak intensities of Cu than that of NGN. Sample also shows two small peaks at 2θ = 35.75° and 78.6° associated with the presence of CuO phase [JCPDS card no. 01-089-5899] in minor quantity. Nano-sized Cu can be readily oxidized by O_2 present in air during sample handling following in situ reduction [156]. Energy dispersive X-ray analysis of Cu_x/NGN also supports this finding as presented in **Fig. 5.7**. The Debey-Scherrer´s equation (equation 3.4) [203] was used to calculate crystallite sizes (d). For this (002) NGN peak (at 2θ = 26.18º) and (111) copper peak (at 2θ = 43.38º) were used to calculate NGN and Cu NPs crystallite size respectively and the results are shown in **Table 5.2**. It is found that with increasing Cu loading on NGN, the crystallite size of Cu NPs increased from 17.50 to 32.53 nm, suggesting a possible grain growth.

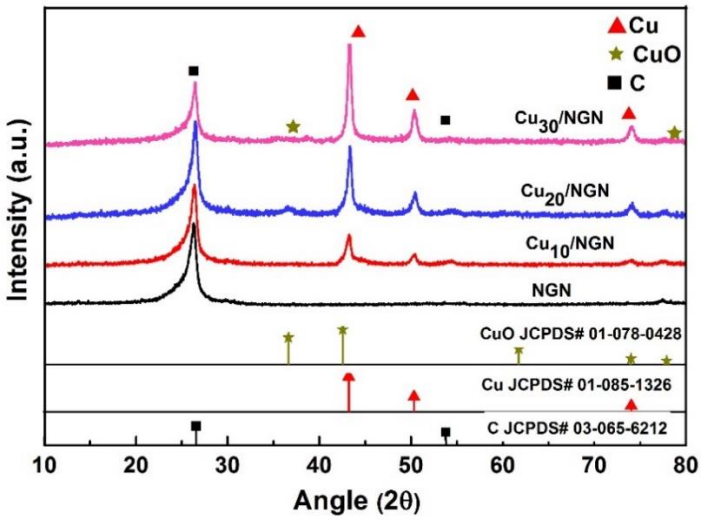

Fig. 5.2 *XRD patterns of NGN, Cu_{10}/NGN, Cu_{20}/NGN and Cu_{30}/NGN*

Table 5.2 *XRD analysis results for the NGN and Cu_x/NGN catalysts*

Catalyst sample	**FWHM (2θ)**	**Crystallite size (nm)**
NGN	0.6368	13.39
Cu_{10}/NGN	0.5132	17.5
Cu_{20}/NGN	0.3814	23.42
Cu_{30}/NGN	0.2746	32.53

5.3.1.2. X-ray photoelectron spectroscopy

X-ray photoelectron spectroscopy (XPS) was used to study the surface composition of the electrodes. The presence of C, N, O and Cu elements in the survey spectrum (**Fig. 5.3**) demonstrates that Cu is present in NGN. The total N-content of 2.36, 2.13, 1.75, and 2.13 atom % was observed in Cu_{20}/NGN, NGN, Cu_{10}/NGN and Cu_{30}/NGN respectively. The N 1s XPS spectra of Cu_{20}/NGN, NGN, Cu_{10}/NGN and Cu_{30}/NGN (**Fig. 5.4**) were deconvoluted into three main component peaks, corresponding to pyridinic N (398.2 eV), pyrrolic N (400.5 eV) and, graphitic N (401.3 eV) [77, 204]. The percentage of pyridinic, pyrrolic, and graphitic N atoms were 21/60/19, 27/67/6, 28/54/18, and 21/68/11 for NGN, Cu_{10}/NGN, Cu_{20}/NGN, and Cu_{30}/NGN, respectively, indicating similar nitrogen groups for all the samples. Many authors have reported that pyridinic N and graphitic N contents adjacent to carbon atoms provide active sites for ECO_2R and the presence of pyrrolic-N suppresses H_2 evolution reaction (HER) [21, 205]. Therefore, the high content of pyridinic-N and coexistence of pyrrolic-N and graphitic-N in the Cu_x/NGN would exhibit a high electro-catalytic activity towards ECO_2R.

The surface composition and oxidation state of Cu inside the Cu_x/NGN was analyzed by the high resolution Cu 2p XPS spectra. The characteristic doublet peaks were observed at ~934.1 eV and 953.8 eV in all Cu_x/NGN samples (**Fig. 5.5**), which is related to Cu 2p3/2 and Cu 2p1/2 respectively confirming the presence of Cu^0 /Cu^+. The shake-up satellite peaks observed at 941.4 eV and 944.6 eV are typical characteristics of presence of CuO on the surface [206]. Moreover, the difference between Cu 2p3/2 and Cu 2p1/2 core-level peak regions is of 19.7 eV which also confirms the presence of Cu^0 /Cu^+ only. In general, since the binding energy values of Cu^0 and Cu^+ regions are very close to each other, it cannot be differentiated. Therefore, to confirm the different oxidation states of the sample present in the surface, the peak positions of LMM-2 Auger transitions were used. From the LMM-2 Auger spectrum, the peak position at 569.0 eV corresponding to the presence of elemental Cu only (88.13 atomic %) [207] with small amount of CuO (11.87 atomic %) on the surface is confirmed.

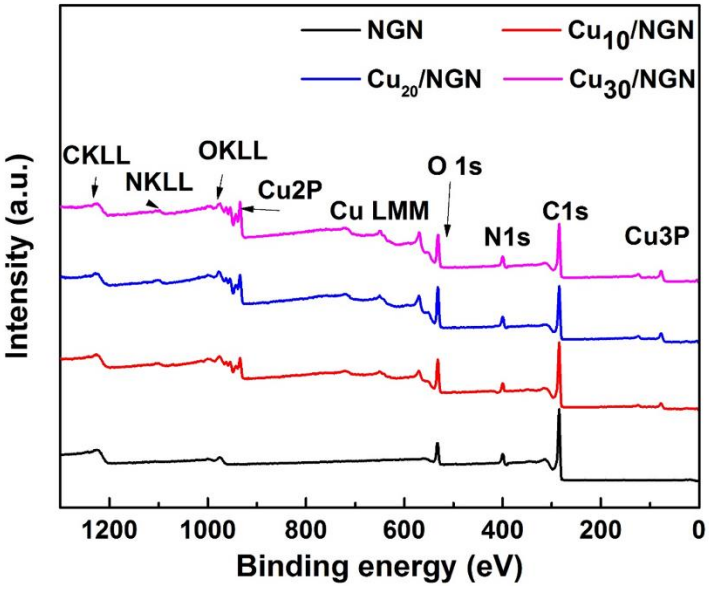

Fig. 5.3 *Full XPS spectra of NGN, Cu_{10}/NGN, Cu_{20}/NGN and Cu_{30}/NGN*

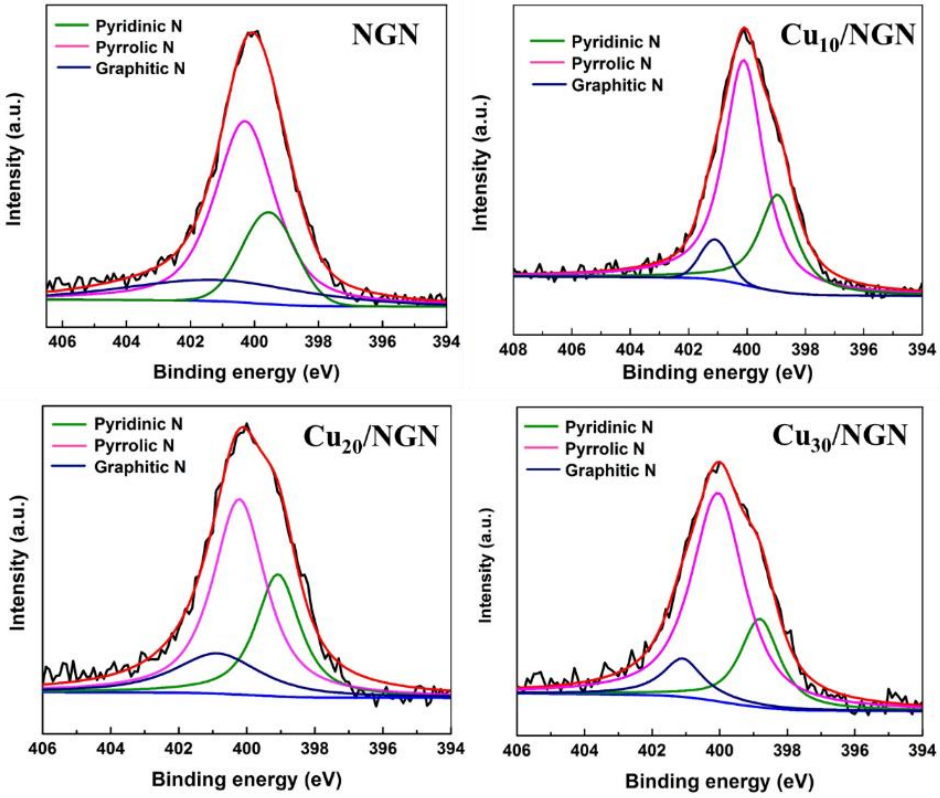

Fig. 5.4 *The XPS spectra of deconvoluted N1s peak of Cu_{10}/NGN, Cu_{20}/NGN, and Cu_{30}/NGN*

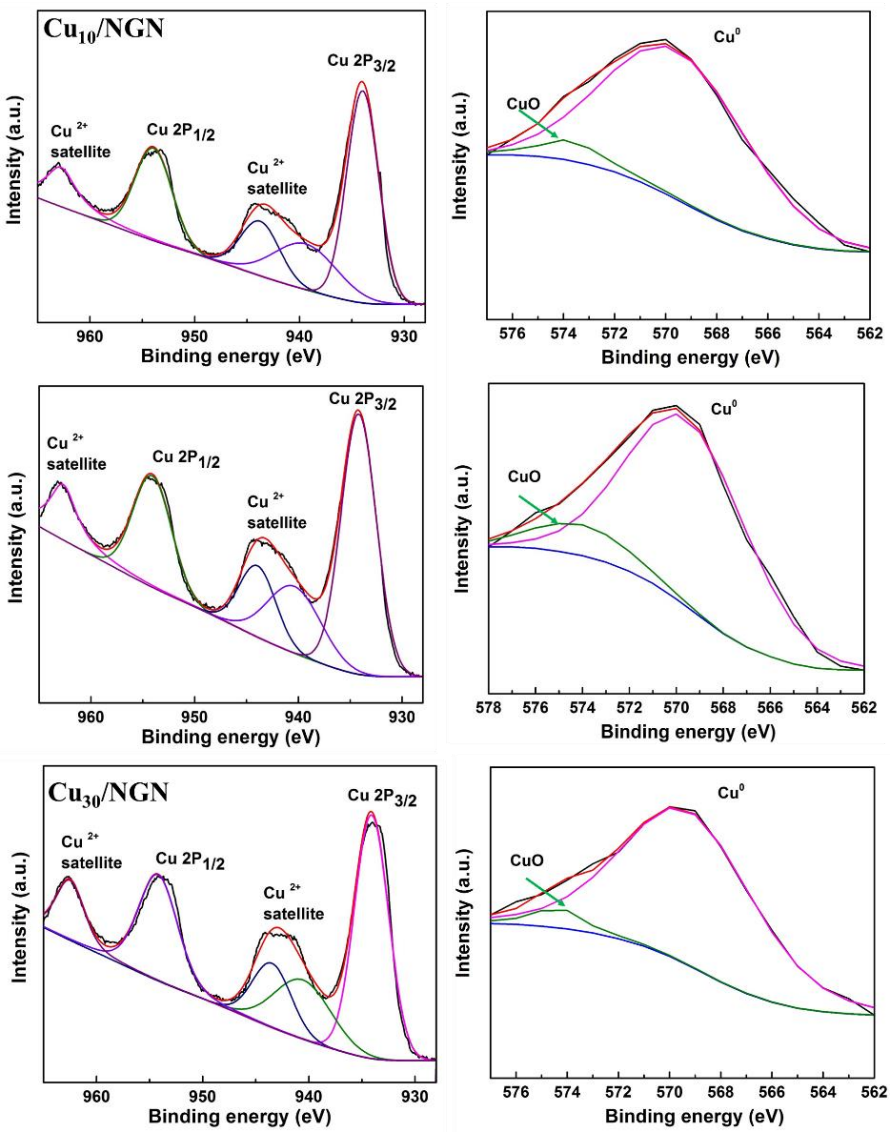

Fig. 5.5 *The XPS spectra of deconvoluted Cu 2P peak of Cu_{10}/NGN, Cu_{20}/NGN, and Cu_{30}/NGN along with Auger spectra*

5.3.1.3. SEM-EDX analysis

Fig. 5.6 shows SEM images of all four electro-catalysts. NGN shows smooth and wrinkled texture. SEM images of Cu_{10}/NGN and Cu_{20}/NGN show that the Cu NPs are homogenously dispersed on the NGN surface. However, further increase in the Cu loading, agglomeration was observed as a result, particle size increased. These results are also supported by XRD. The energy dispersive X-ray spectra (EDX) of Cu/NGN (**Fig. 5.7**) shows the presence of copper and carbon in the sample. This depicts that the Cu is successfully deposited on NGN. Uniform distribution of metals on support enhances the activity of the electro-catalysts [208].

5.3.1.4. TEM analysis

The dispersion of Cu NPs on sheet-like NGN was confirmed by TEM (**Fig. 5.8**). Moreover, increasing the concentration of Cu resulted in the formation of larger particles and agglomerates, suggesting less active sites for CO_2 reduction [209]. HR-TEM image (**Fig. 5.8** inset) shows crystalline domains with an estimated interlayer distance of 0.214 nm, which can be directed as the (111) plane of Cu. The SAED patterns of Cu_x/NGN (**Fig. 5.9**) show well-aligned bright spots with concentric diffraction rings specific to different crystalline planes, suggesting a polycrystalline area consisting of randomly oriented crystallites.

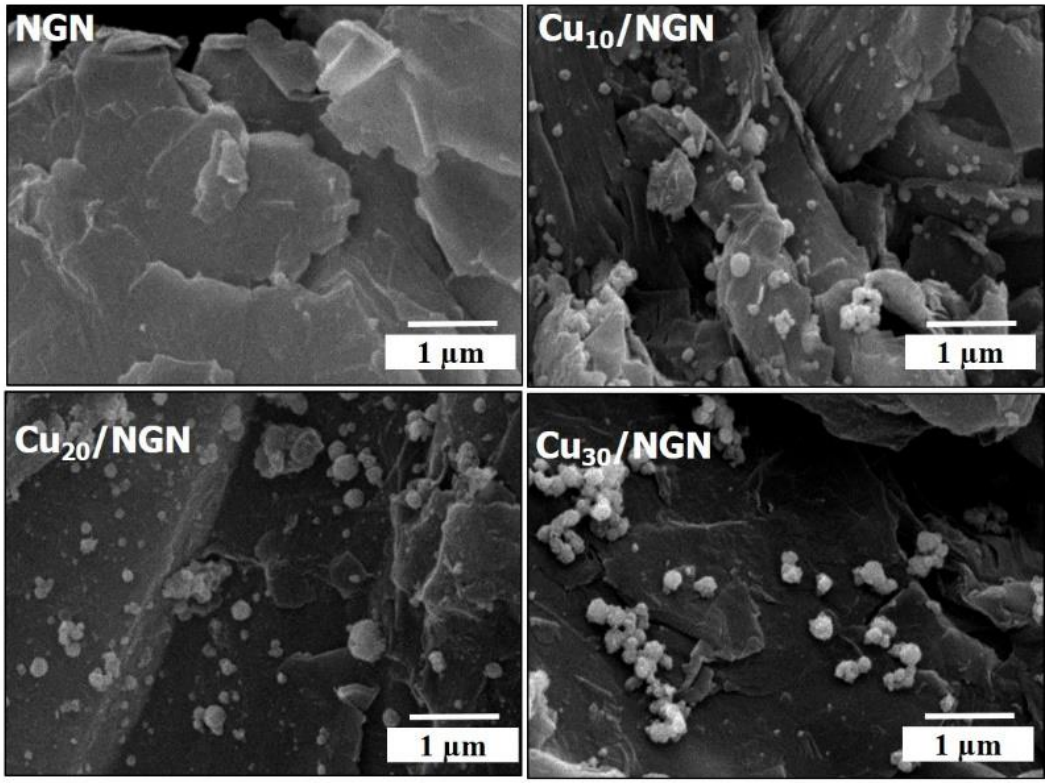

Fig. 5.6 *SEM images of NGN, Cu_{10}/NGN, Cu_{20}/NGN and Cu_{30}/NGN*

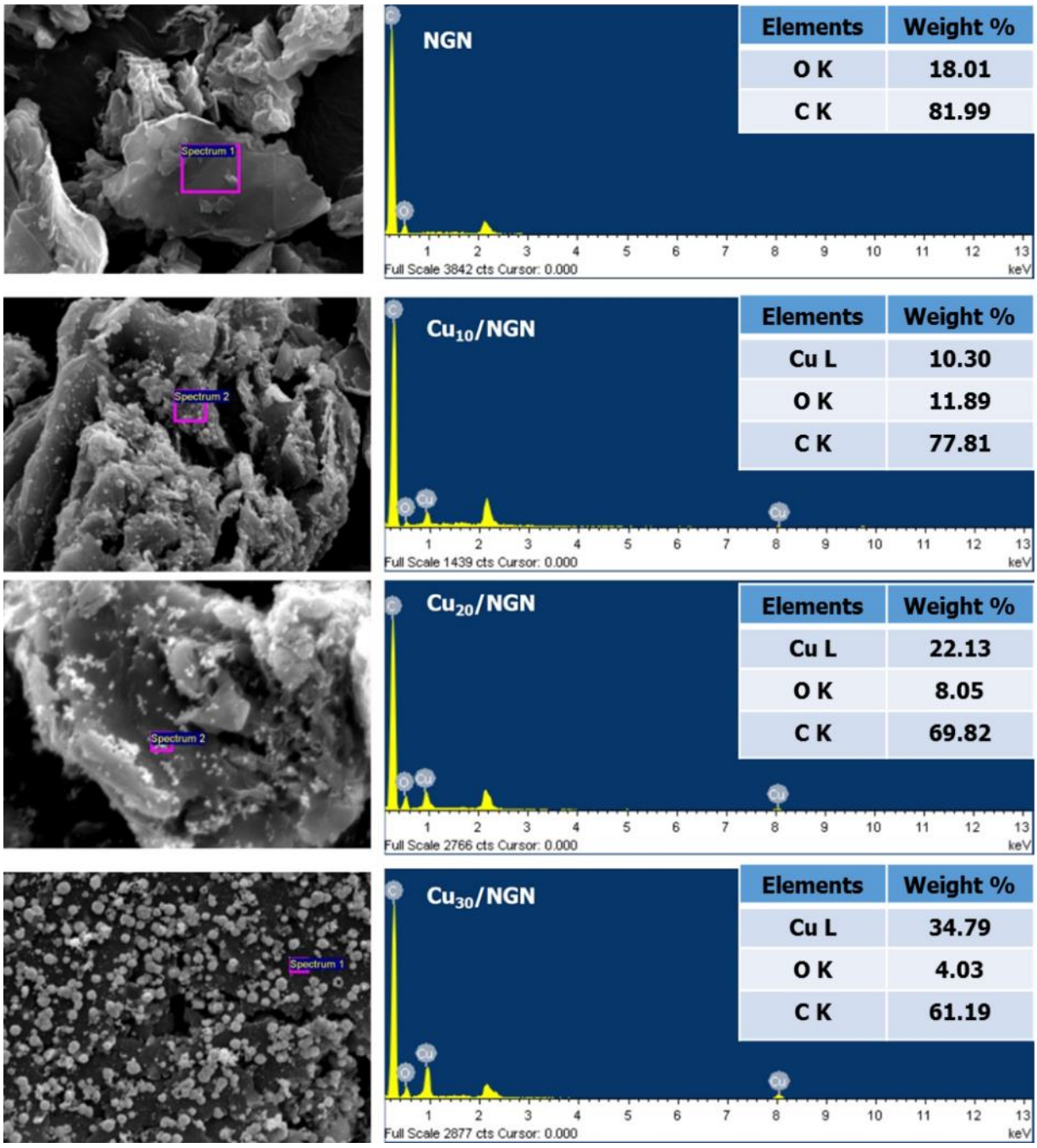

Fig. 5.7 *SEM images of NGN, Cu_{10}/NGN, Cu_{20}/NGN and Cu_{30}/NGN along with EDS spectra*

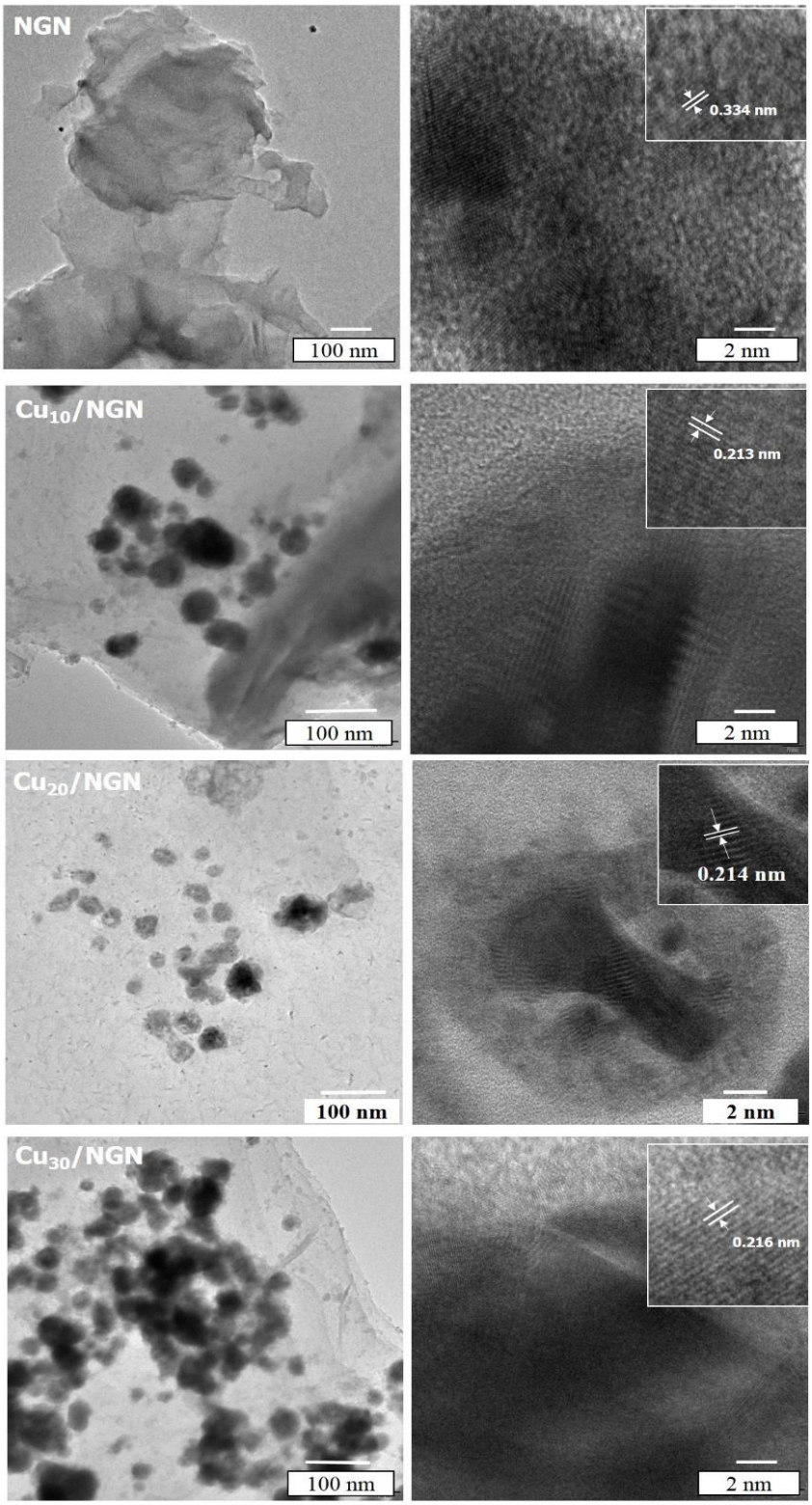

Fig. 5.8 *TEM images of NGN, Cu_{10}/NGN, Cu_{20}/NGN and Cu_{30}/NGN along with high resolution transmission electron images centered on Cu surface (The inset is an enlargement of the lattice, corresponding to atomic plane of Cu.)*

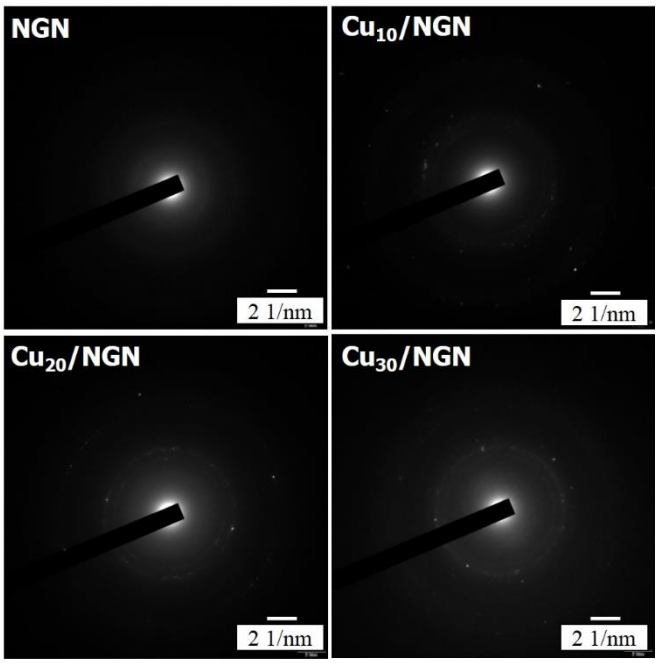

Fig. 5.9 *SAED spots and ring patterns of NGN, Cu_{10}/NGN, Cu_{20}/NGN and Cu_{30}/NGN*

5.3.1.5. Raman spectroscopy

Raman spectroscopy was performed on the samples to characterize structural features of carbonaceous materials. The D-band and G-band peak positions are centered at 1350 cm^{-1} and 1575 cm^{-1} respectively (**Fig. 5.10**). The ratio of I_d/I_g (intensity of the D-band to G-band) of the Cu_x/NGN samples (1.14) is lower than that of the NGN sample (1.83). This indicates that the Cu NPs anchored at the defect sites rather than at ordered surfaces of the NGN. This improves the electron flow, thus enhancing the CD, ultimately giving efficient reduction of CO_2 to different value added products [210]. Additionally, peak which appeared at approximately 620 cm^{-1} in Cu_x/NGN is an indication of presence of CuO [211]. The obtained results are supported by SEM, TEM, XRD, and XPS as discussed in previous sections.

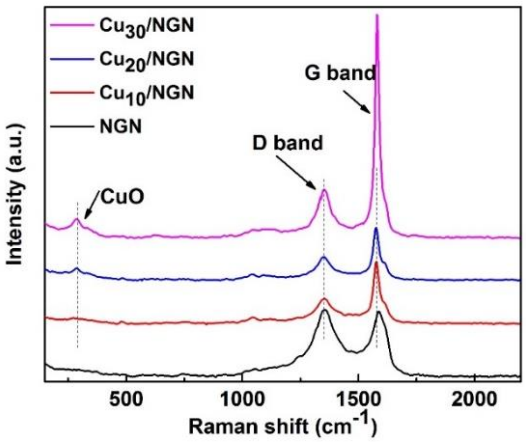

Fig. 5.10 *Raman spectra of NGN, Cu_{10}/NGN, Cu_{20}/NGN and Cu_{30}/NGN*

5.3.1.6. N_2 adsorption isotherms

The surface area and pore size distribution of the electro-catalysts were studied by Brunauer-Emmett-Teller (BET) method. As shown in **Fig. 5.11a**, the NGN shows a type IV adsorption isotherm with a hysteresis loop in the P/Po range of 0.4–1.0, indicating the formation of micro, meso- and macropores in the sample [212]. The Cu_{10}/NGN, and Cu_{20}/NGN show type IV isotherm with larger amounts of meso- and macro-pores of ca. 10-30 nm in diameter, as evidenced by DFT pore size distribution analysis (**Fig. 5.11b**). The Cu_{30}/NGN also shows type IV isotherm but having low surface area and less porosity. The obtained BET specific surface area is 41.56, 17.04, 16.2, and 10.28 $m^2\ g^{-1}$ for NGN, Cu_{10}/NGN, Cu_{20}/NGN and Cu_{30}/NGN, corresponding to the total pore volume of 0.1292, 0.0849, 0.0124, and 0.01 $cm^3\ g^{-1}$, respectively. The specific surface area decreased with increase in Cu loading due to contribution of low surface area Cu NPs compared to NGN. The hierarchically porous structure of NGN promotes mass transfer during the ECO_2R process and provides more active N_2-doped sites, thus enhancing the ECO_2R performance [204].

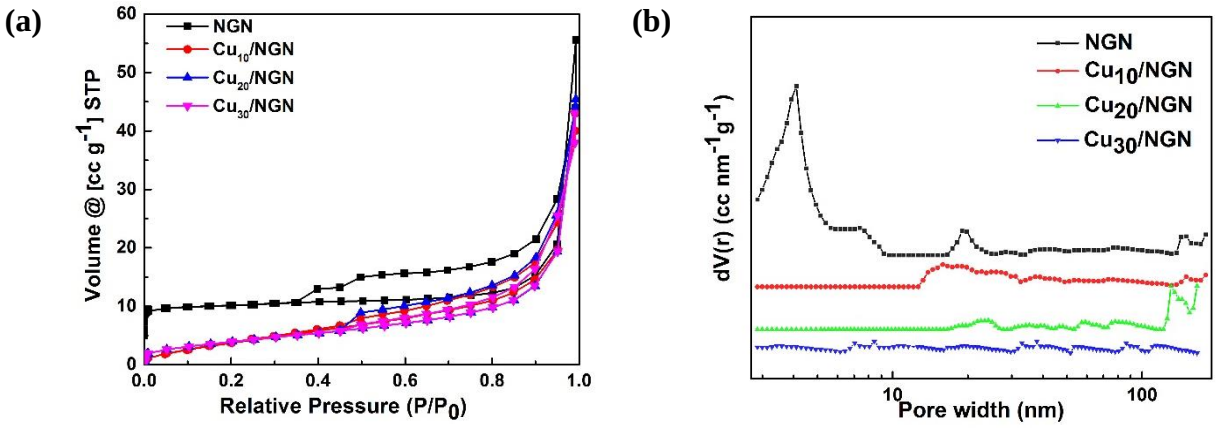

Fig. 5.11 (a) *Nitrogen adsorption/desorption isotherm and* ***(b)*** *pore size distribution curves of NGN, Cu_{10}/NGN, Cu_{20}/NGN and Cu_{30}/NGN*

5.3.2. Electrochemical characterization and performance measurement

5.3.2.1. Linear sweep voltammetry

LSV measurement was performed to study the electrochemical behavior of different Cu loaded electro-catalysts on the ECO_2R. For this, the linear sweep voltammograms were recorded in N_2 and CO_2 saturated 0.1 M $KHCO_3$ solutions between 0.4 to -1.4 V (*vs.* RHE). The current densities of the NGN and Cu_x/NGN with different loadings of Cu NPs (10 to 30 %) were also

plotted as a function of potential range as shown in **Fig. 5.12**. The CD increases with increasing potential for all tested samples. Under N_2 saturation, the CD observed is -4.8 mA cm^{-2} at -1.0 V (vs. RHE). This current is mainly due to the HER [210]. But in case of CO_2 saturated electrolyte, the corresponding CD observed at -1.0 V (vs. RHE) is -8 mA cm^{-2}. The higher value of CD in the CO_2 saturated 0.1 M $KHCO_3$ is due to the occurrence of two different reactions: CO_2 reduction [109] and HER. H_2 evolution is an unwanted side reaction in this process as it consumes significant amounts of electrical energy that was meant for ECO_2R.

In general, the ECO_2R performance is increased by increasing the active metal content in the electro-catalysts. More active sites on surface provide better reaction performance [213]. The LSV results show that the high current densities are recorded for a loading of 20% Cu NPs for the entire potential range, which is therefore considered as optimal loading. Moreover, supporting Cu NPs on NGN surface enhances the ECASA making more active sites for CO_2 within the pores for effective ECO_2R. Also, it traps electrons and assists in enhancing the rate of conversion of the intermediates of $*CO_2^-$ to valuable products. Availability of electrons with surface-bound protons enhances the CD, which results in more CO_2 reduction at lower over-potential. The CD value decreased in 30% Cu NPs loadings compared to 10% and 20 % Cu NPs loading. This decrease in the CD can be ascribed to the formation of agglomerates at higher loading which results in increase in crystallite size, which is further confirmed by different physical characterization methods (i.e. SEM, TEM, and XRD). Therewith, at higher Cu NPs loading, the surface area decreased due to generation of large clusters on the support, which decreases the availability of active sites.

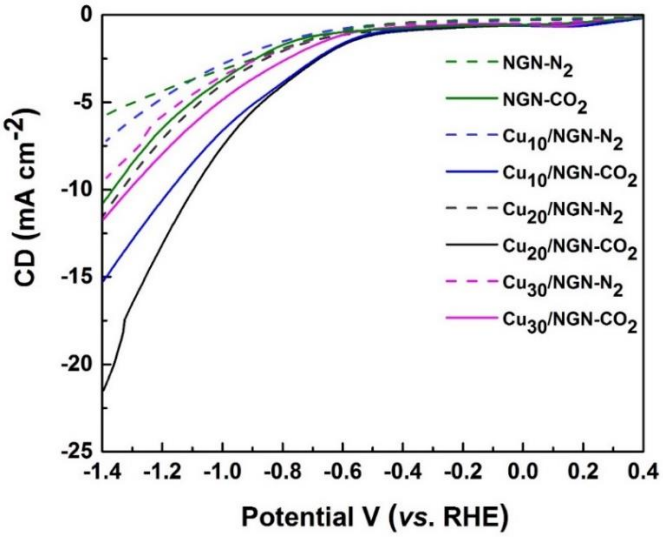

Fig. 5.12 *LSV curves of the various electro-catalysts in N_2 and CO_2-saturated 0.1M $KHCO_3$ aqueous solution*

5.3.2.2. Electrochemical CO_2 reduction and product distribution

In water, CO_2 can exist in three different forms i.e. CO_2(ad)/ H_2CO_3, HCO_3^- (H^+ aq + CO_3^{2-}) and CO_3^{2-} depending on the solution pH [64]. The most electro-active species present between pH 2 and 8.5 is in the form of CO_2(ad)/ H_2CO_3 and HCO_3^- (H^+aq + CO_3^{2-}). Above pH 8.5, only CO_3^{2-} is present and is considered as less active for ECO_2R. The concentration of more electro-active species (CO_2(ad)/ H_2CO_3) is increased by lowering pH of solution, on the other hand, a pH value less than 4.5 increases the HER. Therefore, the final pH of the electrolyte is maintained at 6.9. The reduction potentials of HER and CO_2 reduction are almost the same in the aqueous medium [40]. Thus, the CD observed in the LSV was not only for the reduction of CO_2 but also for H_2 gas generation. Therefore, to differentiate current consumed in ECO_2R and HER, the constant potential electrolysis was performed between -0.6 and -1.2 V (*vs.* RHE) for two hours. Final liquid products were quantified by HPLC and ^{1}H NMR. Formate, acetate, ethanol and n-propanol were observed in the liquid phase.

The highest charge was transferred by Cu_{20}/NGN electro-catalyst at all applied potentials (**Fig. 5.13**). Also, as expected, the CD of the ECO_2R increases with increase in Cu loading until it reaches 20% and then decreases with further increase in Cu content in NGN support as shown in **Fig. 5.14**. This observation is consistent with the results obtained from the LSV. Also, the Cu_x/NGN electro-catalysts with different Cu loadings show different electrochemical behavior in the formation of liquid products.

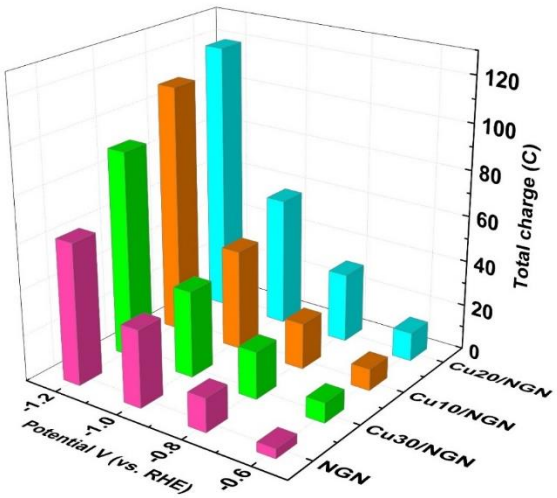

Fig. 5.13 *Total charge obtained as a function of applied potential on different electro-catalysts*

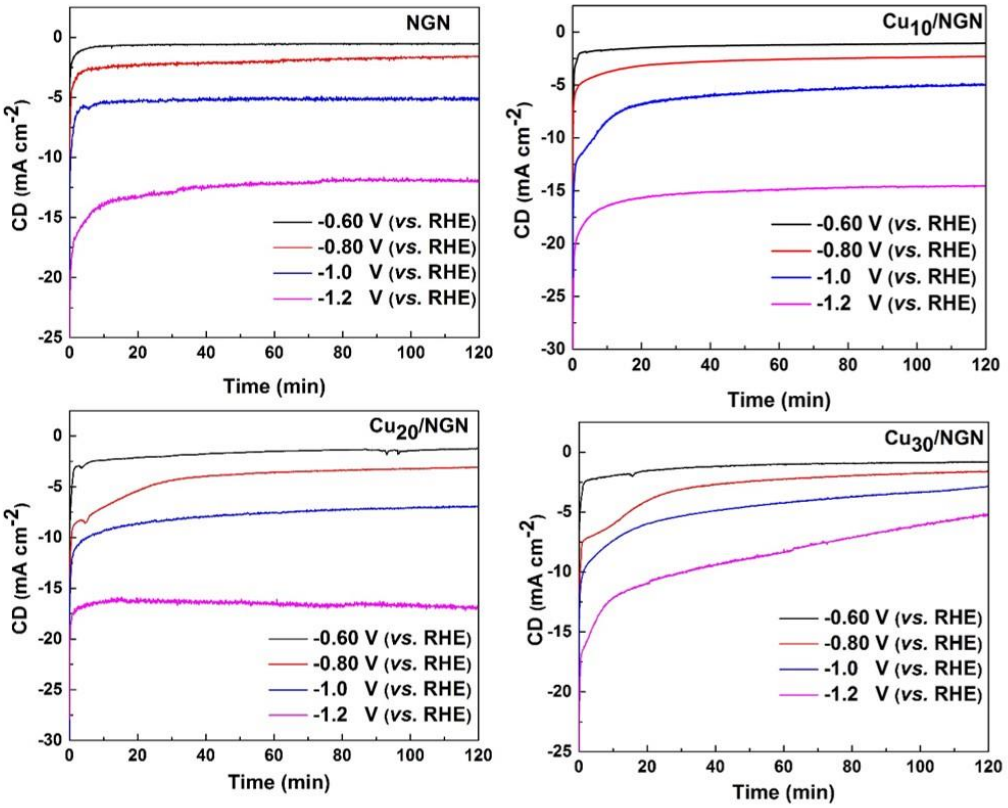

Fig. 5.14 *CD vs. time curves for NGN, Cu_{10}/NGN, Cu_{20}/NGN, and Cu_{30}/NGN in CO_2 saturated 0.1M $KHCO_3$ aqueous solution for different applied potentials*

5.3.2.3. Electrochemical active surface area (ECASA)

The electrochemical double layer capacitance (C_{dl}) was estimated in N_2-saturated 0.1 M $KHCO_3$ solution. Compared with blank carbon paper, C_{dl} increased by many times with electro-catalysts coated carbon paper (**Fig. 5.15** and **Fig. 5.16**). Also, as expected, Cu_x/NGN exhibited 1.5 times higher C_{dl} than that of NGN, showing that the addition of Cu on NGN enhances the intrinsic activity of the electro-catalyst and indicating larger ECASA, and its remarkably larger amount of active sites. Notably, Cu_{20}/NGN showed the C_{dl} value of 10.49 mF cm^{-2} and that of NGN (4.12 mF cm^{-2}), Cu_{10}/NGN (6.98 mF cm^{-2}) and Cu_{30}/NGN (6.53 mF cm^{-2}). Obtained C_{dl} values were in line with the CD values obtained in linear sweep voltammetry.

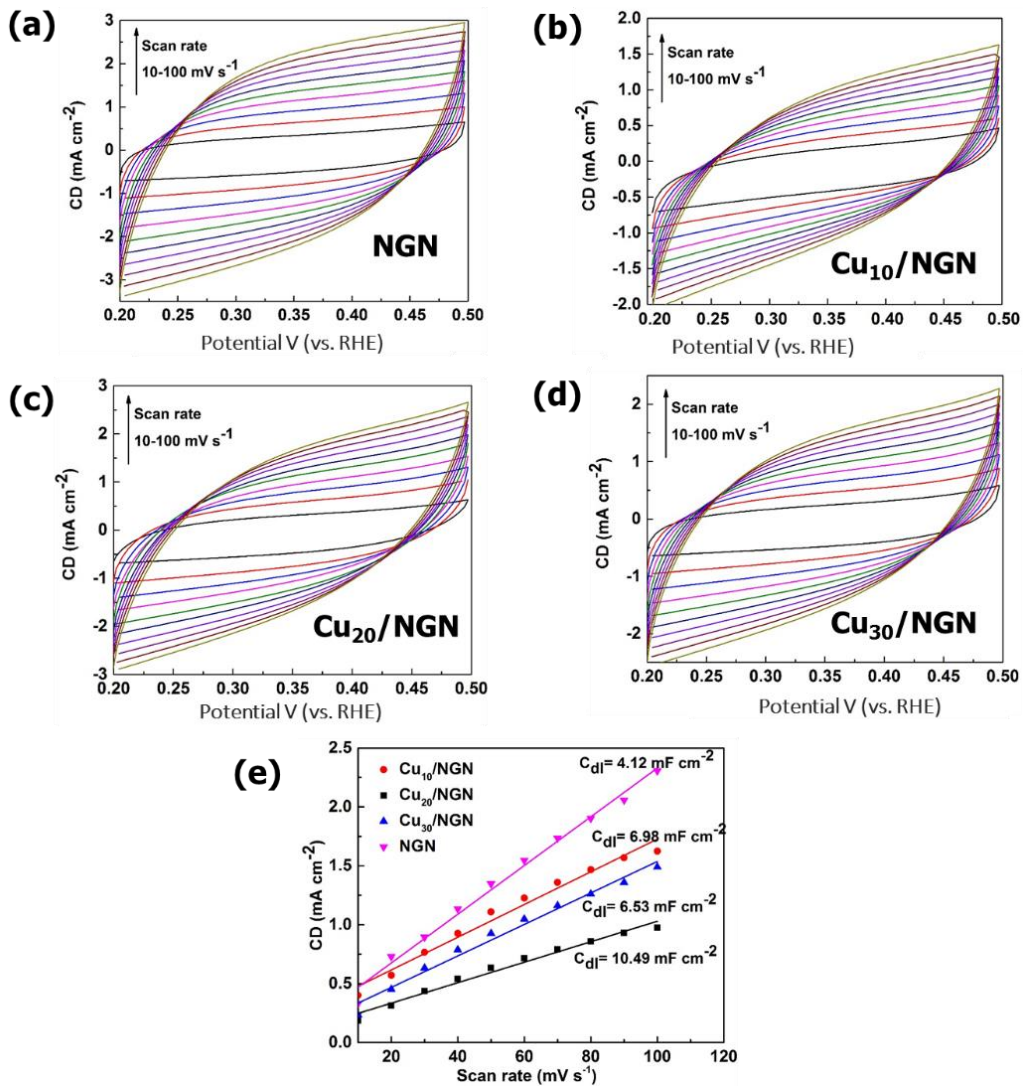

Fig. 5.15 *CV curves of NGN and Cu_x/NGN samples on carbon paper at different scan rates (from 10 to 100 mV·sec^{-1})* ***(a, b, c, d)****; Linear fitting of the current densities at 0.35 V versus scan rates of CV tests* ***(e)***

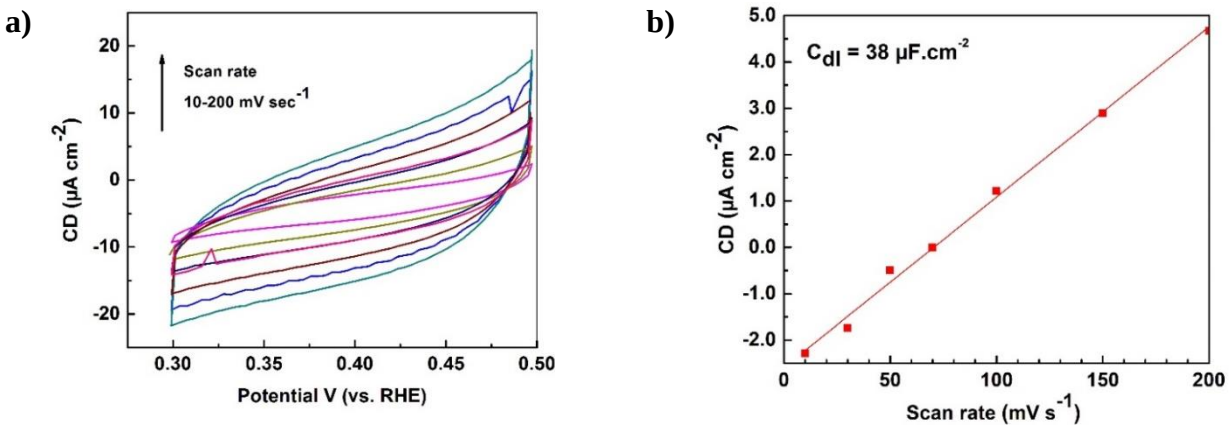

Fig. 5.16 a) *CV curves of blank carbon paper at different scan rates (from 10 to 200 mV·sec^{-1});* ***b)*** *Linear fitting of the current densities at 0.40 V versus scan rates of CV tests*

5.3.3. Products vs. potential

NGN-only electrode (without copper) converts CO_2 to only formate with a production rate of 461 μmol L^{-1} h^{-1} at -1.0 V (*vs.* RHE) (**Table 5.3**). On the same applied potential of -1.0 V (*vs.* RHE), Cu NPs loaded NGN shows different electrochemical behavior. The product formation rate of ethanol was nearly three times using Cu_{20}/NGN than Cu_{10}/NGN and Cu_{30}/NGN (90 vs. 31 μmol L^{-1} h^{-1}). In addition, acetic acid was observed on Cu_x/NGN electrode with a production rate of 20-50 μmol L^{-1} h^{-1} at -1.0 V (*vs.* RHE), whereas NGN produced only formate. The multi-carbon production is increased due to the synergic effect between Cu and N-doped active sites in the electro-catalyst. The increase in ECASA could be one of the key contributors to the enhanced catalytic activity of Cu_{20}/NGN because larger ECASA could provide more catalytically active sites for ECO_2R. Furthermore, as illustrated in the previous reports regarding N-doped carbon electro-catalysts [214, 215], the pyridinic N species provide more active sites, and has higher catalytic ability for ECO_2R [70]. In general, pyridinic N, present on the carbon-based electro-catalyst, might adsorb the COOH* or CO* reaction intermediates [216]. In addition, pyridinic N functionalized on N-doped carbon could be assigned to sp^2 hybridization, resulting in improved electronic conductivity [130]. Fundamental studies showed that increasing the surface concentration of CO* by stabilizing chemisorbed CO* on the Cu metal promotes reaction rate for C−C coupling in ECO_2R [194]. The above findings suggest that, due to the effect of pyridine N and Cu metals in the electro-catalyst, Cu_{20}/NGN provides high conductivity and more active ECO_2R sites. Additional experimental and theoretical works are needed to illustrate the synergic and interfacial effect on reaction paths to multi-carbon product formation on Cu_x/NGN catalysts. To verify the liquid products generated from dissolved CO_2, the electrochemical experiment was performed in N_2 saturated 0.1 M $KHCO_3$ solution (without CO_2 purging) at -1.0 V (vs. RHE) for 2 h. No peaks were observed in HPLC analysis, indicating that all liquid products were coming from CO_2 rather than from electrolyte.

Achieving high FE is still a great challenge for electrochemical CO_2 reduction, especially for producing multi-carbon products such as C_2H_5OH. Here, FE for CO_2 reduction on Cu_x/NGN was determined to further evaluate their performance (**Fig. 5.17**). Notably, Cu_{20}/NGN gives maximum FE for multi-carbon alcohol generation. This is supported by its highest charge utilization tendency (**Fig. 5.13**) in the range of −0.6 to −1.2 V (*vs.* RHE) and its high ECASA amongst other catalysts. The FE of C_2H_5OH formation by Cu_{20}/NGN increased on increase in potential from −0.6 to −1.0 V (*vs.* RHE), reaching a maximum (25.72%) at −1.0 V (*vs.* RHE),

and further increase in potential it decreased (15.2%). A similar pattern was observed for the Cu_{10}/NGN and Cu_{30}/NGN electro-catalysts. NGN alone as electro-catalyst produces only formate with maximum 36.72% FE at -1.0 V (*vs.* RHE). Further increase in applied potential to -1.2 V (vs. RHE), FE decreases to 26% due to competition from H_2 evolution reaction. The total FE was not calculated in the current work due to the absence of gaseous product measurements. In addition to liquid products, CO and H_2 are expected in gaseous products.

Table 5.3 *Production rates of liquid products detected in 2 h ECO_2R*

Catalyst	**Potential V (*vs.* RHE)**	**Production rate (µmol L^{-1} h^{-1})**			
		$HCOO^-$	**CH_3COO^-**	**C_2H_5OH**	**C_3H_7OH**
NGN	-0.6	44.5	0	0	0
	-0.8	178	0	0	0
	-1	461	0	0	0
	-1.2	615	0	0	0
Cu_{10}/NGN	-0.6	63.5	0	0	0
	-0.8	145	0	27.5	0
	-1	458	28.5	31.5	0
	-1.2	518.5	34.5	43	26
Cu_{20}/NGN	-0.6	62.5	0	0	0
	-0.8	86.5	29	42.5	0
	-1	239	51.5	90	17.5
	-1.2	790	55	113.5	27.5
Cu_{30}/NGN	-0.6	55	0	0	0
	-0.8	181	21.5	10	0
	-1	465	17	37.5	0
	-1.2	815	65	53	0

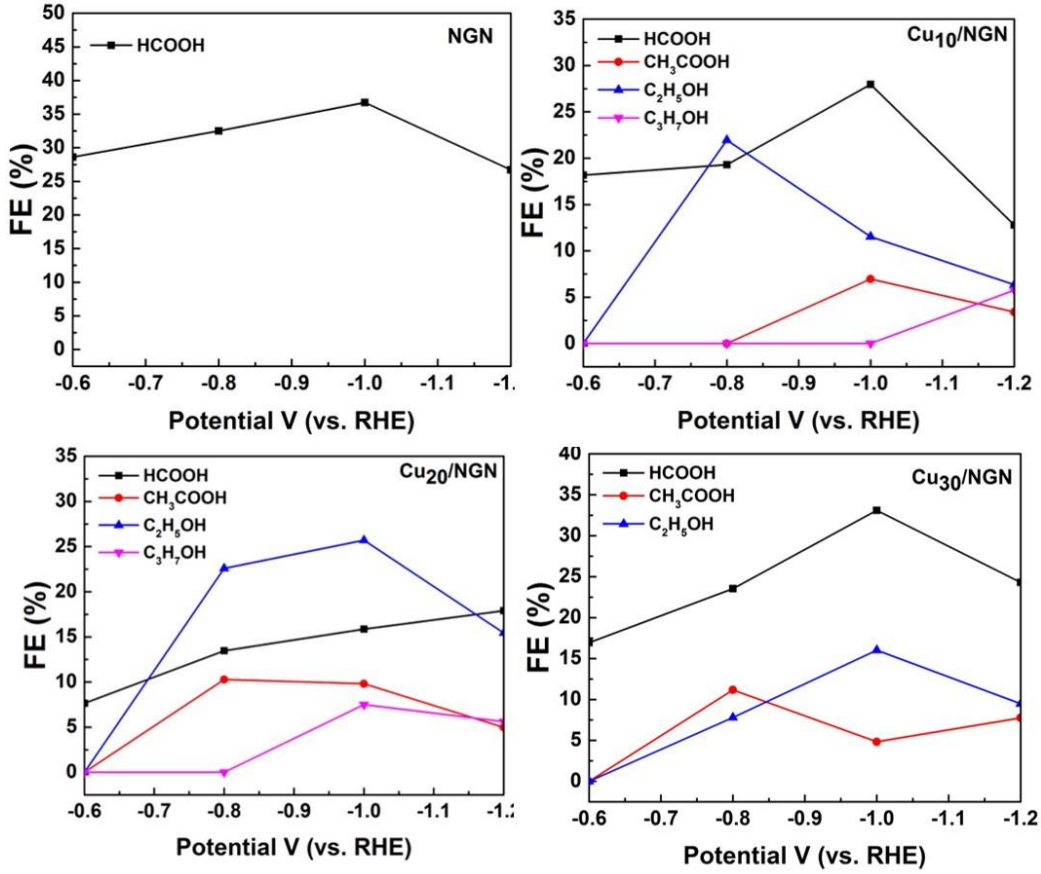

Fig. 5.17 *FEs for liquid products produced by NGN, Cu_{10}/NGN, Cu_{20}/NGN and Cu_{30}/NGN as a function of applied potential*

The significant performance of Cu_{20}/NGN was comparable to recently reported Cu-based and carbon-based catalysts, such as Cu NPs , Cu/CNT [134], Cu/G [133], OD Cu/C [131], B-doped graphene (G) [217], N-doped G (NG) [218], Cu NPs/NG [219] and Cu_2O/ZnO/G [220], which are summarized in **Table 5.4**.

Table 5.4 *Comparison of the catalytic performances of Cu_x/NGN and the similar electro-catalysts reported in literature for the reduction of CO_2 to liquid products*

Electro-catalyst	**Potential**	**Main product**	**FE**	**CD (mA cm^{-2})**	**Ref.**
Cu/G	-0.9 V (*vs.* Ag/AgCl)	Ethanol	9.93	≈ 1	[133]
OD Cu/C	-0.5 V (*vs.* RHE)	Ethanol	34.8	NR	[131]
B-doped graphene (G)	−1.4 V (*vs.* SCE)	Formate	66	1.4	[217]
N-doped G (NG)	−0.84 V (*vs.* RHE)	Formate	73	7.5	[218]

Cu NPs/NG	−1.2 V (*vs.* RHE)	Ethanol	63	~1.7	[219]
Cu_2O/ZnO/G	−1.8 V (*vs.* Ag/AgCl)	N-propanol	30	8	[220]
Cu_{20}/NGN	-1.0 V (*vs.* RHE)	Ethanol	25.72	7.87	This work
NGN	-1.0 V (*vs.* RHE)	Formate	36.72	4.71	
Cu_{20}/NGN	-0.8 V (*vs.* RHE)	Acetate	10.28	4.23	
Cu_{20}/NGN	-1.0 V (*vs.* RHE)	N-propanol	7.50	7.87	

5.3.4. Reaction kinetics/Tafel plot

Tafel plot profiles for different electro-catalysts are plotted to study the intrinsic activity in ECO_2R as shown in **Fig. 5.18** Tafel plots for Cu_{20}/NGN and its comparison with NGN, Cu_{10}/NGN, and Cu_{30}/NGN. According to the Tafel equation, a smaller Tafel slope suggests a good reaction kinetics, because the potential required to overcome the reaction barrier is smaller in the activation step of CO_2 molecule (i.e. the rate-determining step (RDS) is the initial single electron transfer to CO_2 to form CO_2·- intermediate) [206]. The Tafel slope of NGN, Cu_{10}/NGN, Cu_{20}/NGN, and Cu_{30}/NGN, are ca.131, 105, 101 and 115 mv dec^{-1}, respectively which are similar to the other reports available in the literature on Cu-based electrodes [63, 219]. The Tafel slope for the Cu_{20}/NGN is lower (101 mV dec^{-1}) than that of other electro-catalysts which can be associated with the effect of homogeneous dispersion of Cu NPs on NGN surface suggesting lowered kinetic barrier by stabilizing the CO_2^{*-} intermediate on the surface. In other words, it appears that Cu_{20}/NGN can facilitate CO_2 activation by effectively stabilizing the CO_2^{*-} (ads) intermediate. Also, the literature suggests that pyridinic N is the most active site for the CO production from ECO_2R as it exhibits relatively weak binding energy for *CO and facilitates CO desorption [77, 206]. The presence of Cu alters the surface intermediates' (CO_2^{*-}) stability, thereby increasing CO_2 reduction to alcohols rather than H_2 evolution [213]. Cu_x/NGN electro-catalyst for ECO_2R shows high CD and moderate activity. More detailed mechanistic study is needed to understand the overall system for better design of electro-catalyst.

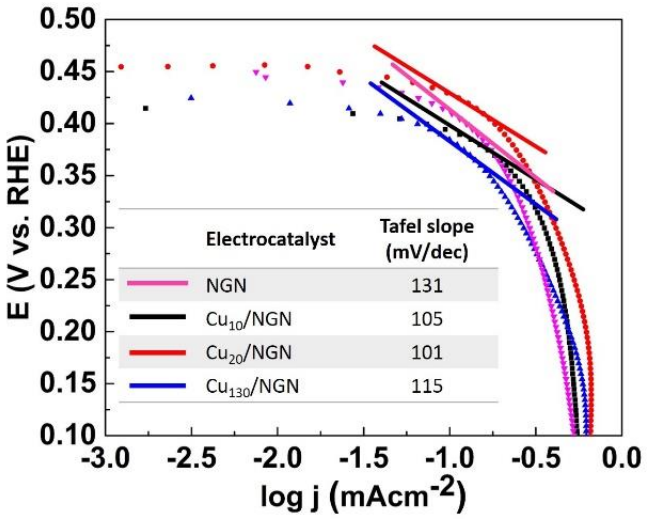

Fig. 5.18 *Tafel plots for Cu_{20}/NGN and its comparison with NGN, Cu_{10}/NGN, and Cu_{30}/NGN*

5.3.5. Long term performance and reusability study

Another important parameter for the development of an efficient electrochemical CO_2 reduction catalyst is its stability for longer reaction time. Therefore, the stability test of Cu_{20}/NGN catalysts was carried out at an applied potential of −1.0 V (*vs.* RHE) in CO_2-saturated 0.1 M $KHCO_3$ aqueous solution with continuous CO_2 bubbling. As shown in **Fig. 5.19a**, the Cu_{20}/NGN shows a thoroughly stable performance during the longer run (for 12 h) without significant loss in CD.

Also, the reusability study of optimized electro-catalyst was carried out in a fresh 0.1 M $KHCO_3$ electrolyte at −1.0 V (*vs.* RHE). The experiment was repeated using same electrode in a fresh electrolyte solution for 6 times. The obtained Faradaic efficiencies for $HCOO^-$, CH_2COO^-, C_2H_5OH and C_3H_7OH are reported in **Fig. 5.19b.** Total Faradaic efficiencies of multi-carbon alcohols (C_2H_5OH and C_3H_7OH) were shown up to 33 % in first two times, later n-propanol was not detected by the HPLC system. The FE for formate was observed constant (12-13 %) in all the 6 runs. The decrease in FE for multi-carbon liquid products is suggesting the deposition of poisoning species (i.e. graphitic carbon, reaction intermediates) on the active sites of the electrode during longer run [167, 201, 202] as shown in section 5.3.6.

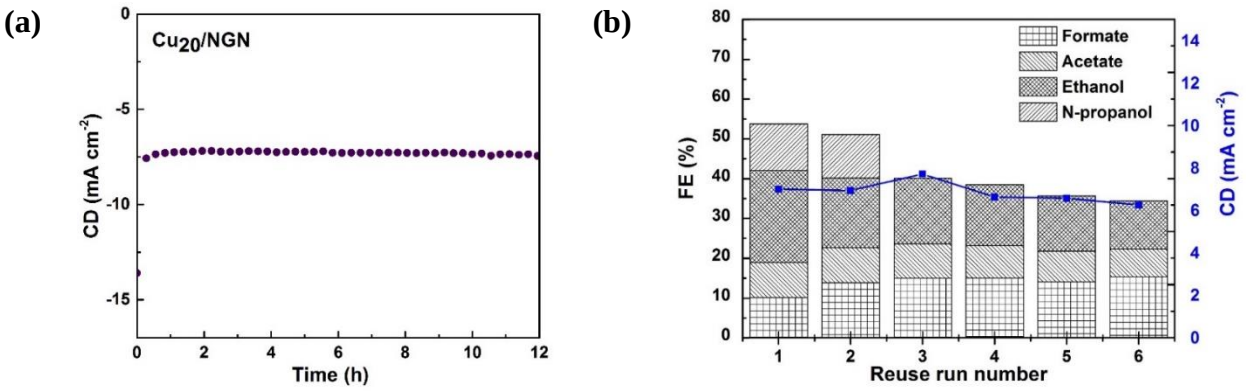

Fig. 5.19 (a) *Long-time test performed at -1.0 V (vs. RHE) cathode potential using Cu_{20}/NGN as electro-catalyst,* ***(b)*** *FE of products during reuse test performed at -1.0 V (vs. RHE) along with obtained total CD*

5.3.6. Post characterization

To provide more insight in nature of active sites for ECO_2R, XRD and EDX analysis of Cu_{20}/NGN dispersed on carbon paper (Cu_{20}/NGN/CP) was performed at different time intervals of ECO_2R. As shown in **Fig. 5.20**, the initial peak of CuO was almost absent after 10 min of ECO_2R at -1.0 V (vs. RHE). This is also supported by no oxygen signal in EDX spectra after 10 min (**Fig. 5.21**). These results suggest that the actual ECO_2R is occurring on metallic Cu^0 sites. Furthermore, previous reports based on in-situ spectroscopy suggest that the mix copper states (CuO, Cu_2O) reduce to metallic Cu^0 under ECO_2R by applying the negative biased treatment probably due to its thermodynamic instability in the applied potential range [108, 221].

Also, at higher current densities, production of OH^- (or H^+ consumption) is higher and K^+ transfer into the catholyte due to concentration gradient. Metallic impurities from electrolyte solution can be adsorbed on catalyst surface of electrode. This is further supported by appearance of K signal in EDX analysis of Cu_{20}/NGN/CP after 12 h of ECO_2R (**Fig. 5.21**). HER continues at the very negative potential on the poisoned surface, but CO_2 reduction to products requiring active Cu surface, decreases. These poisoning species restrict multi-electron and proton transfer resulting in stable FE for formate only.

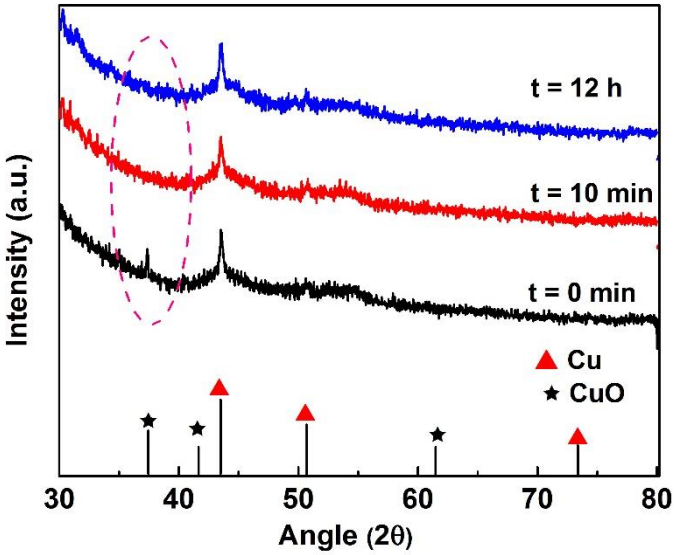

Fig. 5.20 *XRD patterns of Cu_{20}/NGN/CP at t=0 min, t=10 min and t=12 h of ECO_2R*

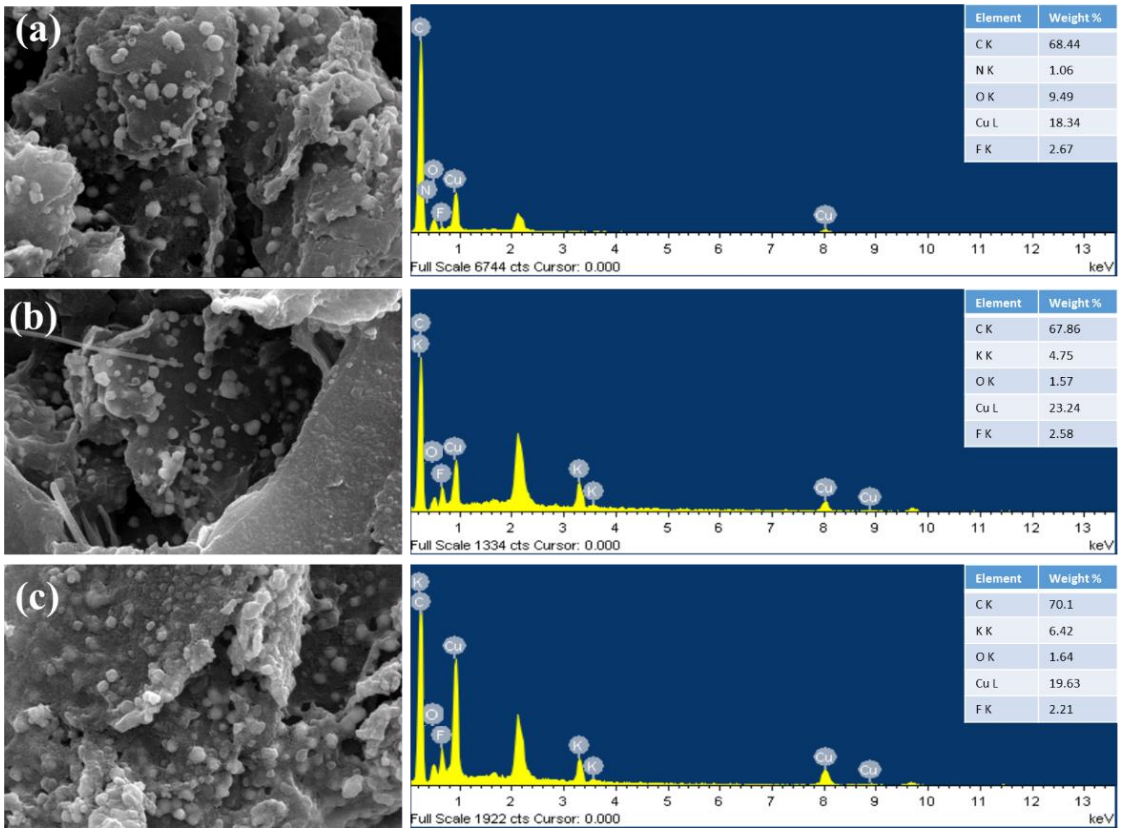

Fig. 5.21 *SEM images of Cu_{20}/NGN/CP at t=0 min (a), t=10 min (b) and t=12 h (c) of ECO_2R with EDX spectra*

5.4. Conclusions

In this work, N-doped graphene supported copper nanoparticles (Cu_x/NGN) were prepared by a simple wet chemical reduction method and used as an electro-catalyst for the ECO_2R in an aqueous 0.1 M $KHCO_3$ electrolyte solution. Optimization of Cu loading on NGN for the ECO_2R reaction was performed by exploring the morphology, particle size, dispersion, and electro-chemical behavior of the catalysts. It showed that they exhibited different selectivities towards CO_2 reduction at different compositions and potential ranges. It is highlighted how metal loading and applied potentials affect the selectivity of CO_2 reduction reactions. Twenty wt.% copper on NGN gives maximum ethanol FE of 25.72% with a high CD of 7.7 mA cm^2 at -1.0 V (vs. RHE). Also, the highest production rate for ethanol (113.5 μmol L^{-1} h^{-1}) is achieved on the same electro-catalyst at -1.2 V (vs. RHE). Moreover, the optimized electro-catalyst shows long term stability without significant loss in CD for 12 h. This work opens up a simple way for efficient transformation of CO_2 into valuable chemicals, and the results are helpful for developing other electrodes for efficient electrochemical reduction of CO_2. The results suggest that designing engineered materials with the higher ECASA by varying the active metal content on the NGN support gives higher activity and selectivity for multi-carbon products. It was intended to improve the multi-carbon production rate by optimizing the loading of Cu by dimerization of COOH*/CO* intermediate. Furthermore, it is expected that enhancing the C–C coupling rate at lower over-potentials, results in longer alcohol chains than ethanol/n-propanol. This work will trigger many interesting work in the future.

(This work has been published in Journal of CO_2 Utilization, 44 (2021) 101382. DOI: https://doi.org/10.1016/j.jcou.2020.101382 (IF =7.132))

Chapter 6- Electrochemical CO_2 reduction on oxide derived $CuZn_x$

6.1. Synthesis of CuO-ZnO_x

Simple co-precipitation method [222] was used to synthesize CuO-ZnO_x (where, x= 5, 10, 15 and 20 wt.% of ZnO) using $Cu(NO_3)_2 \cdot 3H_2O$, $Zn(NO_3)_2 \cdot 6H_2O$, and NaOH as starting materials. Initially, 4 mM of $Cu(NO_3)_2.3H_2O$ was dissolved in 200 mL ultrapure water, and a specific amount of $Zn(NO_3)_2.6H_2O$ was added to the solution as per required condition. This solution is kept under constant stirring and temperature was increased to 80 ^oC. Later, the NaOH solution was added drop-wise under constant stirring until the pH reached 14, resulting in the precipitated product. After that, the as-precipitated reaction product was washed repeatedly with deionized water and ethanol until supernatant pH reached to 7. Finally, the product was kept overnight in an oven at 80 °C. The dried product was then calcined in a tubular furnace at 350 ^0C in air atmosphere for 2 h and then temperature was gradually increased to 700 ^0C to enhance the crystallinity of CuO-ZnO_x. The schematic flowchart for the synthesis of CuO-ZnO_x is shown in **Fig. 6.1**.

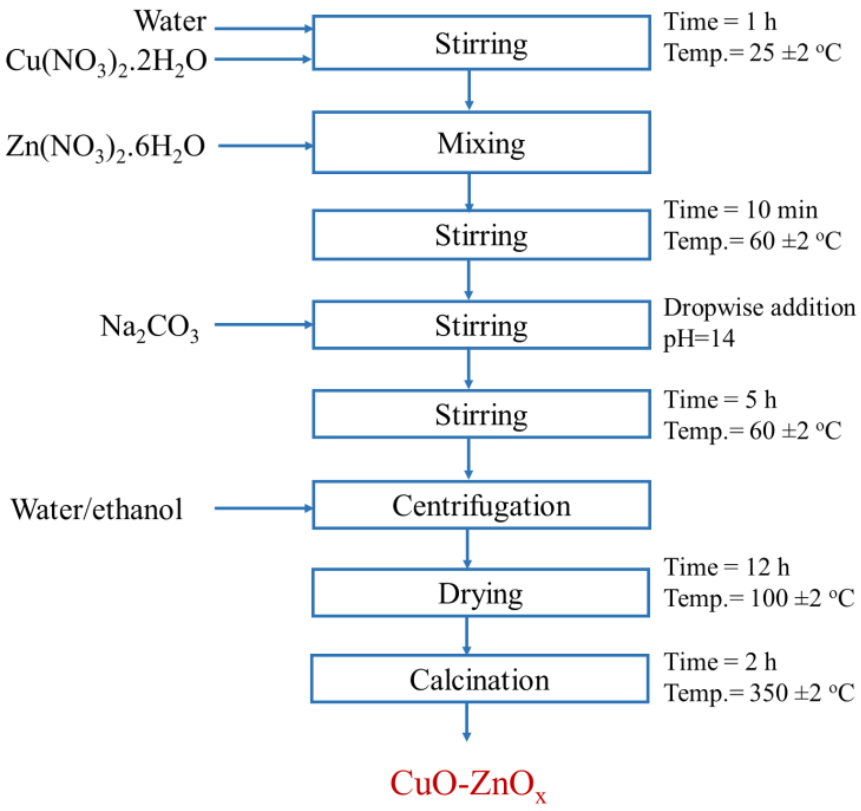

Fig. 6.1 *Process outline for the synthesis of CuO-ZnO_x*

6.2. Preparation of working electrodes

Initially, the mixture of catalyst powder (4 mg), Nafion® 117 solution (30 µL) and isopropanol (1 mL) was sonicated for 30 min for its uniform distribution. Obtained mixture is also called as catalyst ink. This catalyst ink was then sprayed onto a pretreated carbon paper (refer section 3.5.2.) using N_2 carrier gas. The ink coated carbon paper was dried at 60 °C to remove the solvents. Dried carbon paper was denoted with corresponding coated electro-catalyst and used as working electrode in further experiments. For example, carbon paper coated with CuO-ZnO_{10} electro-catalyst, denoted as CuO-ZnO_{10} electrode. Approximately 2.0 mg cm^{-2} catalyst loading was achieved.

6.3. Results and discussion

6.3.1. Physico-chemical characterization

6.3.1.1. X-ray diffraction analysis

The oxide derived bimetallic CuO-ZnO_x catalysts with different wt.% of ZnO were synthesized by the co-precipitation method followed by high temperature calcination. For controlled experiment study, CuO nanoparticles without ZnO content were also prepared. The crystallinity of the catalyst is important for ECO_2R to various useful chemicals [223]. Therefore, the crystalline structures of selected catalysts were evaluated by XRD measurements. As shown in **Fig. 6.2**, the diffraction peaks of CuO dominate the other peaks of ZnO since CuO has higher weight percentage than that of ZnO. Peaks at 2θ of 35.37, 38.56, 48.54, 58.02, and 61.24° correspond to monoclinic CuO (-111), (111), (-202), (202), and (-113) facets, respectively (JCPDS #01-078-0428). The peaks at 2θ of 31.78, 47.55, 56.61, and 67.87° are indexed to hexagonal ZnO (100), (102), (110), and (112) facets, respectively (JCPDS #01-089-0510). Broad diffraction peaks with larger full-width at the half maximum (FWHM) confirm that the CuO and ZnO are in nanoscale size.

The crystallite size (D) of CuO and CuO-ZnO_{10} is calculated from well-known Debye Scherrer equation (equation 3.4) [224]. The intense diffraction peak of CuO at 2θ of 31.77^o was used for calculation. The average crystallite sizes were found to be about 19-22 nm.

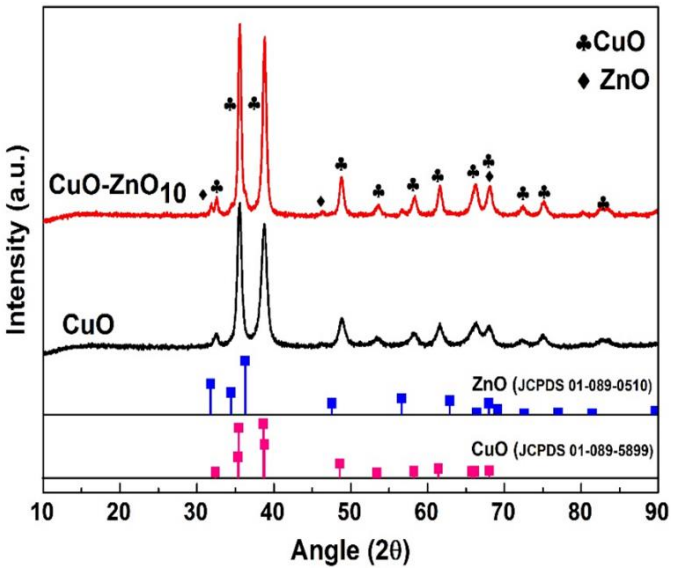

Fig. 6.2 *XRD patterns of CuO, and CuO-ZnO$_{10}$ nanoparticles*

6.3.1.2. X-ray photoelectron spectroscopy

Electrochemical performance is greatly affected by the chemical nature of the electro-catalyst. Therefore, XPS was used to study the surface composition and oxidation state of selected CuO and CuO-ZnO$_{10}$ catalysts. **Fig. 6.3a-b** show the high-resolution Cu 2p XPS spectra deconvoluted into two peaks. Peaks at 933.89 and 954.41 eV correspond to the Cu 2p$_{3/2}$ and Cu 2p$_{1/2}$, respectively. The difference in binding energies of Cu 2p$_{3/2}$ and Cu 2p$_{1/2}$ is found to be 20.52 eV, which is very close to standard value of Cu 2p in CuO, confirming the CuO phase [115]. In addition, satellite peaks at 943.0 and 962.6 eV, confirm the valence state of Cu^{2+}. In **Fig. 6.3c**, the Zn 2p1/2 and Zn 2p3/2 peaks can be found at 1045.39 and 1022.20 eV, respectively. The binding energy difference between Zn 2p$_{1/2}$ and Zn 2p$_{3/2}$ peaks is 23.2 eV, which concurred with the literature value for ZnO [113, 225].

6.3.1.3. Scanning electron microscopy

Morphology and structure of CuO and ZnO were investigated by FESEM and HR-TEM analysis. **Fig. 6.4** shows the FESEM images for CuO and CuO-ZnO$_{10}$ nanoparticles. The samples show a spherical morphology and the average particle size is centered around 40 nm. Since all of the particles are in nanosize, the electrodes should have a better catalytic response due to the high surface to volume ratio, but other factors such as nature, shape, and surface/bulk composition can have a significant impact on electrode efficiency [19, 226]. Elemental analysis shows only Cu, Zn, and O suggesting that prepared sample is free from impurities.

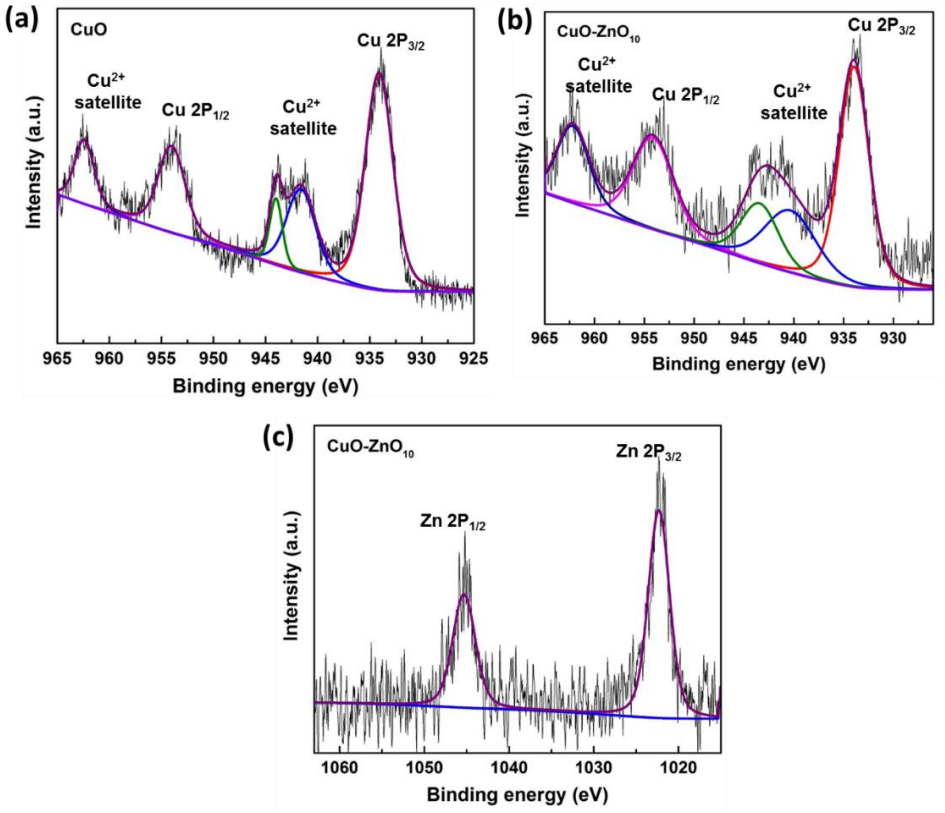

Fig. 6.3 *High resolution Cu 2p core spectra of CuO* ***(a)*** *and CuO-ZnO$_{10}$* ***(b)*** *samples; and high resolution Zn 2p core spectra of CuO-ZnO$_{10}$* ***(c)***

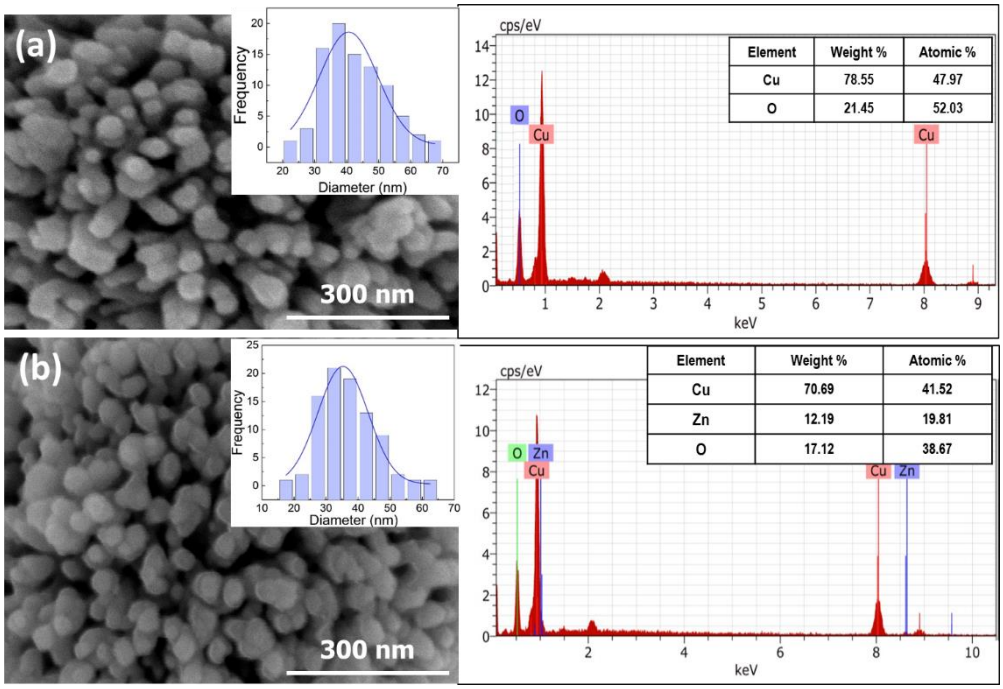

Fig. 6.4 *SEM images and EDX spectra of* ***(a)*** *CuO and* ***(b)*** *CuO-ZnO$_{10}$ electro-catalysts (Inset figure shows the particle size distribution.)*

6.3.1.4. Transmission electron microscopy

Samples exhibit sphere-like morphology with considerable agglomeration (**Fig. 6.5**). The particle sizes are in nanoscale for both CuO and CuO-ZnO_{10} samples. SAED pattern shows small spots with rings in both samples, confirming the polycrystalline nature. All the corresponding crystal planes of ZnO and CuO, indexed in the SAED pattern, are in good agreement with XRD studies. The EDS elemental mapping of selected CuO-ZnO_{10} sample (**Fig. 6.6**) clearly shows the uniform distributions of CuO and ZnO nanoparticles. These results are in line with XRD and FESEM.

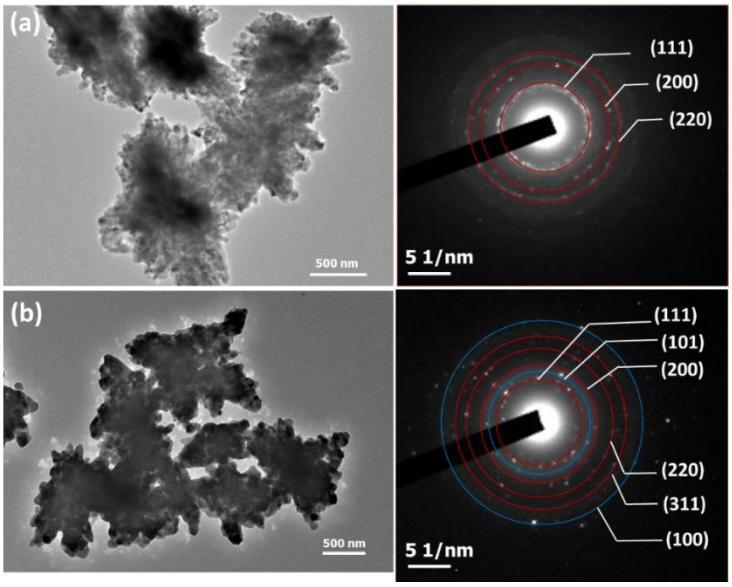

Fig. 6.5 (a) *High-magnification TEM images of CuO and* ***(b)*** *CuO-ZnO_{10} with its SAED patterns (The crystal planes of CuO (white) and ZnO (blue) are marked in SAED patterns.)*

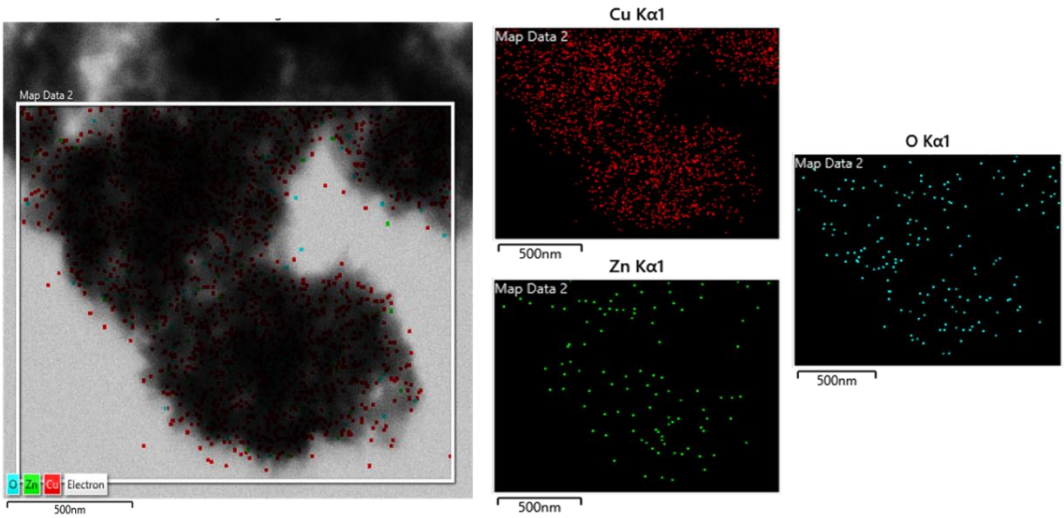

Fig. 6.6 *Elemental mapping patterns of Cu, Zn, and O elements in the CuO-ZnO_{10} electro-catalyst*

6.3.1.5. N_2 adsorption isotherm

It is reported that the high surface area of electro-catalyst can provide suitable porosity to improve the electro-chemical performance. Therefore, the BET surface area and total pore volume of all the CuO-ZnO_x samples were calculated from N_2 sorption isotherms. The samples show typical IV isotherms as shown in **Fig. 6.7**, indicating the mesoporous structure of the sample [227]. As shown in **Table 6.1**, the surface area and total pore volume are decreasing with increasing Zn loading in the catalyst due to the agglomeration at higher loadings of ZnO.

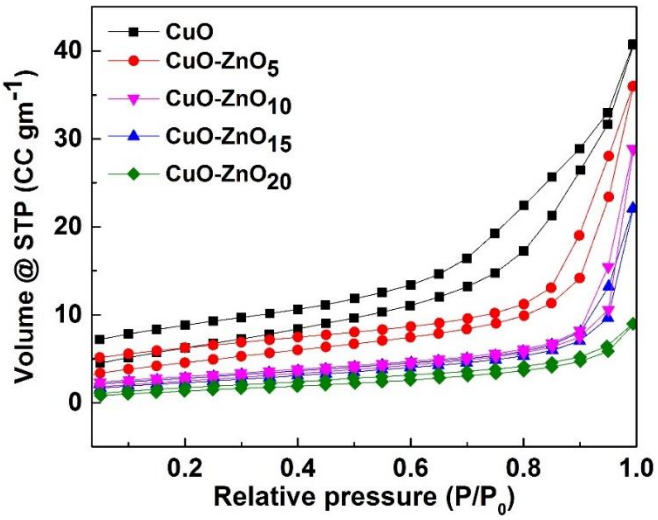

Fig. 6.7 *N_2 sorption isotherms of all CuO-ZnO_x catalysts*

Table 6.1 *Specific surface area and total pore volume of electro-catalysts*

Sample	Surface area (m^2 g^{-1})	Total pore volume (cm^3 g^{-1})
CuO	22.862	0.052
CuO-ZnO_5	16.350	0.045
CuO-ZnO_{10}	9.107	0.029
CuO-ZnO_{15}	8.403	0.023
CuO-ZnO_{20}	5.297	0.11

6.3.2. Electrochemical measurements

6.3.2.1. Linear sweep voltametry

The electro-catalytic performance of the different electrodes was studied by recording LSVs in CO_2 and N_2 saturated 0.1 M $KHCO_3$ aqueous solutions. The electrodes were pre-reduced by performing multiple scans at a scan rate of 50 mV s^{-1} before each LSV experiments. **Fig. 6.8** displays the LSVs on the all CuO/ZnO_x electrodes in CO_2 saturated solution. **Fig. 6.8** also

shows LSV of representative CuO/ZnO_{10} electrode in N_2 saturated electrolyte. The CD observed in CO_2 saturated electrolyte is higher than that of N_2 saturated electrolyte at the potentials greater than -0.6 V (vs. RHE), suggesting $CuO\text{-}ZnO_x$ is active for CO_2 reduction with respect to the HER [40, 228]. Small reduction peak at around -0.4 V (vs. RHE) shows partial reduction of ZnO phase. In addition, when the LSVs of different $CuO\text{-}ZnO_x$ electrodes in CO_2 saturated solution are compared, the CuO electrode shows higher geometric CD than the ZnO loaded electrodes. Furthermore, the CD decreases as the percentage of ZnO in the $CuO\text{-}ZnO_x$ increases. The higher ZnO loaded electrodes should have more exposed Zn surface than Cu surface, as a result, the geometric activity of the Cu-Zn electrode decreases with increasing ZnO content. This is due to the fact that Cu facially favors HER than Zn [157, 228].

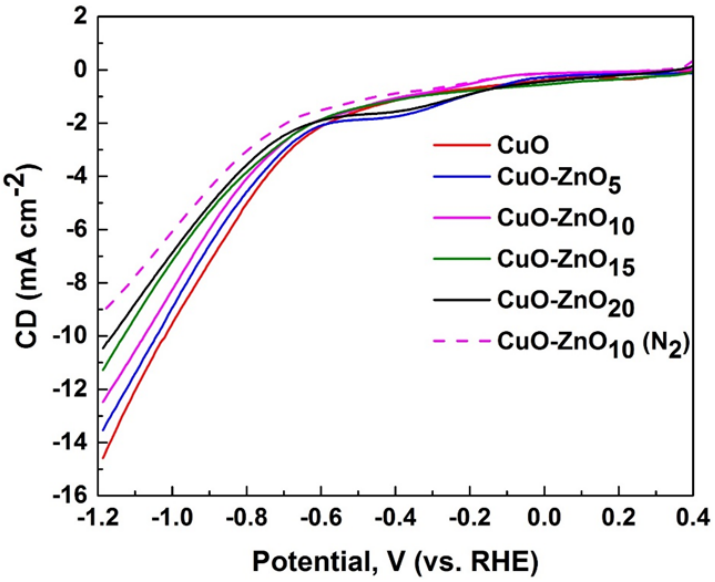

Fig. 6.8 *Linear sweep voltammetry of $CuO\text{-}ZnO_x$ in the CO_2 saturated (dark solid lines) and N_2 saturated (dotted line) 0.1 M $KHCO_3$*

6.3.2.2. Electrochemical CO_2 reduction and product distribution

To study the effect of applied potential on ECO_2R product distribution, CA measurements were carried out in two compartment H-type electrochemical cell at different potentials ranging from -0.4 V to -1.0 V (vs. RHE) for 2 h. Fresh working electrode was used in each experiment. **Fig. 6.9** shows typical current-potential curves for all $CuO\text{-}ZnO_x$ electrodes at different applied potentials. The sudden decrease in CD was observed at initial stage of the experiments due to the reduction of electro-catalyst itself [228]. The CD value reached to a steady value where actual ECO_2R is expected. The summary of charge utilized at different applied potentials using all five electrodes is shown in **Fig. 6.10**. The higher electrode activity was shown by CuO

electrode where total 30.29 C charge was consumed followed by CuO-ZnO_5, CuO-ZnO_{10}, CuO-ZnO_{15}, and CuO-ZnO_{20} where 27.87, 25.16, 23.26, and 20.48 C charge was utilized on the application of -0.8 V (vs. RHE) for 2 h. The results obtained in the CA experiments are in agreement with the LSV analyses.

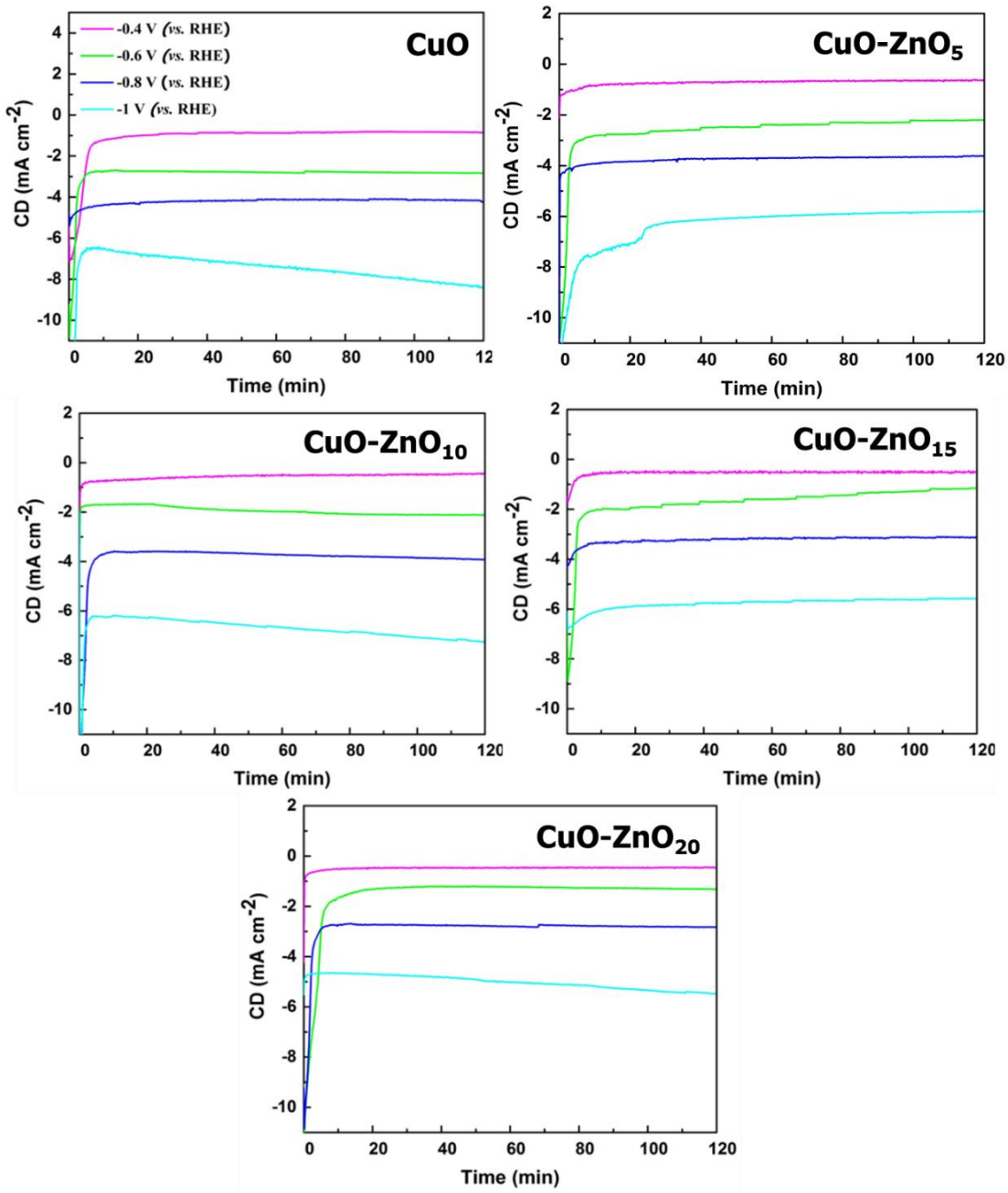

Fig. 6.9 *CA measurement on the CuO-ZnO_x electrodes in CO_2-saturated 0.1 M $KHCO_3$ aqueous solutions at various potentials (The current densities are normalized by geometric electrode area for various catalysts at each potential.)*

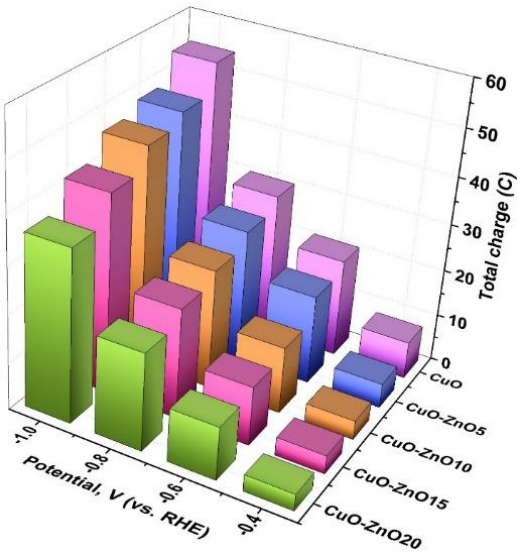

Fig. 6.10 *Total charge consumed by different electrodes in 2 h of ECO_2R*

6.3.2.3. Electrochemical active surface area (ECASA)

The ECASA of all the electrodes was investigated by double-layer capacitance (Cdl) method [229]. For this, the cyclic voltammograms (CV) were recorded in non-Faradaic region at different scan rates (10-100 mV sec^{-1}) using 0.1 M $KHCO_3$ electrolyte solution. As shown in **Fig. 6.11**, there was no active redox peak in the scanning potential range of 0.21 to 0.41 V (vs. RHE). The slope of anodic CD vs. scan rate plot gives Cdl value. The maximum Cdl of 2.6 mF cm^{-2} was found for CuO-ZnO_{10} electrode followed by CuO-ZnO_5 (1.8 mF cm^{-2}), CuO (1.3 mF cm^{-2}), CuO-ZnO_{15} (1.1 mF cm^{-2}), and CuO-ZnO_{20} (0.9 mF cm^{-2}). ECASA was then calculated by dividing the C_{dl} by the capacitance of bare CuO [230]. The ECASA (normalized by CuO) was found to be 1, 1.38, 2, 0.84, and 0.69 for CuO, CuO-ZnO_5, CuO-ZnO_{10}, CuO-ZnO_{15}, and CuO-ZnO_{20} respectively. We have added this on page 14 of the revised manuscript.

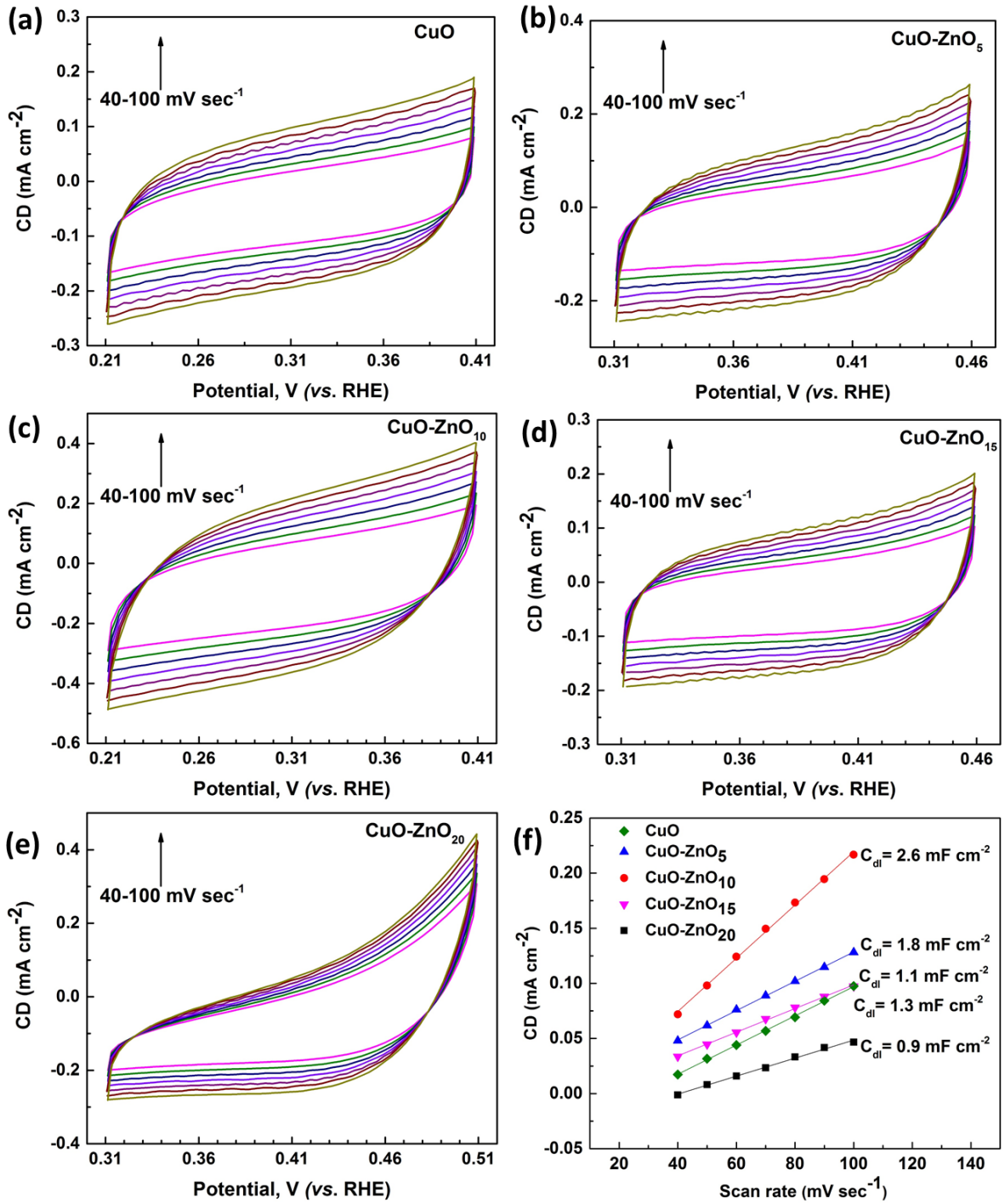

Fig. 6.11 *Cyclic voltamograms of* ***(a)*** *CuO,* ***(b)*** *CuO-ZnO$_5$,* ***(c)*** *CuO-ZnO$_{10}$,* ***(d)*** *CuO-ZnO$_{15}$,* ***(e)*** *CuO-ZnO$_{20}$ at different scan rates, and* ***(f)*** *Double layer capacitive measurement plots of corresponding electrodes*

6.3.3. Product vs. Potential

After the CA experiments for 2 h, the liquid product is stored at 4 ^{o}C to minimize the losses of volatile products. Further, it was analyzed by HPLC and ^{1}H NMR, where four different products, including methanol (CH_3OH), ethanol (CH_3CH_2OH), n-propanol ($CH_3CH_2CH_2OH$), and formate (HCOO-) were detected in most of the samples. The productivity curves for all the electrodes are shown in **Fig. 6.12**. The formate requires only $2e^-$ for generation of one molecule therefore; the formation rate of $HCOO^-$ is higher over alcohols at the all studied potentials. Also, the productivity of formate increased with increase in applied potential starting from nearly 100 μmol $L^{-1}h^{-1}$ at -0.4 V (vs. RHE) to 1000 μmol $L^{-1}h^{-1}$ at -1.0 V (vs. RHE). The similar trend was observed in case of methanol, ethanol, and n-propanol. The highest productivity for ethanol was observed to be 160 μmol $L^{-1}h^{-1}$ at -1.0 V (vs. RHE) using $CuO\text{-}ZnO_{10}$ electrode whereas with CuO, $CuO\text{-}ZnO_5$, $CuO\text{-}ZnO_{15}$, and $CuO\text{-}ZnO_{20}$ electrodes it was 68, 109, 112, and 116 μmol $L^{-1}h^{-1}$ respectively at the same conditions . N-propanol is also detected beyond -0.8 V (vs. RHE) over all studied electrodes. It is also reported that thermodynamically methanol is the least favored product as compared to that of ethanol and n-propanol [106].

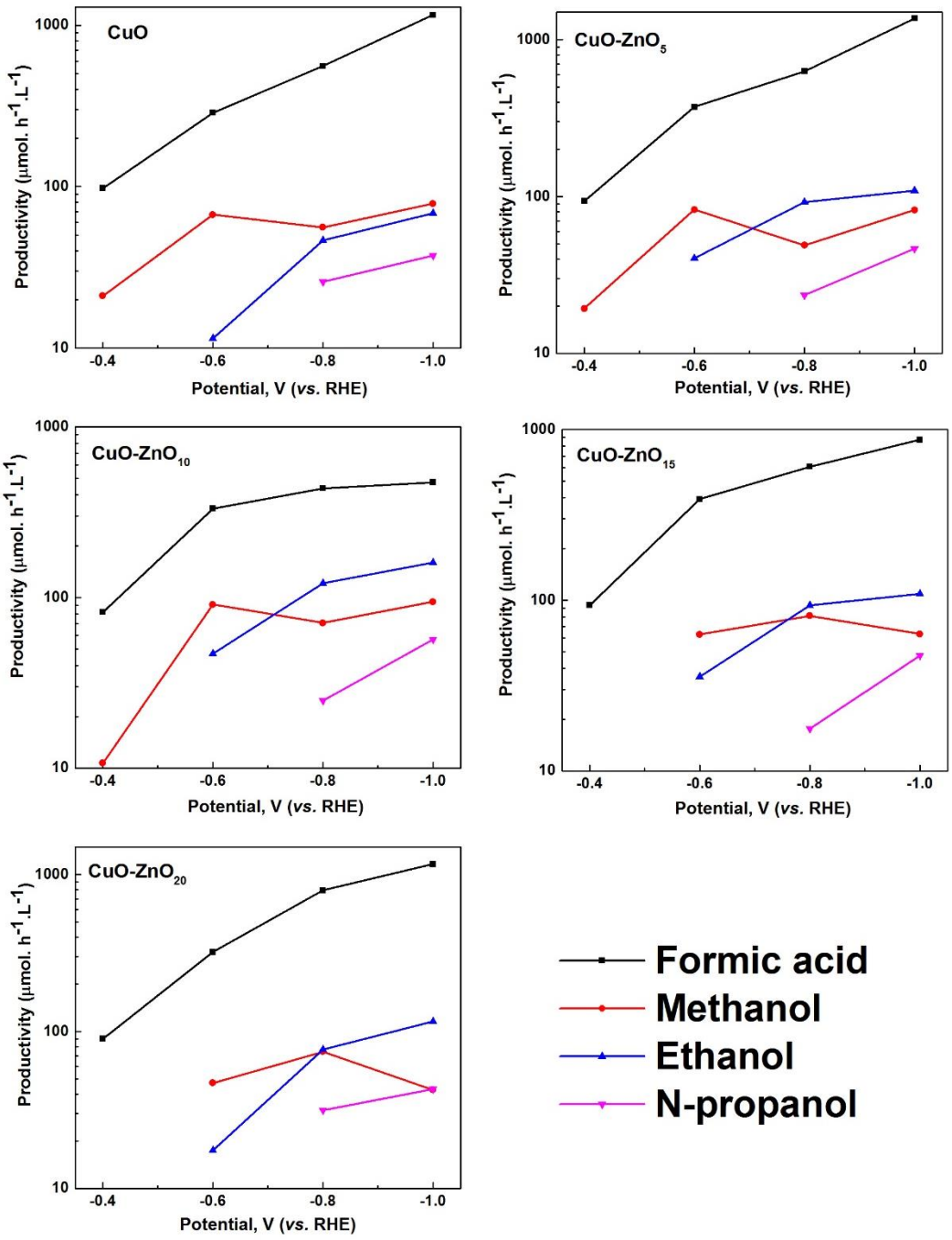

Fig. 6.12 *Comparison of productivity of formic acid, methanol, ethanol and n-propanol over different electrodes*

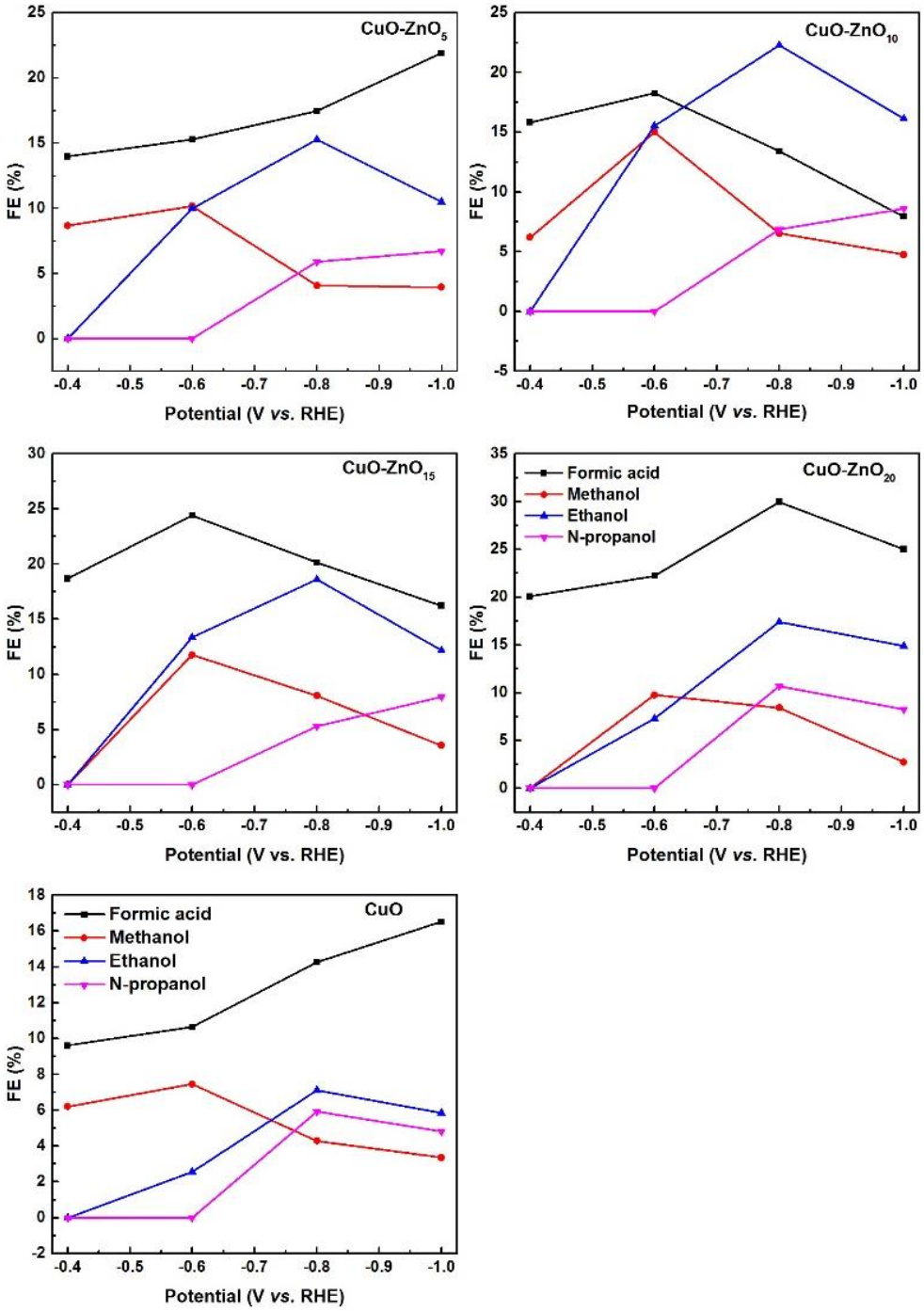

Fig. 6.13 *FE of all the products over different CuO-ZnO$_x$ electrodes*

Production rates are important for industrial deployment of ECO$_2$R process. Similarly, calculation of FE gives idea about selectivity and economic feasibility of the process [231]. Interestingly, the CuO-ZnO$_x$ electrodes showed different FE for methanol, ethanol, n-propanol, and formic acid depending on the CuO to ZnO ratio (**Fig. 6.13**). Incorporating ZnO into CuO enhances the C_{2+} products selectivity, especially ethanol, while suppressing the formation of formic acid in liquid product. Among the five CuO-ZnO$_x$ electro-catalysts, CuO-ZnO$_{10}$ shows

the highest FE for ethanol at -0.8 V (vs. RHE) while the FE for formic acid is lower. For example, the FE of ethanol increased from ~7.10 % for CuO to 22.27 % for CuO-ZnO_{10} while further increase in ZnO loading to 15 and 20 wt.% in the electro-catalyst, the FE decreased to 18.61 and 16.41 % respectively at the similar potential (~-0.8 V vs. RHE). The similar trend was observed in case of methanol and n-propanol. The FE of methanol increased from ~7.44 % to 15.02 % using CuO and CuO-ZnO_{10} respectively at -0.6 V (vs. RHE) and FE of n-propanol increased from 4.5% to 10.23 % on CuO and CuO-ZnO_{20} electrodes at -0.6 V (vs. RHE). The enhanced selectivity of ethanol over CuO-ZnO_{10} may be ascribed to the balanced CuO and ZnO percentage for maximum C-C coupling [115, 230]. Performance of optimized CuO-ZnO_{10} electrode is comparable with other reported work as shown in **Table 6.2**.

Table 6.2 *Comparison of CO_2 reduction performance of similar electro-catalysts reported in the literature*

Catalyst	**Conditions**	**Faradaic efficiency of ethanol (%)**	**CD (mA cm^{-2})**	**Stability (h) and Type of cell**	**Ref.**
Cu-Zn mixture	0.1 M $KHCO_3$ -1.2 V (*vs.* RHE)	2.2	5.7	15 h, H-Type	[232]
Cu/ZnO (1010)	0.1 M $KHCO_3$ -1.4 V (*vs.* RHE)	10.2	--	H-Type	[116]
ZnO-shell/CuO-core bi-metal-oxide	0.1 M $KHCO_3$ -1.05 V (*vs.* RHE)	31	10.5	H-Type	[115]
Cu_4Zn	0.1 M $KHCO_3$ -1.05 V (*vs.* RHE)	29.1	2.1	5 h, H-Type	[113]
HMMP Cu_5Zn_8	0.1 M $KHCO_3$ -0.8 V (*vs.* RHE)	46.6	2.3	11 h, H-Type	[233]
CuAg nanocoral	0.2 M $CsHCO_3$ - 1.00 V (*vs.* RHE)	10	8	Sandwich style, gas flow	[234]
CuAg alloy	0.1 M $KHCO_3$ -1.00 V (*vs.* RHE)	10	--	Sandwich style, gas flow	[76]
CuAu (nanowires)	0.1 M $KHCO_3$ -1.05 V (*vs.* RHE)	22.6	42.87	H-Type	[117]
ZnO	0.1 M $KHCO_3$ -0.8 V (*vs.* RHE)	ND	1.5	H-Type	This work
CuO	0.1 M $KHCO_3$ -0.8 V (*vs.* RHE)	6.2	4.5	H-Type	
CuO-ZnO_{10}	0.1 M $KHCO_3$ -0.8 V (*vs.* RHE)	22.27	3.78	12 h, H-Type	

6.3.4. Reaction kinetics/Tafel plot

To shed light on the kinetic mechanism of the ECO_2R over the $CuO\text{-}ZnO_x$ electrodes, a plot of the log of the overall CD versus the potential (Tafel plot) was obtained by LSV data [227, 235]. As shown in **Fig. 6.14**, CuO electrode shows a Tafel slope of 144 mV dec^{-1} which is nearer to theoretical Tafel slope (118 mV dec^{-1}) for initial e- transfer to CO_2 molecule for the generation of $^{*}CO_2$ [198]. In contrast, ZnO loaded electrodes show higher Tafel slope than CuO alone, and with increase in ZnO loading, the Tafel slope is also increasing. The highest Tafel slop of 208 mV dec^{-1} was observed for $CuO\text{-}ZnO_{20}$, indicating that its reaction kinetics is significantly weaker than that of $CuO\text{-}ZnO_5$, $CuO\text{-}ZnO_{10}$, and $CuO\text{-}ZnO_{15}$ having Tafel slope of 151, 171, and 189 mV dec^{-1} respectively [236]. Tafel slopes of all the electrodes are in agreement with LSV curves. In general, the multi-carbon product selectivity of ECO_2R is governed by the binding strength of adsorbed *CO and *H on the electrode surface. Many authors [113, 115] reported that the Cu has a moderate binding energy for adsorbed *CO, therefore *CO species can further take e- and *H, and combine with another *CO for multi-carbon production. On the other side, Zn electrode has a relatively weak binding strength for adsorbed *CO therefore, *CO desorbs from electrode surface without reacting further and produces CO with high selectivity [157]. Many researchers proposed Cu-Zn composite electro-catalyst for improving multi-carbon production [115, 168, 230, 232]. The generated CO and Zn active sites may have transferred to Cu active site having high binding energy *CO. Two *CO combine by taking required e- and *H for the multi-carbon product generation. Interestingly, in these experiments, with optimized $CuO\text{-}ZnO_{10}$ electrode, ethanol production was found to be higher as compared to that with CuO electrode. That means, $CuO\text{-}ZnO_{10}$ electrode gives balanced CO supply for higher CO dimerization. The ZnO in the electrocatalyst provides supplementary CO to increase the local CO concentration on the Cu surface and in turn, *CO surface coverage, leading to the acceleration of CO-to-ethanol products conversion. An optimal ZnO mass loading, at a specific potential, supplies CO at a rate that achieves a saturation of *CO surface coverage. Moreover, increasing Zn content beyond 10% in the $CuO\text{-}ZnO_x$ electrode, results in an excess supply of CO, and subsequently lowers the *CO dimerization. Hydrogen adsorbs dissociatively on bridge sites between the Cu and Zn atoms, which is an important step in the catalytic hydrogenation of CO_2 to produce ethanol [237, 238]. It is noted that the balance between CO supply rate and CO dimerization rate with balanced hydrogen availability can only determine the optimum FE of C_{2+} products [239]. It is also reported that the formation of C-C bonds on Cu-Zn is thermodynamically favorable because it shows lower energy toward the

bound intermediates *CO-*CO than that on the pure Cu (111). Also, pure Cu (111) surface shows largest C-C distance indicating a poor tendency for the C-C coupling. However, Cu with Zn shows decreased C-C distance indicating a higher possibility for the C-C coupling [233].

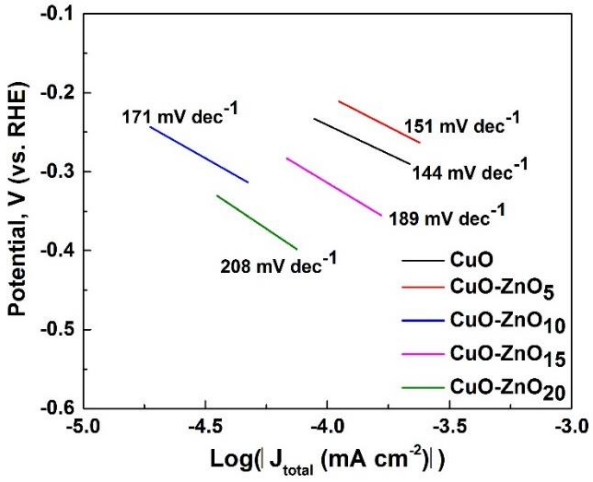

Fig. 6.14 *Tafel plots of CuO, CuO-ZnO$_5$, CuO-ZnO$_{10}$, CuO-ZnO$_{15}$, and CuO-ZnO$_{20}$*

6.3.5. Long term performance and reusability study

To test the long-term durability and stability of the CuO-ZnO$_{10}$ electrode, ECO$_2$R experiments were performed over an extended period at the optimized conditions. The total CD was maintained at around -3.74 mA cm^{-2} during the 12 h running (**Fig. 6.15a**). Moreover, the CuO-ZnO$_{10}$ also kept its original morphology after the stability test (**Fig. 6.17**). Also, post characterization by EDX reveals that the surface composition has changed after ECO$_2$R which suggests the surface poisoning due to adsorption of K+ from the electrolyte or formation of graphitic carbon [201, 202]. Reusability experiments on CuO-ZnO$_{10}$ electrode were also performed for 6 consecutive runs. During reusability experiments, the electrode was washed by water and reused for next run. As shown in **Fig. 6.15b**, the ethanol selectivity is maintained for first 3 reuse runs but later it decreased. The decrease in ethanol selectivity is mainly ascribed to active surface poisoning as discussed earlier.

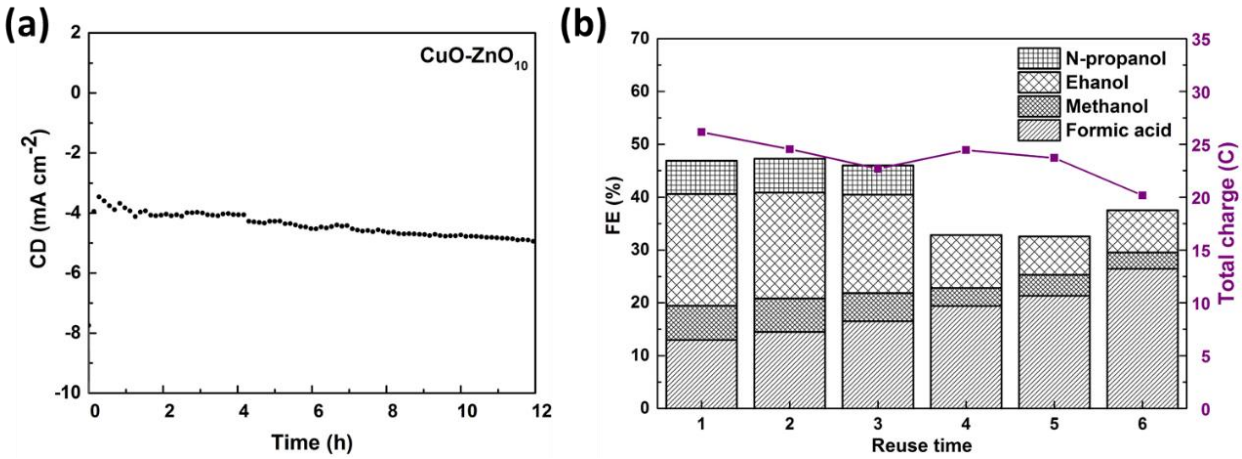

Fig. 6.15 *Long term stability* ***(a)*** *and reuse test performance* ***(b)*** *of representative CuO-ZnO$_{10}$ electrode*

6.3.6. Post characterization

The reaction active sites were studied by performing XRD analysis of working electrode after 0, 10, and 120 min of ECO_2R. The XRD patterns of representative electrodes are shown in **Fig. 6.16**. Before ECO_2R, both the electrodes show CuO and ZnO phases only. After 10 min ECO_2R, the intensity of CuO and ZnO peaks has decreased and intensity of metallic phase Cu has increased due to reduction of CuO and ZnO itself at initial time. Negligible CuO and ZnO intensity peaks are observed after 2 h CO_2 reduction. It is inferred that the CO_2 reduction can take place on metallic sites of Cu and Zn [232].

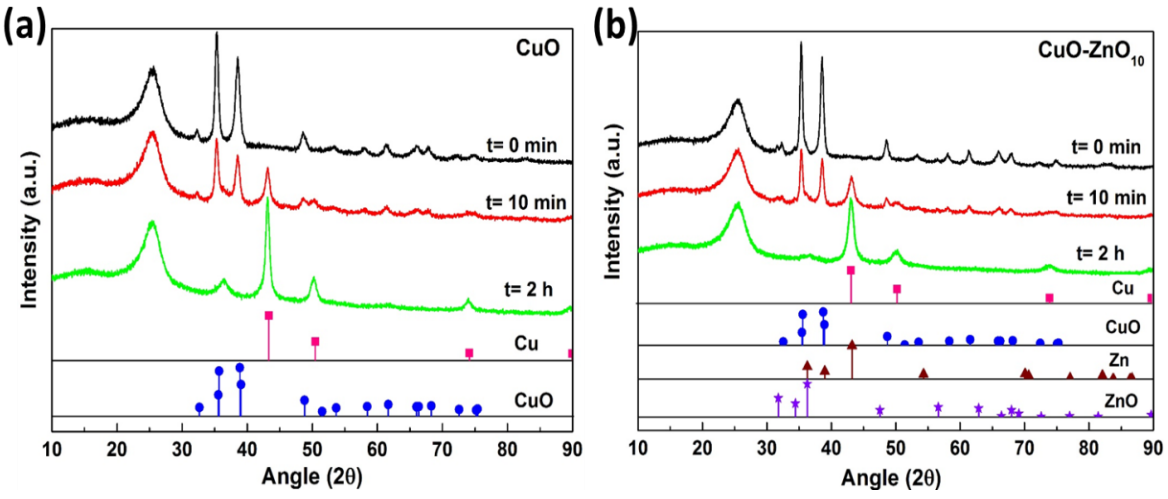

Fig. 6.16 *Post XRD analysis of* ***(a)*** *CuO and* ***(b)*** *CuO-ZnO10 electrodes at different time intervals*

The CuO-ZnO_{10} also kept its original morphology after the stability test (**Fig. 6.17**). Also, post characterization by EDX reveals that the surface composition has changed after ECO_2R which suggests the surface poisoning due to adsorption of K+ from the electrolyte or formation of graphitic carbon [201, 202].

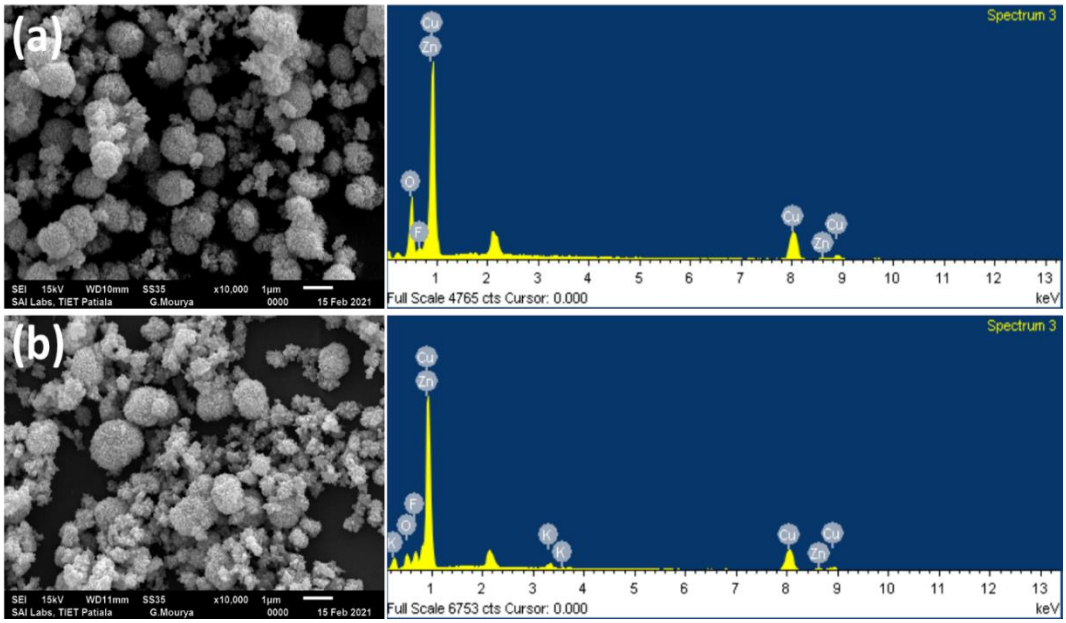

Fig. 6.17 *SEM-EDX analysis of working electrode* ***(a)*** *before and* ***(b)*** *after* ECO_2R *at -0.8 V (vs. RHE) for 2 h*

6.4. Conclusions

The CuO-ZnO_x electro-catalysts were successfully prepared by a simple co-precipitation method and used for electrochemical reduction of CO_2. The Cu/Zn atomic ratios can be adjusted by simply changing the precursor concentrations. The CuO electrode exhibits low selectivity for ethanol with less than 9% FE. In contrast, addition of 10 wt.% ZnO with CuO (i.e. CuO-ZnO_{10}) gives improved catalytic selectivity for ethanol with FE of ~22.3% at −0.8 V (vs. RHE) and a total CD of -3.78 mA cm^{-2}. It is believed that the chemistry of the reduced Cu–Zn interface plays an important role in the ethanol selectivity. Also, the CuO-ZnO_{10} catalyst shows excellent long term stability with no appreciable change in CD for at least 12 h. The current research highlights the significance of bimetallic or even trimetallic materials for ECO_2R applications. Chemical composition of electro-catalysts can be easily tuned by mixing various types of metals/metal oxides. This study could open the opportunities for sustainable development of CO_2 conversion electro-catalysts that are both efficient and may be cost-effective in large-scale manufacturing.

Chapter 7- Electrochemical CO_2 reduction on oxide derived $CuZn_x$/NGN

7.1. Synthesis of $CuZn_x$/NGN catalyst

Initially, the NGN was uniformly dispersed in 100 mL deionized water at room temperature by ultra-sonication for 1 h. Subsequently, $Cu(NO_3)_2 \cdot 3H_2O$ and $Zn(NO_3)_2 \cdot 6H_2O$ were added into the NGN solution. The resulting mixture was stirred at 70 ^oC for 10 min to ensure the complete mixing of $Zn(NO_3)_2 \cdot 6H_2O$ and $Cu(NO_3)_2 \cdot 3H_2O$. Subsequently, 1 M Na_2CO_3 solution was added drop-wise, as a precipitating agent, under constant stirring to reach the pH of the solution to 11 and stirring was continued for 5 h. Later, precipitate was recovered by centrifugation and subsequent washing with ethanol and water. Further, precipitate was kept in a hot air oven at 100 ^oC for 12 h to remove moisture and any volatiles. Finally, the product was calcined in a tubular furnace under air atmosphere at 350 ^oC for 2 h with a heating rate of 5 $^oC\ min^{-1}$. After calcination, the product was stored in air tight bottle for further use. In order to investigate the effect of Zn weight % in the oxide derived $CuZn_x$/NGN electro-catalysts, the $Zn(NO_3)_2 \cdot 6H_2O$ amount was varied in stoichiometric proportion and CuO loading was fixed to 20% as given in section 5.3.2.1. The detailed synthesis recipe is shown in **Table 7.1**. The obtained products are denoted as $CuZn_x$/NGN; where x is the expected loading of ZnO (weight %) in $CuZn_x$/NGN. For the control experiment, the CuO/NGN, ZnO/NGN and $CuZn_{20}$ were prepared using the same procedure as described above without addition of $Zn(NO_3)_2 \cdot 6H_2O$, $Cu(NO_3)_2 \cdot 3H_2O$, and NGN respectively. The outline for preparation of $CuZn_x$/NGN is shown in **Fig. 7.1**.

Table 7.1 *Electro-catalysts prepared with different ZnO loadings (weight %)*

Sr. No.	Electro-catalyst	$Cu(NO_3)_2 \cdot 3H_2O$ (mg)	$Zn(NO_3)_2 \cdot 6H_2O$ (mg)	NGN (mg)
1	CuO/NGN	75.85	0	200
2	$CuZn_{10}$/NGN	75.85	9.13	200
3	$CuZn_{20}$/NGN	75.85	18.26	200
4	$CuZn_{30}$/NGN	75.85	27.39	200
5	$CuZn_{40}$/NGN	75.85	36.52	200

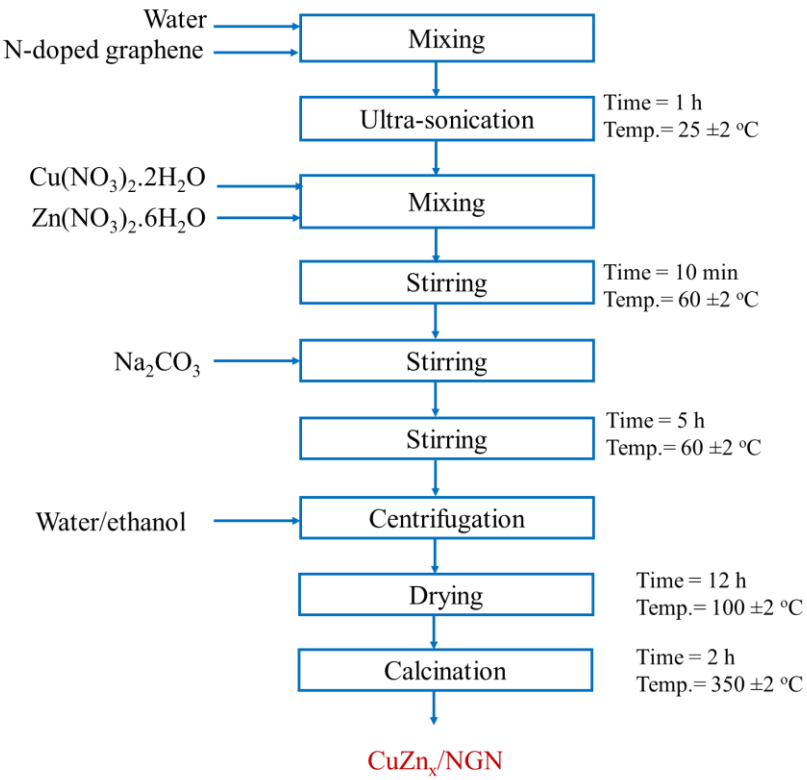

Fig. 7.1 *Schematic for the preparation of $CuZn_x$/NGN*

7.2. Preparation of working electrode

Working electrode was prepared by drop casting method. Briefly, a mixture of catalyst powder, Nafion solution, and iso-propanol were sonicated for 1 hour in water bath for homogeneous mixing. This mixture was uniformly loaded onto a 1 cm × 1 cm pretreated carbon paper (refer section 3.5.2. for pretreatment of carbon paper). The coated electrodes were then dried at 100 °C for 12 h in an oven. At the end, loading of 0.5 mg cm^{-2} was achieved. Each electrode is named as the corresponding coated electro-catalyst. For example, an electrode coated with CuO/NGN electro-catalyst is denoted as CuO/NGN electrode.

7.3. Results and discussion

7.3.1. Physico-chemical characterization

7.3.1.1. X-ray diffraction analysis

The X-ray diffraction measurements were performed at a scan rate of 6^o min^{-1} between $20^o \geq 2\theta \geq 80^o$ to study the crystalline structures of CuO/NGN and $CuZn_x$/NGN. As shown in **Fig. 7.2**, the two strong peaks at 35.5 and 38.7° correspond to (-111) and (111) planes of monoclinic CuO, respectively (JCPDS #01-089-5899). The characteristic peaks at 31.9, 34.5, 36.1, 47.6,

56.7, and 63º are indexed as (100), (002), (101), (102), (110), and (103) facets of hexagonal ZnO structure (JCPDS #01-089-0510). Due to larger weight percentage of CuO compared to that of ZnO, the diffraction peaks of CuO dominate over those of ZnO. The broad diffraction peaks also indicate that the both CuO and ZnO particles are in nanoscale size. Also, the XRD patterns of all the samples show an additional characteristic peak at ~25.2° assigned to the (002) plane of hexagonal graphite structure, suggesting that the oxide derived Cu and Zn are supported on N-doped graphene. Absence of any other peak suggests that the as-prepared samples are of high purity.

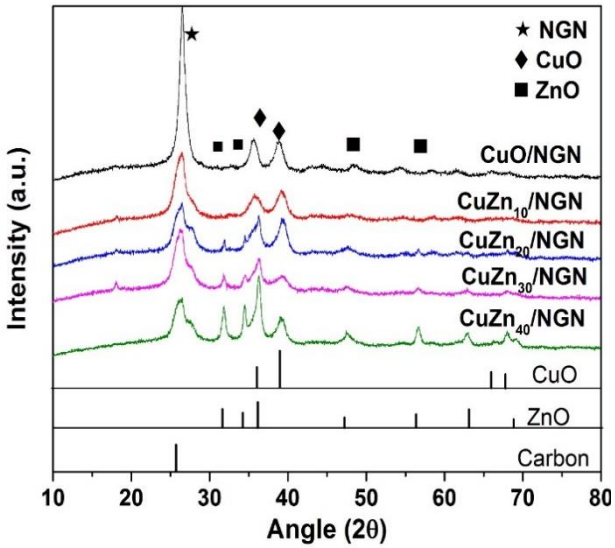

Fig. 7.2 *XRD patterns of different samples*

7.3.1.2. X-ray photoelectron spectroscopy

Types of nitrogen species in NGN and chemical states of Cu and Zn were identified by X-ray photoelectron spectroscopy (XPS). **Fig. 7.3** shows that the survey scan spectra of CuO/NGN and $CuZn_x$/NGN are all composed of C (285 eV, C1s), O (532 eV, O1s), N (399 eV, N1s), Zn (1024 eV, Zn 2P) and Cu (934 eV, Cu2p; 77 eV, Cu3p) elements [230]. Decrease in Cu 2p peak intensity was clearly visible after loading of ZnO. Also, the peaks related to Zn shows higher intensity on increasing the ZnO loading in the $CuZn_x$/NGN. The curve fitting of N1s, Cu 2P, and Zn 2P was performed on XPS Peak Fit software where Gaussian-Lorentzian product function was used with Shirley method for background correction (**Fig. 7.4, Fig. 7.5, Fig. 7.6**) The deconvoluted high-resolution spectrum of N 1s (**Fig. 7.4**) reveals that nitrogen species have been effectively integrated into carbon matrix. Three different N species were observed at ca. 398.3, 400.1, and 402.7 eV, corresponding to pyridinic N, pyrollic N, and pyridinic N-oxide [240]. Nitrogen content in the sample ($CuZn_{20}$/NGN) has been calculated as 8.54 atom

%. The pyridinic N has the highest relative concentration (5.2 atom %) followed by graphitic (2.6 atom %) and pyridinic N-oxide (0.74 atom %).

The high-resolution Cu 2p XPS spectra show two peaks at 952.5 eV and 932.6 eV assigned to the Cu 2p1/2 and Cu 2p3/2 respectively. A binding energy difference between Cu 2p1/2 and Cu 2p3/2 was about 19.75 eV, which is the characteristic of Cu^{2+} ions for all five samples (**Fig. 7.5**) [115]. Furthermore, three satellite peaks at 940.56 eV, 943.07 eV and 962.43 eV confirm the existence of CuO phase. Similarly, the high-resolution XPS spectrum of Zn 2P shows two peaks at 1022.3 and 1045.4 eV which can be, respectively related to Zn 2p3/2 and 2p1/2 [241]. The binding energy difference of 23.2 eV between Zn 2p3/2 and 2p1/2 further confirms the presence of ZnO phase in all the samples (**Fig. 7.6**) [113, 242].

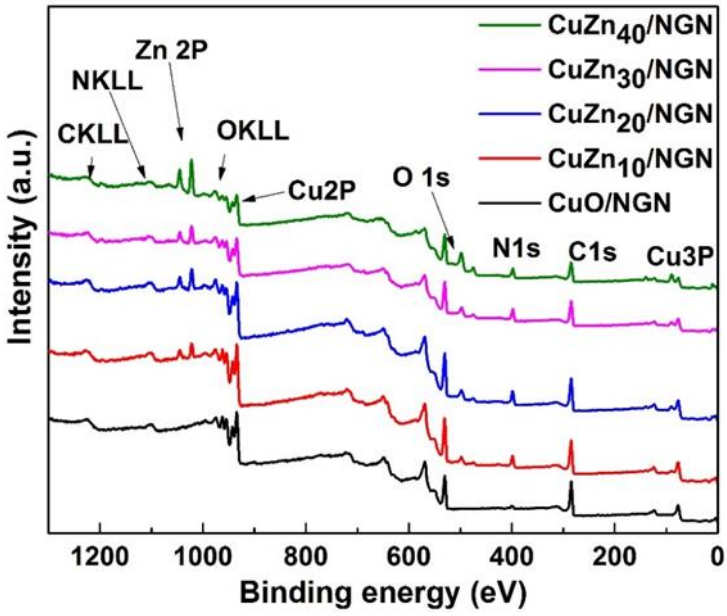

Fig. 7.3 *XPS survey spectra of CuO/NGN, $CuZn_{10}$/NGN, $CuZn_{20}$/NGN, $CuZn_{x30}$/NGN, and $CuZn_{40}$/NGN*

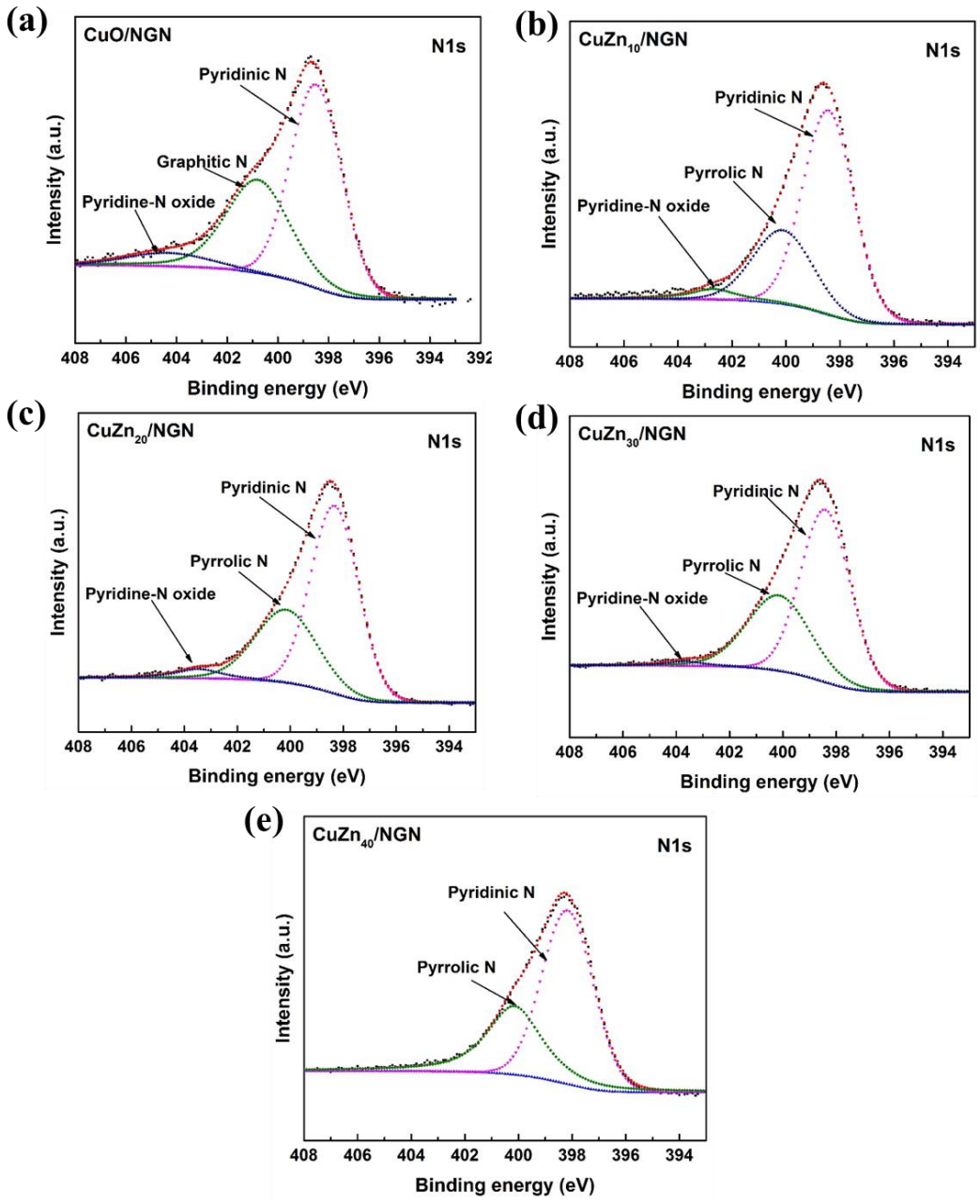

Fig. 7.4 *High resolution XPS spectra of N1s of CuO/NGN* ***(a)***, *CuZn10/NGN* ***(b)***, *CuZn20/NGN* ***(c)***, *CuZnx30/NGN* ***(d)***, *and CuZn40/NGN* ***(e)***

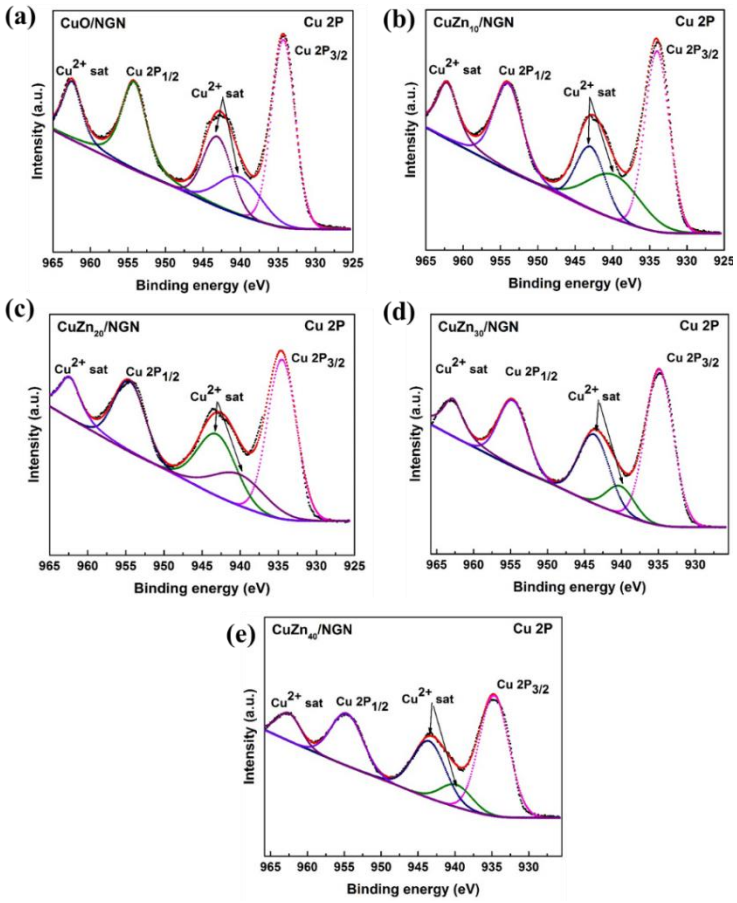

Fig. 7.5 *High resolution XPS spectra of Cu 2P of CuO/NGN* ***(a)***, *$CuZn_{10}$/NGN* ***(b)***, *$CuZn_{20}$/NGN* ***(c)***, *CuZnx$_{30}$/NGN* ***(d)***, *and $CuZn_{40}$/NGN* ***(e)***

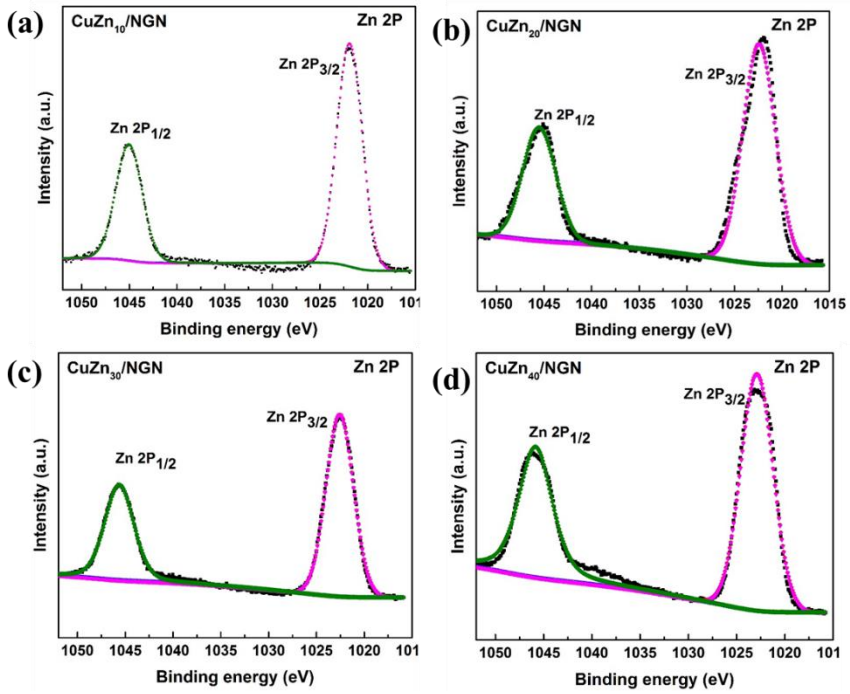

Fig. 7.6 *High resolution XPS spectra of Zn 2P of $CuZn_{10}$/NGN* ***(a)***, *$CuZn_{20}$/NGN* ***(b)***, *CuZnx$_{30}$/NGN* ***(c)***, *and $CuZn_{40}$/NGN (d)*

7.3.1.3. Scanning electron microscopy

Surface morphology and dispersion of active metals in the electrode material considerably influence the activity and selectivity of ECO_2R [19, 226]. SEM images of $CuZn_x$/NGN are shown in **Fig. 7.7**. It shows that CuO and ZnO nanoparticles are uniformly dispersed on NGN support up to 20 weight% ZnO loading. However, further increase in the ZnO loading, particle size increased due to agglomeration. The performance of the electro-catalysts is enhanced by a uniform distribution of metals on the support. The weight ratio of Cu:Zn for all ZnO loaded samples determined by the EDX spectrum is 1:0.09, 1:0.18, 1:0.29, and 1:0.41 (**Fig. 7.8**), which is quite close to the stoichiometric amounts of precursors added during the preparation.

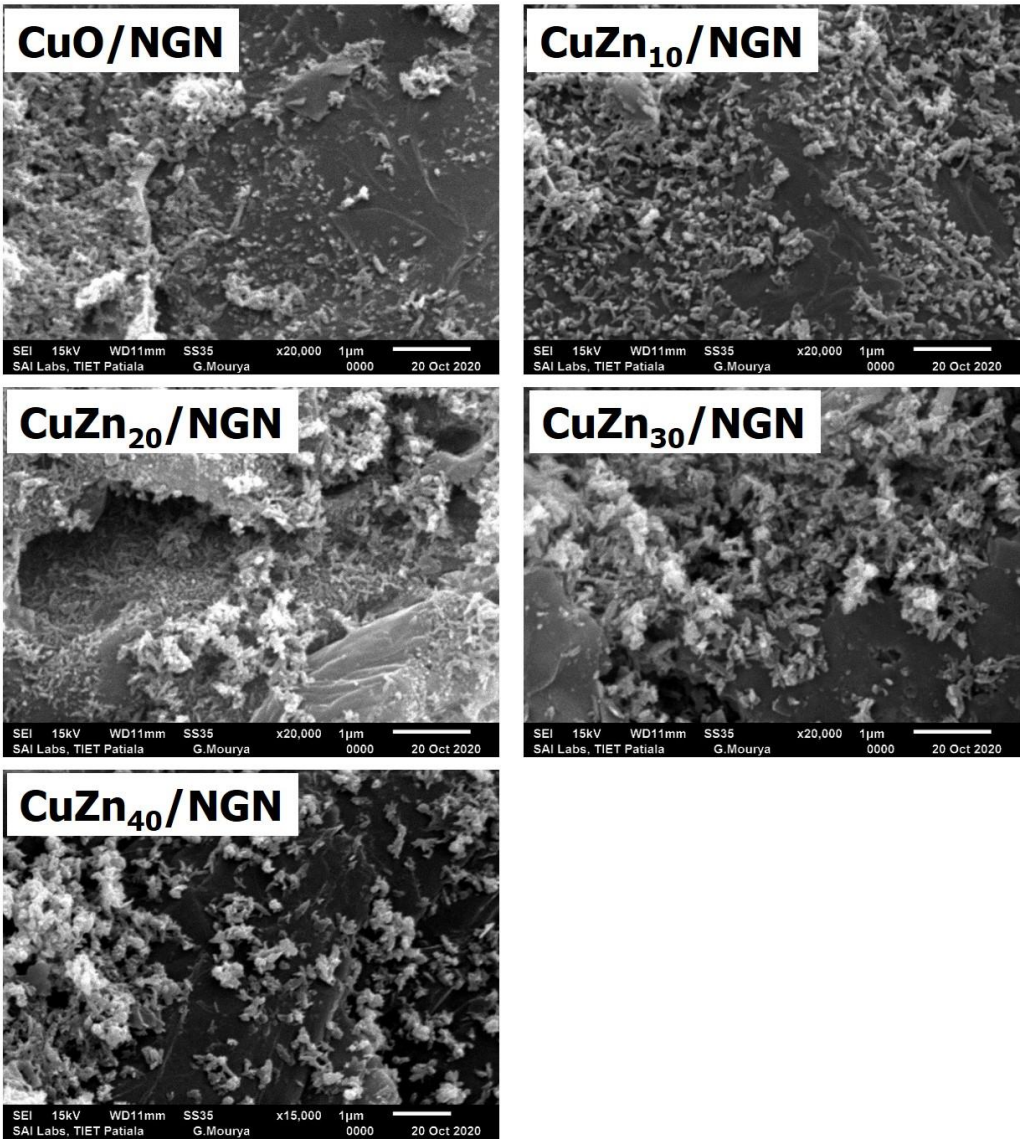

Fig. 7.7 *SEM images of CuO/NGN, $CuZn_{10}$/NGN, $CuZn_{20}$/NGN, $CuZn_{30}$/NGN, and $CuZn_{40}$/NGN*

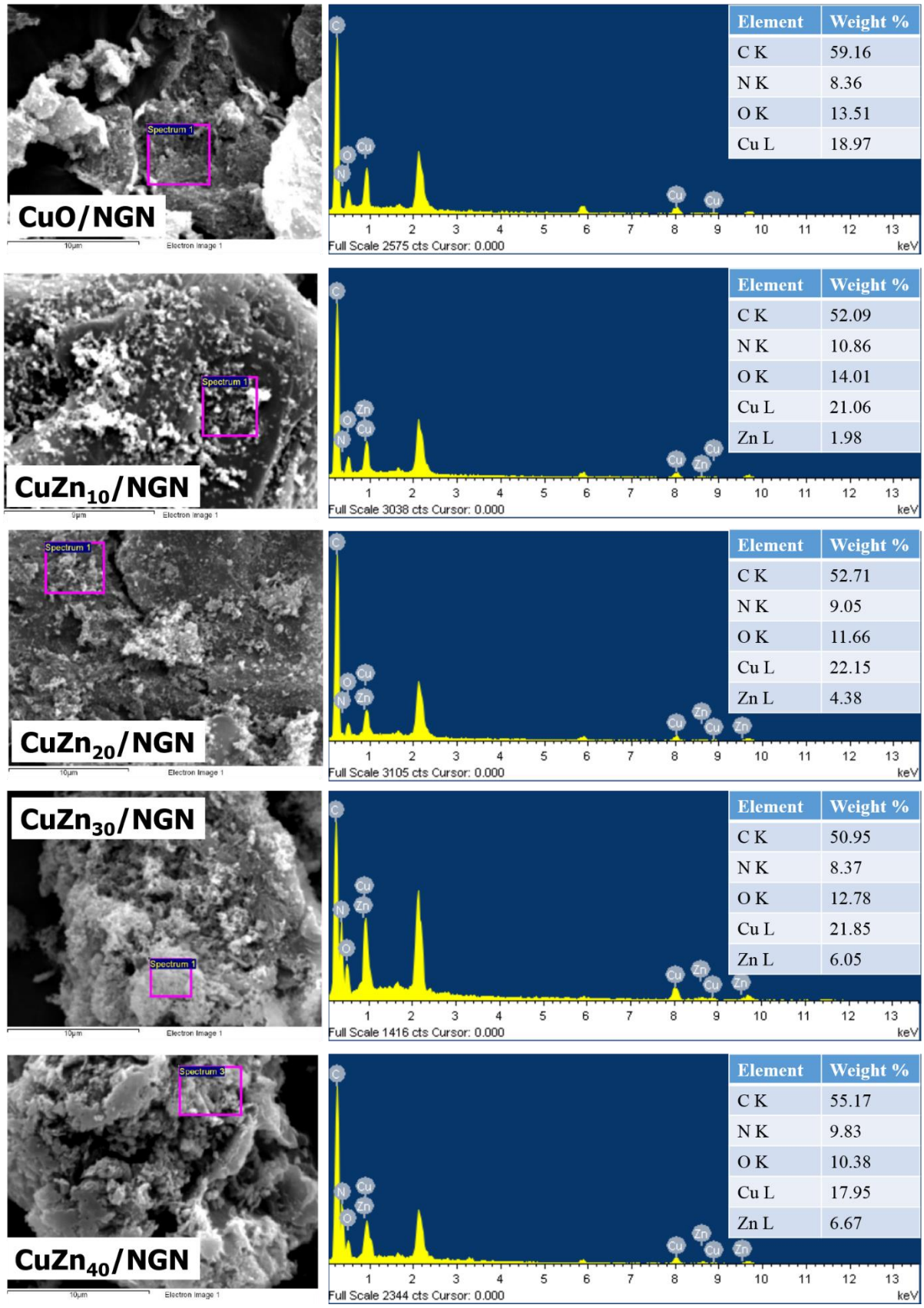

Fig. 7.8 *SEM images of CuO/NGN, $CuZn_{10}$/NGN, $CuZn_{20}$/NGN, $CuZn_{30}$/NGN, and $CuZn_{40}$/NGN with corresponding EDX analysis of the electro-catalysts*

7.3.1.4. Transmission electron microscopy

From **Fig. 7.9**, it is clearly observed that the opaque oxide derived Cu and Zn nanoparticles are tightly attached to the semi-transparent NGN sheets. SAED image (**Fig. 7.9**) shows that sample is crystalline and the diffraction patterns can be indexed to the structure of CuO and ZnO, which is in line with the XRD results. From the EDX elemental mapping of a representative $CuZn_{20}$/NGN nanoparticles (**Fig. 7.10**), it is shown that elements C, O, Zn, and Cu are uniformly distributed. The dispersion of nanoscale CuO and ZnO particles on the high surface area N-doped graphene assists in improving the contact area of CuO and ZnO with electrolyte, which further decreases migration length of the ions to Cu and Zn active sites, and therefore improves the ECO_2R performance.

7.3.1.5. Raman spectroscopy

Fig. 7.11a shows the Raman spectra of NGN, CuO/NGN and other four $CuZn_x$/NGN samples recorded at excitation wavelength of 514 nm. As can be seen from the NGN, CuO/NGN and other four $CuZn_x$/NGN samples, two major peaks at 1350 cm^{-1} and 1575 cm^{-1} were have been observed which are related to D band and G band. The D band was attributed to the distorted hexagonal structure in the graphite layers and G band is caused by in-plane vibrations of sp2 hybridized C−C bonds. The value of I_D/I_G may be used to know the degree of reduction. In the present study, the values of I_D/I_G of all the samples remained unchanged (~1.05) on increasing the ZnO loading, indicating no change in sp2 hybridized carbon atom structure [130].

7.3.1.6. Fourier-transform infrared spectroscopy

For validating the XRD results about the formation of oxide derived $CuZn_x$ on NGN, FT-IR spectroscopy is another useful method. As shown in **Fig. 7.11**b, the main absorption peaks are obtained at 491 and 615 cm^{-1}, which are related to the characteristic stretching vibrations of Cu–O bond in the monoclinic crystal structure of CuO. Also, the strong peak at 454 cm^{-1} can be assigned to Zn–O stretching vibration [228]. However, the intensity of ZnO peak was very low due to its low concentration compared to that of CuO and NGN in the sample. The broad peak around 3400 cm^{-1} and small peaks around 2900 cm^{-1} correspond to OH stretching and CH (acetate) stretching respectively in the graphene material [137]. Above results confirm the dispersion of CuO and ZnO nanoparticles on NGN.

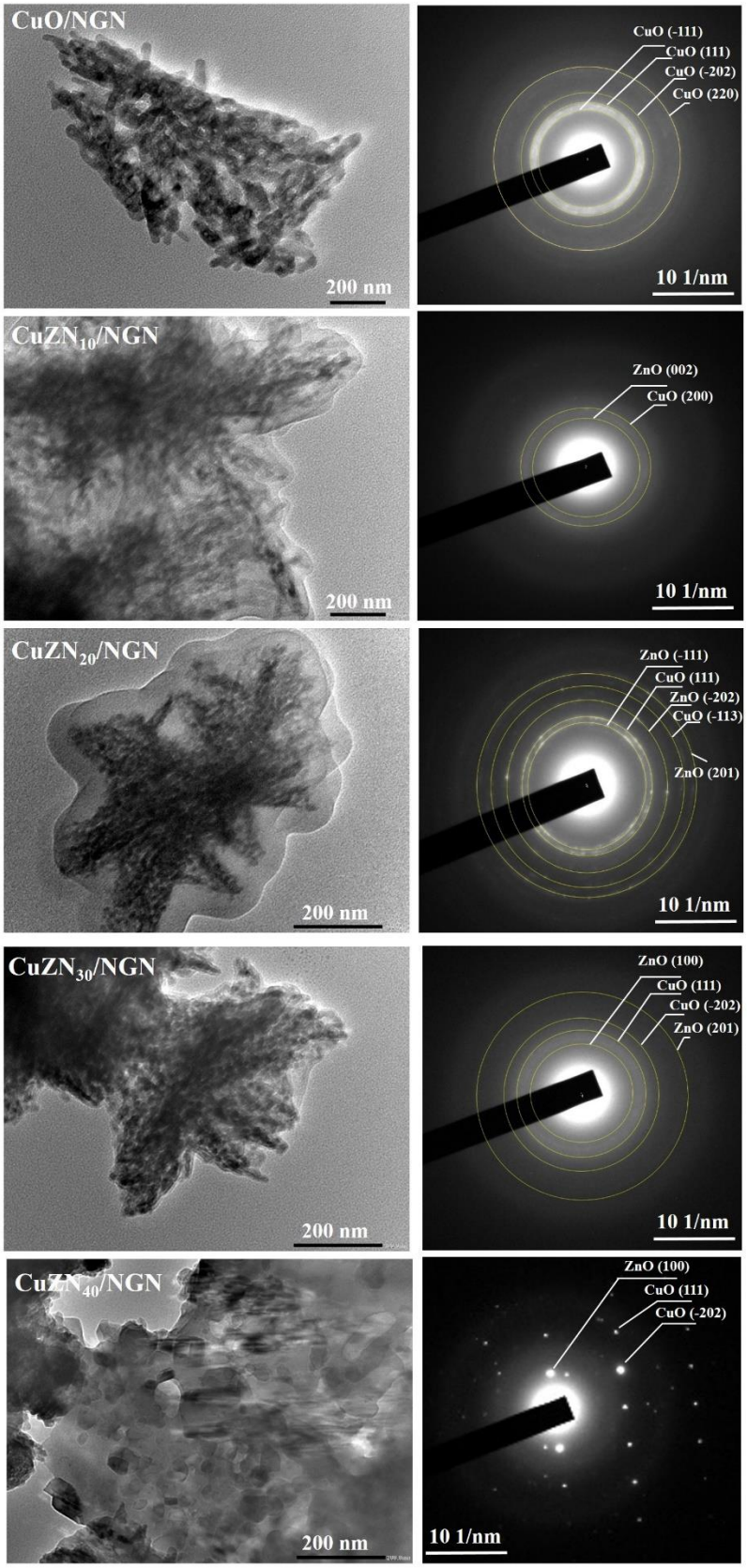

Fig. 7.9 *HR-TEM images of CuO/NGN, CuZn10/NGN, CuZn20/NGN, CuZn30/NGN, and CuZn40/NGN with corresponding SAED patterns*

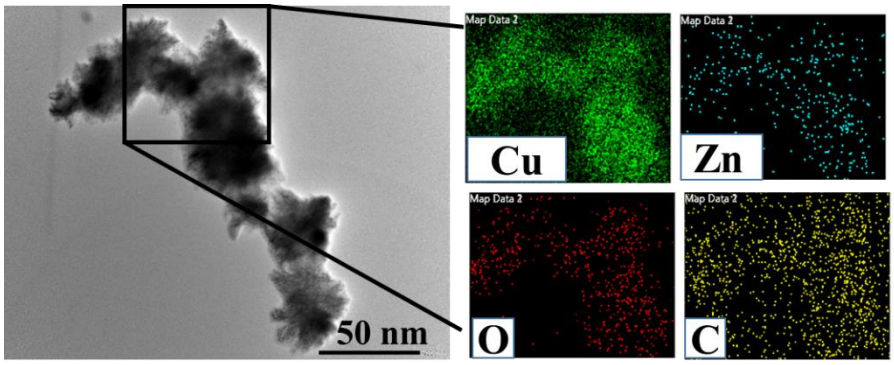

Fig. 7.10 *HRTEM image and elemental mapping results of $CuZn_{20}$/NGN*

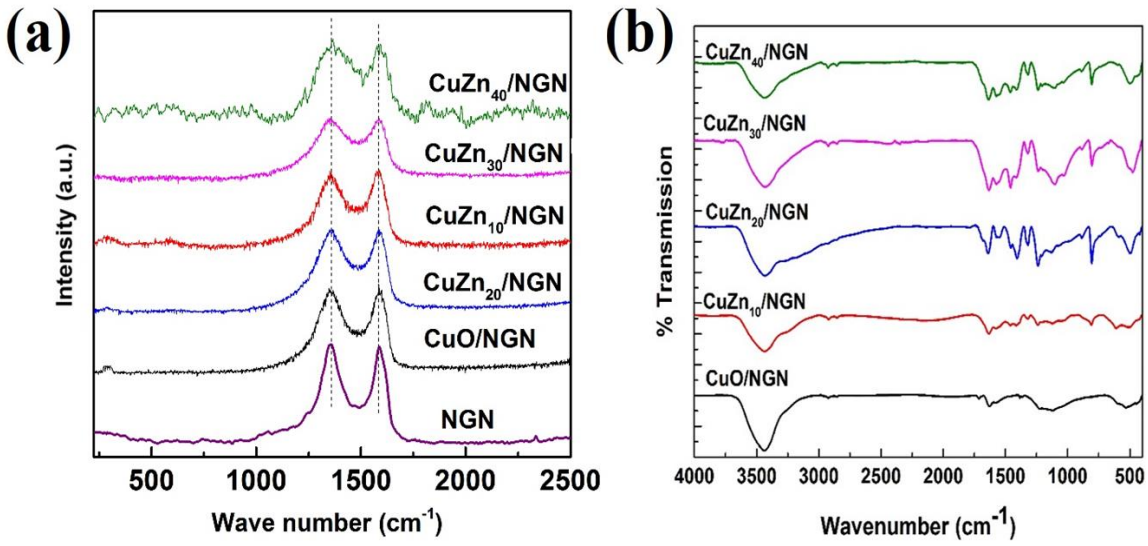

Fig. 7.11 (a) *Raman spectra and* ***(b)*** *FTIR spectra of all the catalysts*

7.3.1.7. N_2 sorption isotherms

The porous structure in electrode materials has a significant role in the overall CO_2 reduction performance. The well-developed hierarchical porous structure of electro-catalyst provides more accessibility to the active sites for ECO_2R. Therefore, the surface area and pore structure of the prepared electro-catalyst was investigated by N_2 adsorption/ desorption isotherms of all the samples. As shown in **Fig. 7.12a**, all the five samples show a type IV isotherm curve according to the IUPAC classification, suggesting the mesoporous structure. The specific surface area was calculated by Brunauer–Emmett–Teller (BET) method. The specific area of samples CuO/NGN, $CuZn_{10}$/NGN $CuZn_{20}$/NGN, $CuZn_{30}$/NGN, and $CuZn_{40}$/NGN were estimated to be 58.43, 54.66, 51.62, 45.60, and 39.77 $m^2\ g^{-1}$ respectively. It is decreased with increase in Zn loading in the electro-catalyst due to the contribution of Zn NPs which may have low surface area. The pore size distribution is studied by Barrett–Joyner–Halenda (BJH) using

the adsorption branch of the isotherm. **Fig. 7.12b** shows different peaks at around 2, 4, 8 and 15 nm, implying that there may be different types of mesopore structures within all the electro-catalysts since NGN is present in all the samples.

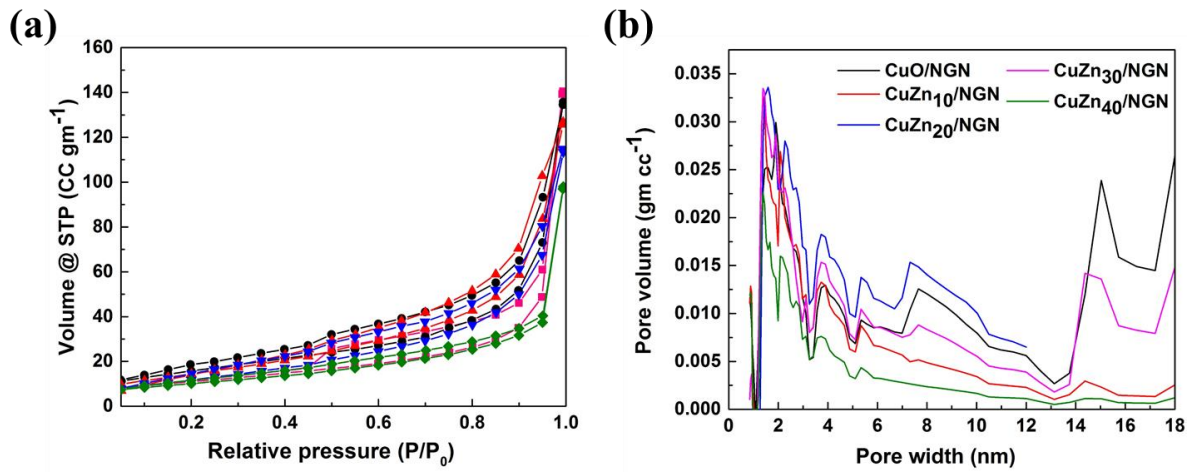

Fig. 7.12 (a) *BET nitrogen adsorption/desorption isotherms and* ***(b)*** *BJH pore size distribution of CuO/NGN, $CuZn_{10}$/NGN, $CuZn_{20}$/NGN, $CuZn_{30}$/NGN, and $CuZn_{40}$/NGN*

7.3.1.8. Thermogravimetric analysis

The thermal degradation of different precursors used in the synthesis of $CuZn_x$/NGN and representative electro-catalyst ($CuZn_{20}$/NGN) was investigated by thermogravimetric analysis (TGA). For this, the samples were heated up to 800 ^oC at a ramp rate of 10 ^oC min^{-1} under air atmosphere. As shown in **Fig. 7.13**, the oxidation of the NGN starts beyond 420 ^oC. Also, the nitrates of Cu and Zn are converted to corresponding CuO and ZnO respectively after annealing at 330 ^oC [243] which is further supported by no weight loss beyond 330 ^oC. Further, the rate of change in weight loss of $CuZn_{20}$/NGN is higher than that of NGN alone which confirms that the electro-catalyst is less thermally stable as compared to the NGN, probably because the loading of oxide derived Cu and Zn on the NGN matrix for enhancing the electronic properties of the electro-catalyst. However, this is not a concern in the current experiments as all the electro-catalysts are synthesized at 350 ^oC which is below the oxidation temperature.

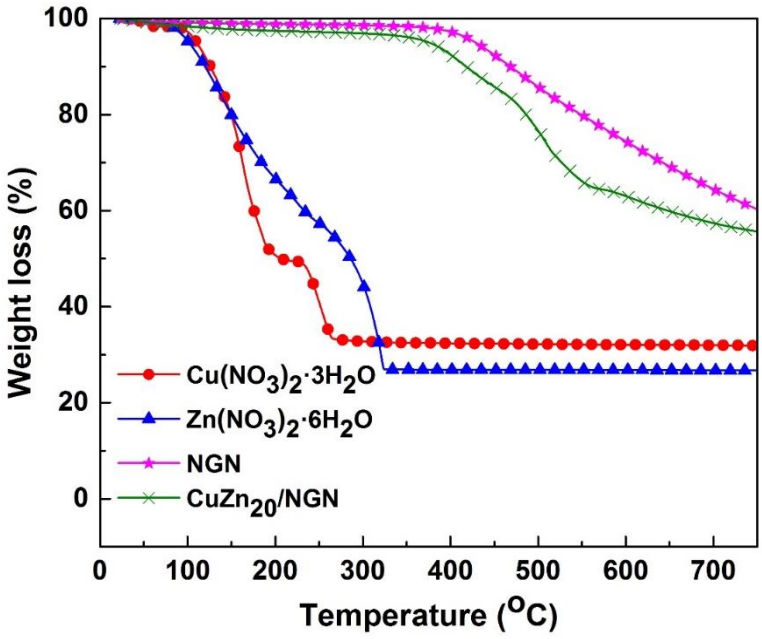

Fig. 7.13 *Thermogravimetric analysis (TGA) of copper nitrate, zinc nitrate, NGN and representative $CuZn_{20}$/NGN (under air atmosphere)*

7.3.2. Electrochemical characterization

7.3.2.1. Linear sweep voltammetry (LSV)

The ECO_2R activity of the electrodes was studied by recording linear sweep voltamogram (LSV) in CO_2 and N_2 saturated aqueous 0.1 M $KHCO_3$ solutions with scan rate of 10 mV s^{-1}. For this, high purity CO_2 or N_2 gas was bubbled at a rate of 15 mL min^{-1} in the 0.1 M $KHCO_3$ for 30 min before tests. In the pretreatment step, the electrodes were pre-reduced by performing cyclic voltammetry (CV) for 30 cycles at a scan rate of 50 mV s^{-1}. The recorded LSV scans are shown in **Fig. 7.14a**. The CD response for all the electro-catalysts in N_2-saturated electrolyte is smaller than that in CO_2-saturated electrolyte. The smaller CD under N_2 is attributed to only due to hydrogen evolution reaction (HER) whereas larger CD response in CO_2 is due to both reduction of CO_2 and the HER [40, 228]. Therefore, a catalyst that exhibits a higher CD in CO_2 electrolyte than that in N_2 one is considered as active for ECO_2R with respect to the HER at the corresponding applied potential. Comparing the LSVs in the CO_2 electrolyte, the CuO/NGN electrode shows increased CD than that of ZnO loaded electrodes. Furthermore, it is observed that increasing ZnO loading in the $CuZn_x$/NGN electro-catalyst, the corresponding electrode shows a lower CD response. Since the electrodes were prepared with the same catalyst loading of Cu, the one containing higher ZnO percentage in $CuZn_x$/NGN is expected to have more exposed Zn surface than Cu surface. Therefore, the decrease in ECO_2R

performance of the $CuZn_x$/NGN electrode on increasing the ZnO loading is due to the development of less active Zn sites with simultaneous decrease of more active Cu sites. Obtained LSV response for $CuZn_x$/NGN is in agreement with the literature [244].

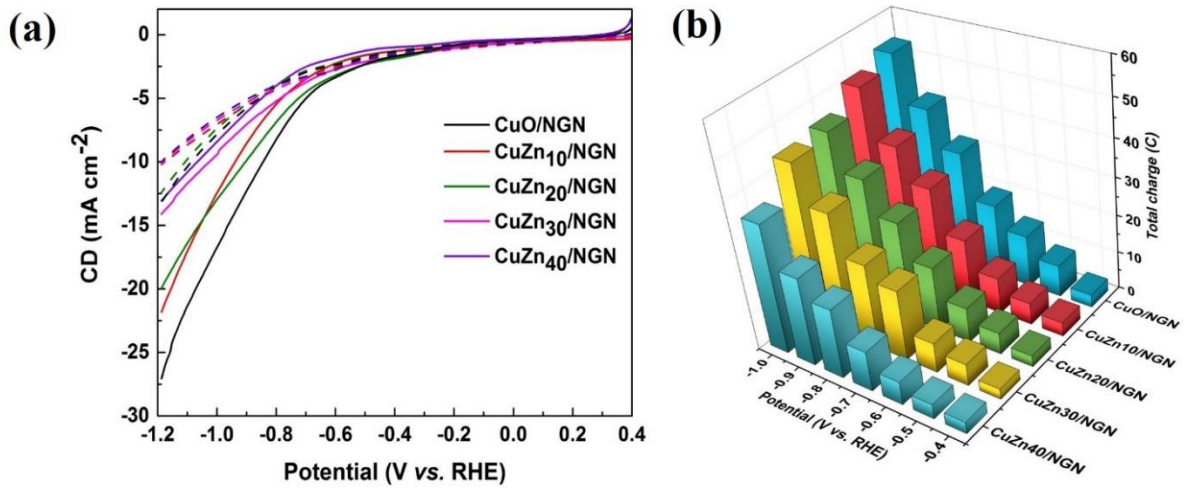

Fig. 7.14 (a) *LSV recorded at a sweep rate of 10 mV s^{-1} in N_2 (dashed line) and in CO_2 (solid line) saturated 0.1M $KHCO_3$ solution;* ***(b)*** *Total charge consumed at different applied voltages in 2 h reaction time*

7.3.2.2. Electrochemical CO_2 reduction and product distribution

For the catalytic activity of the different electro-catalysts, potentiostatic electrolysis in CO_2 saturated 0.1M $KHCO_3$ solution was performed at different applied potentials (from -0.4 to -1.0 V (*vs.* RHE) for 120 min. The total charge (Q_{Total}) utilized by the different electro-catalysts at different potentials are represented in **Fig. 7.14** (corresponding chronoamperograms are presented in **Fig. 7.15**). In comparison to higher loading of ZnO, lower ZnO loading catalysts showed higher current densities and utilized higher total charge in ECO_2R activity. This could be due to the differences in their ECASA (**Fig. 7.16**) as well as the higher reactivity of reduced CuO than that of ZnO towards ECO_2R. Previous reports also suggest that polycrystalline Zn required higher over-potential of 100−300 mV than Cu to handle 5 mA cm^{-2} CD during CO_2 reduction [157].

All the chronoamperometry curves (**Fig. 7.15**) show rapid decrease in the CD at the beginning and further attaining a steady state. This can be due to the reduction of the electro-catalysts themselves and the decrease in the local H^+ and CO_2 concentration close to the working electrode and double layer charging. Stable CD response at different applied potentials suggests good stability of $CuZn_x$/NGN during the ECO_2R experiments. Liquid products were collected

for identification and quantification of products using ^{1}H NMR and HPLC. In the liquid-phase, only formic acid, acetic acid, methanol, ethanol, and n-propanol were detected.

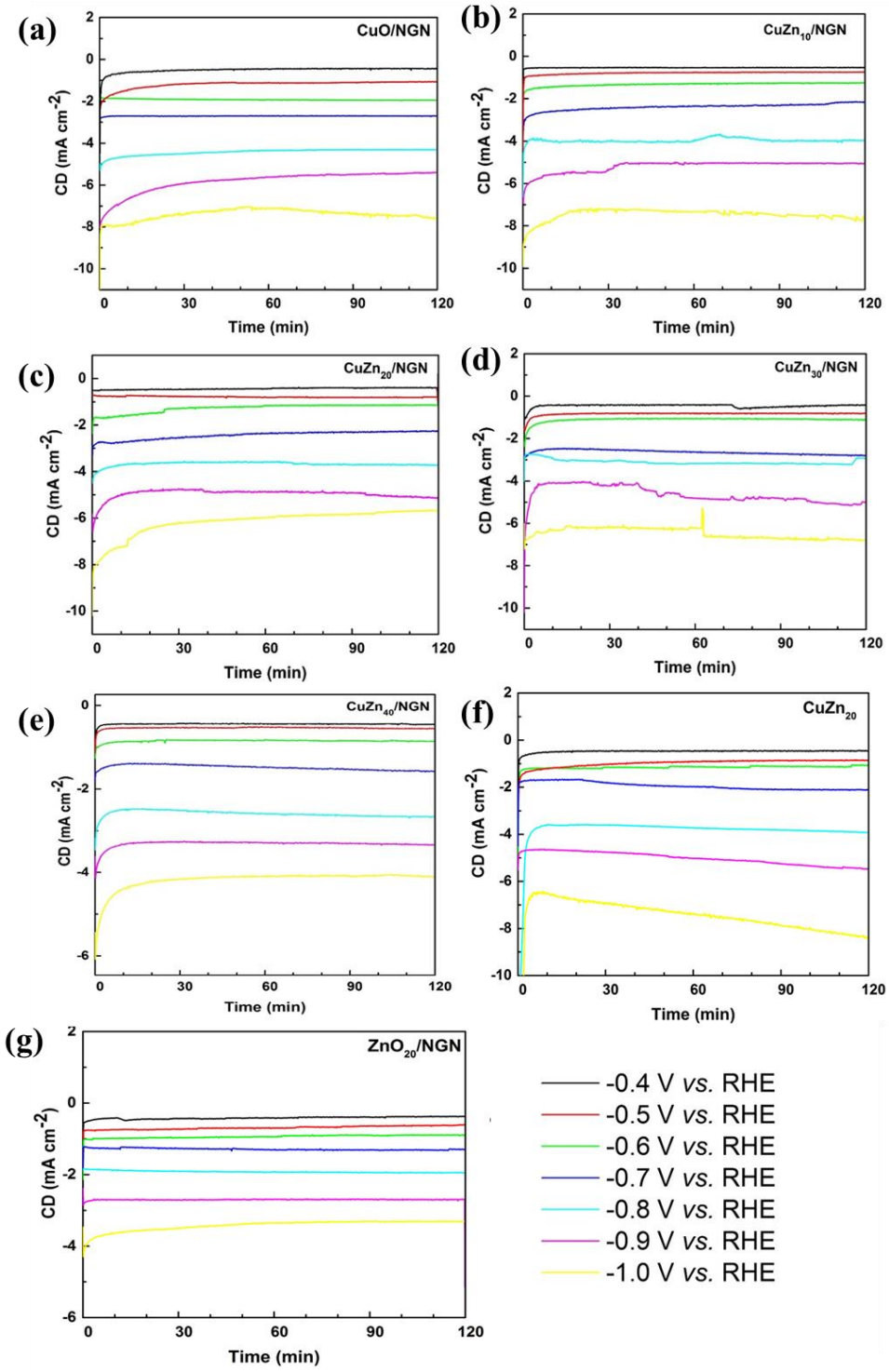

Fig. 7.15 *Chronoamperometric measurements at various potentials in a CO_2-saturated 0.1 M $KHCO_3$ aqueous solution on different electrodes (CuO/NGN, $CuZn_{10}$/NGN, $CuZn_{20}$/NGN, $CuZn_{30}$/NGN, $CuZn_{40}$/NGN, $CuZn_{20}$ and ZnO/NGN)*

7.3.2.3. Electrochemical active surface area (ECASA)

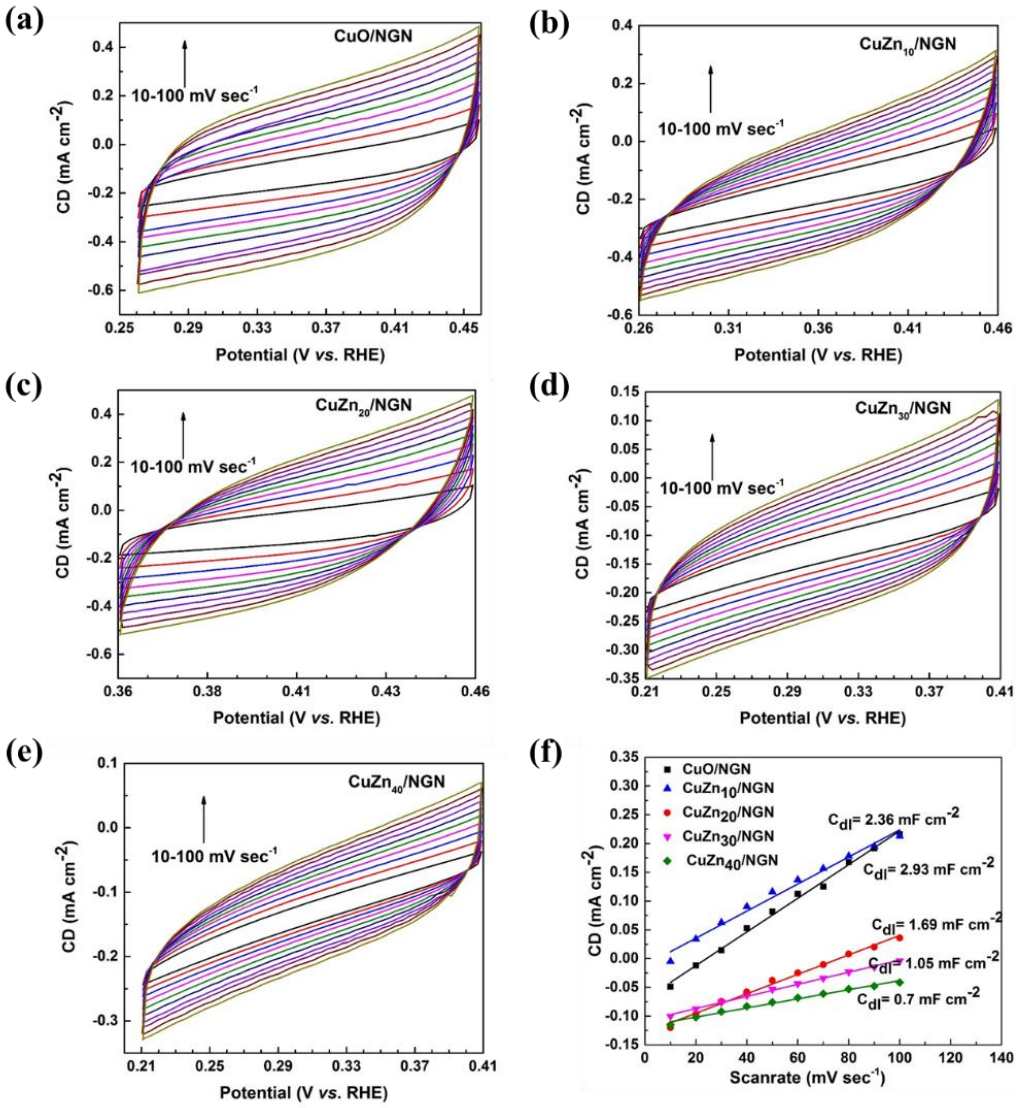

Fig. 7.16 *ECASA characterization of CuO/NGN, $CuZn_{10}$/NGN, $CuZn_{20}$/NGN, $CuZn_{30}$/NGN, and $CuZn_{40}$/NGN electrodes;* ***(a-e)*** *Cyclic voltammograms at scan rates of 10 to 100 mV s^{-1} and* ***(f)*** *linear correlation between non-Faradaic CD and scan rate*

7.3.3. Product vs. potential

The effect of applied potential on product formation rate (productivity) is studied by plotting productivity of obtained products as a function of applied potential (**Fig. 7.17**). The rate of ethanol formation at $CuZn_{20}$/NGN electrode is found to be 20 to 195 μmol L^{-1} h^{-1} within the applied potential range which is higher than that of other studied electrodes - ranging from 18 to 41 μmol L^{-1} h^{-1} with CuO/NGN, from 17 to 105 μmol L^{-1} h^{-1} with $CuZn_{10}$/NGN; from 10 to 65 μmol L^{-1} h^{-1} with $CuZn_{30}$/NGN; and from 13 to 33 μmol L^{-1} h^{-1} with $CuZn_{40}$/NGN.

Interestingly, productivity of ethanol increased with potential from –0.5 V to -0.8 V (*vs.* RHE) and reached a maximum value of 195 μmol L^{-1} h^{-1} at −0.8 V (*vs.* RHE).

At low overpotentials (before reaching -0.7 V vs. RHE), only formate and methanol are observed. At the lowest overpotentials (-0.4 V vs. RHE) only formate was detected in liquid product. As the overpotential increases, the percentage of the current going to hydrogen evolution and C1 product formation decreases while the percent going to C_{2+} reduction products increases. At -0.7 V (vs. RHE), ethanol and n-propanol are the first alcohols to be observed. The productivities for all C_{2+} products continue to increase with increasing overpotential, until a peak is reached around -0.8 V (vs. RHE). At this potential, the FE for formate, acetate, and methanol have declined to values below 10 % FE. At very high overpotentials, beyond -0.8 V (vs. RHE), selectivities towards all C_{2+} products are declined. At the most negative potential investigated in this study, -1.0 V vs. RHE, formate, acetate, methanol, ethanol, and n-propanol account for over 43% of the Faradaic efficiency. At higher overpotential mass transport limitation of CO_2 to the electrode can occur and the productivity is decreased, as CO_2 has a poor solubility in aqueous electrolytes (~34 mM at 25 °C). Additionally, as the total current increased with applied overpotential, there will also be a buildup of OH^- near the electrode surface, i.e., an increase in local pH. Increased gas bubble formation was clearly visible at both the electrode surfaces at higher applied potentials. These bubbles are probably due to gaseous product generation and HER. This will cause a decrease in local concentration of CO_2 near the electrode surface, resulting in the fall in CO_2 reduction productivities.

From **Fig. 7.17**, it is also observed that the formation of multi-carbon product is changing with the ZnO loading in the electro-catalysts and $CuZn_{20}$/NGN electrode produces ethanol with higher formation rate. Moreover, the formation rate of formic acid with all the electrodes is quite high at all the applied potentials in comparison with other products. Formic acid requires only two electrons to be produced by ECO_2R therefore, formation rates typically increased with potential from –0.4 V to – 1.0 V (*vs.* RHE). In case of multi-electron transfer process (i.e. during the production of ethanol, n-propanol, and acetic acid where 12, 18, and 8 electrons respectively are required) [40], formation rates typically increased with potential up to certain value and then it decreased due to weak interaction of reaction intermediates at higher applied potentials [40]. Similar trend was observed for all multi-carbon products.

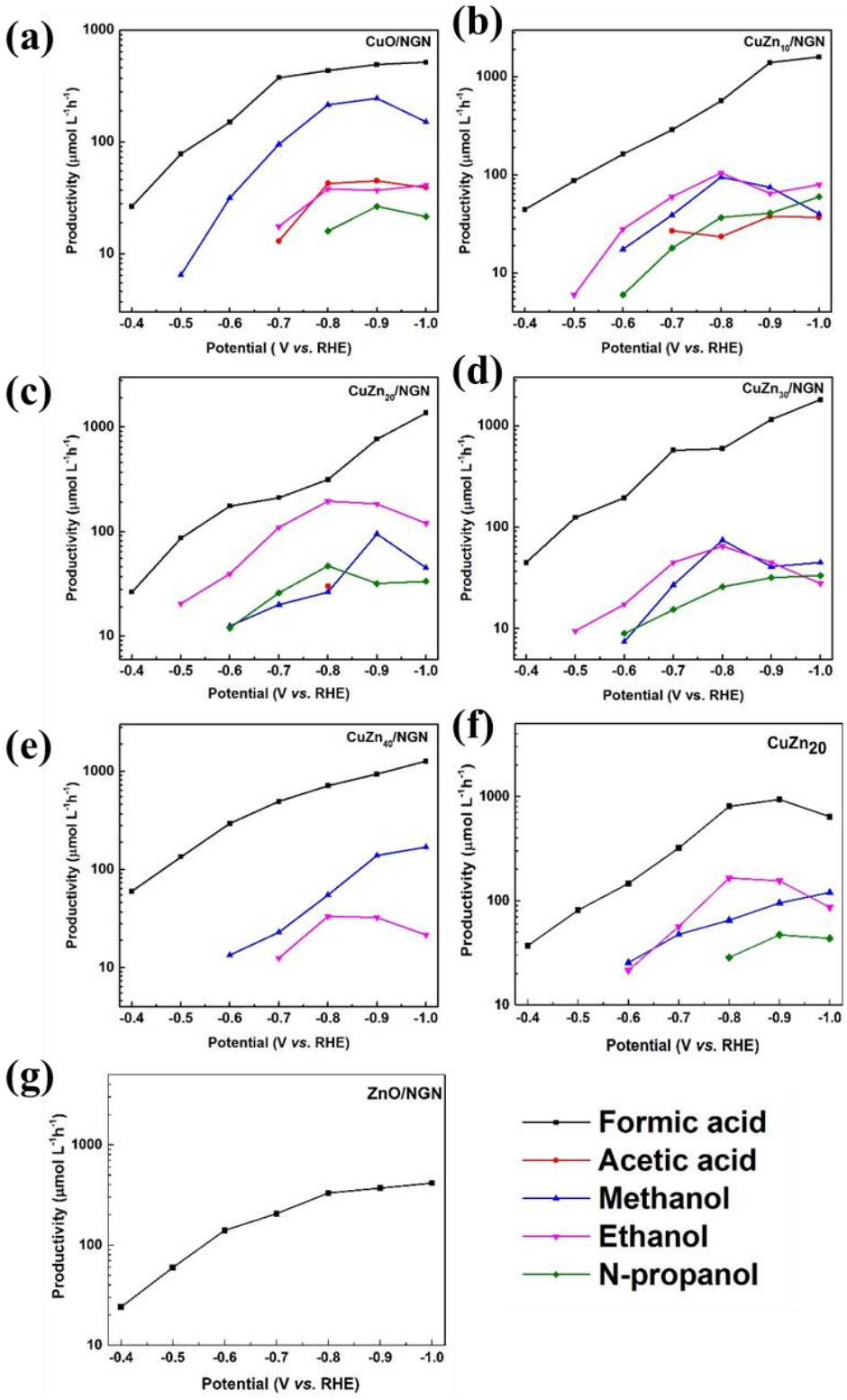

Fig. 7.17 *Productivity of formic acid, acetic acid, methanol, ethanol and n-propanol for CuO/NGN, $CuZn_{10}$/NGN, $CuZn_{20}$/NGN, $CuZn_{30}$/NGN, $CuZn_{40}$/NGN, $CuZn_{20}$ and ZnO/NGN*

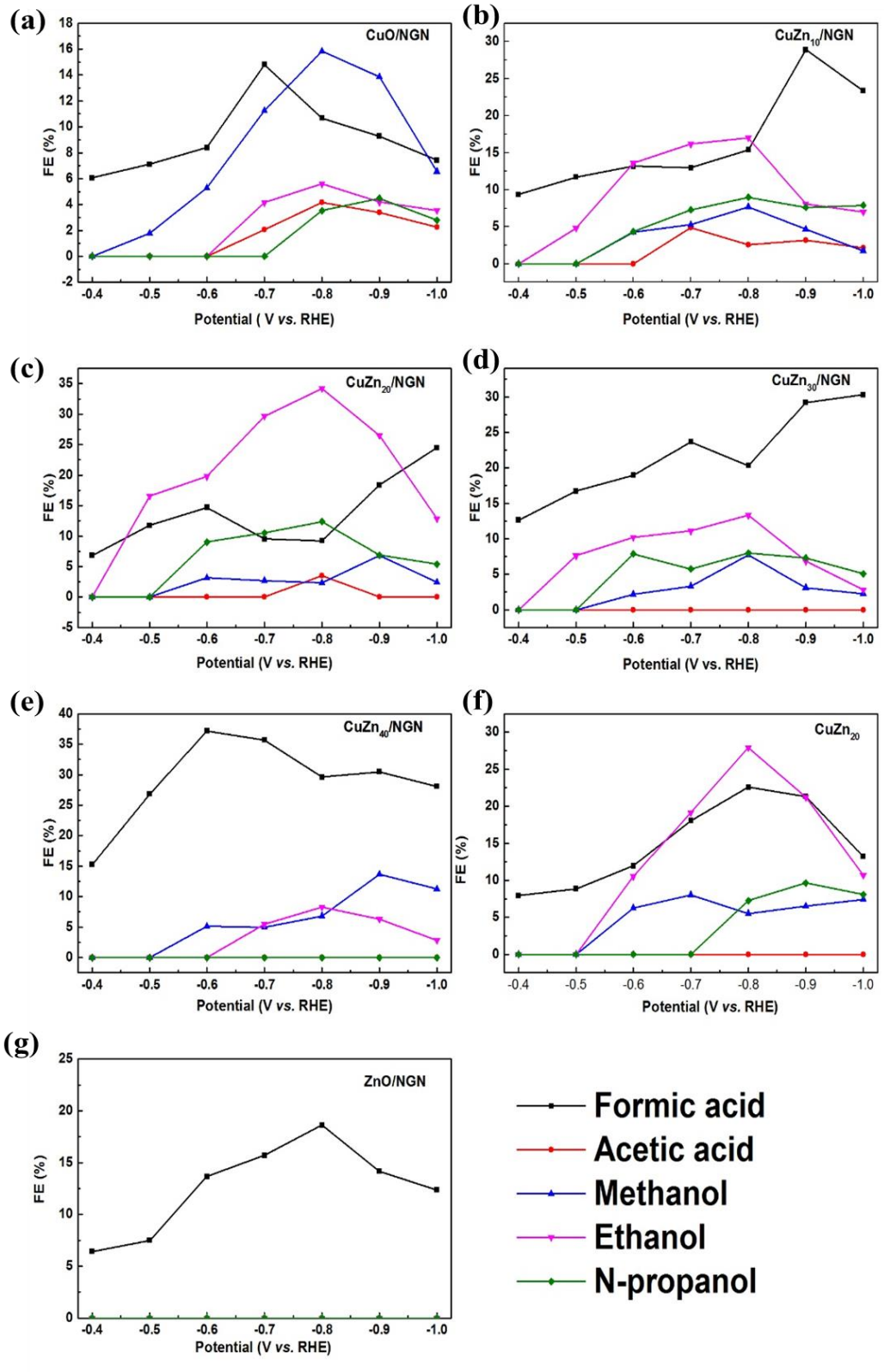

Fig. 7.18 *FE of formic acid, acetic acid, methanol, ethanol and n propanol for CuO/NGN, $CuZn_{10}$/NGN, $CuZn_{20}$/NGN, $CuZn_{30}$/NGN, $CuZn_{40}$/NGN, $CuZn_{20}$, and ZnO/NGN electrodes at different potentials*

The production rate holds great relevance from practical point of view but the FE is equally important for studying the selectivity of products [231]. The FEs of ethanol increased from 5.6 % (on CuO/NGN) to 34.2 % (on $CuZn_{20}$/NGN) and then decreased to 7.5% after further increase in ZnO loading ($CuZn_{40}$/NGN). This can be attributed to the fact that the exposed surface area of ZnO increases with increasing the ZnO percentage and more selective reaction sites can be generated for ethanol. $CuZn_{20}$/NGN electrode has higher $FE_{ethanol}$ as compared to $CuZn_{30}$/NGN and $CuZn_{40}$/NGN, indicating that further increasing ZnO in the electrode could be less favorable for ethanol formation since the ZnO electrode has satisfactory CO selectivity as widely reported in the literature [244, 245]. The good performance of $CuZn_{20}$/NGN electrodes could be attributed to the balance of ZnO and CuO contents on NGN. Sufficient Cu content is also required to enhance electric conductivity and to obtain high electrode activity.

As mentioned earlier, in $CuZn_x$/NGN catalyst, Zn and Cu had synergistically acted to facilitate the ethanol selectivity. This synergy could be demonstrated by analyzing the FE of multi-carbon products at CuO/NGN and ZnO/NGN. If ZnO/NGN had functioned independently, only formate (FE = 7-17 %) could be detected in liquid product. Also, CuO/NGN alone showed high selectivity for methanol (i.e. FE = 15.8 % at -0.8 V (vs. RHE) and less selectivity for CO_2 reduction to ethanol (FE = 5.6 %), acetic acid (FE = 4.1 %) and n-propanol (FE =3.5 %) as shown in **Fig. 7.18**. It is interesting to note that although $CuZn_{20}$/NGN electro-catalyst produces formate with maximum formation rate of 315 μmol L^{-1} h^{-1} but the FE for ethanol was higher (34.5 % at -0.8 V (vs. RHE)). The decrease in formate selectivity on the $CuZn_{20}$/NGN electrode indicates that the binding energy of *COOH to the catalyst might be enhanced by optimized Cu:Zn ratio and its distribution on NGN. The $CuZn_{10}$/NGN electrode contained the smallest loading of Zn, catalyzed formate and ethanol with good selectivity across the different potentials investigated. Many authors reported more CO generation at reduced ZnO sites which helped in enhanced ethanol formation [244]. Thus, it can be concluded that gaseous CO generated at the Zn sites may have further reacted at neighboring reduced CuO sites to give ethanol. The remarkable performance of the $CuZn_{20}$/NGN was comparable to that of other Cu-Zn composite catalysts reported recently, such as Cu_4Zn [113], Cu/ZnO (1010) [116], HMMP Cu_5Zn_8 [233], ZnO-shell/CuO-core bi-metal-oxide [115], 8CuO/2ZnO/C [230], and Cu-Zn mixture [232] as summarized in **Table 7.2**.

Table 7.2 *Comparison of performance of electro-catalysts reported in the literature for the electrochemical reduction of CO_2 to ethanol and multi-carbon products (n-propanol, ethanol, and acetic acid)*

Catalyst	Conditions	FE (%)		CD (mA cm^{-2})	Stability (h) and Type of cell	Ref.
		Ethanol	Multi-carbon products			
Cu_4Zn	0.1 M $KHCO_3$ -1.05 V (*vs.* RHE)	29.1	51.3	2.1	5 h, H-Type	[113]
Cu/ZnO (1010)	0.1 M $KHCO_3$ -1.4 V (*vs.* RHE)	10.2	20.3		H-Type	[116]
HMMP Cu_5Zn_8	0.1 M $KHCO_3$ -0.8 V (*vs.* RHE)	46.6	58.3	2.3	11 h, H-Type	[233]
ZnO-shell/CuO-core bi-metal-oxide	0.1 M $KHCO_3$ -1.15 V (*vs.* RHE)	32	41	-10.5	H-Type	[115]
8CuO/2ZnO/C	0.1 M $KHCO_3$ -0.75 V (*vs.* RHE)	21	74	110	Flow cell	[230]
Cu-ZnO	0.1 M $KHCO_3$ -1.7 V (*vs.* RHE)	ND	60	5.5	H-Type	[99]
Cu-Zn mixture	0.1 M $KHCO_3$ -1.2 V (*vs.* RHE)	2.2	8	5.7	15 h, H-Type	[232]
$CuZn_{20}$/NGN	0.1 M $KHCO_3$ -0.8 V (*vs.* RHE)	34.25	50.14	3.95	24 h, H-Type	This work

To determine the origin of the product, control experiments were conducted in N_2-saturated 0.1 M $KHCO_3$ using $CuZn_{20}$/NGN electrode. No product was observed in the HPLC and ^1H NMR analysis even after application of -0.8 V (*vs.* RHE) for 2 h, confirming that formate, acetate, methanol, ethanol, and n-propanol were generated by reduction of CO_2 only.

7.3.4. Reaction kinetics/Tafel plot

The Tafel slope analysis (**Fig. 7.19a**) was performed to gain more insights on reaction kinetics of ECO_2R. The smaller Tafel slope of 84 mV dec^{-1} for $CuZn_{20}$ is observed compared to that of other electro-catalysts. Also, Tafel slope for CuO/NGN is 90 mV dec^{-1}, comparatively smaller than all ZnO loaded electro-catalysts. It reveals that CuO/NGN exhibits a faster rate of electron transfer causing a better reaction kinetics in ECO_2R [236]. Moreover, Tafel slope of $CuZn_x$/NGN catalyst increased with increase in ZnO loading due to its lower electro-catalytic activity compared to Cu suggesting higher over potential requirement to start the catalytic reaction. Highest Tafel slope of ZnO/NGN (171 mV dec^{-1}) supports this conclusion. These values of Tafel slope are consistent with the integral activity as shown by the LSV curves.

As reported by other researchers, the formation of the C-C bond (e.g., *CO-CHO and *CO-CH_2) is considered to be important during ethanol production by ECO_2R [246, 247]. It requires twelve proton-electron transfers and follows complicated reaction pathways with multiple reaction intermediates. Among them, the co-adsorption of two carbon-based intermediates is very important and critical, since the two adsorbed C1 species is required for generation of C2 species of ethanol [233]. Recent theoretical studies have shown that the combination of two hydrogenated C1 species is highly favored over two *CO species, as the activation energy required for combining two hydrogenated C1 species is much smaller than that of two bare *CO species. Ren and co-workers [113, 115] suggested that the generation of closely adsorbed *CH_2 and *CO is of crucial importance for improving ethanol selectivity on Cu-Zn composite electrodes. Moreover, according to Su et al. [85] incorporation of Zn to Cu efficiently decreases the C-C distance encouraging a greater possibility for the C-C coupling. Based on the above discussion, the possible mechanism of ECO_2R on $CuZn_x$/NGN is proposed. At the initial stage, the adsorption of CO_2 molecules and protons are taking place on Cu/Zn-based and pyridinic-N sites. Electrons are transferred to adsorbed CO_2 molecule to form *CO species. This *CO species are further converted to *CH_2 intermediate through a hydrogenation process by utilizing four protons and electron pairs. In the next step, proton and electron pairs are transferred to the other *CO species for the formation of *COH. Previously formed *CH_2 is combined with *COH to generate C-C bond through formation of *CH_2COH intermediate. Lastly, three protons and electron pair are transferred to *CH_2COH intermediate to produce ethanol molecule, followed by desorption into electrolyte solution [233] as illustrated in **Fig. 7.19b**.

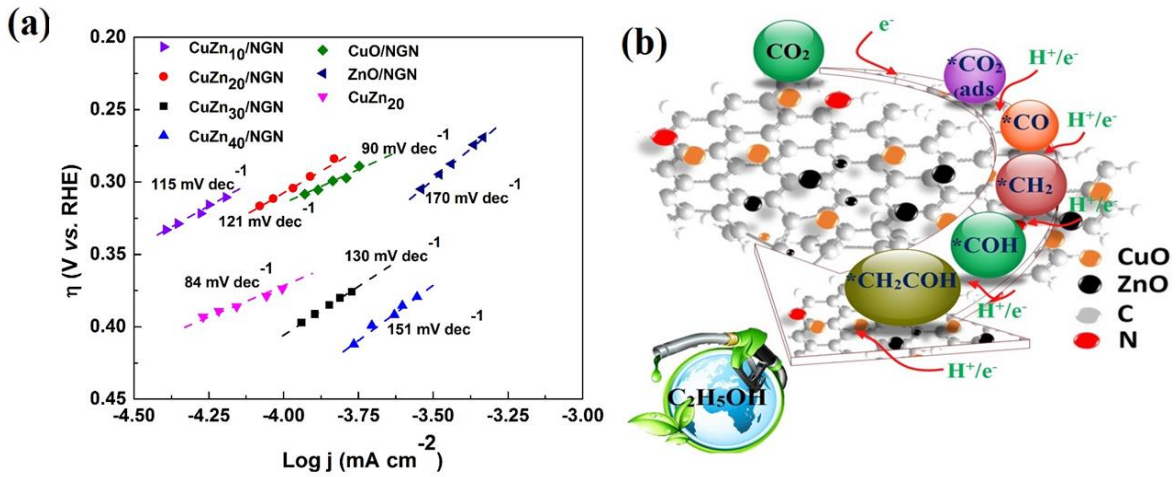

Fig. 7.19 (a) *Tafel plot analysis and* ***(b)*** *Schematic of proposed reaction pathway for ECO_2R to ethanol*

7.3.5. Long term performance and reusability study

In addition to the good activity and excellent selectivity, stability and reusability is equally important when developing CO_2 reduction catalysts for commercial purpose. A longer test was performed with $CuZn_{20}$/NGN at optimized potential of -0.8 V (*vs.* RHE) for 24 h (**Fig. 7.20a**). A small drop in CD was observed during 24 h of electrolysis. During the reuse test performance, after each cycle, electrode was thoroughly washed with water and used for next run. As shown in **Fig. 7.20b**, the initial ethanol FE was 34% which decreased to 28% after repeating the 6 runs at −0.8 V (*vs.* RHE). Similar trend was observed for other multi-carbon products. On the other hand, a FE for formate increased from 8.7% to 13.9% in 6 repeated runs. The electro-catalytic activity of $CuZn_{20}$/NGN for ethanol and other multi-carbon products decreased significantly due to the adsorption of poisoning species on the surface of the electrode, especially metals ions and organic/inorganic substances present in the electrolyte, as demonstrated by Hori et al. and other researchers [201, 202].

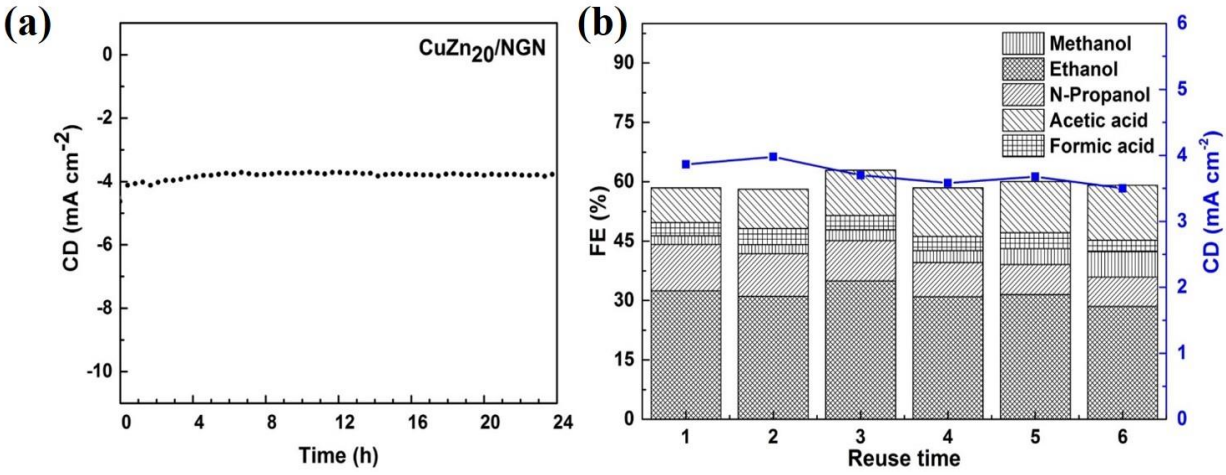

Fig. 7.20 (a) *CD response of $CuZn_{20}$/NGN as a function of time for long-time test performance and* ***(b)*** *Reuse test performance at −0.8 V (*vs. *RHE) using $CuZn_{20}$/NGN as working electrode*

7.3.6. Post characterization

After the long term performance, the structure and composition of the $CuZn_{20}$/NGN electrode was analyzed by SEM-EDX, XRD and ECASA. As seen from **Fig. 7.21**, the morphology of the $CuZn_{20}$/NGN was preserved after 24 hours running. But in EDX analysis, the additional signals corresponding to potassium (K) was observed, which might support the electrode deactivation by adsorption of K+ ions as described in previous paragraph. Furthermore, initial ECASA (**Fig. 7.22**) was found to be decreased after long term performance. It should also be

noted that the HER still remained at the very negative potential on the poisoned surface, but CO_2 reduction to products, requiring active Cu and Zn surface, decreased. These poisoning species restrict multi-electron and proton transfer resulting in increased formate FE after consecutive recycle tests [201, 202].

To confirm the active sites for the generation of corresponding products, XRD analysis was performed at different time intervals of ECO_2R at -0.8 V (*vs.* RHE). As shown in **Fig. 7.23**, initial oxide peaks of Cu and Zn are almost absent after 10 min of applied potential. Therefore, it can be concluded that the reduction of CO_2 occurred probably on metallic sites rather than on metal oxides [232].

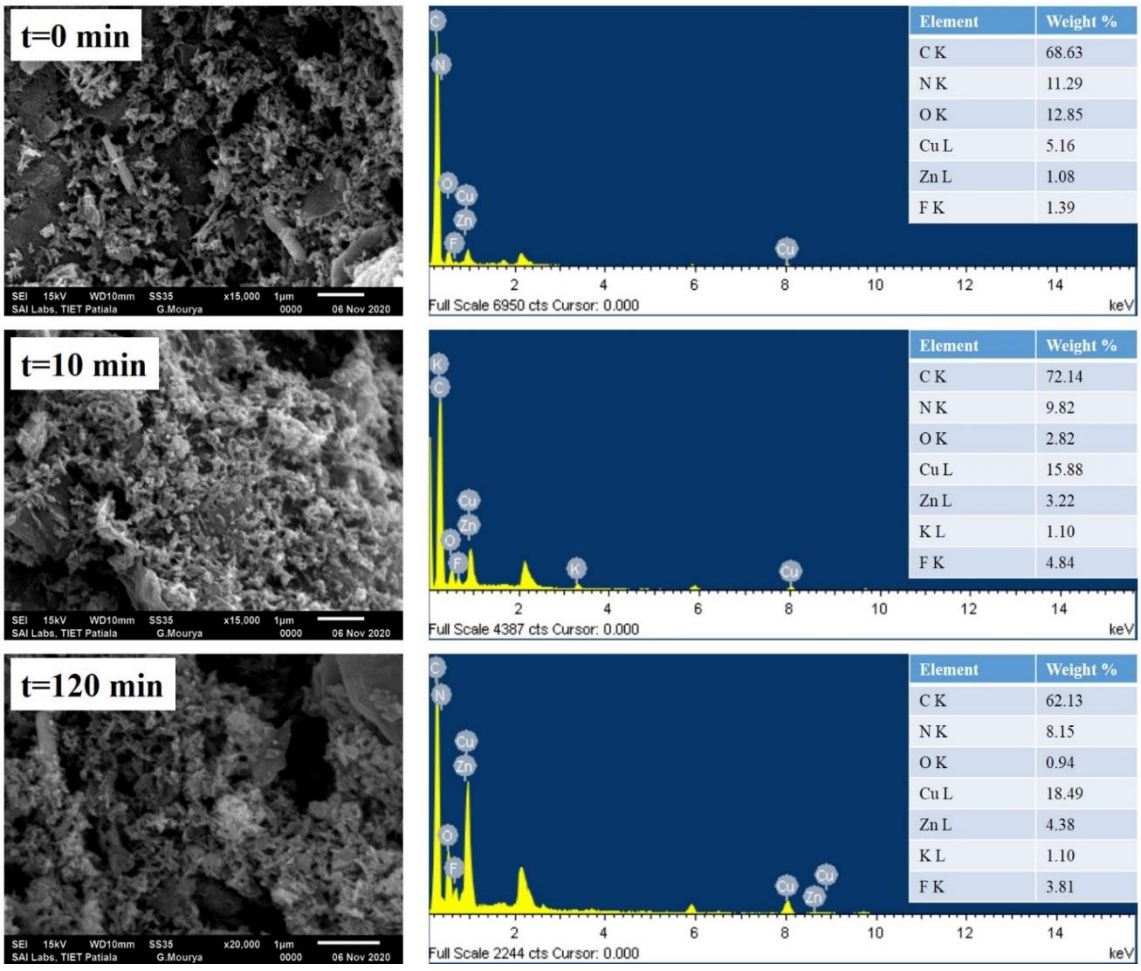

Fig. 7.21 *SEM images and corresponding EDX spectra of $CuZn_{20}$/NGN electrode at different time intervals of ECO_2R*

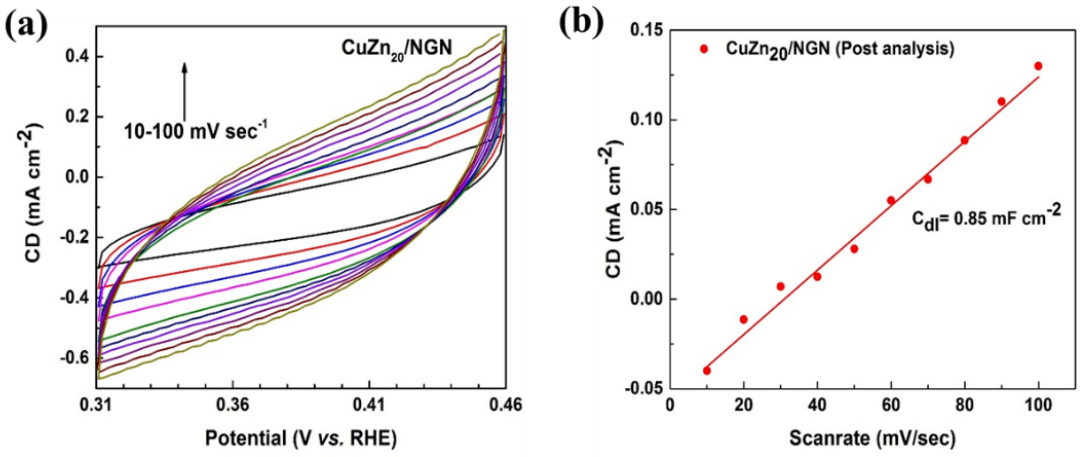

Fig. 7.22 *Post analysis of ECASA characterization of $CuZn_{20}$/NGN electrodes* ***(a)*** *Cyclic voltammograms at scan rates of 10 to 100 mV s^{-1} and* ***(b)*** *linear correlation between non-Faradaic CD and scan rate*

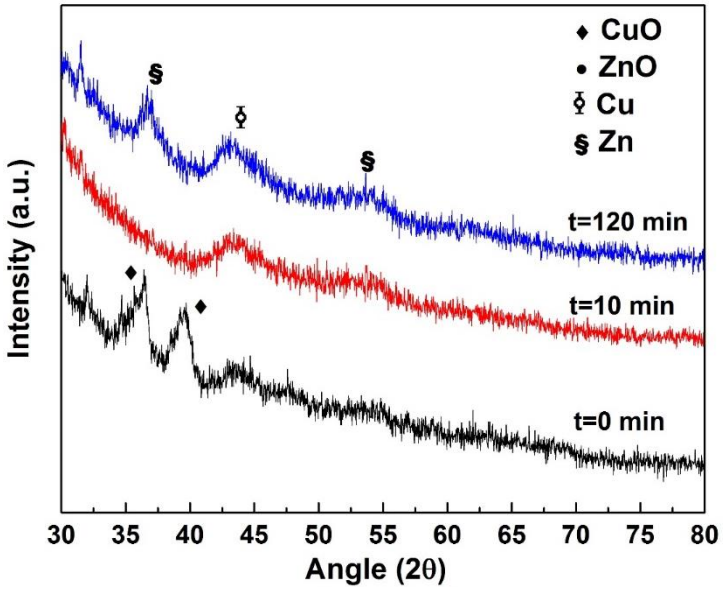

Fig. 7.23 *XRD patterns of $CuZn_{20}$/NGN electrode at different time intervals of ECO_2R*

7.4. Conclusions

The present work demonstrates the significance of rational design of oxide derived composite materials supported on N-doped graphene for the electrochemical CO_2 reduction (ECR) application. Electro-catalysts with desired characteristics can be prepared through a conventional co-precipitation method where electro-catalyst composition is simply controlled by varying the ratio of Cu and Zn precursors. Different key variables have been studied for the reduction of CO_2 to ethanol and other C2 chemicals. Copper supported on nitrogen doped graphene (CuO/NGN) electrode exhibits low selectivity for ethanol and other C2 chemicals.

In contrast, the electrode with 20 weight% Zn with copper on NGN ($CuZn_{20}$/NGN) displayed the highest selectivity for ethanol production (FE=34.25 %) with formation rate of 195 µmol L^{-1} h^{-1} at -0.8 V (*vs.* RHE). The enhanced performance of the $CuZn_{20}$/NGN electrodes can be assigned to the selective active sites derived from reduced CuO and ZnO. The Cu–Zn interface seems to play an important role in the production of C_{2+} species. This work may guide to the development of effective and less expensive electro-catalysts for CO_2 conversion in large-scale processing. There are still several issues that need to be tackled for this technology to have highly active, selective and stable catalyst(s). Research efforts must be continued for multi-carbon production with practical and economic feasibility in the coming years.

(This work have been published in Applied Surface Science, 556 (2021) 149790. DOI: https://doi.org/10.1016/j.apsusc.2021.149790 (IF =6.707))

Chapter 8- Conclusions and recommendations for future work

8.1. Conclusions

Four different nanostructured metal based electro-catalysts, namely metallic Cu nanoparticles (Cu NPs), Cu NPs on N-doped graphene (Cu_x/NGN), oxide derived copper-zinc nanoparticles (CuO-ZnO_x) and CuO-ZnO_x supported on N-doped grapheme, have been prepared for the ECO_2R with an aim to produce alcohol. Effects of metallic loading and applied potential have been studied using H-type electrolytic cell in aqueous 0.1 M $KHCO_3$ electrolyte. The optimum results with the four types of electro-catalysts are given in the following table.

Electro-catalyst	Applied potential	Faradaic efficiency (%)					Stability (h)
		Formic acid	Acetic acid	Methanol	Ethanol	N-propanol	
Cu NPs	-0.8 V	46	1.8	ND	6.5	5	20
Cu_{20}/NGN	-1 V	15.86	9.81	ND	25.71	7.50	12
CuO-ZnO_{20}	-0.8 V	13.40	ND	6.53	22.27	6.87	12
$CuZn_{20}$/NGN	-0.8 V	9.22	3.51	2.32	34.25	12.38	24

The electro-catalyst consisting of 20 weight% ZnO with CuO on NGN ($CuZn_{20}$/NGN) displays the highest selectivity for ethanol production (FE=34.25 %) with formation rate of 195 µmol L^{-1} h^{-1} at -0.8 V (*vs.* RHE). This electrode has shown long-term stability of at least 24 h under optimum conditions. Post characterization of the electrode indicates that carbon dioxide reduction takes place on reduced oxide sites (metallic sites) rather than on metal oxide.

Nano-porous Cu NPs have great potential in developing efficient and green routes for ECO_2R to produce useful chemicals and fuels. The Cu–Zn interface seems to play an important role in the production of C_{2+} species. The multi-carbon production is increased due to the synergistic effect between Cu, Zn and N doped active sites in the electro-catalyst.

This research work provides a few examples of the development of effective and less expensive electro-catalysts for CO_2 conversion. It also highlights the effect of active metal loading, composition of electrocatalysts, and applied potentials on the alcohol selectivity of CO_2 reduction reactions. This work opens up a simple way for efficient transformation of CO_2 into

valuable chemicals, and the results are helpful for developing other electrodes for efficient CO_2 reduction.

However, there are still several issues that need to be tackled for this technology to have highly active, selective and stable catalyst(s). Research efforts must be continued for multi-carbon production with practical and economic feasibility in the coming years.

8.2. Recommendations for future research

i. Solving the issue of low CO_2 solubility in electrolyte solution by designing suitable reactors such as liquid-flow cells, gas-diffusion cells, and use of different reaction media, such as ionic liquids (ILs) and solid polymer electrolytes.

ii. Developing more advanced electro-catalysts with better structures (e.g., more hierarchical or having suitable binding energies for different reaction intermediates) are suggested. This can be achieved by combination of different synthesis techniques and developing appropriate novel compositions (e.g., 2D transition metal oxides, supported metals, introducing molecular modifiers, materials with atomic dopant/defect/surface curvature, etc.).

iii. The majority of the systems have been tested for few hours only; therefore, designing of more stable and low-cost electro-catalysts (such as metal-free electro-catalyst, complex catalysts with heteroatom doping) with more appropriate active sites are needed to accelerate the ECO_2R performance for higher alcohol selectivity.

iv. For getting the mechanistic insights, combination of experimental, analytical (both in situ and ex situ), and computational approaches are required.

v. Natural power sources (like solar, wind, etc.) need to be utilized to drive ECO_2R process. This can be done by generating electrical energy from direct utilization of natural powers or using photo-electrochemical reduction technique from reduction of CO_2 to ethanol.

References

[1] Global Monitoring Laboratory, National Oceanic and Atmospheric Administration (NOAA), https://gml.noaa.gov/, Accessed on May 12, 2021.

[2] https://www.CO_2.earth/2100-projections, accessed on May 12, 2021.

[3] Sixth Assessment Report, Climate Change 2021: Impacts, Adaptation and Vulnerability, The Intergovernmental Panel on Climate Change, World Meteorological Organization (WMO) and the United Nations Environment Programme (UNEP), Geneva 2 Switzerland. (2021).

[4] Y. Gao, X. Gao, X. Zhang, The 2 C global temperature target and the evolution of the long-term goal of addressing climate change - from the United Nations framework convention on climate change to the Paris agreement, Engineering, 3 (2017) 272-278.

[5] S.C. Peter, Reduction of CO_2 to chemicals and fuels: a solution to global warming and energy crisis, ACS Energy Letters, 3 (2018) 1557-1561.

[6] S. Sengupta, A. Jha, P. Shende, R. Maskara, A.K. Das, Catalytic performance of Co and Ni doped Fe-based catalysts for the hydrogenation of CO_2 to CO via reverse water-gas shift reaction, Journal of Environmental Chemical Engineering, 7 (1) (2019) 102911.

[7] A. Adamu, F. Russo-Abegao, K. Boodhoo, Process intensification technologies for CO_2 capture and conversion – a review, BMC Chemical Engineering, 2 (2020) 1-18.

[8] I. Ghiat, T. Al-Ansari, A review of carbon capture and utilisation as a CO_2 abatement opportunity within the EWF nexus, Journal of CO_2 Utilization, 45 (2021) 101432.

[9] A. Saravanan, D.-V.N. Vo, S. Jeevanantham, V. Bhuvaneswari, V.A. Narayanan, P. Yaashikaa, S. Swetha, B. Reshma, A comprehensive review on different approaches for CO_2 utilization and conversion pathways, Chemical Engineering Science, 236 (2021) 116515.

[10] A. Taheri Najafabadi, CO_2 chemical conversion to useful products: an engineering insight to the latest advances toward sustainability, International Journal of Energy Research, 37 (2013) 485-499.

[11] Y. Song, W. Chen, W. Wei, Y. Sun, Advances in clean fuel ethanol production from electro-, photo-and photoelectro-catalytic CO_2 reduction, Catalysts, 10 (2020) 1287.

[12] S. Pandey, V.C. Srivastava, V. Kumar, Comparative thermodynamic analysis of CO_2 based dimethyl carbonate synthesis routes, The Canadian Journal of Chemical Engineering, 99 (2021) 467-478.

[13] P.P. Sharma, X.D. Zhou, Electrocatalytic conversion of carbon dioxide to fuels: a review on the interaction between CO_2 and the liquid electrolyte, Wiley Interdiscip. Rev. Energy Environ., 6 (2017) 21.

[14] Y.W. Li, S.H. Chan, Q. Sun, Heterogeneous catalytic conversion of CO_2: a comprehensive theoretical review, Nanoscale, 7 (2015) 8663-8683.

[15] A.T. Najafabadi, CO_2 chemical conversion to useful products: An engineering insight to the latest advances toward sustainability, Int. J. Energy Res., 37 (2013) 485-499.

[16] J. Schneider, H.F. Jia, J.T. Muckerman, E. Fujita, Thermodynamics and kinetics of CO_2, CO, and H^+ binding to the metal centre of CO_2 reduction catalysts, Chem. Soc. Rev., 41 (2012) 2036-2051.

[17] J. Hong, W. Zhang, J. Ren, R. Xu, Photocatalytic reduction of CO_2: a brief review on product analysis and systematic methods, Analytical methods, 5 (2013) 1086-1097.

[18] Z. Sun, T. Ma, H. Tao, Q. Fan, B. Han, Fundamentals and challenges of electrochemical CO_2 reduction using two-dimensional materials, Chem, 3 (2017) 560-587.

[19] K. Malik, S. Singh, S. Basu, A. Verma, Electrochemical reduction of CO_2 for synthesis of green fuel, Wiley Interdisciplinary Reviews: Energy and Environment, 6 (2017) e244.

[20] F.N. Al-Rowaili, A. Jamal, M.S.B. Shammakh, A. Rana, A review on recent advances for electrochemical reduction of carbon dioxide to methanol using metal-organic framework (MOF) and non-MOF catalysts: challenges and future prospects, ACS Sustainable Chemistry & Engineering, 6 (2018) 15895-15914.

[21] S. Liu, H. Yang, X. Su, J. Ding, Q. Mao, Y. Huang, T. Zhang, B. Liu, Rational design of carbon-based metal-free catalysts for electrochemical carbon dioxide reduction: a review, Journal of Energy Chemistry, 36 (2019) 95-105.

[22] S. Garg, M. Li, A.Z. Weber, L. Ge, L. Li, V. Rudolph, G. Wang, T.E. Rufford, Advances and challenges in electrochemical CO_2 reduction processes: an engineering and design perspective looking beyond new catalyst materials, Journal of Materials Chemistry A, 8 (2020) 1511-1544.

[23] S. Das, The National Policy of biofuels of India–A perspective, Energy Policy, 143 (2020) 111595.

[24] M.S. Luchansky, J. Monks, Supply and demand elasticities in the US ethanol fuel market, Energy Economics, 31 (2009) 403-410.

[25] A. Demirbas, M. Balubaid, A. Basahel, W. Ahmad, M. Sheikh, Octane rating of gasoline and octane booster additives, Petroleum Science and Technology, 33 (2015) 1190-1197.

[26] A. Mohsenzadeh, A. Zamani, M.J. Taherzadeh, Bioethylene production from ethanol: A review and techno-economical evaluation, ChemBioEng Reviews, 4 (2017) 75-91.

[27] M. Arshad, M. Abbas, S. Javed, M. Adil, M.I. Shahzad, M. Iqbal, Sustainable ethanol production: An overview, sustainable ethanol and climate change, Springer International Publishing, (2021) 1-14.

[28] R. Chauhan, V. Srivastava, Advances in Electrocatalyst for Ethanol Electro-Oxidation, Nanomater. Materials Research Foundations, 49 (2019) 293-320.

[29] Y. Hori, K. Kikuchi, S. Suzuki, Production of CO and CH_4 in electrochemical reduction of CO_2 at metal electrodes in aqueous hydrogen carbonate solution, Chemistry Letters, 14 (1985) 1695-1698.

[30] Y. Hori, H. Wakebe, T. Tsukamoto, O. Koga, Electrocatalytic process of CO selectivity in electrochemical reduction of CO_2 at metal-electrodes in aqueous-media, Electrochimica Acta, 39 (1994) 1833-1839.

[31] Z.Q. Chen, T. Wang, B. Liu, D.F. Cheng, C.L. Hu, G. Zhang, W.J. Zhu, H.Y. Wang, Z.J. Zhao, J.L. Gong, Grain-boundary-rich copper for efficient solar-driven electrochemical CO_2 reduction to ethylene and ethanol, Journal of the American Chemical Society, 142 (2020) 6878-6883.

[32] J. Yuan, J.J. Zhang, M.P. Yang, W.J. Meng, H. Wang, J.X. Lu, CuO nanoparticles supported on TiO_2 with high efficiency for CO_2 electrochemical reduction to ethanol, Catalysts, 8 (4) (2018) 171.

[33] J. Yuan, L. Liu, R.-R. Guo, S. Zeng, H. Wang, J.-X. Lu, Electroreduction of CO_2 into ethanol over an active catalyst: copper supported on titania, Catalysts, 7 (2017) 220.

[34] D. Ren, Y.L. Deng, A.D. Handoko, C.S. Chen, S. Malkhandi, B.S. Yeo, Selective electrochemical reduction of carbon dioxide to ethylene and ethanol on copper(I) oxide catalysts, ACS Catalysis, 5 (2015) 2814-2821.

[35] D. Chi, H. Yang, Y. Du, T. Lv, G. Sui, H. Wang, J. Lu, Morphology-controlled CuO nanoparticles for electroreduction of CO_2 to ethanol, RSC Advances, 4 (2014) 37329-37332.

[36] S. Zhu, E.P. Delmo, T. Li, X. Qin, J. Tian, L. Zhang, M. Shao, Recent advances in catalyst structure and composition engineering strategies for regulating CO_2 electrochemical reduction, Advanced Materials, (2021) 2005484.

[37] D. Karapinar, C.E. Creissen, J.G. Rivera de la Cruz, M.W. Schreiber, M. Fontecave, Electrochemical CO_2 reduction to ethanol with copper-based catalysts, ACS Energy Letters, 6 (2021) 694-706.

[38] J. Du, P. Zhang, H. Liu, Electrochemical reduction of carbon dioxide to ethanol: An approach to transforming greenhouse gas to fuel source, Chemistry - An Asian Journal, 16 (2021) 588-603.

[39] J. Qiao, Y. Liu, J. Zhang, Electrochemical Reduction of Carbon Dioxide: Fundamentals and Technologies, CRC Press, 2016 (ISBN 9780367870836).

[40] K.P. Kuhl, E.R. Cave, D.N. Abram, T.F. Jaramillo, New insights into the electrochemical reduction of carbon dioxide on metallic copper surfaces, Energy & Environmental Science, 5 (2012) 7050-7059.

[41] M. Li, S. Garg, X. Chang, L. Ge, L. Li, M. Konarova, T.E. Rufford, V. Rudolph, G. Wang, Toward excellence of transition metal-based catalysts for CO_2 electrochemical reduction: an overview of strategies and rationales, Small Methods, 4 (2020) 2000033.

[42] T.T. Hoang, S. Ma, J.I. Gold, P.J. Kenis, A.A. Gewirth, Nanoporous copper films by additive-controlled electrodeposition: CO_2 reduction catalysis, ACS Catalysis, 7 (2017) 3313-3321.

[43] B. Schmid, C. Reller, S.S. Neubauer, M. Fleischer, R. Dorta, G. Schmid, Reactivity of copper electrodes towards functional groups and small molecules in the context of CO_2 electro-reductions, Catalysts, 7 (5) (2017) 161.

[44] W.W. Zhu, K.M. Zhao, S.Q. Liu, M. Liu, F. Peng, P.D. An, B.H. Qin, H.M. Zhou, H.M. Li, Z. He, Low over-potential selective reduction of CO_2 to ethanol on electrodeposited Cu_xAu_y nanowire arrays, Journal of Energy Chemistry, 37 (2019) 176-182.

[45] G.O. Larrazabal, A.J. Martin, F. Krumeich, R. Hauert, J. Perez-Ramirez, Solvothermally-prepared Cu_2O electrocatalysts for CO_2 reduction with tunable selectivity by the introduction of p-block elements, Chemsuschem, 10 (2017) 1255-1265.

[46] C. Yang, H.C. Shen, A.X. Guan, J.L. Liu, T.F. Li, Y.L. Ji, A.M. Al-Enizi, L.J. Zhang, L.P. Qian, G.F. Zheng, Fast cooling induced grain-boundary-rich copper oxide for electrocatalytic carbon dioxide reduction to ethanol, Journal of Colloid and Interface Science, 570 (2020) 375-381.

[47] A. Dutta, I.Z. Montiel, R. Erni, K. Kiran, M. Rahaman, J. Drnec, P. Broekmann, Activation of bimetallic AgCu foam electrocatalysts for ethanol formation from CO_2 by selective Cu oxidation/reduction, Nano Energy, 68 (2020). 104331

[48] Y.X. Duan, F.L. Meng, K.H. Liu, S.S. Yi, S.J. Li, J.M. Yan, Q. Jiang, Amorphizing of Cu nanoparticles toward highly efficient and robust electrocatalyst for CO_2 reduction to liquid fuels with high Faradaic efficiencies, Advanced Materials, 30 (2018) 1706194.

[49] T.M. Suzuki, T. Ishizaki, S. Kosaka, N. Takahashi, N. Isomura, J. Seki, Y. Matsuoka, K. Oh-ishi, A. Oshima, K. Kitazumi, K. Sekizawa, T. Morikawa, Electrochemical CO_2 reduction over nanoparticles derived from an oxidized Cu-Ni intermetallic alloy, Chemical Communications, 56 (2020) 15008-15011.

[50] Y. Song, J.R. Junqueira, N. Sikdar, D. Öhl, S. Dieckhöfer, T. Quast, S. Seisel, J. Masa, C. Andronescu, W. Schuhmann, B-Cu-Zn gas diffusion electrodes for CO_2 electroreduction to C2+ products at high current densities, Angewandte Chemie International Edition, 60 (2021) 9135-9141.

[51] Y. Song, W. Chen, C. Zhao, S. Li, W. Wei, Y. Sun, Metal-free nitrogen-doped mesoporous carbon for electroreduction of CO_2 to ethanol, Angewandte Chemie International Edition, 56 (2017) 10840-10844.

[52] J. Du, S.P. Li, S.L. Liu, Y. Xin, B.F. Chen, H.Z. Liu, B.X. Han, Selective electrochemical reduction of carbon dioxide to ethanol via a relay catalytic platform, Chemical Science, 11 (2020) 5098-5104.

[53] E.E. Benson, C.P. Kubiak, A.J. Sathrum, J.M. Smieja, Electrocatalytic and homogeneous approaches to conversion of CO_2 to liquid fuels, Chem. Soc. Rev., 38 (2009) 89-99.

[54] D.D. Zhu, J.L. Liu, S.Z. Qiao, Recent advances in inorganic heterogeneous electrocatalysts for reduction of carbon dioxide, Adv. Mater., 28 (2016) 3423-3452.

[55] A.A. Al-Omari, Z.H. Yamani, H.L. Nguyen, Electrocatalytic CO_2 reduction: From homogeneous catalysts to heterogeneous-based reticular chemistry, Molecules, 23 (2018) 2835.

[56] B. Kumar, J.P. Brian, V. Atla, S. Kumari, K.A. Bertram, R.T. White, J.M. Spurgeon, New trends in the development of heterogeneous catalysts for electrochemical CO_2 reduction, Catal Today, 270 (2016) 19-30.

[57] N. Theaker, J.M. Strain, B. Kumar, J.P. Brian, S. Kumari, J.M. Spurgeon, Heterogeneously catalyzed two-step cascade electrochemical reduction of CO_2 to ethanol, Electrochimica Acta, 274 (2018) 1-8.

[58] S. Gonglach, S. Paul, M. Haas, F. Pillwein, S.S. Sreejith, S. Barman, R. De, S. Mullegger, P. Gerschel, U.P. Apfel, H. Coskun, A. Aljabour, P. Stadler, W. Schofberger, S. Roy, Molecular cobalt corrole complex for the heterogeneous electrocatalytic reduction of carbon dioxide, Nat. Commun., 10 (2019) 3864.

[59] D. Gao, I. Zegkinoglou, N.J. Divins, F. Scholten, I. Sinev, P. Grosse, B. Roldan Cuenya, Plasma-activated copper nanocube catalysts for efficient carbon dioxide electroreduction to hydrocarbons and alcohols, ACS Nano, 11 (2017) 4825-4831.

[60] Y. Huang, C.W. Ong, B.S. Yeo, Effects of electrolyte anions on the reduction of carbon dioxide to ethylene and ethanol on copper (100) and (111) surfaces, Chemsuschem, 11 (2018) 3299-3306.

[61] V.S.K. Yadav, M.K. Purkait, Solar cell driven electrochemical process for the reduction of CO_2 to HCOOH on Zn and Sn electrocatalysts, Solar Energy, 124 (2016) 177-183.

[62] Y.S. Zhou, F.L. Che, M. Liu, C.Q. Zou, Z.Q. Liang, P. De Luna, H.F. Yuan, J. Li, Z.Q. Wang, H.P. Xie, H.M. Li, P.N. Chen, E. Bladt, R. Quintero-Bermudez, T.K. Sham, S. Bals, J. Hofkens, D. Sinton, G. Chen, E.H. Sargent, Dopant-induced electron localization drives CO_2 reduction to C-2 hydrocarbons, Nature Chemistry, 10 (2018) 974-980.

[63] W.C. Ma, S.J. Xie, T.T. Liu, Q.Y. Fan, J.Y. Ye, F.F. Sun, Z. Jiang, Q.H. Zhang, J. Cheng, Y. Wang, Electrocatalytic reduction of CO_2 to ethylene and ethanol through hydrogen-assisted C-C coupling over fluorine-modified copper, Nature Catalysis, 3 (2020) 478-487.

[64] P. Bose, C. Mukherjee, A.K. Golder, A Ni-II complex of the tetradentate salen ligand H_2L_2NH comprising an anchoring $-NH_2$ group: synthesis, characterization and

electrocatalytic CO_2 reduction to alcohols, Inorganic Chemistry Frontiers, 6 (2019) 1721-1728.

[65] H.P. Yang, Y.N. Yue, S. Qin, H. Wang, J.X. Lu, Selective electrochemical reduction of CO_2 to different alcohol products by an organically doped alloy catalyst, Green Chemistry, 18 (2016) 3216-3220.

[66] T. Roman, O. Conquest, A. Marianov, Y. Jiang, C. Stampfl, Enhancing the performance of cobalt porphyrin-based electrocatalysts for CO_2 reduction, Bulletin of the American Physical Society, 56 (23) (2021) 6468-6472.

[67] N. Sakamoto, Y.F. Nishimura, T. Nonaka, M. Ohashi, N. Ishida, K. Kitazumi, Y. Kato, K. Sekizawa, T. Morikawa, T. Arai, Self-assembled cuprous coordination polymer as a catalyst for CO_2 electrochemical reduction into C-2 products, ACS Catalysis, 10 (2020) 10412-10419.

[68] J. Albo, D. Vallejo, G. Beobide, O. Castillo, P. Castano, A. Irabien, Copper-based metal-organic porous materials for CO_2 electrocatalytic reduction to alcohols, Chemsuschem, 10 (2017) 1100-1109.

[69] H. Xu, D. Rebollar, H. He, L. Chong, Y. Liu, C. Liu, C.-J. Sun, T. Li, J.V. Muntean, R.E. Winans, Highly selective electrocatalytic CO_2 reduction to ethanol by metallic clusters dynamically formed from atomically dispersed copper, Nature Energy, 5 (2020) 623-632.

[70] J. Yuan, M.P. Yang, W.Y. Zhi, H. Wang, H. Wang, J.X. Lu, Efficient electrochemical reduction of CO_2 to ethanol on Cu nanoparticles decorated on N-doped graphene oxide catalysts, Journal of CO_2 Utilization, 33 (2019) 452-460.

[71] Y.M. Liu, Y.J. Zhang, K. Cheng, X. Quan, X.F. Fan, Y. Su, S. Chen, H.M. Zhao, Y.B. Zhang, H.T. Yu, M.R. Hoffmann, Selective electrochemical reduction of carbon dioxide to ethanol on a boron- and nitrogen-co-doped nanodiamond, Angewandte Chemie-International Edition, 56 (2017) 15607-15611.

[72] J.J. Wu, S.C. Ma, J. Sun, J.I. Gold, C. Tiwary, B. Kim, L.Y. Zhu, N. Chopra, I.N. Odeh, R. Vajtai, A.Z. Yu, R. Luo, J. Lou, G.Q. Ding, P.J.A. Kenis, P.M. Ajayan, A metal-free electrocatalyst for carbon dioxide reduction to multi-carbon hydrocarbons and oxygenates, Nature Communications, 7 (2016) 13869.

[73] I. Hjorth, M. Nord, M. Ronning, J. Yang, D. Chen, Electrochemical reduction of CO_2 to synthesis gas on CNT supported $Cu_xZn_{1-x}O$ catalysts, Catal Today, 357 (2020) 311-321.

[74] G.L. Chai, Z.X. Guo, Highly effective sites and selectivity of nitrogen-doped graphene/CNT catalysts for CO_2 electrochemical reduction, Chemical Science, 7 (2016) 1268-1275.

[75] J. Yuan, M. P. Yang, Q. L. Hu, S. M. Li, H. Wang, J. X. Lu, Cu/TiO2 nanoparticles modified nitrogen-doped graphene as a highly efficient catalyst for the selective electroreduction of CO_2 to different alcohols, Journal of CO_2 Utilization, 24 (2018) 334-340.

[76] E.L. Clark, C. Hahn, T.F. Jaramillo, A.T. Bell, Electrochemical CO_2 reduction over compressively strained CuAg surface alloys with enhanced multi-carbon oxygenate selectivity, Journal of the American Chemical Society, 139 (2017) 15848-15857.

[77] H. Han, Y. Noh, Y. Kim, S. Park, W. Yoon, D. Jang, S.M. Choi, W.B. Kim, Selective electrochemical CO_2 conversion to multicarbon alcohols on highly efficient N-doped porous carbon-supported Cu catalysts, Green Chemistry, 22 (2020) 71-84.

[78] M. Gonçalves, A. Gomes, J. Condeço, T. Fernandes, T. Pardal, C. Sequeira, J. Branco, Electrochemical conversion of CO_2 to C2 hydrocarbons using different ex situ copper electrodeposits, Electrochimica Acta, 102 (2013) 388-392.

[79] V.S.K. Yadav, M.K. Purkait, Electrochemical studies for CO_2 reduction using synthesized Co_3O_4 (Anode) and Cu_2O (Cathode) as electrocatalysts, Energy & Fuels, 29 (2015) 6670-6677.

[80] Y. Wang, H.Y. Liu, J.L. Yu, B.H. Hu, H. Zhao, P. Tsiakaras, S.Q. Song, Copper oxide derived nanostructured self-supporting Cu electrodes for electrochemical reduction of carbon dioxide, Electrochimica Acta, 328 (2019) 135083.

[81] Y. Hori, I. Takahashi, O. Koga, N. Hoshi, Electrochemical reduction of carbon dioxide at various series of copper single crystal electrodes, Journal of Molecular Catalysis A - Chemical, 199 (2003) 39-47.

[82] N.T. Suen, Z.R. Kong, C.S. Hsu, H.C. Chen, C.W. Tung, Y.R. Lu, C.L. Dong, C.C. Shen, J.C. Chung, H.M. Chen, Morphology manipulation of copper nanocrystals and product selectivity in the electrocatalytic reduction of carbon dioxide, ACS Catalysis, 9 (2019) 5217-5222.

[83] A.A. Permyakova, J. Herranz, M. El Kazzi, J.S. Diercks, M. Povia, L.R. Mangani, M. Horisberger, A. Patru, T.J. Schmidt, On the oxidation state of Cu_2O upon electrochemical CO_2 reduction: An XPS study, Chemphyschem, 20 (2019) 3120-3127.

[84] Y. Lum, J.W. Ager, Evidence for product-specific active sites on oxide-derived Cu catalysts for electrochemical CO_2 reduction, Nature Catalysis, 2 (2019) 86-93.

[85] N.S.R. Cuellar, C. Scherer, B. Kackar, W. Eisenreich, C. Huber, K. Wiesner-Fleischer, M. Fleischer, O. Hinrichsen, Two-step electrochemical reduction of CO_2 towards multi-carbon products at high current densities, Journal of CO_2 Utilization, 36 (2020) 263-275.

[86] C.S. Chen, J.H. Wan, B.S. Yeo, Electrochemical reduction of carbon dioxide to ethane using nanostructured Cu_2O-derived copper catalyst and palladium(II) chloride, Journal of Physical Chemistry C, 119 (2015) 26875-26882.

[87] W.L. Fu, Z. Liu, T.Y. Wang, J.S. Liang, S. Duan, L.F. Xie, J.T. Han, Q. Li, Promoting C_{2+} production from electrochemical CO_2 reduction on shape-controlled cuprous oxide nanocrystals with high-index facets, ACS Sustainable Chemistry & Engineering, 8 (2020) 15223-15229.

[88] L.R.L. Ting, R. Garcia-Muelas, A.J. Martin, F.L.P. Veenstra, S.T.J. Chen, Y.J. Peng, E.Y.X. Per, S. Pablo-Garcia, N. Lopez, J. Perez-Ramirez, B.S. Yeo, Electrochemical reduction of carbon dioxide to 1-butanol on oxide-derived copper, Angewandte Chemie-International Edition, 59 (2020) 21072-21079.

[89] M. Rahaman, A. Dutta, A. Zanetti, P. Broekmann, Electrochemical reduction of CO_2 into multicarbon alcohols on activated Cu mesh catalysts: an identical location (IL) study, ACS Catalysis, 7 (2017) 7946-7956.

[90] J. Albo, A. Irabien, Cu_2O-loaded gas diffusion electrodes for the continuous electrochemical reduction of CO_2 to methanol, Journal of Catalysis, 343 (2016) 232-239.

[91] H. Xiang, S. Rasul, K. Scott, J. Portoles, P. Cumpson, E.H. Yu, Enhanced selectivity of carbonaceous products from electrochemical reduction of CO_2 in aqueous media, Journal of CO_2 Utilization, 30 (2019) 214-221.

[92] K.J. Puring, D. Siegmund, J. Timm, F. Mollenbruck, S. Schemme, R. Marschall, U.P. Apfel, Electrochemical CO_2 reduction: tailoring catalyst layers in gas diffusion electrodes, Advanced Sustainable Systems, 5 (2021) 2000088.

[93] Z.P. Ma, C. Tsounis, P.V. Kumar, Z.J. Han, R.J. Wong, C.Y. Toe, S.J. Zhou, N.M. Bedford, L. Thomsen, Y.H. Ng, R. Amal, Enhanced electrochemical CO_2 reduction of $Cu@Cu_xO$ nanoparticles decorated on 3D vertical graphene with intrinsic $sp^{(3)}$-type defect, Advanced Functional Materials, 30 (2020) 1910118.

[94] J. Zhang, W. Luo, A. Zuttel, Self-supported copper-based gas diffusion electrodes for CO_2 electrochemical reduction, Journal of Materials Chemistry A, 7 (2019) 26285-26292.

[95] J.-T. Luo, G.-L. Zang, C. Hu, An efficient 3D ordered mesoporous Cu sphere array electrocatalyst for carbon dioxide electrochemical reduction, Journal of Materials Science & Technology, 55 (2020) 95-106.

[96] Y. Kwon, Y. Lum, E.L. Clark, J.W. Ager, A.T. Bell, CO_2 electroreduction with enhanced ethylene and ethanol selectivity by nanostructuring polycrystalline copper, ChemElectroChem, 3 (2016) 1012-1019.

[97] A. Vasileff, Y.P. Zhu, X. Zhi, Y.Q. Zhao, L. Ge, H.M. Chen, Y. Zheng, S.Z. Qiao, Electrochemical reduction of CO_2 to ethane through stabilization of an ethoxy intermediate, Angewandte Chemie-International Edition, 59 (2020) 19649-19653.

[98] N.S.R. Cuellar, K. Wiesner-Fleischer, M. Fleischer, A. Rucki, O. Hinrichsen, Advantages of CO over CO_2 as reactant for electrochemical reduction to ethylene, ethanol and n-propanol on gas diffusion electrodes at high current densities, Electrochimica Acta, 307 (2019) 164-175.

[99] S. Munir, A.R. Varzeghani, S. Kaya, Electrocatalytic reduction of CO_2 to produce higher alcohols, Sustainable Energy & Fuels, 2 (2018) 2532-2541.

[100] M. Ma, K. Djanashvili, W.A. Smith, Controllable hydrocarbon formation from the electrochemical reduction of CO_2 over Cu nanowire arrays, Angewandte Chemie-International Edition, 55 (2016) 6680-6684.

[101] G. Iijima, T. Inomata, H. Yamaguchi, M. Ito, H. Masuda, Role of a hydroxide layer on Cu electrodes in electrochemical CO_2 reduction, ACS Catalysis, 9 (2019) 6305-6319.

[102] C.S. Le Duff, M.J. Lawrence, P. Rodriguez, Role of the adsorbed oxygen species in the selective electrochemical reduction of CO_2 to alcohols and carbonyls on copper electrodes, Angewandte Chemie-International Edition, 56 (2017) 12919-12924.

[103] F. Dattila, R. García-Muelas, N.r. López, Active and selective ensembles in oxide-derived copper catalysts for CO_2 reduction, ACS Energy Letters, 5 (2020) 3176-3184.

[104] E.L. Clark, A.T. Bell, Direct observation of the local reaction environment during the electrochemical reduction of CO_2, Journal of the American Chemical Society, 140 (2018) 7012-7020.

[105] E. Bertheussen, A. Verdaguer-Casadevall, D. Ravasio, J.H. Montoya, D.B. Trimarco, C. Roy, S. Meier, J. Wendland, J.K. Nørskov, I.E. Stephens, Acetaldehyde as an intermediate in the electroreduction of carbon monoxide to ethanol on oxide-derived copper, Angewandte Chemie International Edition, 55 (2016) 1450-1454.

[106] K.A. Adegoke, S.G. Radhakrishnan, C.L. Gray, B. Sowa, C. Morais, P. Rayess, E.R. Rohwer, C. Comminges, K.B. Kokoh, E. Roduner, Highly efficient formic acid and carbon dioxide electro-reduction to alcohols on indium oxide electrodes, Sustainable Energy & Fuels, 4 (2020) 4030-4038.

[107] T. Hatsukade, K.P. Kuhl, E.R. Cave, D.N. Abram, T.F. Jaramillo, Insights into the electrocatalytic reduction of CO_2 on metallic silver surfaces, Physical Chemistry Chemical Physics, 16 (2014) 13814-13819.

[108] S.D. Giri, S.M. Mahajani, A. Suresh, A. Sarkar, Electrochemical reduction of CO_2 on activated copper: Influence of surface area, Materials Research Bulletin, 123 (2020) 110702.

[109] K. Malik, N.K. Bajaj, A. Verma, Effect of catalyst layer on electrochemical reduction of carbon dioxide using different morphologies of copper, Journal of CO_2 Utilization, 27 (2018) 355-365.

[110] S. Lee, D. Kim, J. Lee, Electrocatalytic production of C3-C4 compounds by conversion of CO_2 on a chloride-induced bi-phasic Cu_2O-Cu catalyst, Angewandte Chemie, 127 (2015) 14914-14918.

[111] S. Lee, G. Park, J. Lee, Importance of Ag–Cu biphasic boundaries for selective electrochemical reduction of CO_2 to ethanol, ACS Catalysis, 7 (2017) 8594-8604.

[112] T.T. Hoang, S. Verma, S. Ma, T.T. Fister, J. Timoshenko, A.I. Frenkel, P.J. Kenis, A.A. Gewirth, Nanoporous copper–silver alloys by additive-controlled electrodeposition for the selective electroreduction of CO_2 to ethylene and ethanol, Journal of the American Chemical Society, 140 (2018) 5791-5797.

[113] D. Ren, B.S.-H. Ang, B.S. Yeo, Tuning the selectivity of carbon dioxide electroreduction toward ethanol on oxide-derived Cu_x Zn catalysts, ACS Catalysis, 6 (2016) 8239-8247.

[114] S. Ikeda, Y. Tomita, A. Hattori, K. Ito, H. Noda, M. Sakai, Selective ethanol formation by electrochemical reduction of carbon-dioxide on electrodes comprised of the mixtures of copper and zinc-oxides, Denki Kagaku, 61 (1993) 807-809.

[115] D. Ren, J. Gao, L. Pan, Z. Wang, J. Luo, S.M. Zakeeruddin, A. Hagfeldt, M. Grätzel, Atomic layer deposition of ZnO on CuO enables selective and efficient electroreduction of carbon dioxide to liquid fuels, Angewandte Chemie, 131 (2019) 15178-15182.

[116] E. Andrews, M.M. Ren, F. Wang, Z.Y. Zhang, P. Sprunger, R. Kurtz, J. Flake, Electrochemical reduction of CO_2 at Cu nanocluster/(100) ZnO electrodes, Journal of the Electrochemical Society, 160 (2013) H841-H846.

[117] J. Gao, D. Ren, X.Y. Guo, S.M. Zakeeruddin, M. Gratzel, Sequential catalysis enables enhanced C-C coupling towards multi-carbon alkenes and alcohols in carbon dioxide reduction: a study on bifunctional Cu/Au electrocatalysts, Faraday Discussions, 215 (2019) 282-296.

[118] G. Iijima, H. Yamaguchi, T. Inomata, H. Yoto, M. Ito, H. Masuda, Methanethiol SAMs induce reconstruction and formation of Cu^+ on a Cu catalyst under electrochemical CO_2 reduction, ACS Catalysis, 10 (2020) 15238-15249.

[119] H.P. Yang, S. Qin, Y.N. Yue, L. Liu, H. Wang, J.X. Lu, Entrapment of a pyridine derivative within a copper-palladium alloy: a bifunctional catalyst for electrochemical reduction of CO_2 to alcohols with excellent selectivity and reusability, Catalysis Science & Technology, 6 (2016) 6490-6494.

[120] F. Li, Y.C. Li, Z. Wang, J. Li, D.-H. Nam, Y. Lum, M. Luo, X. Wang, A. Ozden, S.-F. Hung, Cooperative CO_2-to-ethanol conversion via enriched intermediates at molecule–metal catalyst interfaces, Nature Catalysis, 3 (2020) 75-82.

[121] Q. Zhu, X. Sun, D. Yang, J. Ma, X. Kang, L. Zheng, J. Zhang, Z. Wu, B. Han, Carbon dioxide electroreduction to C2 products over copper-cuprous oxide derived from electrosynthesized copper complex, Nature Communications, 10 (2019) 1-11.

[122] K. Ogura, N. Endo, Electrochemical reduction of CO_2 with a functional gas-diffusion electrode in aqueous solutions with and without propylene carbonate, Journal of the Electrochemical Society, 146 (1999) 3736.

[123] Y. Jiao, Y. Zheng, P. Chen, M. Jaroniec, S.Z. Qiao, Molecular scaffolding strategy with synergistic active centers to facilitate electrocatalytic CO_2 reduction to hydrocarbon/alcohol, Journal of the American Chemical Society, 139 (2017) 18093-18100.

[124] H. Li, T. Liu, P. Wei, L. Lin, D. Gao, G. Wang, X. Bao, High-rate CO_2 electroreduction to C_{2+} products over a copper-copper iodide catalyst, Angewandte Chemie, (2021).

[125] H. Li, X.X. Qin, T.W. Jiang, X.Y. Ma, K. Jiang, W.B. Cai, Changing the product selectivity for electrocatalysis of CO_2 reduction reaction on plated Cu electrodes, Chemcatchem, 11 (2019) 6139-6146.

[126] N. Roy, Y. Shibano, C. Terashima, K. Katsumata, K. Nakata, T. Kondo, M. Yuasa, A. Fujishima, Ionic-liquid-assisted selective and controlled electrochemical CO_2 reduction at Cu-modified boron-doped diamond electrode, Chemelectrochem, 3 (2016) 1044-1047.

[127] D. Karapinar, N.T. Huan, N. Ranjbar Sahraie, J. Li, D. Wakerley, N. Touati, S. Zanna, D. Taverna, L.H. Galvão Tizei, A. Zitolo, Electroreduction of CO_2 on single-site copper-nitrogen-doped carbon material: selective formation of ethanol and reversible restructuration of the metal sites, Angewandte Chemie International Edition, 58 (2019) 15098-15103.

[128] Y.-S. Cheng, X.-P. Chu, M. Ling, N. Li, K.-L. Wu, F.-H. Wu, H. Li, G. Yuan, X.-W. Wei, An MOF-derived copper@ nitrogen-doped carbon composite: the synergistic effects of N-types and copper on selective CO_2 electroreduction, Catalysis Science & Technology, 9 (2019) 5668-5675.

[129] M. Perfecto-Irigaray, J. Albo, G. Beobide, O. Castillo, A. Irabien, S. Perez-Yanez, Synthesis of heterometallic metal-organic frameworks and their performance as electrocatalyst for CO_2 reduction, RSCAdvances, 8 (2018) 21092-21099.

[130] K.L. Lv, Y.C. Fan, Y. Zhu, Y. Yuan, J.R. Wang, Y. Zhu, Q.F. Zhang, Elastic Ag-anchored N-doped graphene/carbon foam for the selective electrochemical reduction of carbon dioxide to ethanol, Journal of Materials Chemistry A, 6 (2018) 5025-5031.

[131] K. Zhao, Y. Liu, X. Quan, S. Chen, H. Yu, CO_2 electroreduction at low overpotential on oxide-derived Cu/carbons fabricated from metal organic framework, ACS Applied Materials & Interfaces, 9 (2017) 5302-5311.

[132] H.P. Yang, Q. Lin, H.W. Zhang, Y. Wu, L.D. Fan, X.Y. Chai, Q.L. Zhang, J.H. Liu, C.X. He, Selective electrochemical reduction of CO_2 by a binder-free platinum/nitrogen-doped carbon nanofiber/copper foil catalyst with remarkable efficiency and reusability, Electrochemistry Communications, 93 (2018) 138-142.

[133] R.A. Geioushy, M.M. Khaled, A.S. Hakeem, K. Alhooshani, C. Basheer, High efficiency graphene/Cu_2O electrode for the electrochemical reduction of carbon dioxide to ethanol, J. Electroanal. Chem., 785 (2017) 138-143.

[134] B.C. Marepally, C. Ampelli, C. Genovese, F. Tavella, L. Veyre, E.A. Quadrelli, S. Perathoner, G. Centi, Role of small Cu nanoparticles in the behaviour of nanocarbon-based electrodes for the electrocatalytic reduction of CO_2, Journal of CO_2 Utilization, 21 (2017) 534-542.

[135] L. Ji, L. Li, X.Q. Ji, Y. Zhang, S.Y. Mou, T.W. Wu, Q. Liu, B.H. Li, X.J. Zhu, Y.L. Luo, X.F. Shi, A.M. Asiri, X.P. Sun, Highly Selective electrochemical reduction of CO_2 to alcohols on a FeP nanoarray, Angewandte Chemie-International Edition, 59 (2020) 758-762.

[136] L. Ji, L. Chang, Y. Zhang, S.Y. Mou, T. Wang, Y.L. Luo, Z.M. Wang, X.P. Sun, Electrocatalytic CO_2 reduction to alcohols with high selectivity over a Two-Dimensional $Fe_2P_2S_6$ nanosheet, ACS Catalysis, 9 (2019) 9721-9725.

[137] J. Yuan, W.Y. Zhi, L. Liu, M.P. Yang, H. Wang, J.X. Lu, Electrochemical reduction of CO_2 at metal-free N-functionalized graphene oxide electrodes, Electrochimica Acta, 282 (2018) 694-701.

[138] Y.Y. Birdja, M.T.M. Koper, The importance of cannizzaro-type reactions during electrocatalytic reduction of carbon dioxide, Journal of the American Chemical Society, 139 (2017) 2030-2034.

[139] J.W. Vickers, D. Alfonso, D.R. Kauffman, Electrochemical carbon dioxide reduction at nanostructured gold, copper, and alloy materials, Energy Technology, 5 (2017) 775-795.

[140] S. Gu, A.N. Marianov, H. Xu, Y. Jiang, Effect of TiO_2 support on immobilization of cobalt porphyrin for electrochemical CO_2 reduction, Journal of Materials Science & Technology, 80 (2021) 20-27.

[141] I. Masood ul Hasan, L. Peng, J. Mao, R. He, Y. Wang, J. Fu, N. Xu, J. Qiao, Carbon-based metal-free catalysts for electrochemical CO_2 reduction: Activity, selectivity, and stability, Carbon Energy, 3 (2021) 24-49.

[142] D.M. Fernandes, A.F. Peixoto, C. Freire, Nitrogen-doped metal-free carbon catalysts for (electro) chemical CO_2 conversion and valorisation, Dalton Transactions, 48 (2019) 13508-13528.

[143] X. Duan, J. Xu, Z. Wei, J. Ma, S. Guo, S. Wang, H. Liu, S. Dou, Metal-free carbon materials for CO_2 electrochemical reduction, Advanced Materials, 29 (2017) 1701784.

[144] D. Guo, R. Shibuya, C. Akiba, S. Saji, T. Kondo, J. Nakamura, Active sites of nitrogen-doped carbon materials for oxygen reduction reaction clarified using model catalysts, Science, 351 (2016) 361-365.

[145] P.S. Murthy, W. Liang, Y. Jiang, J. Huang, Cu-based nanocatalysts for CO_2 hydrogenation to methanol, Energy & Fuels, 35 (2021) 8558-8584.

[146] D. Ren, J. Fong, B.S. Yeo, The effects of currents and potentials on the selectivities of copper toward carbon dioxide electroreduction, Nature Communications, 9 (2018) 1-8.

[147] N. Gupta, M. Gattrell, B. MacDougall, Calculation for the cathode surface concentrations in the electrochemical reduction of CO_2 in $KHCO_3$ solutions, Journal of Applied Electrochemistry, 36 (2006) 161-172.

[148] M.M. de Salles Pupo, R. Kortlever, Electrolyte effects on the electrochemical reduction of CO_2, ChemPhysChem, 20 (2019) 2926.

[149] S. Garg, M. Li, Y. Wu, M. Nazmi Idros, H. Wang, A.J. Yago, L. Ge, G.G. Wang, T.E. Rufford, Understanding the effects of anion interactions with Ag electrodes on electrochemical CO_2 reduction in choline halide electrolytes, ChemSusChem, 14 (12) (2021) 2601-2611.

[150] N. Uemoto, M. Furukawa, I. Tateishi, H. Katsumata, S. Kaneco, Electrochemical carbon dioxide reduction in methanol at Cu and Cu_2O-deposited carbon black electrodes, ChemEngineering, 3 (1) (2019) 15.

[151] S.T. Ahn, I. Abu-Baker, G.T.R. Palmore, Electroreduction of CO_2 on polycrystalline copper: Effect of temperature on product selectivity, Catal Today, 288 (2017) 24-29.

[152] C.S. Wong, P.Y. Tishchenko, W.K. Johnson, Solubility of carbon dioxide in aqueous HCl and $NaHCO_3$ solutions from 278 to 298 K, Journal of Chemical & Engineering Data, 50 (2005) 817-821.

[153] J.T. Song, H. Song, B. Kim, J. Oh, Towards higher rate electrochemical CO_2 conversion: from liquid-phase to gas-phase systems, Catalysts, 9 (2019) 224.

[154] S. Verma, X. Lu, S. Ma, R.I. Masel, P.J. Kenis, The effect of electrolyte composition on the electroreduction of CO_2 to CO on Ag based gas diffusion electrodes, Physical Chemistry Chemical Physics, 18 (2016) 7075-7084.

[155] L. Fan, C. Xia, F. Yang, J. Wang, H. Wang, Y. Lu, Strategies in catalysts and electrolyzer design for electrochemical CO_2 reduction toward C2+ products, Science Advances, 6 (2020) eaay3111.

[156] J.J. Lv, M. Jouny, W. Luc, W. Zhu, J.J. Zhu, F. Jiao, A highly porous copper electrocatalyst for carbon dioxide reduction, Advanced Materials, 30 (2018) 1803111.

[157] K.P. Kuhl, T. Hatsukade, E.R. Cave, D.N. Abram, J. Kibsgaard, T.F. Jaramillo, Electrocatalytic conversion of carbon dioxide to methane and methanol on transition metal surfaces, Journal of the American Chemical Society, 136 (2014) 14107-14113.

[158] M.R. Singh, E.L. Clark, A.T. Bell, Effects of electrolyte, catalyst, and membrane composition and operating conditions on the performance of solar-driven electrochemical reduction of carbon dioxide, Physical Chemistry Chemical Physics, 17 (2015) 18924-18936.

[159] D. Kim, C.S. Kley, Y. Li, P. Yang, Copper nanoparticle ensembles for selective electroreduction of CO_2 to C2–C3 products, Proceedings of the National Academy of Sciences, 114 (2017) 10560-10565.

[160] I. Merino-Garcia, J. Albo, A. Irabien, Productivity and selectivity of gas-phase CO_2 electroreduction to methane at copper nanoparticle-based electrodes, Energy Technology, 5 (2017) 922-928.

[161] M.N. Hossain, J. Wen, A. Chen, Unique copper and reduced graphene oxide nanocomposite toward the efficient electrochemical reduction of carbon dioxide, Scientific Reports, 7 (2017) 1-10.

[162] D. Hursán, A.A. Samu, L. Janovák, K. Artyushkova, T. Asset, P. Atanassov, C. Janáky, Morphological attributes govern carbon dioxide reduction on N-doped carbon electrodes, Joule, 3 (2019) 1719-1733.

[163] R.A. Tufa, D. Chanda, M. Ma, D. Aili, T.B. Demissie, J. Vaes, Q. Li, S. Liu, D. Pant, Towards highly efficient electrochemical CO_2 reduction: Cell designs, membranes and electrocatalysts, Applied Energy, 277 (2020) 115557.

[164] X. Wang, Z. Wang, F.P.G. de Arquer, C.-T. Dinh, A. Ozden, Y.C. Li, D.-H. Nam, J. Li, Y.-S. Liu, J. Wicks, Efficient electrically powered CO_2-to-ethanol via suppression of deoxygenation, Nature Energy, 5 (2020) 478-486.

[165] S. Ma, M. Sadakiyo, M. Heima, R. Luo, R.T. Haasch, J.I. Gold, M. Yamauchi, P.J. Kenis, Electroreduction of carbon dioxide to hydrocarbons using bimetallic Cu–Pd catalysts with different mixing patterns, Journal of the American Chemical Society, 139 (2017) 47-50.

[166] T.K. Todorova, M.W. Schreiber, M. Fontecave, Mechanistic understanding of CO_2 reduction reaction (CO_2RR) toward multicarbon products by heterogeneous copper-based catalysts, ACS Catalysis, 10 (2019) 1754-1768.

[167] R. Kortlever, J. Shen, K.J.P. Schouten, F. Calle-Vallejo, M.T.M. Koper, Catalysts and reaction pathways for the electrochemical reduction of carbon dioxide, Journal of Physical Chemistry Letters, 6 (2015) 4073-4082.

[168] Q. Fan, M. Zhang, M. Jia, S. Liu, J. Qiu, Z. Sun, Electrochemical CO_2 reduction to C2+ species: heterogeneous electrocatalysts, reaction pathways, and optimization strategies, Materials Today Energy, 10 (2018) 280-301.

[169] B. Endrődi, E. Kecsenovity, A. Samu, F. Darvas, R. Jones, V. Török, A. Danyi, C. Janáky, Multilayer electrolyzer stack converts carbon dioxide to gas products at high pressure with high efficiency, ACS Energy Letters, 4 (2019) 1770-1777.

[170] S.D. Sajjad, Y. Gao, Z. Liu, H. Yang, R. Masel, Tunable-High performance sustainion™ anion exchange membranes for electrochemical applications, ECS Transactions, 77 (2017) 1653.

[171] J.M. Spurgeon, B. Kumar, A comparative technoeconomic analysis of pathways for commercial electrochemical CO_2 reduction to liquid products, Energy & Environmental Science, 11 (2018) 1536-1551.

[172] X. Wang, Z. Wang, F.P.G. de Arquer, C.-T. Dinh, A. Ozden, Y.C. Li, D.-H. Nam, J. Li, Y.-S. Liu, J. Wicks, Efficient electrically powered CO_2-to-ethanol via suppression of deoxygenation, Nature Energy, 5 (2020) 478-486.

[173] National Academies of Sciences, Medicine, Gaseous carbon waste streams utilization: Status and research needs, National Academies Press, 2019.

[174] W. Knoche, Chemical reactions of CO_2 in water. In: Bauer C., Gros G., Bartels H. (eds) Biophysics and Physiology of Carbon Dioxide. Proceedings in Life Sciences. Springer, Berlin, Heidelberg. (1980) 3-11.

[175] M. Naderi, Surface Area: Brunauer–Emmett–Teller (BET), in: Progress in filtration and separation, Elsevier, 2015, 585-608.

[176] S. Storck, H. Bretinger, W.F. Maier, Characterization of micro-and mesoporous solids by physisorption methods and pore-size analysis, Applied Catalysis A: General, 174 (1998) 137-146.

[177] A. Kamat, A. Huth, O. Klein, S. Scholl, Chronoamperometric investigations of the electrode–electrolyte interface of a commercial high temperature PEM fuel cell, Fuel Cells, 10 (2010) 983-992.

[178] L. Wang, S. Nitopi, A.B. Wong, J.L. Snider, A.C. Nielander, C.G. Morales-Guio, M. Orazov, D.C. Higgins, C. Hahn, T.F. Jaramillo, Electrochemically converting carbon monoxide to liquid fuels by directing selectivity with electrode surface area, Nature Catalysis, 2 (2019) 702-708.

[179] M.E. LaCourse, W.R. LaCourse, General instrumentation in HPLC, in: Liquid Chromatography, Elsevier, 2017, pp. 417-429.

[180] K. Zia, T. Siddiqui, S. Ali, I. Farooq, M.S. Zafar, Z. Khurshid, Nuclear magnetic resonance spectroscopy for medical and dental applications: A comprehensive review, European Journal of Dentistry, 13 (2019) 124-128.

[181] S. Chatterjee, N.C. Maji, A.H. Shaik, J. Chakraborty, Economical and high throughput synthesis of copper nanopowder using continuous stirred tank and tubular flow reactors, Chemical Engineering Journal, 304 (2016) 241-250.

[182] T. Ghodselahi, M. Vesaghi, A. Shafiekhani, A. Baghizadeh, M. Lameii, XPS study of the Cu@ Cu_2O core-shell nanoparticles, Applied Surface Science, 255 (2008) 2730-2734.

[183] S. Sengupta, V. Amte, R. Dongara, A.K. Das, H. Bhunia, P.K. Bajpai, Effects of the adsorbent preparation method for CO_2 capture from flue gas using K_2CO_3/Al_2O_3 adsorbents, Energy & Fuels, 29 (2015) 287-297.

[184] X. Zou, E. Ying, S. Dong, Seed-mediated synthesis of branched gold nanoparticles with the assistance of citrate and their surface-enhanced Raman scattering properties, Nanotechnology, 17 (2006) 4758.

[185] S. Singh, R.K. Gautam, K. Malik, A. Verma, Ag-Co bimetallic catalyst for electrochemical reduction of CO_2 to value added products, Journal of CO_2 Utilization, 18 (2017) 139-146.

[186] C.G. Morales-Guio, E.R. Cave, S.A. Nitopi, J.T. Feaster, L. Wang, K.P. Kuhl, A. Jackson, N.C. Johnson, D.N. Abram, T. Hatsukade, C. Hahn, T.F. Jaramillo, Improved CO_2 reduction activity towards C2+ alcohols on a tandem gold on copper electrocatalyst, Nature Catalysis, 1 (2018) 764-771.

[187] Y. Hori, H. Wakebe, T. Tsukamoto, O. Koga, Adsorption of CO accompanied with simultaneous charge transfer on copper single crystal electrodes related with electrochemical reduction of CO_2 to hydrocarbons, Surface Science, 335 (1995) 258-263.

[188] L. Hou, J. Han, C. Wang, Y. Zhang, Y. Wang, Z. Bai, Y. Gu, Y. Gao, X. Yan, Ag nanoparticle embedded Cu nanoporous hybrid arrays for the selective electrocatalytic reduction of CO_2 towards ethylene, Inorganic Chemistry Frontiers, 7 (2020) 2097-2106.

[189] D. Yang, Q. Zhu, X. Sun, C. Chen, L. Lu, W. Guo, Z. Liu, B. Han, Nanoporous Cu/Ni oxide composites: efficient catalysts for electrochemical reduction of CO_2 in aqueous electrolytes, Green Chemistry, 20 (2018) 3705-3710.

[190] S. Sen, D. Liu, G.T.R. Palmore, Electrochemical reduction of CO_2 at copper nanofoams, ACS Catalysis, 4 (2014) 3091-3095.

[191] A. Loiudice, P. Lobaccaro, E.A. Kamali, T. Thao, B.H. Huang, J.W. Ager, R. Buonsanti, Tailoring copper nanocrystals towards C2 products in electrochemical CO_2 reduction, Angewandte Chemie International Edition, 55 (2016) 5789-5792.

[192] A.D. Handoko, C.W. Ong, Y. Huang, Z.G. Lee, L. Lin, G.B. Panetti, B.S. Yeo, Mechanistic insights into the selective electroreduction of carbon dioxide to ethylene on Cu_2O-derived copper catalysts, The Journal of Physical Chemistry C, 120 (2016) 20058-20067.

[193] D. Ren, N.T. Wong, A.D. Handoko, Y. Huang, B.S. Yeo, Mechanistic insights into the enhanced activity and stability of agglomerated Cu nanocrystals for the electrochemical reduction of carbon dioxide to n-propanol, The Journal of Physical Chemistry Letters, 7 (2016) 20-24.

[194] Y. Hori, A. Murata, R. Takahashi, Formation of hydrocarbons in the electrochemical reduction of carbon-dioxide at a copper electrode in aqueous-solution, Journal of the Chemical Society-Faraday Transactions I, 85 (1989) 2309-2326.

[195] R. Kas, R. Kortlever, A. Milbrat, M.T.M. Koper, G. Mul, J. Baltrusaitis, Electrochemical CO_2 reduction on Cu_2O-derived copper nanoparticles: controlling the catalytic selectivity of hydrocarbons, Physical Chemistry Chemical Physics, 16 (2014) 12194-12201.

[196] D. Kim, S. Lee, J.D. Ocon, B. Jeong, J.K. Lee, J. Lee, Insights into an autonomously formed oxygen-evacuated Cu_2O electrode for the selective production of C_2H_4 from CO_2, Physical Chemistry Chemical Physics, 17 (2015) 824-830.

[197] C.S. Chen, A.D. Handoko, J.H. Wan, L. Ma, D. Ren, B.S. Yeo, Stable and selective electrochemical reduction of carbon dioxide to ethylene on copper mesocrystals, Catalysis Science & Technology, 5 (2015) 161-168.

[198] Q. Lu, J. Rosen, Y. Zhou, G.S. Hutchings, Y.C. Kimmel, J.G. Chen, F. Jiao, A selective and efficient electrocatalyst for carbon dioxide reduction, Nature Communications, 5 (2014) 1-6.

[199] X. Chang, A. Malkani, X. Yang, B. Xu, Mechanistic insights into electroreductive C–C coupling between CO and acetaldehyde into multicarbon products, Journal of the American Chemical Society, 142 (2020) 2975-2983.

[200] D.F. Cox, K.H. Schulz, Interaction of CO with Cu^+ cations: CO adsorption on Cu_2O (100), Surface Science, 249 (1991) 138-148.

[201] D.W. DeWulf, T. Jin, A.J. Bard, Electrochemical and surface studies of carbon dioxide reduction to methane and ethylene at copper electrodes in aqueous solutions, Journal of the Electrochemical Society, 136 (1989) 1686.

[202] Y. Hori, H. Konishi, T. Futamura, A. Murata, O. Koga, H. Sakurai, K. Oguma, Deactivation of copper electrode in electrochemical reduction of CO_2, Electrochimica Acta, 50 (2005) 5354-5369.

[203] A. Patterson, The Scherrer formula for X-ray particle size determination, Physical Review, 56 (1939) 978.

[204] Y. Song, S. Wang, W. Chen, S. Li, G. Feng, W. Wei, Y. Sun, Enhanced ethanol production from CO_2 electroreduction at micropores in nitrogen-doped mesoporous carbon, ChemSusChem, 13 (2020) 293-297.

[205] W.L. Dai, W.W. Xiong, J.J. Yu, S.Q. Zhang, B. Li, L.X. Yang, T.Y. Wang, X.B. Luo, J.P. Zou, S.L. Luo, Bi_2MoO_6 quantum dots in situ grown on reduced graphene oxide layers: A novel electron-rich interface for efficient CO_2 reduction, ACS Applied Materials & Interfaces, 12 (2020) 25861-25874.

[206] I. Merino-Garcia, J. Albo, J. Solla-Gullón, V. Montiel, A. Irabien, Cu oxide/ZnO-based surfaces for a selective ethylene production from gas-phase CO_2 electroconversion, Journal of CO_2 Utilization, 31 (2019) 135-142.

[207] M. Devaraj, R. Saravanan, R. Deivasigamani, V.K. Gupta, F. Gracia, S. Jayadevan, Fabrication of novel shape Cu and Cu/Cu_2O nanoparticles modified electrode for the determination of dopamine and paracetamol, Journal of Molecular Liquids, 221 (2016) 930-941.

[208] H.S. Jeon, J. Timoshenko, F. Scholten, I. Sinev, A. Herzog, F.T. Haase, B.R. Cuenya, Operando insight into the correlation between the structure and composition of CuZn nanoparticles and their selectivity for the electrochemical CO_2 reduction, Journal of the American Chemical Society, 141 (2019) 19879-19887.

[209] H. Xie, T. Wang, J. Liang, Q. Li, S. Sun, Cu-based nanocatalysts for electrochemical reduction of CO_2, Nano Today, 21 (2018) 41-54.

[210] M.I. Malik, Z.O. Malaibari, M. Atieh, B. Abussaud, Electrochemical reduction of CO_2 to methanol over MWCNTs impregnated with Cu_2O, Chemical Engineering Science, 152 (2016) 468-477.

[211] J. Shu, S. Cheng, H. Xia, L. Zhang, J. Peng, C. Li, S. Zhang, Copper loaded on activated carbon as an efficient adsorbent for removal of methylene blue, RSC Advances, 7 (2017) 14395-14405.

[212] Y. Hou, Y. L. Liangc, P. C. Shi, R. Coaa, Atomically dispersed Ni species on N-doped carbon nanotubes for electroreduction of CO_2 with nearly 100% CO selectivity, Appl Catal B - Environ, 271 (2020) 118929.

[213] W. Ni, C. Li, X. Zang, M. Xu, S. Huo, M. Liu, Z. Yang, Y.-M. Yan, Efficient electrocatalytic reduction of CO_2 on Cu_xO decorated graphene oxides: an insight into the role of multivalent Cu in selectivity and durability, Appl Catal B - Environ, 259 (2019) 118044.

[214] X. Cui, W. An, X. Liu, H. Wang, Y. Men, J. Wang, C_2N-graphene supported single-atom catalysts for CO_2 electrochemical reduction reaction: Mechanistic insight and catalyst screening, Nanoscale, 10 (2018) 15262-15272.

[215] Q. Huang, H. Liu, W. An, Y. Wang, Y. Feng, Y. Men, Synergy of a metallic NiCo dimer anchored on a C_2N–graphene matrix promotes the electrochemical CO_2 reduction reaction, ACS Sustainable Chemistry & Engineering, 7 (2019) 19113-19121.

[216] J. Chen, J. Xu, S. Zhou, N. Zhao, C.-P. Wong, Nitrogen-doped hierarchically porous carbon foam: a free-standing electrode and mechanical support for high-performance supercapacitors, Nano Energy, 25 (2016) 193-202.

[217] N. Sreekanth, M.A. Nazrulla, T.V. Vineesh, K. Sailaja, K.L. Phani, Metal-free boron-doped graphene for selective electroreduction of carbon dioxide to formic acid/formate, Chem Commun, 51 (2015) 16061-16064.

[218] H. Wang, Y. Chen, X. Hou, C. Ma, T. Tan, Nitrogen-doped graphenes as efficient electrocatalysts for the selective reduction of carbon dioxide to formate in aqueous solution, Green Chemistry, 18 (2016) 3250-3256.

[219] Y. Song, R. Peng, D.K. Hensley, P.V. Bonnesen, L. Liang, Z. Wu, H.M. Meyer, M. Chi, C. Ma, B.G. Sumpter, High-selectivity electrochemical conversion of CO_2 to ethanol using a copper nanoparticle/N-doped graphene electrode, ChemistrySelect, 1 (2016) 6055-6061.

[220] R. Geioushy, M.M. Khaled, K. Alhooshani, A.S. Hakeem, A. Rinaldi, Graphene/ZnO/Cu_2O electrocatalyst for selective conversion of CO_2 into n-propanol, Electrochimica Acta, 245 (2017) 456-462.

[221] N. Altaf, S. Liang, L. Huang, Q. Wang, Electro-derived Cu-Cu_2O nanocluster from LDH for stable and selective C2 hydrocarbons production from CO_2 electrochemical reduction, Journal of Energy Chemistry, 48 (2020) 169-180.

[222] N. Thaweesaeng, S. Supankit, W. Techidheera, W. Pecharapa, Structure properties of as-synthesized Cu-doped ZnO nanopowder synthesized by co-precipitation method, Energy Procedia, 34 (2013) 682-688.

[223] S. Kusama, T. Saito, H. Hashiba, A. Sakai, S. Yotsuhashi, Crystalline copper (II) phthalocyanine catalysts for electrochemical reduction of carbon dioxide in aqueous media, ACS Catalysis, 7 (2017) 8382-8385.

[224] B. Cullity, S. Stock, Elements of X-ray Diffraction, Prentice Hall, Upper Saddle River, NJ, USA (2001) 388.

[225] S. Das, V.C. Srivastava, An overview of the synthesis of CuO-ZnO nanocomposite for environmental and other applications, Nanotechnology Reviews, 7 (2018) 267-282.

[226] G. Liu, T. Tran-Phu, H. Chen, A. Tricoli, A Review of metal-and metal-oxide-based heterogeneous catalysts for electroreduction of carbon dioxide, Advanced Sustainable Systems, 2 (2018) 1800028.

[227] Y. Zhang, Y. Sun, Z. Cai, S. You, X. Li, Y. Zhang, Y. Yu, N. Ren, J. Zou, Stable CuO with variable valence states cooperated with active Co^{2+} as catalyst/co-catalyst for oxygen reduction/methanol oxidation reactions, Journal of Colloid and Interface Science, 593 (2021) 345-358.

[228] K. Malik, B.M. Rajbongshi, A. Verma, Syngas production from electrochemical reduction of CO_2 at high current density using oxide derived Zn/Cu nanocomposite, Journal of CO_2 Utilization, 33 (2019) 311-319.

[229] J. Huang, M. Mensi, E. Oveisi, V. Mantella, R. Buonsanti, Structural sensitivities in bimetallic catalysts for electrochemical CO_2 reduction revealed by Ag–Cu nanodimers, Journal of the American Chemical Society, 141 (2019) 2490-2499.

[230] Z. Li, R.M. Yadav, L. Sun, T. Zhang, J. Zhang, P.M. Ajayan, J. Wu, CuO/ZnO/C electrocatalysts for CO_2-to-C_{2+} products conversion with high yield: On the effect of geometric structure and composition, Applied Catalysis A: General, 606 (2020) 117829.

[231] M. Jouny, W. Luc, F. Jiao, General techno-economic analysis of CO_2 electrolysis systems, Industrial & Engineering Chemistry Research, 57 (2018) 2165-2177.

[232] Y. Feng, Z. Li, H. Liu, C. Dong, J. Wang, S.A. Kulinich, X. Du, Laser-prepared CuZn alloy catalyst for selective electrochemical reduction of CO_2 to ethylene, Langmuir, 34 (2018) 13544-13549.

[233] X. Su, Y. Sun, L. Jin, L. Zhang, Y. Yang, P. Kerns, B. Liu, S. Li, J. He, Hierarchically porous Cu/Zn bimetallic catalysts for highly selective CO_2 electroreduction to liquid C2 products, Appl Catal B - Environ, 269 (2020) 118800.

[234] J. Bullock, D.F. Srankó, C.M. Towle, Y. Lum, M. Hettick, M. Scott, A. Javey, J. Ager, Efficient solar-driven electrochemical CO 2 reduction to hydrocarbons and oxygenates, Energy & Environmental Science, 10 (2017) 2222-2230.

[235] Q. Zhang, T. Li, J. Luo, B. Liu, J. Liang, N. Wang, X. Kong, B. Li, C. Wei, Y. Zhao, Ti/Co-S catalyst covered amorphous Si-based photocathodes with high photovoltage for the HER in non-acid environments, Journal of Materials Chemistry A, 6 (2018) 811-816.

[236] Z. Chen, K. Mou, S. Yao, L. Liu, Zinc-coordinated nitrogen-codoped graphene as an efficient catalyst for selective electrochemical reduction of CO_2 to CO, ChemSusChem, 11 (2018) 2944-2952.

[237] M. Hus, V.D. Dasireddy, N.S. Stefancic, B. Likozar, Mechanism, kinetics and thermodynamics of carbon dioxide hydrogenation to methanol on Cu/$ZnAl_2O_4$ spinel-type heterogeneous catalysts, Applied Catalysis B: Environmental, 207 (2017) 267-278.

[238] M. Huš, D. Kopac, N.S. Stefancic, D.L. Jurkovic, V.D. Dasireddy, B. Likozar, Unravelling the mechanisms of CO_2 hydrogenation to methanol on Cu-based catalysts using first-principles multiscale modelling and experiments, Catalysis Science & Technology, 7 (2017) 5900-5913.

[239] T. Zhang, Z. Li, J. Zhang, J. Wu, Enhance CO_2-to-C_{2+} products yield through spatial management of CO transport in Cu/ZnO tandem electrodes, Journal of Catalysis, 387 (2020) 163-169.

[240] U. Legrand, R. Boudreault, J. Meunier, Decoration of N-functionalized graphene nanoflakes with copper-based nanoparticles for high selectivity CO_2 electroreduction towards formate, Electrochimica Acta, 318 (2019) 142-150.

[241] M. Molla, A. Islam, M. Furukawa, I. Tateishi, H. Katsumata, S. Kaneco, Studies of effects of calcination temperature on the crystallinity and optical properties of Ag-doped ZnO nanocomposites, Journal of Composites Science, 3 (2019) 18.

[242] P. Sharma, N. Kumar, R. Chauhan, V. Singh, V.C. Srivastava, R. Bhatnagar, Growth of hierarchical ZnO nano flower on large functionalized rGO sheet for superior photocatalytic mineralization of antibiotic, Chemical Engineering Journal, 392 (2020) 123746.

[243] R. Nikolic, S. Zec, V. Maksimovic, S. Mentus, Physico-chemical characterization of thermal decomposition course in zinc nitrate-copper nitrate hexahydrates, Journal of Thermal Analysis and Calorimetry, 86 (2006) 423-428.

[244] J. Zeng, T. Rino, K. Bejtka, M. Castellino, A. Sacco, M.A. Farkhondehfal, A. Chiodoni, F. Drago, C.F. Pirri, Coupled copper-zinc catalysts for electrochemical reduction of carbon dioxide, ChemSusChem, 13 (2020) 4128.

[245] J. Rosen, G.S. Hutchings, Q. Lu, R.V. Forest, A. Moore, F. Jiao, Electrodeposited Zn dendrites with enhanced CO selectivity for electrocatalytic CO_2 reduction, ACS Catalysis, 5 (2015) 4586-4591.

[246] Y.-T. Chan, I.-S. Huang, M.-K. Tsai, Enhancing C–C bond formation by surface strain: a computational investigation for C2 and C3 intermediate formation on strained Cu surfaces, Physical Chemistry Chemical Physics, 21 (2019) 22704-22710.

[247] J.D. Goodpaster, A.T. Bell, M. Head-Gordon, Identification of possible pathways for C–C bond formation during electrochemical reduction of CO_2: new theoretical insights from an improved electrochemical model, The Journal of Physical Chemistry Letters, 7 (2016) 1471-1477.

List of Publications

1. In Peer-Reviewed (SCI) Journals

1.1 Published (05)

i. **Saudagar Dongare**, Neetu Singh, Haripada Bhunia, Electro catalytic reduction of CO_2 to useful chemicals on copper nanoparticles, *Applied Surface Science, 537 (2021) 148020. DOI:* https://doi.org/10.1016/j.apsusc.2020.148020. ***(Impact Factor: 6.707)***

ii. **Saudagar Dongare**, Neetu Singh, Haripada Bhunia, Nitrogen-doped graphene supported copper nanoparticles for electrochemical reduction of CO_2, *Journal of* CO_2 *Utilization, 44 (2021) 101382.* DOI: https://doi.org/10.1016/j.jcou.2020.101382 ***(Impact Factor: 7.132)***

iii. **Saudagar Dongare**, Neetu Singh, Haripada Bhunia, Oxide-derived Cu-Zn nanoparticles supported on N-doped graphene for electrochemical reduction of CO_2 to ethanol, *Applied Surface Science, 556 (2021) 149790. DOI:* https://doi.org/10.1016/j.apsusc.2021.149790 ***(Impact Factor: 6.707)***

iv. **Saudagar Dongare**, Neetu Singh, Haripada Bhunia, Pramod K. Bajpai, Electrochemical reduction of CO_2 using oxide based Cu and Zn bimetallic catalyst, *Electrochimica Acta, 392* (2021) 138988 DOI: https://doi.org/10.1016/j.electacta.2021.138988 ***(Impact Factor: 6.901)***

v. **Saudagar Dongare**, Neetu Singh, Haripada Bhunia, Pramod K. Bajpai, Asit Kumar Das, Electrochemical reduction of carbon dioxide to ethanol: A review, *Chemistry Select*, Manusript No. slct.202102829R3, ***(Impact Factor: 2.109)*** **(Accepted for publication)**

2. Conferences

2.1 In International Conferences (03)

i. **Saudagar Dongare**, Neetu Singh, Haripada Bhunia, 2021. Study of copper and copper supported on N-doped graphene nanoparticles for enhanced electrochemical reduction of CO_2 to ethanol. *239th ECS Meeting, organized by The Electrochemical Society*, Chicago, IL, May 30-June 3, 2021

ii. **Saudagar Dongare**, Neetu Singh, Haripada Bhunia, 2020. Utilization of carbon dioxide to useful chemicals by electro catalytic reduction on nanostructured copper surface. *Proc. of the International Conference on Electrochemistry EIHE-2020*, Indian Society for ElectroAnalytical Chemistry (ISEAC), Bhabha Atomic Research Centre (BARC), Trombay, Mumbai, India, January 20-25. pp. 193.

iii. **Saudagar Dongare**, Neetu Singh, Haripada Bhunia, 2019. Metal/metal oxide supported electro-catalysts for CO_2 reduction. *Proc. of the 12th International Symp. on Advances in Electrochemical Science and Technology (iSAEST-12)*, Society for Advancement of Electrochemical Science and Technology (SAEST) Karaikudi and CSIR-Central

Electrochemical Research Institute (CSIR-CECRI) Karaikudi, Tamil Nadu, India, January 8 – 10, pp. 123.

2.2 In National Conferences (06)

i. **Saudagar Dongare**, Neetu Singh, Haripada Bhunia, 2021. Improved catalytic activity and selectivity on metal oxide electro-catalysts for low temperature aquous-phase CO_2 reduction" in *Innovative Development in Chemical Technology (IDCT-2021)* organized by University School of Chemical Technology, GGSIPU, New Delhi, India. March 19-20, 2021.

ii. **Saudagar Dongare**, Neetu Singh, Haripada Bhunia, 2020. Electro-reduction of carbon dioxide to ethanol using nanostructured copper-based Electro-catalysts, *New Generation Ideation Contest (NGIC) – 2020*, organized by HPCL Green R&D Centre, Bengaluru, January 05-07, 2021.

iii. **Saudagar Dongare**, Neetu Singh, Haripada Bhunia, 2020. Recent trends in copper based electrocatalyst for CO_2 reduction. *Proc. of the Engineering Science Section, 107th Indian Science Congress,* University of Agricultural Sciences, GKVK, Bangalore, India, January 03-07.

iv. **Saudagar Dongare**, Neetu Singh, Haripada Bhunia, 2019. Synthesis and characterization of copper nanoparticles: Potential application towards electrochemical reduction of carbon dioxide. *Proc. of the 3rd National Symp. on Shaping the Energy Future: Challenges & Opportunities (SEFCO 2019),* CSIR-Indian Institute of Petroleum, Dehradun, India, May 10-11, pp. 46

v. **Saudagar Dongare**, Neetu Singh, Haripada Bhunia, 2018. Recent trends in electrocatalyst for CO_2 conversion. *Proc. of the 71th Annual Session of Indian Institute of Chemical Engineers (CHEMCON–2018),* Department of Chemical Engineering, Dr. B. R. Ambedkar National Institute of Technology Jalandhar, India, December 27-30, pp. 43.

vi. **Saudagar Dongare**, Neetu Singh, Haripada Bhunia, Pramod K. Bajpai, 2021. Bimetallic Cu-Zn electrocatalysts for conversion of CO_2 to alcohols. *Proc. of the 5th National Symp. on Shaping the Energy Future: Challenges & Opportunities (SEFCO 2021),* CSIR-Indian Institute of Petroleum, Dehradun, India, August 27, 2021, pp-60.

Reprints of published articles

Applied Surface Science 537 (2021) 148020

Contents lists available at ScienceDirect

Applied Surface Science

journal homepage: www.elsevier.com/locate/apsusc

Electrocatalytic reduction of CO_2 to useful chemicals on copper nanoparticles

Saudagar Dongare, Neetu Singh, Haripada Bhunia*

Department of Chemical Engineering, Thapar Institute of Engineering and Technology (Deemed to be University), Patiala 147004, Punjab, India

ARTICLE INFO

Keywords:
Copper nanoparticles
CO_2 reduction
nanoporous Cu electrode
Faradaic efficiency

ABSTRACT

One of the best options to utilize CO_2 is to convert it to useful chemicals, which may lead to economic and environmental benefits. In the present work, highly stable metallic copper nanoparticles (Cu NPs) have been synthesized and characterized by different physio-chemical characterization techniques like X-ray photoelectron spectroscopy (XPS), high-resolution transmission electron microscopy (HR-TEM), X-ray diffraction (XRD), Brunauer-Emmet-Teller (BET), etc. The prepared Cu NPs exhibit porous morphology in pure metallic state with high surface area of 630 $m^2.g^{-1}$. From electrochemical experiments, total Faradaic efficiency (FE) for the liquid products reached to ~58% at −0.8 V (vs. RHE) using prepared Cu NPs as an electrocatalyst. The Cu NPs majorly produced formic acid (2.3 mM) with small quantities of acetic acid (13 μM), ethanol (51 μM), and n-propanol (32 μM) under studied conditions. In addition, FE for formic acid remained constant around ~40% at −0.8 V vs. RHE) when reusing the same electrode number of times. The good performance of Cu NPs might be due to the presence of lots of micropores on the surface, which increases CO_2 adsorption for its conversion to chemicals.

1. Introduction

Naturally available fuels (crude oil, coal, etc.) are used as the world's primary source of energy [1]. The utilization of naturally available fuel is drastically increasing to fulfill the world's energy demand due to rapid rise in population and its low cost. Fossil fuel accounts for more than 85% usage for energy generation [2]. Therefore, the atmospheric carbon dioxide (CO_2) concentration has been increasing drastically [3]. This increase in the concentration of CO_2 is a very sincere concern as it creates high impact on global climate change. In addition, increasing the CO_2 concentration in the atmosphere is resulting in ocean acidification and influencing the growth of many aquatic species present in the ocean [4].

The atmospheric CO_2 could be reduced by converting it into useful chemicals using electrochemical reduction of CO_2 (ECO_2R) driven by renewable energy. Several metal complexes [5–8], pure metals [9], polymer [10], alloys [11–14] and metal free [15,16] electrocatalysts have been studied for ECO_2R. However, different electrocatalytic properties were shown by various metal electrodes to produce different chemicals. The copper has a unique ability to reduce CO_2 to many products like methanol, ethanol, propanol [17], formic acid/formate (depending on pH), etc. which are relatively value-added commodity chemicals. Therefore, there is great interest in studying Cu to improve product selectivity for maximizing economic and environmental benefits (see Supporting Information, SI-1).

To date, different Cu based electrocatalysts have been investigated to improve the selectivity and activity, including the exposed surface facets [18], particle size [19], the control of macrostructure [20], and bimetallic alloys formation with the use of secondary metals [21]. High overpotential and poor selectivity due to the hydrogen evolution reaction (HER) remains a huge challenge for selective ECO_2R [22]. Therefore, recent investigations have focused on suppressing HER and improving carbonaceous product selectivity.

The use of copper electrode for ECO_2R is extensively studied by many researchers [9,23–31]. The very first report was available in 1989 by Hori et al. [25], where the authors studied Cu in the aqueous inorganic electrolyte and observed CO, CH_4, C_2H_4, C_2H_5OH, and C_3H_7OH at ambient conditions. Recently, cuprous oxide (Cu_2O) derived copper nanoparticles was reported by Kas et al. [26] for ECO_2R. From their online electrochemical mass spectroscopy study, they reported that all ECO_2R actually proceeds on the newly formed metallic copper particles (*in-situ*) and not on as-deposited Cu_2O. Formic acid with 22% FE was observed in the liquid phase. Two separate studies were carried out by Frese et al. [27] and Le et al. [5] on the effect of different pretreatment methods on Cu foils. Both have reported methanol as the main product with the highest production rate on Cu_2O films deposited on stainless

* Corresponding author.
E-mail addresses: saudagar1108@gmail.com (S. Dongare), neetu.singh1479@gmail.com (N. Singh), hbhunia@thapar.edu (H. Bhunia).

https://doi.org/10.1016/j.apsusc.2020.148020
Received 6 August 2020; Received in revised form 19 September 2020; Accepted 26 September 2020
Available online 30 September 2020
0169-4332/

Journal of CO2 Utilization 44 (2021) 101382

Contents lists available at ScienceDirect

Journal of CO2 Utilization

journal homepage: www.elsevier.com/locate/jcou

Nitrogen-doped graphene supported copper nanoparticles for electrochemical reduction of CO_2

Saudagar Dongare, Neetu Singh, Haripada Bhunia *

Department of Chemical Engineering, Thapar Institute of Engineering and Technology (Deemed to be University), Patiala, 147004, Punjab, India

ARTICLE INFO

Keywords:
Alcohol
Carbon dioxide
Cu/NGN
Electrochemical reduction

ABSTRACT

Increasing CO_2 concentration in the atmosphere causes a negative impact on the global climate. Utilization of CO_2 into value-added chemical products by electrochemical reduction method has attracted great attention to reduce the CO_2 emissions and achieve net-zero carbon footprints. Herein, we report a nanostructured electrocatalyst consisting of N-doped graphene (NGN) supported Cu nanoparticles (Cu NPs) with high catalytic activity for electrochemical CO_2 reduction (ECR). The electrocatalyst was optimized for loading of Cu NPs on NGN. The physico-chemical properties of electrocatalysts were studied by SEM, TEM, Raman spectroscopy, XPS, *etc.* Characterization results show that the high loading of Cu (30 wt. %) increases the size of Cu NPs due to agglomeration of particles. ECR experiments were carried out in a two-compartment electrochemical cell. High performance liquid chromatography (HPLC) was employed to analyze the liquid products. Amongst all tested electrocatalysts, Cu_{20}/NGN shows the highest activity for ECR in the entire potential range studied. It gives a total 54 % Faradaic efficiency at -1.0 V (*vs.* RHE) for the liquid products. The study also demonstrates that the electronic and structural properties of the electrode were improved by the addition of Cu NPs on NGN surface, which in turn enhanced the performance of the catalyst as confirmed by potential-controlled electrocatalysis.

1. Introduction

In recent years, the total usage of fossil fuels (*e.g.* petroleum, coal, and natural gas) comprises ~ 81.5 % of global energy resources due to the progress of human society and rapid industrialization [1]. This is enhancing the carbon dioxide (CO_2) concentration in the atmosphere. Therefore, great efforts have been devoted to find out an alternative pathway to capture and convert it into other value-added products. Among several existing methods available for CO_2 utilization [2], electrochemical CO_2 reduction (ECR) has attracted increasing interest in recent years, because it is easily controlled by electrode potential and operated at ambient conditions [3]. Also, electrical energy required to drive ECR can be generated from renewable sources (like geothermal power, wind, tidal, and solar) which help to achieve net-zero carbon footprints. However, CO_2 is a very stable molecule and huge negative potentials are required for triggering ECR reaction which produces multiple products [4]. Therefore, efficient electrocatalyst is needed which can control the multi-electron and multi-proton transfer pathways for ECR at low overpotential and also can provide high selectivity for different products [5]. So far, only few catalysts are available which could give single end product [6–8].

From past few years, different heterogeneous electrocatalysts were studied by many researchers including mono-metals (*e.g.*, Zn, Cu, *etc.*) [9,10], bi-metals (*e.g.*, Cu-CO, Cu-Zn, *etc.*) [11,12], oxides (*e.g.*, SnO_2, CuO, Cu_2O, ZnO, *etc.*) [13], carbon-based materials [14–16], and metal organic frameworks [17,18]. Compared with these different materials, carbon-based materials, specifically N-doped graphene (NGN) are promising and desirable materials for ECR due to its low-cost, high surface area, a mesoporous and microporous structure, and excellent electrical conductivity [19]. Also, NGN is favorable to assimilate metallic and nonmetallic species on account of its high specific area [14]. This offers higher degrees of freedom to incorporate the corresponding catalytic active sites.

Recently, Song et al. [19] studied Cu/CN (Cu NPs decorated on a N-doped carbon Nano spike film) for the ECR. Cu/CNS gives high selectivity for ethanol formation (FE = 63 %) at −1.2 V *vs.* the reversible hydrogen electrode (RHE). Han et al. [20] reported Cu/NPC-800 electrocatalyst with high selectivity toward the multi-carbon alcohols. According to their report, the multi-carbon alcohols are produced due to the combined effect of Cu nanoparticles as a catalytic site and pyridinic

* Corresponding author.
E-mail addresses: saudagar1108@gmail.com (S. Dongare), neetu.singh1479@gmail.com (N. Singh), hbhunia@thapar.edu (H. Bhunia).

https://doi.org/10.1016/j.jcou.2020.101382
Received 30 July 2020; Received in revised form 25 October 2020; Accepted 18 November 2020

Applied Surface Science 556 (2021) 149790

Contents lists available at ScienceDirect

Applied Surface Science

journal homepage: www.elsevier.com/locate/apsusc

Full Length Article

Oxide-derived Cu-Zn nanoparticles supported on N-doped graphene for electrochemical reduction of CO_2 to ethanol

Saudagar Dongare, Neetu Singh, Haripada Bhunia *

Department of Chemical Engineering, Thapar Institute of Engineering and Technology (Deemed to be University), Patiala 147004, Punjab, India

ARTICLE INFO

Keywords:
Electrochemical CO_2 reduction
Ethanol production
Co-precipitation
Faradaic efficiency
Heterogeneous catalyst

ABSTRACT

The oxide-derived Cu and Zn nanoparticles (prepared by co-precipitation method) supported on N-doped graphene ($CuZn_x$/NGN) were prepared and ZnO loading was optimized for efficient electrochemical CO_2 reduction (ECR) to multi-carbon products. The ECR experiments were performed in aqueous 0.1 M $KHCO_3$ electrolyte at ambient pressure. Results suggest that the Faradaic efficiency (FE) for multicarbon products could be tuned by varying the loading of Zn in the $CuZn_x$/NGN. The catalyst with 20 wt% ZnO loading ($CuZn_{20}$/NGN) gives the highest FE of 34.25% for ethanol production and 12.38% for N-propanol at −0.8 V (*vs.* RHE) with the total current density of 3.95 mA cm^{-2}. The $CuZn_{20}$/NGN electrode shows long term stability of at least 24 h at optimized conditions. It is suggested that CO generated at the reduced ZnO nanoparticles increases the local surface coverage of *CO on the reduced CuO, which improves the C-C coupling rate, facilitating the multi-carbon production (i.e. ethanol).

1. Introduction

Carbon dioxide (CO_2) is a most common greenhouse gas in our planet. Unfortunately, with the intensified industrial activities by mankind and global consumption of fossil fuels, more CO_2 is released to the environment, causing Earth–carbon imbalance, leading to possible global warming and climate change issue [1]. Consequently, the reduction of the CO_2 emissions and the conversion of CO_2 into useful products seem to be important, indeed essential, for the conservation of the environment [2]. Different governments around the world have expressed their concern by growing their expenditure in research to address the CO_2 problem [3]. Amongst various techniques available for CO_2 conversion [2], electrochemical CO_2 reduction (ECR) reactions is considered as best because it can be carried out under ambient conditions through the application of an external electrical bias [4]. Many useful products like acids, ethers, and alcohols can be derived from ECR but now a days many researchers are targeting high energy density products such as alcohols due to its application in gasoline blends for fuel [5]. The global alcohol industry size was approximately USD 131.8 billion in 2019 and is projected to rise at an average annual growth rate of 8.3 percent from 2020 to 2027 [6]. The product selectivity in ECR depends on the type of electrocatalyst used. Till date, no electrocatalyst is reported which shows 100% selectivity for single product due to its high over-potential and competing hydrogen evolution reaction (HER) [7].

Therefore, researchers devoted considerable effort in electrocatalyst developments for the ECR. Amongst all the reported catalysts so far for ECR in aqueous media, Copper (Cu) alone has a capacity to generate a large range of chemicals beyond CO*, including hydrocarbons and alcohols [8]. However, Cu shows a low activity and selectivity for the C2 products like ethanol and ethylene [9]. While huge amount of literature is available on Cu catalyst for basic understanding of the effect of nanostructures, surface crystal facets, and morphologies on activity and selectivity of the products [10]. Unfortunately, selective electrochemical CO_2 reduction to multi-carbon products has not fulfilled the industrial requirement. Density functional theory (DFT) suggests that the formation of the C-C bond is the important step towards the formation of C2 chemicals [11,12]; that is, the coupling of the intermediate *CO takes place on electrocatalyst surface. Also, C-C coupling for multi-carbon reaction products is facilitated by higher local CO concentration. Many interesting studies are available on modification of Cu surface with organic/inorganic molecules (e.g., N-arylpyridinium, polyaniline, Ag, Au, Co, Cu NPs@C, etc.) for multi-carbon product selectivity [5,13–16]. According to these reports, the stabilization of *CO intermediate on Cu surface increases CO partial pressure which further enhances the CO dimerization rate. In general, increased partial pressure of

* Corresponding author.
E-mail address: hbhunia@thapar.edu (H. Bhunia).

https://doi.org/10.1016/j.apsusc.2021.149790
Received 16 January 2021; Received in revised form 13 March 2021; Accepted 6 April 2021
Available online 18 April 2021

Electrochimica Acta 392 (2021) 138988

Contents lists available at ScienceDirect

Electrochimica Acta

journal homepage: www.elsevier.com/locate/electacta

Electrochemical reduction of CO_2 using oxide based Cu and Zn bimetallic catalyst

Saudagar Dongare[a], Neetu Singh[a], Haripada Bhunia[a,*], Pramod K. Bajpai[b,1]

[a] Department of Chemical Engineering, Thapar Institute of Engineering and Technology (Deemed to be University), Patiala-147004, Punjab, India
[b] Ex-Distinguished Professor, Department of Chemical Engineering, Thapar Institute of Engineering and Technology (Deemed to be University), Patiala-147004, Punjab, India

ARTICLE INFO

Article history:
Received 3 June 2021
Revised 12 July 2021
Accepted 22 July 2021
Available online 28 July 2021

Keywords:
Bimetallic catalyst
Ethanol
CO_2 reduction
High efficiency
Fuel additive

ABSTRACT

Electrochemical reduction of carbon dioxide ($ERCO_2$) driven by non-conventional sources of energy is a favorable approach to generate closed loop CO_2 cycle. It will reduce CO_2 emissions by lowering CO_2 levels in the atmosphere and converting it into high-energy-density carbon-based fuels like alcohols and hydrocarbons. Monometallic copper based catalysts are largely reported for $ERCO_2$ to a variety of industrially important carbon products. But, challenges such as high over potential, uncontrollable product selectivity, and catalyst deactivation inhibit their progress. Oxide derived bimetallic $CuZn_x$ electrocatalysts have been suggested as alternatives for achieving high selectivity for different valuable products. In this study, the co-precipitation approach has been used to prepare CuO with various quantities of ZnO dopants. HRTEM, FESEM, XRD, and XPS were used to conduct detailed morphological and elemental studies on the electrode. The electrochemical performance was measured using H-type electrochemical cell in aqueous 0.1 M $KHCO_3$ electrolyte. The evaluation of different CuO-ZnO_x (where x=5, 10, 15 and 20 wt.%) catalysts for ethanol productivity and Faradaic efficiency are of particular importance. Amongst studied electrocatalysts, the highest Faradaic efficiency of 22.27 % was obtained for ethanol using CuO-ZnO_{10} at -0.80 V (vs RHE) with the production rate of about 121 μmol h^{-1} L^{-1}. The optimized electrode (CuO-ZnO_{10}) shows long term stability for at least 12 h. Post characterization of the catalyst was also conducted to obtain an insight into the active sites, which indicated that CO_2 reduction took place on reduced oxide sites (i.e. metallic sites) rather than metal oxides.

1. Introduction

The global transportation industry is confronted with three big issues, namely crude oil price instability, fossil fuel depletion, and strict environmental policies [1, 2]. Among various alternatives [3, 4], biofuels are being aggressively explored as an option because they have less complexities in terms of processing, storage, transportation, and usage in internal combustion engines [5]. Ethanol is regarded as one of the most desirable renewable fuel because of its comparable higher heating value (23.4 MJ/L) [6], competitiveness, superior fuel efficiency, and many environmental advantages [7, 8]. Many countries introduced ethanol blending program in recent years [9]. Therefore, conversion of waste CO_2 to ethanol by electrochemical reduction may be helpful to fulfill world increasing ethanol demand and at the same time it will also decrease the CO_2 emissions from the atmosphere [10].

Electrochemical reduction of CO_2 ($ERCO_2$) to ethanol is $12e^-$ transfer process [11]. The coupling of the main reaction intermediate *CO on the electrocatalysts surface for the C-C bond formation, is considered as important and complex step in the production of ethanol [10]. Also, CO_2 is highly stable molecule and requires high energy for conversion, which makes $ERCO_2$ process more difficult [12]. To make this process feasible at an industrial scale, both the low selectivity of desired products and high reaction over potential must be taken into account [13, 14]. To overcome these limitations, highly active, inexpensive, long-lasting, energy-efficient, and selective electrocatalysts must be created. Different strategies have been suggested to improve the efficiency of metal catalysts, including designing the metal/electrolyte interface [15], nanostructuring the metals [16, 17], or adding a secondary metal to establish bimetallic structure [18-20]. The addition of co-catalysts has been reported by many groups for the in-situ feedstock of mobile CO reactant for Cu

* Corresponding author.
E-mail addresses: saudagar1108@gmail.com (S. Dongare), neetu.singh1479@gmail.com (N. Singh), hbhunia@thapar.edu (H. Bhunia), pramod.iitk77@gmail.com (P.K. Bajpai).
[1] Present address: P.K. Bajpai, G-1 Ekta Apartment, 120/912 Ranjeet Nagar, Kanpur-208005, Uttar Pradesh, India

https://doi.org/10.1016/j.electacta.2021.138988
0013-4686/